

71-18,059

NEEDHAM, Paul Eugene, 1929-  
THE FORMATION AND EVALUATION OF DETAILED  
GEOPOTENTIAL MODELS BASED ON POINT MASSES.

The Ohio State University, Ph.D., 1970  
Geodesy

University Microfilms, A XEROX Company , Ann Arbor, Michigan

**THE FORMATION AND EVALUATION OF DETAILED  
GEOPOTENTIAL MODELS BASED ON POINT MASSES**

**DISSERTATION**

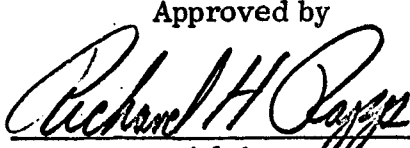
**Presented in Partial Fulfillment of the Requirements  
for the Degree Doctor of Philosophy  
in the Graduate School of The Ohio State University**

**By**

**Paul Eugene Needham, B.S., M.Sc.**

\*\*\*\*\*

**The Ohio State University  
1970**

Approved by  
  
\_\_\_\_\_  
Adviser  
Department of Geodetic Science

## ACKNOWLEDGEMENTS

The writer wishes to acknowledge the support and assistance given by the faculty, staff, and students of the Department of Geodetic Science.

Dr. R. H. Rapp, my adviser for this study, generously furnished unpublished gravity data and some supplemental computer programs, but most valuably, he furnished encouragement and advice.

Special thanks are due to Dr. U. A. Uotila, Dr. Gabriel F. T. Obenson, Mr. John Snowden, and Mr. Francis Fajemirokun for their patience in listening to and criticizing the various concepts involved in this investigation. Mr. Snowden should also be singled out for the extensive advice that he provided on computer programming.

The reading committee, Dr. R. H. Rapp, Dr. I. I. Mueller, and Dr. U. A. Uotila deserve thanks for the assistance they gave in refining and clarifying my original draft.

The extensive computer support required for this study was provided by The Ohio State University Instruction and Research Computer Center.

## VITA

August 19, 1929. . . . .	Born - Oskaloosa, Iowa
1951. . . . .	B.S., Forestry, Iowa State University
1952. . . . .	M.S., Silviculture, New York State College of Forestry
1952. . . . .	Entered active duty, U. S. Air Force
1960. . . . .	M.Sc., Geodesy, The Ohio State University
1967. . . . .	Began studies for Ph. D. at The Ohio State University

## FIELDS OF STUDY

### Major Field: Geodetic Science

Studies in Geometric Geodesy. Professors Richard H. Rapp and Simo H. Laurila.

Studies in Astronomy and Satellite Geodesy. Professor Ivan I. Mueller.

Studies in Adjustment Computations. Professors Urho A. Uotila and Simo H. Laurila .

Studies in Physical Geodesy. Professors Ivan I. Mueller and Weikko A. Heiskanen.

Studies in Electronic Surveying. Professors Simo H. Laurila and Peter Richardus.

Studies in Photogrammetry. Professors Fred C. Doyle, Sanjib K. Ghosh, and Dean C. Merchant.

**Studies in Map Projections. Professors Simo A. Laurila and Richard  
H. Rapp.**

## TABLE OF CONTENTS

ACKNOWLEDGEMENTS.....	ii
VITA .....	iii
LIST OF TABLES .....	viii
LIST OF FIGURES.....	x
INTRODUCTION.....	1
Chapter	
1. THE COMBINATION OF SATELLITE AND TERRESTRIAL GRAVITY DATA .....	5
1.1 General.....	5
1.2 Utilization of Gravity Information.....	8
2. POINT MASS REPRESENTATION OF AN EQUIVALENT LAYER SURFACE.....	14
2.1 An Equivalent Layer Model of the Disturbing Potential ..	14
2.2 The Relationship Between Gravity Anomalies and Elemental Point Masses on an Equivalent Layer Surface.	17
2.3 The Relationship Between a Point Mass Approximation and a Surface Integral Approximation.....	22
2.4 The Point Mass Model as a Representation of a Smoothed Geopotential Field.....	29
2.5 Practical Consequences of the Geometry of the Point Mass Solution .....	33
3. THE SPHEROP 14 REFERENCE SYSTEM.....	36

4.	ERRORS CAUSED BY THE USE OF LIMITED AREAS OF GRAVITY INFORMATION .....	50
4.1	General .....	50
4.2	Comparison of Truncation Errors for Geoid Heights Computed with Respect to Ellipsoidal and Spherop Reference Surfaces.....	53
4.3	The Effect of Neglected High Order Anomaly Degree Variances .....	55
4.4	The Effect of Discrepancies Between the Reference Model and the True Earth .....	63
4.5	Truncation Errors in the Computation of Gravitational Disturbance Components .....	65
5.	THE COMPUTATION OF POINT MASS SETS .....	72
5.1	General .....	72
5.2	Assumptions Regarding Data .....	72
5.3	Conditions Imposed on the Solution .....	73
5.4	Superpositioned Mass Sets.....	78
5.5	Generation of Contiguous Mass Sets .....	85
5.6	The Point Mass Solution Computer Program .....	89
5.6.1	General.....	89
5.6.2	Computation Control Parameters .....	90
5.6.3	Input Data.....	91
5.6.4	Mass Positioning .....	92
5.6.5	Formation of Normal Equations.....	92
5.6.6	Matrix Inversion.....	95
5.6.7	Results and Statistics Produced by the Point Mass Solution Program.....	96
5.6.8	Geoid Computation .....	97
6.	THE DATA USED IN FORMING GEOPOTENTIAL MODELS...	99
6.1	Basic Data Used in Computations.....	99
6.1.1	Spherical Harmonic Coefficients.....	99
6.1.2	Five Degree by Five Degree Mean Anomaly Set ..	100
6.1.3	One Degree by One Degree Mean Anomaly Set....	101
6.1.4	Thirty Minute by Thirty Minute and Five Minute by Five Minute Mean Anomalies .....	101
6.2	The Relation Between the Anomaly Sets.....	102
6.3	Conversion of Mean Anomalies from The International Gravity Formula System to the GRS 67 and Spherop 14 Systems.....	102
6.4	Reconciliation of Anomalies .....	108

<b>7. COMPUTATION OF STANDARDS OF COMPARISON.....</b>	<b>115</b>
<b>7.1 General.....</b>	<b>115</b>
<b>7.2 The Comparison Gravimetric Geoid.....</b>	<b>117</b>
<b>7.2.1 General.....</b>	<b>117</b>
<b>7.2.2 Compatibility of Anomaly Data .....</b>	<b>122</b>
<b>7.2.3 Computation of the Comparison Gravimetric Geoid .....</b>	<b>125</b>
<b>7.2.4 Comparison with an Astrogeodetic Geoid .....</b>	<b>130</b>
<b>7.3 The Gravity Disturbance Component Standard .....</b>	<b>138</b>
<b>7.3.1 General.....</b>	<b>137</b>
<b>7.3.2 The Direct Integration Method.....</b>	<b>139</b>
<b>7.3.3 Computation of the Gravity Disturbance Component Standard.....</b>	<b>141</b>
<b>8. POINT MASS COMPUTATIONS AND COMPARISONS.....</b>	<b>143</b>
<b>8.1 Computation of a Point Mass Set to Describe the Potential Field in the Central United States .....</b>	<b>143</b>
<b>8.2 A Point Mass Geoid for the Comparison Test Area.....</b>	<b>147</b>
<b>8.3 Computation of Point Mass Sets for Gravity Disturbance Component Computation.....</b>	<b>155</b>
<b>8.4 Computation of Gravity Disturbance Components from Point Masses .....</b>	<b>156</b>
<b>8.5 Computation of Gravity Disturbances at the Test Points .</b>	<b>160</b>
<b>8.6 Comparison of Computer Time Requirements .....</b>	<b>168</b>
<b>9. CONCLUSIONS AND RECOMMENDATIONS .....</b>	<b>172</b>
<b>9.1 Summary and Conclusions.....</b>	<b>172</b>
<b>9.2 Possibilities for Further Investigation.....</b>	<b>175</b>
<b>APPENDIX</b>	
<b>A .....</b>	<b>177</b>
<b>B .....</b>	<b>194</b>
<b>C .....</b>	<b>197</b>
<b>D .....</b>	<b>200</b>
<b>E .....</b>	<b>209</b>
<b>F .....</b>	<b>219</b>
<b>G .....</b>	<b>233</b>
<b>BIBLIOGRAPHY.....</b>	<b>246</b>

## LIST OF TABLES

Table	Title	Page
1.	General Comparison of Integrated and Point Mass Kernels..	26
2.	Comparison of Integrated and Point Mass Kernels for Blocks Directly Under Computation Point ( $s=0$ ).....	27
3.	Comparison of Integrated and Point Mass Kernels at Different Lateral Distances for Shallow Depths ( $d=.8$ ).....	28
4.	Anomaly Degree Variances According to Rapp.....	54
5.	Root Mean Square Truncation Error $\overline{\Delta N\psi}$ .....	55
6.	Hypothesised Undulation Computation Errors Due to Neglected High Order Terms .....	61
7.	Anomaly Degree Variances for Altered Gravity Field Referred to Spherop 14 .....	64
8.	Influence of Conditions on Point Mass Solutions.....	78
9.	Point Mass Solution Characteristics.....	80
10.	Suggested Anomaly Block Sizes for Disturbance Computations (Hirvonen and Moritz).....	81
11.	Recent Determinations of Absolute Gravity.....	103
12.	Mean Anomaly Sets Formed.....	104
13.	Statistics on $1^\circ \times 1^\circ$ Mean Anomaly Sets.....	106
14.	Comparison of Spherop 14 and GRS 67 $1^\circ \times 1^\circ$ Mean Free Air Anomalies Averaged Over $19^\circ \times 19^\circ$ Blocks.....	107
15.	Mean 1927 NAD Datum Shifts .....	136

16.	Comparison of Deflections at 1927 NAD Origin .....	137
17.	Point Mass Solutions Using $1^\circ \times 1^\circ$ Mean Anomalies .....	145
18.	Summary of Superimposed Point Mass Set Solutions.....	158
19.	Comparison of Point Mass and Direct Integration Gravity Disturbance Component Computations .....	161
20.	Mean Difference Between Comparison Standard and Point Mass Gravity Components.....	165
21.	Comparison of Point Mass and Direct Integration Gravity Disturbance Components (Reduced Field of $5' \times 5'$ Mean Anomalies).....	166
22.	Orlin's Computation of Gravity Disturbance Vector Components .....	167
23.	Comparison of Time Required to Compute 1000 Geoid Heights .....	170
24.	Comparison of Time Required to Compute Gravity Disturbance Components at 45 Points.....	170
25.	Time Required to Form Point Mass Sets.....	171

## LIST OF FIGURES

Figure	Title	Page
1.	A Fictitious Model Earth.....	17
2.	Notation of Point Mass Derivations.....	19
3.	Geometry of the Planar Approximation .....	24
4.	Undulation Error Due to Truncation of Anomaly Field - Ellipsoidal Reference Surface .....	56
5.	Undulation Error Due to Truncation of Anomaly Field - Spherop 14 Reference Surface .....	57
6.	Total Undulation Error Due to Truncation of Anomaly Field - Spherop 14 Reference Surface .....	62
7.	Total Undulation Error Due to Truncation of Anomaly Field - Spherop 14 Reference Surface (Based on Altered Gravity Field) .....	66
8.	Errors in Deflections and Horizontal Components of Anomalous Gravity as a Function of Truncation Angle $\psi_0$ .....	69
9.	Correlation Coefficients for Members of a Point Mass Array	86
10.	Arrangement of Contiguous Anomaly Areas .....	89
11.	Average Reconciliation Correction to $1^\circ \times 1^\circ$ Mean Anomalies	113
12.	Corrections Applied to $5^\circ \times 5^\circ$ Mean Anomalies .....	114
13.	Area of $1^\circ \times 1^\circ$ Mean Anomalies and Comparison Test Area..	118
14.	Geoid from Stokes' Equation.....	127
15	Geoid from Spherical Harmonic Coefficients .....	128

16.	Astrogeodetic Geoid .....	134
17.	Point Mass Geoid .....	148
18.	Geoid Height Difference - (14, 14) Spherical Harmonic Minus Point Mass .....	150
19.	Geoid Height Differences - Stokes' Minus Point Mass Solution	151
20.	Comparison of Geoid Profiles - 35°N Parallel .....	153
21.	Superposed Mass Set Area and Trajectory Foot Points .....	157
22.	Gravity Disturbance Components at 20 Kilometers Elevation Arranged in Geographic Location .....	162

## INTRODUCTION

Treatises on the theories of gravimetric geodesy very generally start with a basic mathematical description of the gravitational potential of the earth of the form:

$$(I-1) \quad V = k \int_M \frac{dM}{\ell}$$

where:  $V$  = gravitational potential at a point;

$k$  = gravitational constant;

$dM$  = mass element; and

$\ell$  = distance between the computation point

and the mass element  $dM$ .

[Heiskanen and Moritz, 1967, p. 3]

Although the concept is basic to the entire development of gravimetric geodesy, these publications quickly point out that this equation has no practical value in the computation of the earth's gravitational potential or its derivatives since the mass distribution within the earth is not known. As a result, emphasis is shifted to formulations depending on forces actually measurable on or above the surface of the earth. It is further pointed out that problems such as determining the potential and its first derivative and thus the mass of the earth and the shape of its exterior equipotential

can be solved without knowledge of the density distribution within the earth [Heiskanen and Moritz, 1967, p. 64]. This is fortunate for there is no solution by which a unique internal mass distribution generating a given potential can be determined from measurements of that potential [Heiskanen and Moritz, 1967, p. 17; Bullard and Cooper, 1948].

The simplicity of equation (I-1) and its various directional derivatives have stimulated various investigations to attempt to synthesize a mass distribution model that would generate an observed potential field.

Weightman [1967] in 1965 suggested the use of "point sources" or "buried masses" as the basis for such a mathematical model for geodetic purposes.

He credited an earlier paper that used dipoles as a model for the geomagnetic field [Aldridge and Horovitz, 1964] for suggesting some facets of his development. There are, however, many examples in geophysical literature of attempts to interpret gravimetric data in terms of anomalous masses.

Examples are given by Garland [1965] and Bullard and Cooper [1948]. In these examples, the location, size, and anomalous density of the masses producing an observed field are sought for their geophysical implications.

This type of geophysical problem is much different than the problem of finding an arbitrary mass distribution that will produce a given potential field and, as noted, it has no unique solution. Most geophysical discussions of mass solutions as a result are rather unrelated to Weightman's proposal. An exception is the "equivalent source technique" in which discrete point masses on a buried plane are used in a very localized area to aid in inter-

polating a regular grid of Bouguer anomalies from irregularly-spaced obser-vations [Dampney, 1969].

Probably the best known utilization of point masses to geodesists is the work done by Muller, Sjogren, and others as part of the Lunar Orbiter Program. In this program, point masses were used to model the lunar potential [Muller and Sjogren, 1968]. These studies have shown that under the special situation pertaining to the Lunar Orbiter Program, point masses have contributed significantly to describing the local structure of the poten-tial field [Wong, et al., 1969].

A lesser known investigation utilizing point masses has been conduced by Geodynamics Corporation under the auspices of the United States Air Force. This study is related to the compensation of ballistic weapons sys-tems for anomalous gravity accelerations. The existence of this effort and its general outlines are not classified military information, but specific parameter values and requirements are classified. No information has been published in the open scientific literature, to the knowledge of the author, on these studies and the author has had no access to classified documents. Through personal communication with individuals at various Air Force activi-ties, it has been determined that the point mass concept currently appears to be applicable to some Air Force requirements, but that many theoretical and practical aspects of the concepts have not been completely resolved. There was a strong interest at all activities contacted in encouraging inde-pendent studies utilizing point masses.

This dissertation is therefore oriented toward the use of point masses in geodesy. Specifically it treats the use of point masses as a means of describing more detailed gravitational fields than are represented by current spherical harmonic models. The approach has been to see what can be done in a practical manner with actual data rather than to offer a purely theoretical discussion. In some respects, as is often the case in actual practice, the available data was somewhat inadequate. It seemed preferable, nevertheless, to use this real data rather than to attempt to construct model gravitational fields. The construction of such fields is too closely related to the point mass concept to insure that the techniques employed in the study would not be unconsciously biased toward resolving the components of the specific model originally postulated.

## CHAPTER 1

### THE COMBINATION OF SATELLITE AND TERRESTRIALLY OBSERVED GRAVITY DATA

#### 1.1 General

The external anomalous gravity field of the earth is commonly described by a truncated spherical harmonic expansion obtained from satellite analysis, or by the explicit listing of anomalies derived from surface observations and reduced to a defined surface. Neither system is fully satisfactory for modern applications in geodesy and the missile and space fields. New and proposed uses for gravity data as typified by rocket trajectory computations and inertial navigation system calibration and operation have presented problems that are not easily solved using these representations. These difficulties arise primarily because, with the data available today, neither method alone can be used to successfully describe the full spectrum of the variation in the gravity field. The two methods are complimentary and the best current model of the external gravity field must include data obtained from both sources. This is the subject of much current research and reference will be made in subsequent sections to investigations concerned with specific aspects of this problem.

To date, practically all data on the gravitational field of the earth that

has been obtained by the analysis of satellite orbits has been obtained initially in the form of spherical harmonic coefficients. Less than 300 terms in this infinite series of coefficients have currently been determined with any reliability [Gaposchkin and Lambeck, 1970]. Some current research deals with the direct determination of surface gravity or surface density layers [Obenson, 1970; Rapp, 1970; Koch and Morrison, 1970], but irrespective of the form of the data, the current methods of satellite analysis will be limited to forming models of a complexity comparable to that shown by the spherical harmonic models [Kaula, 1969]. This is inherent in the fact that a satellite reacts to the potential field through which it moves. At satellite heights, the high frequency variations which occur in the near earth field are damped out. If the wavelength,  $\theta$ , of a variation is given by:

$$(1.1) \quad \theta = \frac{2\pi a_e}{n}$$

where  $a_e$  is the equatorial radius of the earth and  $n$  is an arbitrary integer, then the potential field variations are damped with elevation by the factor:

$$(1.2) \quad \left(\frac{a_e}{r}\right)^n \quad \text{or} \quad \left(\frac{a_e}{r}\right)^{\left(\frac{2\pi a_e}{\theta}\right)}$$

where  $r$  is the satellite geocentric radius. Thus, the shorter the wavelength of the variation, the greater the attenuation of the disturbance to the normal field and the less the observable perturbation of the nominal satellite orbit. It is apparent that conventional satellite orbit analysis is not an optimum technique for defining the very detailed structure of the near earth gravity field. It should be noted parenthetically that new satellite techniques using data

other than the motion of the satellite relative to earth fixed stations may be expected to yield more detailed information in the future. For example, satellite altimetry may considerably improve the knowledge of the fine structure of the geopotential over oceanic areas [Young, 1970].

A converse situation exists with respect to terrestrial gravimetry. Huge quantities of very detailed information exist as a result of ground gravity observations, but this information is poorly distributed over the earth. In a recent effort to develop a spherical harmonic coefficient set from observed terrestrial anomalies, only 1470 of the  $2592\ 5^\circ \times 5^\circ$  mean anomalies over the earth could be estimated from actual observations [Rapp, 1969a]. This situation does not allow a strong determination of the spherical harmonic coefficients describing the gravitational field of the earth. Gravity anomalies are known in great detail in many areas, particularly in the United States and Europe, but the lack of worldwide gravity information prevents the fullest utilization of this material. In effect, we know the short wavelength variations in the field in limited areas, but do not have adequate information to fully define larger scale features from terrestrial observations.

In recent years, several investigators have utilized both satellite information and terrestrial gravity information to determine spherical harmonic coefficient sets. These combination solutions are essentially the result of all of the available observational material concerning the variations in the geopotential field. They provide a bridge between the satellite derived coefficients and the terrestrial gravity observations, but because of

the limited availability of ground observations in the context of a worldwide solution, the coefficient sets have not been carried to a high degree and order. Examples of such coefficient sets derived from combination solutions are Rapp's (14,14) set [1969b], Gaposchkin and Lambeck's (16,16) set [1970], and Kaula's (12,12) set [1966]. These solutions provide more detail than the purely satellite solution, and the inclusion of the terrestrial material improves the reliability of the detail that is described.

### 1.2 Utilization of Gravity Information

Many of the applications of gravity data require worldwide knowledge of the gravity field at least in theory. Examples are computations of geoid undulations, of deflections of the vertical, and of the gravitational disturbance components that are needed in trajectory and orbit analysis. In each of these cases, detailed gravity information is needed in some "inner zone" surrounding the computation point while more generalized information will suffice for distant areas [Heiskanen and Moritz, 1967].

Prior to the development of satellite geodesy, a considerable portion of the effort in gravimetric geodesy was devoted to the practical solution of problems where only the inner field was known. In these cases, the local variations in the geopotential field and the consequences of these variations could be determined with some accuracy. These computations were of value in applications such as interpolating deflections between astrogeodetic deflection stations [Rice, 1967]. In these computations, the effect of the outer zone was considered to be constant resulting in systematic errors in localized com-

putation areas. Undulations or deflections determined in this manner could not be considered to be measured in an absolute earth centered coordinate system and do not share in this primary advantage that gravimetric methods enjoy when worldwide gravity data is available. The magnitude of the systematic errors introduced by the neglect of outer anomaly fields has been studied by Molodenskii et al. [1962] and will be discussed further in Chapter 4.

The spherical harmonic coefficient sets that have become available since the advent of dynamic satellite geodesy provide a means of computing functions of the geopotential that are defined in an absolute geocentric coordinate system. Many examples are available in the literature of the use of these coefficient sets to solve for various quantities of interest in geodesy and the space sciences [Rapp, 1966; Lundquist and Veis, 1966; Mueller, 1964; Kaula, 1965]. Because these series are truncated at a relatively low order, they yield highly smoothed representations of the various functions of the geopotential. For example, the actual absolute deflection of the vertical attains magnitudes of 60 seconds of arc [Bomford, 1962], but the maximum deflections computed from current spherical harmonic coefficient sets are less than 10 seconds [Lundquist and Veis, 1966, Vol. 3]. This smoothing, the result of the neglect of short wavelength variations in the geopotential, is a serious deficiency for applications near the surface of the earth. Functions computed in this manner are described in a geocentric coordinate system, but the smoothed value at an individual computation point may have only a tenuous relation to the actual value of a rapidly varying function near the sur-

face of the earth. Since these short wavelength variations are damped at high altitudes, the functions computed from truncated spherical harmonic sets at satellite altitudes are much more representative of the actual value of the function than is the case at lower elevations. For applications at high elevations, the truncated series are satisfactory models of the geopotential [Kaula, 1969].

To achieve a detailed representation of a geopotential function in a given area that is properly related to a mass centered reference system, it is necessary to combine the worldwide knowledge of the geopotential obtained from satellite studies with the detailed gravity information obtained from terrestrial surveys. One manner in which this has been done is to compute anomalies at the center of  $5^\circ \times 5^\circ$  squares using satellite derived spherical harmonic coefficient sets and assume that these are satisfactory representations of  $5^\circ \times 5^\circ$  mean anomalies for use as an outer gravity field. This data is then combined with detailed inner zone terrestrial anomaly data to provide a worldwide gravity field [Rapp, 1967, 1969b]. Another method is to obtain an outer field from the available terrestrial data that has been adjusted to be consistent with a set of spherical harmonic coefficients derived from a combination solution [Snowden and Rapp, 1968]. This method has the advantage, over the preceding method, of retaining a larger amount of the available information on the outer anomaly field. It is a less smoothed field than that obtained from evaluation of spherical harmonic coefficients, yet it is fully compatible with the set of coefficients used in adjusting the field.

This method will be discussed in more detail in Chapter 6. Outer anomaly fields derived in this manner have been used together with detailed inner terrestrial anomaly fields by Rapp [1968], Mather [1969], and Siebenhüner [1969].

Another approach that has been discussed theoretically is the use of a high order reference system [Molodenskii, 1962; de Witte, 1966a; Wong and Gore, 1969]. The common reference systems of physical geodesy, for example, the International, adopted in 1930, and the Geodetic Reference System of 1967, are based on the concept of an ellipsoid as a reference figure. In the terminology used here, a high order, or spherop, reference system is one that is based on a more complex figure than the ellipsoid and that is defined by a finite set of spherical harmonic coefficients.

The traditional normal gravity field is typified by a gravity formula of the type:

$$(1.3) \quad \gamma_\varphi = \gamma_a (1 + \beta_1 \sin^2 \varphi + \beta_2 \sin^2 2\varphi)$$

where:  $\gamma_\varphi$  = normal gravity at latitude  $\varphi$ ;

$\gamma_a$  = equatorial gravity; and

$\beta_1, \beta_2$  = coefficients depending on a set of ellipsoid

parameters such as:

- 1) equatorial radius;
- 2) mass;
- 3) flattening; and
- 4) rotational velocity  
of the earth.

This formula is a truncation of a series expansion of a formula describing the gravity field on the surface of a rotating level ellipsoid [Mueller, 1969; Mueller and Rockie, 1966]. Gravity anomalies at a point are then defined by:

$$(1.4) \quad \Delta g_i = g_i - \gamma_\varphi$$

where  $g_i$  is the observed gravity reduced to the geoid at point i. This procedure reduces the observed gravity information to a perturbation of a normal field. Quantities computed from these anomalies, for example, undulations, deflections, or disturbances at high altitudes, are then similarly perturbations from the normal field or normal reference figure. The ellipsoidal reference figure is simply an approximation to the true shape of the sea level equipotential surface. In a completely analogous manner, a high order, or spherop, reference figure can be defined that is more complex and is a closer approximation to the sea level equipotential surface. For example, the surface might be described in terms of the position dependent radius,  $R_{\varphi'}, \lambda$ , defined by:

$$(1.5) \quad R_{\varphi'}, \lambda = r_{\varphi'} + N_{\varphi'}, \lambda$$

where:  $r_{\varphi'}$  = geocentric radius to a point at geocentric latitude  $\varphi'$  on a defined reference ellipsoid; and

$N_{\varphi'}, \lambda$  = distance between the high order reference surface and the reference ellipsoid along the radius vector  $r_{\varphi'}$ .

A method of defining  $N_{\varphi'}, \lambda$  and of determining the normal gravity on

this surface will be described in Chapter 3. If computations are carried out using anomalies referred to this high order reference surface, then the undulations, deflections, and disturbances are given with reference to this reference figure or its associated gravitational field. In theory the results of these computations, and the results of the usual computations using anomalies referred to a specified ellipsoid should be identical, after reduction to some common reference system, if identical gravity information extending over the entire earth is used in the two computations. If adequate data is available over the entire earth and this data is used in all computations, there is no apparent advantage in using a high order reference system. In practice, the use of a high order reference system minimizes the importance of the outer anomaly field to such a degree that anomaly information need be used only in an inner zone surrounding the computation point. If the spherical harmonic coefficient set used to define the spherop reference is considered to be derived primarily from satellite data and the inner zone anomalies from terrestrial observations, then this procedure is in effect another way of combining satellite and terrestrial data to obtain a detailed geopotential field referenced to a mass centered system. The procedures involved in defining a spherop reference system are described in Chapter 4 and the errors incurred by neglecting the outer anomaly field are treated in Chapter 5.

## CHAPTER 2

### POINT MASS REPRESENTATION OF AN EQUIVALENT LAYER SURFACE

#### 2.1 An Equivalent Layer Model of the Disturbing Potential

The potential field,  $W$ , of the earth is commonly divided into two parts to facilitate both practical and theoretical operations. One part, the normal field  $U$ , consists of some defined reference field. The remainder, known as the disturbing or anomalous potential  $T$ , consists of perturbations to the normal reference field. This may be expressed as:

$$(2.1) \quad W = U + T$$

The anomalous potential  $T$  could be expressed as:

$$(2.2) \quad T = k \int_M \frac{dM}{\ell}$$

where  $dM$  represents differential anomalous mass elements,  $\ell$  represents the distance between a mass element and the point of computation of  $T$ , and the integral is extended over all anomalous mass.

Since  $U$  is a defined potential field, the mass distribution which generates the field  $U$  need not be known. We will assume that the reference field is generated by a mean earth ellipsoid that has the same mass, flattening, and rotation rate as the earth and the same boundary potential as the geoid. This will

imply that:

$$(2.3) \quad \int_M dM = 0$$

$$(2.4) \quad \int_{\sigma} T d\sigma = 0$$

where  $\sigma$  is an equipotential surface and  $d\sigma$  represents a differential area element on that surface. The external geopotential field can be fully described if an anomalous mass distribution is known so that equation (2.2) can be solved at all points on or above the geop exterior to all of the mass of the earth. The mass distribution used for this purpose could be purely imaginary. Indeed "anomalous mass" can have little interpretable meaning where no "normal" mass distribution has been specified.

The task of finding a mass distribution that will generate the true disturbance potential  $T$  is simplified by the fact that we need only find a mass distribution that generates the true potential  $T$  on all points of a given surface  $S$  that encloses all of the anomalous masses to assure that this mass distribution will generate the true disturbance potential throughout the space exterior to the closed surface  $S$ . This statement follows from Stokes' Theorem which states, "...there is only one harmonic function  $V$  that assumes given boundary values on a surface  $S$ , provided that such a harmonic function exists" [Heiskanen and Moritz, 1967, p. 17]. The existence of such a function is assured by Dirichlet's principle [Heiskanen and Moritz, 1967, p. 18].

The problem can be still further simplified by specifying that all of

the anomalous mass be concentrated into an equivalent layer on an equipotential surface that is external to all of the anomalous masses that generate the disturbing potential but internal to the surface S. By Chasles' Theorem we know that it is possible to specify a surface density for this layer that will generate an exterior potential field identical to that generated by the original anomalous masses [Heiskanen and Moritz, 1967, p. 16; Ramsey, 1959, p. 110]. With this condition that the anomalous mass will be found as an equivalent layer on a specified equipotential surface, the determination of the required mass distribution, or the analytic definition of the harmonic function T resolves to the Dirichlet-Neuman Inverse Problem which is stated by Zidarov [1965] as "...the determination of a simple or double layer situated on a surface S lying inside a surface  $S_0$  at which the values of the potential or of its normal derivative due to this layer are known." It is important to note that the problem is now reduced to the determination of masses (differential elements of a layer) in pre-defined locations. Unfortunately, neither the anomalous potential, nor its normal derivative for a given surface are available from terrestrial gravity measurements. Rather, gravity measurements lead to the determination of gravity anomalies. From consideration of the spherical approximation of the basic equation of physical geodesy:

$$(2.5) \quad \Delta g = -\frac{\partial T}{\partial R} - \frac{2T}{R}$$

where:  $\partial T / \partial R$  = the radial (approximately the normal) derivative  
of T, and

$R$  = the mean radius of the earth,

we see that a gravity anomaly is a linear combination of the disturbing potential and its normal derivative. A solution of this equation to obtain an expression for  $T$  is sometimes called the third boundary value problem or the boundary value problem of physical geodesy [Heiskanen and Moritz, 1967, p. 37]. Stokes' Integral provides one method of determining the disturbing potential from gravity anomalies.

## 2.2 The Relationship Between Gravity Anomalies and Elemental Point Masses on an Equivalent Layer Surface

For purposes of deriving another solution for  $T$  by obtaining a defined equivalent anomalous mass distribution, consider a model earth such as shown in Figure 1.

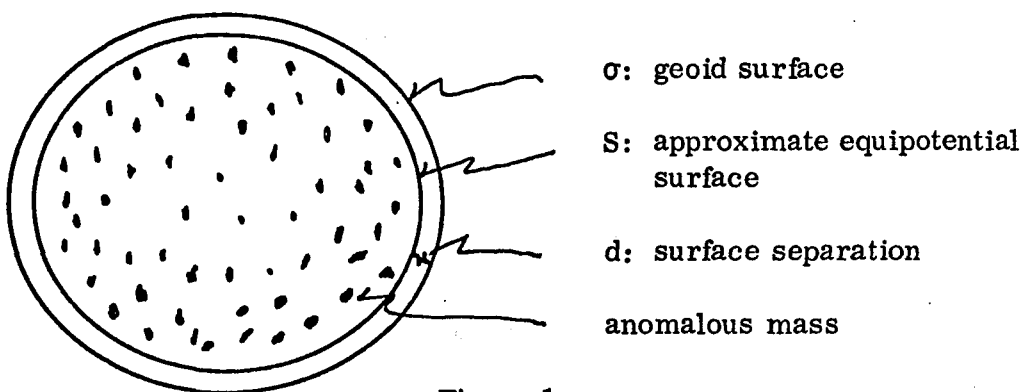


Figure 1

A Fictitious Model Earth

In this figure, the outer surface  $\sigma$  is the true geoid. We will approximate this figure by an ellipsoid thereby introducing, according to most geoid maps, a maximum error on the order of 100 meters in the geocentric radius of the

surface. The inner surface  $S$  encloses all anomalous masses and is separated from the surface  $\sigma$  by a constant distance  $d$ . This surface is not precisely an ellipsoid nor can it be shown that it is an equipotential surface. If, however, the distance  $d$  is kept small relative to the axes of the earth, it is reasonable to assume that this  $S$  surface is a close approximation to an equipotential surface. It is therefore a suitable surface upon which an equivalent density layer can be found that will generate the potential  $T$ .

To find this mass distribution from a consideration of gravity anomalies, we will base the solution on equation (2.5), but express the anomalous potential  $T$  and its normal derivative in terms of differential mass elements on the surface  $S$ . For computational purposes we will express the integration over the surface  $S$  as a summation of differential mass elements over that surface. Thus we express the potential  $T$  at any point  $P_i$  as:

$$(2.6) \quad T_{P_i} = \sum_j \frac{kM_j}{\ell_{ij}}$$

where:  $\ell_{ij}$  = the distance between point  $P_i$  and mass element  $M_j$ ;  
 $k$  = the gravitational constant ( $6.673 \times 10^{-8} \text{ cm}^3 \text{ g}^{-1} \text{ sec}^{-2}$ );  
 $M_j$  = the  $j^{\text{th}}$  mass element.

Figure 2 illustrates the relationship between a computation point  $P_i$ , a mass element  $M_j$ , and the coordinate systems used in the following derivations. The subscripts  $i$  indicate that a value pertains to a point on the geoid  $\sigma$  and the subscript  $j$  indicates a relationship with a mass element making up part of the surface  $S$ . For example,  $\vec{R}_i$  is the radius vector to the  $i^{\text{th}}$  point

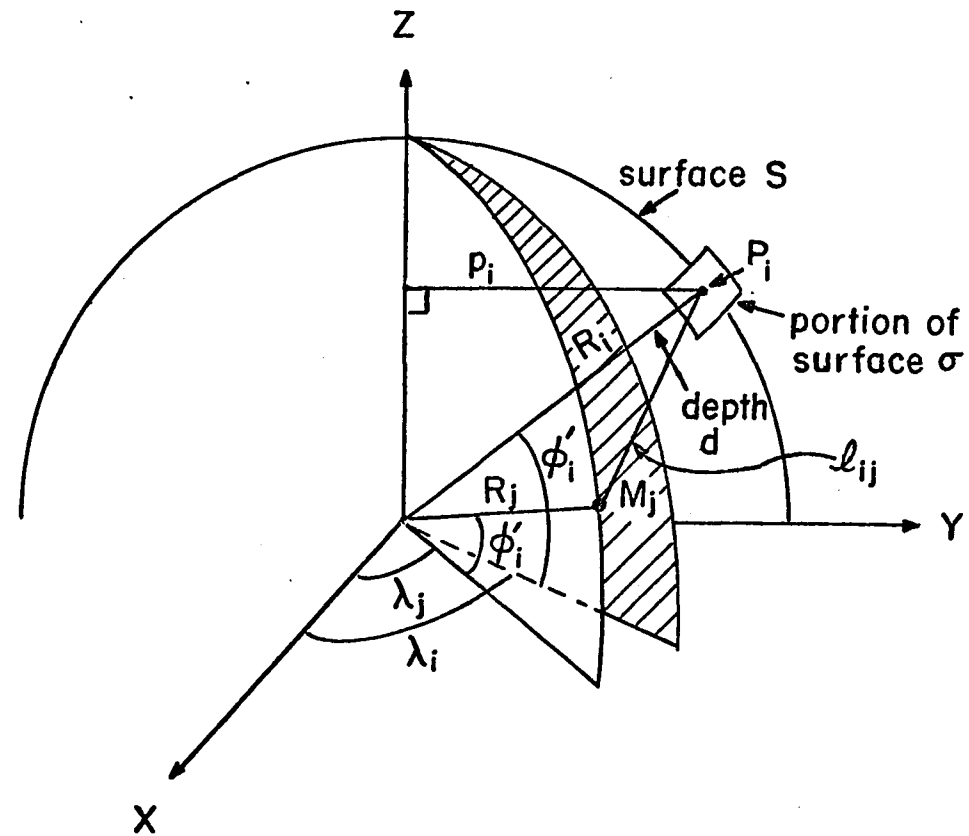


Figure 2

Notation of Point Mass Derivations

on the geoid;  $\vec{R}_j$  is the radius vector to the  $j^{\text{th}}$  mass element;  $\ell_{ij}$  is the distance between the  $i^{\text{th}}$  computation point and the  $j^{\text{th}}$  mass element. The general notation required in this and subsequent developments is as follows:

$X, Y, Z$  Geocentric Cartesian coordinates of a computation point or mass element. This system has the  $Z$  axis along the mean rotation axis of the earth, positive North, the  $X$  axis positive through the Greenwich Meridian, and is right handed.

$R$  Length of radius vector  $\vec{R}$  to a point or mass

$\ell_{ij}$  Distance between computation point  $i$  and mass element  $j$

$\varphi'$  Geocentric latitude

$\varphi$  Geodetic latitude

$\lambda$  Geodetic longitude (positive to East)

$F_{ij}$  Dot product  $\vec{R}_i \cdot \vec{R}_j$

$p$  Distance of a point from the rotational axis of the earth,  
i.e.  $p_i = (X_i^2 + Y_i^2)^{1/2}$

The following equations are listed for subsequent reference:

$$(2.7) \quad X_i = R_i \cos \varphi'_i \cos \lambda_i$$

$$(2.8) \quad Y_i = R_i \cos \varphi'_i \sin \lambda_i$$

$$(2.9) \quad Z_i = R_i \sin \varphi'_i$$

$$(2.10) \quad F_{ij} = X_i X_j + Y_i Y_j + Z_i Z_j$$

$$(2.11) \quad \ell_{ij} = ((X_i - X_j)^2 + (Y_i - Y_j)^2 + (Z_i - Z_j)^2)^{1/2}$$

Making the approximation that the radial derivative of the disturbing potential is the practical equivalent of the normal derivative, equation (2.6)

can be differentiated to find the gravity disturbance at the  $i^{\text{th}}$  computation point in terms of the  $j$  elemental masses on the  $S$  surface.

$$(2.12) \quad \frac{\partial T_i}{\partial R_i} = - \sum_j \frac{kM_j \frac{\partial \ell_{ij}}{\partial R_i}}{\ell_{ij}^2}$$

From differentiating (2.11) we obtain:

$$(2.13) \quad \frac{\partial \ell_{ij}}{\partial R_i} = \frac{1}{\ell_{ij}} \left( (X_i - X_j) \frac{dX_i}{dR_i} + (Y_i - Y_j) \frac{dY_i}{dR_i} + (Z_i - Z_j) \frac{dZ_i}{dR_i} \right)$$

Differentiating equations (2.7), (2.8), and (2.9), we obtain:

$$(2.14) \quad \frac{dX_i}{dR_i} = \frac{X_i}{R_i}$$

$$(2.15) \quad \frac{dY_i}{dR_i} = \frac{Y_i}{R_i}$$

$$(2.16) \quad \frac{dZ_i}{dR_i} = \frac{Z_i}{R_i}$$

Substituting equation (2.14), (2.15), and (2.16) into equation (2.13), simplifying and taking advantage of equation (2.10), one obtains:

$$(2.17) \quad \frac{d\ell_{ij}}{dR_i} = \frac{R_i^2 - F_{ij}}{\ell_{ij} R_i}$$

Inserting equation (2.17) into equation (2.12) yields the gravity disturbance:

$$(2.18) \quad \frac{\partial T_i}{\partial R_i} = - \sum_j kM_j \left( \frac{R_i^2 - F_{ij}}{\ell_{ij}^3 R_i} \right)$$

Equations (2.6) and (2.18) can then be substituted into equation (2.5) to give an expression connecting gravity anomalies on the geoid surface  $\sigma$  with mass elements on the equivalent layer surface  $S$ . This basic equation is:

$$(2.19) \Delta g_i = \sum_j \left( \frac{R_i^2 - F_{ij}}{\ell_{ij}^3 R_i} - \frac{2}{\ell_{ij} R_i} \right) k M_j$$

### 2.3 The Relationship Between a Point Mass Approximation and a Surface Integral Approximation

The development of equation (2.19) was based on equation (2.6) which replaced an integral over the equivalent mass layer surface with a summation of differential mass elements of that surface. Implicitly therefore the subscript  $j$  runs from 1 to infinity.

If any computational use is to be made of equation (2.19), the number of masses must be restricted to some finite number. When this is done, the differential mass element  $M_j$  must be redefined. If one specifies that the equivalent layer surface is to be divided into  $m$  "blocks" of the same area, two obvious interpretations of  $M_j$  arise. One is that  $M_j$  is a dimensionless mass point situated at the center of the block that represents the mass in the portion of the equivalent layer included in that block. In this case, the equivalent layer is approximated by an evenly spaced grid of point masses on an otherwise empty surface. Equation (2.19) is unchanged, but the position of  $M_j$  is defined to be at the center of the block.

The second interpretation is that  $M_j$  consists of a uniform mass distribution over the equivalent layer within the block. That is:

$$(2.20) M_j = \rho_j dS_j \quad \text{or} \quad M_j = \rho_j \int_{dS_j} da$$

where  $\rho_j$  is the constant surface density on the surface element  $dS_j$ , and  $da$  is a differential area element of  $dS_j$ . If this interpretation is accepted, the

simplicity of equation (2.19) is destroyed and the relationship becomes:

$$(2.21) \quad \Delta g_1 = k \sum_{j=1}^m \rho_j \int dS_j \left( \frac{R_i^2 - F_{ij}}{\ell^3 R_i} - \frac{2}{\ell R_i} \right) da$$

where the integrations are carried out over each of the m blocks on the equivalent layer surface. Both of these interpretations must of course be considered as approximations. The mass making up the equivalent layer that satisfies Chasles' Theorem does not consist of discrete points or plates of constant surface density, but is rather a continuously varying function on that surface [Ramsey, 1965, p. 110].

The second interpretation as expressed by equation (2.21) is obviously the theoretically better of the two approximations. It is in fact an approximation only in so far that the density is considered constant in some small area. As m increases to infinity and  $dS_j$  decreases to  $da$ , equation (2.21) becomes exact. It is therefore appropriate to compare equation (2.19) to equation (2.21) to determine the errors that will arise from use of the more computationally practicable point mass concept.

The analytical evaluation of equation (2.21) would involve a difficult if not impossible integration over a nearly ellipsoidal surface. Fortunately, for the purposes of comparing equations (2.19) and (2.21), this problem can be avoided. The equivalency of the two equations is evident if the distance between the computation point and mass area is large with respect to the dimensions of the represented area on the equivalent layer surface. Equations (2.19) and (2.21) are identical if the kernel of equation (2.21) is effec-

tively constant over the element  $dS_j$ . We need consider then, only that area on the equivalent layer surface which is near the gravity anomaly observation point. This area can be treated as a plane making the computations much more tractible. We will therefore reformulate equations (2.19) and (2.21) in a planar approximation and evaluate the equivalency of the point mass and integrated block coefficients for different layer depths and different block positions with respect to the anomaly point. The geometry of this approximation is shown in Figure 3.

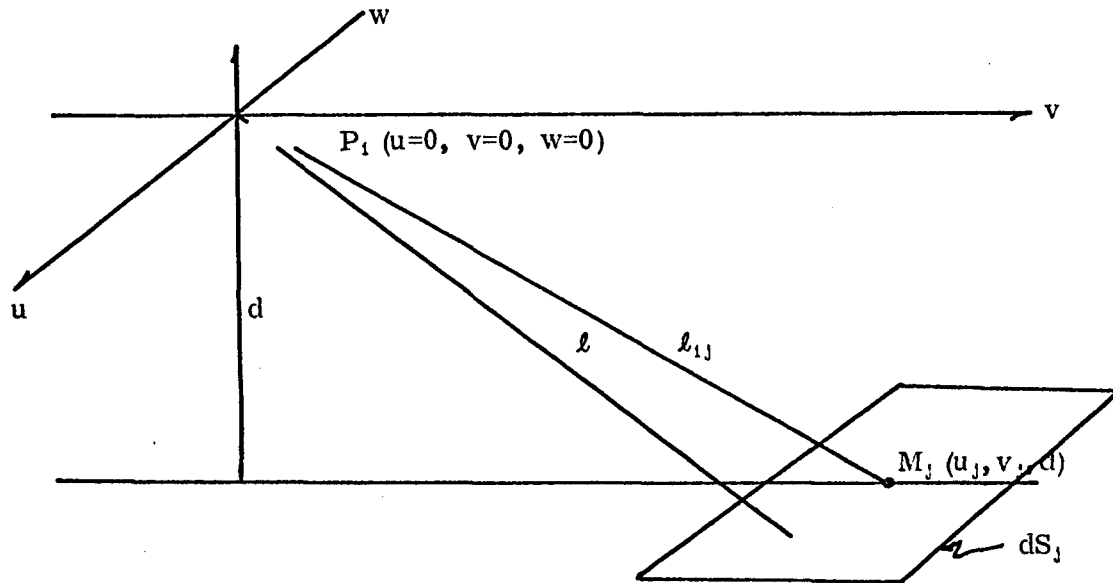


Figure 3

#### Geometry of the Planar Approximation

In this geometry and with a constant surface density  $\rho_j$ , the potential at  $P_1$  from the density layer on  $dS_j$  is given by:

$$(2.22) \quad T_1 = k \rho_j \int_{dS_j} \frac{1}{\ell} da = k \rho_j \iint_{dS_j} \frac{1}{(u^2 + v^2 + w^2)^{1/2}} du dv$$

Differentiating (2.22) with respect to the normal direction  $w$  at  $P_1$ :

$$(2.23) \frac{\partial T_1}{\partial R} = -k \rho_j \iint_{dS_j} \frac{1}{(u^2 + v^2 + w^2)^{3/2}} dudv$$

Inserting equations (2.22) and (2.23) into the basic equation (2.5), one obtains the planar form for integrated coefficients corresponding to the kernel of equation (2.21):

$$(2.24) k \rho_j \iint_{dS_j} \left( \frac{w}{(u^2 + v^2 + w^2)^{3/2}} - \frac{2}{(u^2 + v^2 + w^2)^{1/2}} R_1 \right) dudv$$

The planar approximation of the point mass equation consists merely of specializing equation (2.24) so that  $u = u_j$ ,  $v = v_j$  where  $(u_j, v_j, d)$  are the coordinates of the center of  $dS_j$  and the mass  $M_j$  is identified as equal to  $\rho_j \iint_{dS_j} dudv$ . If for purposes of comparison, the values of  $k$ ,  $\rho_j$ , and  $dS_j$  are specified as unity, the comparison may be carried out between the kernels  $K_{INT}$  and  $K_{PM}$  representing the surface integral and point mass assumptions respectively.

$$(2.25) K_{INT} = \iint_{dS_j} \frac{d}{(u^2 + v^2 + d^2)^{3/2}} - \frac{2}{(u^2 + v^2 + d^2)^{1/2}} R_1 dudv$$

$$(2.26) K_{PM} = \frac{d}{(u_j^2 + v_j^2 + d^2)^{3/2}} - \frac{2}{(u_j^2 + v_j^2 + d^2)^{1/2}} R_1$$

The  $K_{INT}$  kernel, (2.25), can be integrated with difficulty yielding an unwieldy expression. See for example Hirvonen and Moritz [1963, p. 73] and Nagy [1966]. To compare the integrated kernel with the point mass kernel for this investigation, a numerical integration was used in which the sur-

face regions  $dS_j$  were divided into 100 elements.

If we restrict consideration to square elements on the surface, it is possible to describe the geometry required for this comparative investigation in terms of only two variables: the depth  $d$  of the equivalent layer surface beneath the computation point and the lateral distance  $s$ , measured horizontally, from the computation point to the center of the block in question. If both of these variables are expressed in units of the length of a block side, the interrelationship between the kernels and element spacing and depth is made more apparent. Table 1 shows a comparison of the integrated ( $K_{INT}$ ) and point mass kernels ( $K_{PM}$ ) as determined by equations (2.25) and (2.26), for three different depth/side ratios and five lateral distances. In these comparisons,  $R_i$  was taken as 63.8 block side lengths. Similar tests for  $R_i$  equal to 638.0 block side lengths lead to comparable results.

Table 1

General Comparison of Integrated and Point Mass Kernels

Lateral Distance Between Point and Block	Depth of Mass Layer In Units of Block Sides					
	$d = 0.8$		$d = 1.0$		$d = 2.0$	
$s = 0$	$K_{INT}$ 1.106	$K_{PM}$ 1.523	$K_{INT}$ .778	$K_{PM}$ .969	$K_{INT}$ .220	$K_{PM}$ .234
$s = 1$	.379	.356	.338	.331	.161	.165
$s = 2$	.070	.065	.080	.075	.078	.077
$s = 3$	.018	.017	.023	.022	.035	.034
$s = 4$	.004	.004	.007	.007	.016	.015

It is apparent that the two kernels are in close agreement except when consid-

ering relatively shallow blocks directly under the computation point. Supplemental computations were therefore made to investigate the variation with depth for blocks directly under the computation point (Table 2), and the variation with small lateral distances for  $d = 0.8$  (Table 3).

Table 2

Comparison of Integrated and Point Mass Kernels  
For Blocks Directly Under Computation Point ( $s = 0$ )

Kernel	Depth of Mass Layer in Units of Block Sides						
	.8	1.0	1.2	1.4	1.6	1.8	2.0
K <sub>INT</sub>	1.106	.778	.570	.432	.338	.270	.220
K <sub>P.M.</sub>	1.523	.969	.668	.488	.371	.291	.234

Tables 2 and 3 show that the agreement between the integrated kernels and the point mass kernels improve rapidly as either the vertical distance or the horizontal distance between the computation point and the block center increases. For a given computation point  $P_1$  at which  $\Delta g_1$  is related to  $m$  mass points  $M_j$  in the sense of equation (2.19), an absolute maximum of two mass points could lie within the interval,  $0 < s < 0.5$ , if we restrict the mass points and computation points to square arrays. For the worst case considered,  $d = 0.8$ , the relative spacing of the mass points and the mean anomaly block centers for the computations performed in this study is such that just one mass point could lie in this interval for a given computation point. Only a small fraction of the mass point coefficients could thus differ from the integrated coefficients by more than a few percent. From this

analysis, I conclude that equation (2.19) in its point mass interpretation is a satisfactory approximation of the more rigorous equation (2.21) if a depth/side ratio of at least 0.8 is maintained. As such, it is an appropriate tool to use under the previously outlined assumptions in defining a discrete point mass distribution that approximates an equivalent layer. To illustrate the basic use

Table 3

Comparison of Integrated and Point Mass Kernels  
at Different Lateral Distances for Shallow Depths ( $d = 0.8$ )

<u>Lateral Distance Between Point and Block Center</u>	$K_{INT}$	$K_{PM}$
$s = 0.00$	1.106	1.523
$s = 0.25$	1.027	1.321
$s = 0.50$	.823	.920
$s = 0.75$	.580	.578
$s = 1.00$	.379	.356

of equation (2.19) for this purpose, consider a series of equations representing  $n$  points of observation of anomalous gravity. These equations may be written in matrix form as:

$$(2.27) \quad G = AM$$

where  $G$  is an  $n \times 1$  vector of gravity anomalies,  $M$  is an  $m \times 1$  vector of point masses, and  $A$  is an  $n \times m$  matrix of the point mass kernels. If  $n$  is equal to  $m$ , this system can be solved directly for the  $m$  point masses. If  $n$  is greater than  $m$ , recourse may be made to standard least squares procedures to find a solution for  $M$ .

## 2.4 The Point Mass Model as a Representation of a Smoothed Geopotential Field

The preceding discussion of the possibility of defining a set of anomalous masses approximating an equivalent layer presupposed an earth such as is shown in Figure 1 containing no anomalous masses outside of the equivalent layers. Such an earth model could not exhibit the same short wavelength variations in the gravitational field on the geoid as a model that allowed anomalous masses between the geoid and the equivalent layer surface. There is ample evidence that many of the fluctuations of the earth's gravitational and potential fields arise from structural features near the surface [Garland, 1965]. It is evident that, at best, an equivalent layer surface can only provide a model for a smoothed representation of the true fields. The technique of finding this mass distribution should therefore be oriented toward determining the best smoothed field rather than trying to recover irregularities which cannot even theoretically be modeled. A natural step toward this goal would be to use smoothed gravity anomalies as the input data to the solution. This can be done by using the area weighted mean of the gravity anomalies over some specified tesseral element of the geoidal surface to represent the gravity anomaly at the center of the element. By this process, the spectral components of gravity anomalies having a wavelength less than the side of the element are filtered out of the observations [McGinnis, 1970]. This procedure is routine in the practical evaluation of the integral formula of physical geodesy, as typified by Stokes' or Vening Meinez's functions. In

these numerical integrations, the gravitational field is invariably smoothed by using mean anomalies over some finite area. Upon reflection, it can be seen that this smoothing is closely related to an anomalous mass distribution of the type shown in Figure 1. Short wavelength variations in gravity, from the nature of the inverse square law of gravitation must result from density variations occurring near the surface of the earth. Filtering out the short wavelength anomaly changes by using mean anomalies is analogous to denying the existence of short wavelength, near surface, density variations.

A further smoothing of the field is the natural result of reducing the number of parameters used to describe the field. If this reduction in parameters, or mass points, is accompanied by a similar reduction in observations, there is no guarantee that the model field will be a smoothed representation of the real field but may be simply a fit to the observation points that deviates widely from the true field at uncontrolled intermediate points. Least squares procedures offer a method of securing an optimized fit of a smoothed geopotential field to the real field by minimizing the sum of squares of the differences between the two fields at all known points of the real field. Smoothing the model field by reducing the number of parameters within reasonable limits and increasing the density of observation points will both tend to insure against large discrepancies at any arbitrary position. This over-determination, or more explicitly, avoidance of over-parameterization is a standard safeguard when fitting data to an empirical model [Pugh and Winslow, 1966]. In the point mass case, it can be given a physical

meaning related to the model earth illustrated in Figure 1.

To illustrate, assume that a solution is sought for  $n$  point masses from  $n$  mean anomaly observations and furthermore, assume that several of the anomalies actually arise primarily from large anomalous masses near the anomaly points and well above the defined equivalent layer surface. A distribution of mass on the equivalent layer surface that would completely satisfy the observations could be found from the relationship:

$$(2.28) \quad M = A^{-1}G$$

where the  $A$  matrix was formed under the condition that all anomalous masses lay on the equivalent layer surface. Since the mathematical model is wrong, a false mass set would be forced into this surface that could be expected to generate an erroneous anomaly field at all points other than the original observation points. This field also would fail to generate the true potential field even at the observation points. The anomalous potential depends only on the distance from the anomalous masses and their magnitudes and not on the false mathematical model, the  $A$  matrix, that generated these masses.

If, however, there were redundant observations and a least squares adjustment were performed so that:

$$(2.29) \quad M = [A'A]^{-1} A'G$$

it would be found that no set of masses in the specified locations could exactly satisfy the observed anomalies. In essence, the adjustment would reject the components of the anomalies that were caused by anomalous masses above the equivalent layer surface and yield only a set of masses on that surface that

could generate some portion of the observed anomalies. The components of the anomalies that were actually caused by near surface anomalous masses would appear as residual differences between the solution model and the observed field. In effect, a further smoothing of the observed field would take place as a result of filtering out the influence of anomalous masses outside of the equivalent layer surface. Again, the over-determined least squares solution would contribute toward finding a model earth of the type shown in Figure 1.

The filtering effects mentioned in the preceding discussions would not be completely effective and the mass distribution found by the outlined procedures would not conform exactly to that of an earth smoothed according to the model shown in Figure 1. The mass distribution found in this manner and under these assumptions can only be considered as a basis for an approximate model of a smoothed geopotential or gravitational field. The intent of this discussion is simply to indicate that there is some rationale that makes it plausible to consider constructing an anomalous mass model of the earth where the mass points are arbitrarily fixed in a regular pattern at specified depth. Theoretical discussions of the degree of approximation that arises in this procedure could only be speculative since the errors that arise will be intimately connected with the unknown detailed mass distribution of the earth. Rather than construct questionable models that might be biased unconsciously toward the method of solution used, this investigation will use real data to compare geopotential functions derived through the point mass concept with

similar functions obtained through more traditional methods. This comparison will be deferred to Chapter 8.

## 2.5 Practical Consequences of the Geometry of the Point Mass Solution

Several criteria for developing a point mass representation of an equivalent layer have been implied during the preceding discussion that interrelate to set bounds on the various parameters of a point mass solution. For example, a ratio of at least 0.8 between the mass depth and mass spacing is desirable; the mass depth should be shallow and the masses should be closely spaced to obtain maximum detail. At the same time, the mass unknowns should be over-determined by observed mean anomalies. These guidelines allow some more specific interpretation of the previous generalized discussion and lead to some further conclusions about the nature of a point mass solution.

If the entire earth were considered in the solution under the assumptions of  $d = 100$  kilometers and depth/side ratio of 0.8, then some 32,000 point masses would be required to represent the anomalous mass distribution of the earth. This, in turn, would require a minimum of 32,000 mean gravity anomaly observations evenly dispersed over the earth. The lack of such a set of observations and the obvious computation difficulties of solving for 32,000 unknowns make a worldwide solution impracticable. Such a solution is not a goal of this investigation, which is rather directed toward the determination of detailed potential fields over restricted areas. Chapters 5 and 6 will return

to the possibilities of adequately describing a localized field by sets of masses of less than worldwide extent. It is appropriate at this point, however, to note the rapid decrease in the values of the coefficients relating anomalies and masses in equation (2.19) as the distance between an anomaly computation point and the masses increase. As can be seen from Table 1, a shallow mass (depth/side ratio = 0.8) more than 3 or 4 masses from the computation point has practically no effect on the anomaly at that point. A point mass and a gravity anomaly separated by such a distance are therefore essentially unrelated and the anomaly could not contribute significantly to a solution for the mass point. This has both advantages and disadvantages in practical applications. Favorably, it means that an isolated point mass array can be found from a set of anomaly observations covering an area only slightly larger than the array desired. If point masses are fitted under a limited area of anomaly observations, the point mass magnitudes near the edge will be slightly distorted because of an edge effect but the central array, more than 3 or 4 rows of masses from the edge, will be the equivalent of the masses that would have been found from a simultaneous solution covering a much larger area. This conclusion is intuitive from a consideration of the coefficients given in Tables 1 through 3. Numerical examples of computations illustrating the validity of the conclusion will, however, be given in Chapter 5. This fact that point masses are determined primarily by the immediate gravity field is an essential element of the concept of using point masses to determine detailed local potential fields.

A less desirable consequence of the independence of point masses and distant anomalies is the result that a point mass cannot be well determined if there are no gravity anomaly observations in the immediate vicinity of the point mass. Limited experimentation indicates that obviously aberrant results will be obtained if more than one contiguous mass point underlies an area lacking gravity anomaly observations. When a dense array of point masses at a shallow depth is desired to develop the maximum detail in the model potential field, the observed gravity anomaly field should be complete in the area of interest. Unobserved areas will naturally result in uncontrolled mass magnitudes. A transformation from a description of the field by means of gravity anomalies to a model based on point masses obviously cannot add real detail to the described field. The model field can be seriously distorted, however, by unrealistic mass values determined by weak solutions based on inadequate gravity anomaly information.

## CHAPTER 3

### THE SPHEROP 14 REFERENCE SYSTEM

The concept of a reference surface and associated normal gravity field based on a set of spherical harmonic potential coefficients was introduced in Chapter 1. This concept will be used in the point mass investigations to obtain the most effective use of localized gravity anomaly information. In this study we will refer to spherop reference surfaces, spherop normal gravity fields, and spherop gravity anomalies to distinguish the elements of such a system from those of the more familiar ellipsoidal reference system.

The spherop normal gravity field used in this investigation is the field determined by the kM and equatorial radius specified for the Geodetic Reference System of 1967 and by a specific 14th degree and order set of spherical harmonic coefficients developed by Rapp [1969]. These coefficients, which are discussed in Chapter 6, will hereafter be designated as Rapp's (14, 14) coefficient set. The spherop reference surface based on these coefficients will be identified as Spherop 14 to indicate the order and degree of the coefficient set used in the definition. This surface is an undulating surface which is defined to have a normal potential equal to that asso-

ciated with the GRS 67 ellipsoid. It holds a meaning in the spherop system that is analogous in many respects to the ellipsoid in the GRS 67 but does not replace the ellipsoid. An ellipsoid is retained for computational convenience. As will subsequently be seen, the elements of the Spherop 14 system are described as perturbations to the GRS 67 system.

A spherop gravity anomaly is defined as the difference between a gravity measurement, reduced to the geoid, and the spherop normal gravity at the corresponding point on the spherop reference surface.

The mechanics of defining the spherop reference surface are based on a spherical harmonic representation of the potential field of the form:

$$(3.1) \quad U_S = \frac{kM}{r} \left[ 1 + \sum_{n=2}^{\infty} \left( \frac{a_e}{r} \right)^n \sum_{m=0}^n (\bar{C}_{nm} \cos m\lambda + \bar{S}_{nm} \sin m\lambda) \cdot \bar{P}_{nm}(\sin \varphi') \right] + 1/2 \omega^2 r^2 \cos^2 \varphi'$$

In this notation:

- $U_S$  = Normal potential
- $kM$  = Newton's gravitational constant times the mass of the earth (specified by GRS 67)
- $a_e$  = Equatorial radius of earth (specified by GRS 67)
- $r$  = Geocentric radius to point of computation
- $\omega$  = Rate of rotation of the earth
- $\varphi'$  = Geocentric latitude of computation point
- $\lambda$  = Geocentric longitude of computation point

$\bar{C}_{nm}\bar{S}_{nm}$  = Fully normalized dimensionless spherical harmonic coefficients

$\bar{P}_{nm}(\sin\varphi')$  = Fully normalized associated Legendre functions:

$$= \left( (2-\delta)(2n+1) \frac{(n-m)!}{(n+m)!} \right)^{1/2} 2^{-n} \cos^m \varphi' \sum_{i=0}^k (-1)^i$$

$$\cdot \frac{(2n-2i)!(\sin\varphi')^{n-m-2i}}{i!(n-i)!(n-m-2i)!}$$

where:  $\delta = 1$  if  $m = 0$

$\delta = 0$  if  $m \neq 0$

$k$  = integer part of  $\frac{n-m}{2}$

One set of orthogonal components of the gravity field can be obtained by differentiating this function with respect to length units in the geocentric coordinate system of equation (3.1). These components are:

$$(3.2) \quad \gamma_r = \frac{\partial U}{\partial r}; \quad \gamma_\varphi' = \frac{1}{r} \frac{\partial U}{\partial \varphi}; \quad \gamma_\lambda = \frac{1}{r \cos \varphi} \frac{\partial U}{\partial \lambda}$$

or:

$$(3.3) \quad \gamma_r = -\frac{kM}{r^2} \left[ 1 + \sum_{n=2}^{\infty} (n+1) \left( \frac{ae}{r} \right)^n \sum_{m=0}^n (\bar{C}_{nm} \cos m\lambda + \bar{S}_{nm} \sin m\lambda) \right]$$

$$+ \bar{S}_{nm} \sin m\lambda) \frac{\partial \bar{P}_{nm}(\sin\varphi')}{\partial \varphi} + \omega^2 r \cos^2 \varphi'$$

$$(3.4) \quad \gamma_\varphi' = \frac{kM}{r^2} \sum_{n=2}^{\infty} \left( \frac{ae}{r} \right)^n \sum_{m=0}^n (\bar{C}_{nm} \cos m\lambda + \bar{S}_{nm} \sin m\lambda) \frac{d\bar{P}_{nm}(\sin\varphi')}{d\varphi}$$

$$- \omega^2 r^2 \sin \varphi' \cos \varphi'$$

$$(3.5) \quad \gamma_\lambda = \frac{-kM}{r^2 \cos \varphi} \sum_{n=2}^{\infty} \left( \frac{ae}{r} \right)^n \sum_{m=0}^n m(\bar{C}_{nm} \sin m\lambda - \bar{S}_{nm} \cos m\lambda) \frac{\partial \bar{P}_{nm}(\sin\varphi')}{\partial \lambda}$$

These equations are most conveniently evaluated using recursive relationships [Obenson, 1970]. Splitting the fully normalized associated Legendre function into a conventional Legendre function and a normalizing factor, the following relationships may be used.

$$(3.6) \quad \bar{P}_{nm} = Q_{nm} P_{nm}$$

$$(3.7) \quad Q_{nm} = \left[ (2-\delta)(2n+1) \frac{(n-m)!}{(n+m)!} \right]^{1/2}$$

$$(3.8) \quad P_{n0} = \frac{2n-1}{n} \sin\varphi' P_{n-1,0} - \frac{n-1}{n} P_{n-2,0}$$

$$(3.9) \quad P_{nn} = (2n-1) \cos\varphi' P_{n-1,n-1}$$

$$(3.10) \quad P_{nm} = P_{n-2,m} + (2n-1) \cos\varphi' P_{n-1,m-1}$$

These relationships also furnish a convenient algorithm for deriving and computing the derivatives of  $P_{nm}$  with respect to  $\varphi'$  [Obenson, 1970].

$$(3.11) \quad \frac{dP_{n0}}{d\varphi'} = \frac{(2n-1)}{n} \left[ \sin\varphi' \frac{dP_{n-1,0}}{d\varphi'} + \cos\varphi' P_{n-1,0} \right] - \frac{n-1}{n} \frac{dP_{n-2,0}}{d\varphi'}$$

$$(3.12) \quad \frac{dP_{nn}}{d\varphi'} = (2n-1) \left[ \cos\varphi' \frac{dP_{n-1,n-1}}{d\varphi'} - \sin\varphi' P_{n-1,n-1} \right]$$

$$(3.13) \quad \frac{dP_{nm}}{d\varphi'} = \frac{dP_{n-2,m}}{d\varphi'} + (2n-1) \left[ \cos\varphi' \frac{dP_{n-1,m-1}}{d\varphi'} - \sin\varphi' P_{n-1,m-1} \right]$$

In the preceding equations:

$$P_{0,0} = 1 ; \quad P_{1,0} = \sin\varphi' \quad P_{1,1} = \cos\varphi'$$

$$\frac{dP_{0,0}}{d\varphi} = 0 ; \quad \frac{dP_{1,0}}{d\varphi} = \cos\varphi' ; \quad \frac{dP_{1,1}}{d\varphi} = -\sin\varphi'$$

$$P_{n-2,n} = 0 \text{ if } m > n-2 ; \quad \delta = 0 \text{ if } m \neq 0$$

$$\frac{dP_{n-2,n}}{d\varphi} = 0 \text{ if } m > n-2 ; \quad \delta = 1 \text{ if } m = 0$$

In addition,  $\cos m\lambda$  and  $\sin m\lambda$  can be computed recursively through the relations:

$$(3.14) \cos m\lambda = 2\cos\lambda \cos(m-1)\lambda - \cos(m-2)\lambda$$

$$(3.15) \sin m\lambda = 2\cos\lambda \sin(m-1)\lambda - \sin(m-2)\lambda$$

The orthogonal components  $\gamma_r$ ,  $\gamma_{\varphi}'$ , and  $\gamma_\lambda$  given by equations (3.3), (3.4), and (3.5) are vectors in a left-handed coordinate system with origin at the computation point, the  $X_1$  axis to the east along the prime vertical, the  $X_2$  axis to the north along the meridian, and the  $X_3$  axis upward along the radius vector from the mass center of the earth. Corresponding components in a similar coordinate system but based on the normal to the ellipsoid rather than the radius vector can be obtained by the rotation:

$$(3.16) \begin{bmatrix} \gamma_\lambda \\ \gamma_{\varphi} \\ \gamma_N \end{bmatrix} = \begin{bmatrix} 1 & 0 & 0 \\ 0 & \cos(\varphi' - \varphi) & \sin(\varphi' - \varphi) \\ 0 & -\sin(\varphi' - \varphi) & \cos(\varphi' - \varphi) \end{bmatrix} \begin{bmatrix} \gamma_\lambda \\ \gamma_{\varphi}' \\ \gamma_r \end{bmatrix}$$

The total gravity vector, normal to the spherop reference surface, is given by:

$$(3.17) \gamma_s = (\gamma_{\varphi}'^2 + \gamma_\lambda^2 + \gamma_N^2)^{1/2} \quad \text{or} \quad \gamma_s = (\gamma_\lambda^2 + \gamma_{\varphi}'^2 + \gamma_r^2)^{1/2}$$

The angles in the meridian and prime vertical directions between the normal to the spherop and the normal to the GRS-67 ellipsoid are given by:

$$(3.18) \xi_s = -\frac{\gamma_{\varphi}}{\gamma}$$

$$(3.19) \eta_s = -\frac{\gamma_\lambda}{\gamma}$$

In these equations,  $\xi_s$  and  $\eta_s$  have the same sense as the components per-

taining to astrogeodetic deflections [Mueller, 1969]. That is,  $\eta_s$  positive indicates that the spherop surface slopes downward with respect to the ellipsoid in the direction of increasing longitude and  $\xi_s$  positive indicates that the surface slopes downward with respect to increasing latitude.

The shape of the spherop is determined by considering the  $U_s$  field to be a perturbation of the GRS-67 potential field. The disturbance  $T_s$  is defined as:

$$(3.20) \quad T_s = U_s - U_{GRS}$$

The separation or undulation of the spherop reference surface with respect to the ellipsoid is then given by Bruns' Formula [Heiskanen and Moritz, 1967, p. 85]:

$$(3.21) \quad N_s = \frac{T_s}{\gamma}$$

For all reasonable spherical harmonic representations of the earth's potential field, the radius vector to the harmonic surface,  $r_s$ , can be determined by assuming  $N_s$  and the radius vector to be parallel so that:

$$(3.22) \quad r_s = r_{GRS} + N_s$$

The normal gravitation potential  $V$  ( $U$  less the centrifugal potential) of an equipotential ellipsoid of rotation is given by [Heiskanen and Moritz, 1967, p. 230]:

$$(3.23) \quad V = \frac{kM}{r} \left[ 1 - \sum_{n=1}^{\infty} J_{2n} \left( \frac{a_e}{r} \right)^{2n} P_{2n}(\sin \varphi') \right]$$

This expression is normally truncated at  $n = 2$  [Mueller, 1964, p. 357].

$J_{2n}$  is related to  $\bar{C}_{2n}$  by the relationship [Mueller, 1964, p. 186].

$$(3.24) \quad \bar{C}_{2n} = -\frac{J_{2n}}{Q_{2n,0}}$$

where  $Q$  is defined as in equation (3.7).

For a specific equipotential ellipsoid [Heiskanen and Moritz, 1967, p. 73]:

$$(3.25) \quad J_{2n} = (-1)^{n+1} \frac{3e^{2n}}{(2n+1)(2n+3)} \left( 1 - n - 5n \frac{J_2}{e^2} \right)$$

where  $e^2$  is the first eccentricity of the ellipsoid. Various formulations for computing  $J_2$  are available. See for examples Mueller [1964] and Heiskanen and Moritz [1967]. Kaula [1966] gives direct expressions for both  $J_2$  and  $J_4$  of the form:

$$(3.26) \quad J_2 = \frac{2}{3} f \left( 1 - \frac{1}{2} f \right) - \frac{1}{3} m \left( 1 - \frac{3}{2} m - \frac{2}{7} f \right) + \dots$$

$$(3.27) \quad J_4 = -\frac{4}{35} f (7f - 5m) + \dots$$

In these equations:

$$f = \frac{a_e - b}{a_e}$$

$$m = \frac{\omega^2 a_e}{g_e}$$

$b$  = semi-minor axis of the ellipsoid

$a_e$  = equatorial radius

$g_e$  = equatorial gravity

$\omega$  = mean angular rotation rate of the earth

Using equations (3.1), (3.7), (3.20), (3.23) and (3.24) a direct expression for

$T_s$  can be written as:

$$(3.28) \quad T_s = \frac{kM}{r} \sum_{n=2}^{\infty} \left( \frac{a_e}{r} \right)^n \sum_{m=0}^n (\bar{C}_{nm}^* \cos m\lambda + \bar{S}_{nm} \sin m\lambda) \bar{P}_{nm}(\sin \varphi')$$

where  $\bar{C}_{nm}^*$  denotes a set of coefficients where the  $\bar{C}_{no}^*$  terms are the differences between the original terms and the  $\bar{C}_{no}$  appropriate to a specified ellipsoid.

Making the approximations:

$$\gamma \approx kM/r^2$$

$$a_e/r \approx 1$$

$$r \approx R \text{ (mean radius = 6371 km)}$$

and substituting equation (3.28) into equation (3.21), we obtain:

$$(3.29) \quad N_s = 6371000 \sum_{n=2}^{\infty} \sum_{m=0}^n (\bar{C}_{nm}^* \cos m\lambda + \bar{S}_{nm} \sin m\lambda) \bar{P}_{nm}(\sin \varphi')$$

This value is substituted into equation (3.22) to obtain the value of  $r_s$  needed to evaluate equations (3.3), (3.4), and (3.5).

The equations in the preceding paragraphs suffice to define the separation between the spherop and the GRS 67 ellipsoid, the angular orientation of the surfaces in the meridian and prime vertical directions, and the value of spherop normal gravity.

An alternate approach to the determination of  $\gamma_s$  can be based on equation (3.28) and the spherical approximation of the basic equation of physical geodesy.

$$(3.30) \quad \Delta g = \frac{-\partial T}{\partial R} - \frac{2T}{R}$$

Differentiating equation (3.28) and substituting the values of  $\partial T/\partial R$  and  $T$  into equation (3.30), we obtain, after making approximations equivalent to those in equation (3.29):

$$(3.31) \quad \Delta g_S = \gamma \sum_{n=2}^{\infty} (n-1) \sum_{m=0}^n (\bar{C}_{nm}^* \cos m\lambda + \bar{S}_{nm} \sin m\lambda) \bar{P}_{nm}(\sin \varphi')$$

In practice, a single mean value such as 979.8 gals is used for  $\gamma$  [Rapp, 1967a].

The  $\Delta g_S$  computed from equation (3.31) can be interpreted as the difference between normal gravity on the ellipsoid, and gravity computed on the spherop. Therefore,  $\gamma_S$ , which in our definition is normal gravity on the spherop, is given by:

$$(3.32) \quad \gamma_S = \Delta g_S + \gamma_{GRS}$$

The defined parameters of the Geodetic Reference System of 1967 are [IAG, 1967]:

$$a_e = 6378160 \text{ meters}$$

$$J_2 = 10827 \times 10^{-7}$$

$$kM = 3.98603 \times 10^{20} \text{ cm}^3 \text{sec}^{-2}$$

The corresponding reciprocal flattening is 298.247167427. These values, together with the angular rotation rate of:

$$\omega = 7.2921151467 \times 10^{-5} \text{ rad sec}^{-1}$$

suffice to define  $\gamma_{GRS}$  [IAG, 1970].

$$(3.33) \quad \gamma_{GRS} = 978031.8 (1 + .0053024 \sin^2 \varphi - .0000059 \sin^2 2\varphi)$$

Equation (3.32) with (3.33) and (3.31) should yield the same result as equa-

tion (3.17) using the components from equations (3.3), (3.4), and (3.5).

Both sets of equations were used in an effort to verify the programs written to compute the components of the gravity field. Normal Spherop 14 gravity was computed for the centers of  $10^\circ \times 10^\circ$  areas covering the earth using the two formulations. The agreement between the two methods was excellent below  $\pm 45^\circ$  latitude with few discrepancies over .25 milligals. The vast majority in this area agreed within 0.1 milligal. Over the entire earth, the disagreement reached a maximum of 1.05 milligals. Only 2% of the discrepancies out of the 648 computed were over 1.0 milligals, and all were at  $65^\circ$  latitude or greater. No readily discernible pattern was evident except that the maximum absolute discrepancies were associated with sharp inflexions in the spherop occurring at high latitudes. Anomalies computed by the two methods were integrated over the earth to determine if  $\Delta g_s$  satisfied the relation:

$$(3.34) \int_{\sigma} \Delta g_s d\sigma = 0$$

and did not exhibit any zero order component. In these computations, the above integral was approximated by:

$$(3.35) \overline{\Delta g} = \frac{1}{4\pi} \sum_{n=1}^{648} \Delta g_s \cos \varphi d\varphi d\lambda$$

For the equation (3.17) method,  $\overline{\Delta g}$  was 0.06 milligals and for the equation (3.31) method,  $\overline{\Delta g}$  was 0.01 milligals. These values were accepted as reasonably equivalent and satisfactory fulfillments of equation (3.34) con-

sidering the approximations which have been previously outlined. It is probable that the discrepancies between the two computations arise from the approximation  $a_e/r \approx 1$ . This approximation becomes increasingly incorrect as the latitude increases toward the poles. This effect is compounded for the higher degree coefficients since the term enters the computation as  $(a_e/r)^n$ . If this inaccuracy is multiplied with a relatively large high order sub-sum of the spherical harmonic expansion, as might be expected near the inflexion points of the surface, then the larger discrepancies that were observed might be expected. The discrepancies noted at high latitudes were not important in this investigation since spherop anomaly computations were limited to latitudes below  $50^\circ$ .

Current literature contains many examples of the use of spherical harmonic expansions of the potential field of the earth for the determinations of geoidal undulations, deflections of the vertical, and gravity anomalies. In these applications mention is usually made of convergence problems in a series such as equation (3.1) when the point of interest is inside a sphere which just includes all attracting masses [Rapp, 1968a]. If the earth were a perfectly homogeneous ellipsoid, equation (3.1) would converge down to a sphere whose diameter is defined by the foci of the meridian, i.e., the potential expansion would be valid well below the surface of the earth [Morrison, 1969]. The earth does not have this property of homogeneity, however, and the series must be considered formally divergent at or near the terrestrial surface [Heiskanen and Moritz, 1967; Mueller, 1964, p. 368]. This defect is more

theoretical than actual in the usual applications since the series are truncated to yield smoothed approximations of the true functions. Groten [1968] considers the errors irrelevant for the order of coefficients derived currently from satellite studies. Levallois [1969] has stated that the potential field derived from satellites can be continued to the earth level and that it is possible to extend the series to about hundredth order. He further states that, "The so obtained geoid cannot differ by more than a few meters from the correct one." On the basis of Groten's and Levallois' studies, it seems justified to use a (14,14) spherical harmonic expansion to define a reference surface approximating a smoothed geoid. Morrison [1969] raises the possibility that even though a function may be well approximated by a truncated series, its derivatives may not be approximated by the series obtained through termwise differentiation. For example, the potential or potential disturbance might be adequately approximated by a truncated series, but the components of the gravity vector or the gravity disturbance vector might not be obtainable with comparable precision by differentiating the original series.

For a meaningful reference equipotential surface, it is essential that the derivatives of the potential be well defined on the described surface. A check was therefore made to insure that the derivatives used in equations (3.3), (3.4), and (3.5) were consistent with the shape of the reference surface. Five areas were selected spaced over the globe. These were:

	$\phi$	$\lambda$
1) The Icelandic High	$65^\circ$	$345^\circ$
2) The South Atlantic High	$-50^\circ$	$358^\circ$

3) Mid United States	$35^\circ$	$260^\circ$
4) Bahama Low	$25^\circ$	$290^\circ$
5) Java Slope	$0^\circ$	$100^\circ$

These areas provided a varied sample of geoidal features, latitudes and longitudes. In each area undulation profiles were run along meridians and parallels. The deflection components in the direction of the profile were computed from spherical harmonic series at points spaced about 10 kilometers apart along the profile. These components were compared with the actual slopes of the profiles obtained through the numerical differentiation of the geoid height (from equation (3.29)) using the equations:

$$(3.36) \quad \eta_i = -\frac{1}{2} \left( \frac{N_{i-1}-N_i}{R_i \cos \varphi_i (\lambda_{i-1}-\lambda_i)} + \frac{N_i-N_{i+1}}{R_i \cos \varphi_i (\lambda_i-\lambda_{i+1})} \right)$$

$$(3.37) \quad \xi_i = -\frac{1}{2} \left( \frac{N_{i-1}-N_i}{R_i(\varphi_{i+1}-\varphi_i)} + \frac{N_i-N_{i+1}}{R_i(\varphi_i-\varphi_{i+1})} \right)$$

Both the geoidal heights and  $\frac{1}{2}$   $\left( \frac{N_{i-1}-N_i}{R_i(\varphi_{i+1}-\varphi_i)} + \frac{N_i-N_{i+1}}{R_i(\varphi_i-\varphi_{i+1})} \right)$  were smoothly varying functions. In all cases the deflection components computed by differentiation of the potential function agreed with those computed by the numerical differentiation of the geoidal surface to within 0.1".

Rapp [1967] has reported one other test which has verified the legitimacy of defining an equipotential reference surface through the use of spherical harmonics. In the process of testing a computer program for geoid undulations using Stokes' equation, he introduced gravity anomalies computed according to equation (3.31). The resulting undulations were subsequently compared to undulations computed in the manner of equation (3.29). The dif-

ferences in the two computations were on the order of 0.1 to 0.3 meters and were considered insignificant in light of the precision of the computation.

On the basis of the preceding tests and discussions it seems safe to say that it is possible to define a reference surface and associated normal gravity function based on the parameters of a given ellipsoid and a set of spherical harmonic coefficients. In this sense, equation (3.17) is a normal gravity formula. Equations (3.18), (3.19), and (3.29) define the position and local orientation of the spherop reference surface with respect to the ellipsoid.

## CHAPTER 4

### ERRORS CAUSED BY USE OF LIMITED AREAS OF GRAVITY INFORMATION

#### 4.1 General

The lack of detailed gravity data over large portions of the earth's surface has traditionally been a limiting factor in the use of gravimetric methods for the computation of geoid heights and other indicators of disturbances in the normal gravitational field [Uotila, 1959]. Because of the absence of worldwide data, evaluations of surface integrals, such as Stokes' integral for the anomalous potential, have been truncated to include a limited area of known gravity data around the computation point. These integrals must in theory be extended over the entire earth and failure to do so results in an error that is a function of the generally unknown anomalies outside of the truncated integration cap. A similar situation exists when a point mass model is established from anomalies located in a limited area.

A number of investigators have studied the relationship between the radius of the integration cap and the error arising from the neglect of gravity anomalies outside of this inner zone [Cook, 1951; Molodenskii et al., 1962; Hirvonen & Moritz, 1963; deWitte, 1966a; Wong & Gore, 1969]. A rather elegant means of estimating the influence of distant zones on the potential field

that is based on a knowledge of the spherical harmonic expansion of the geo-potential field has evolved through these studies. Complete derivations of this method, sometimes called Molodenskii's method of computing the effect of remote zones, are given in the above cited references. In outline, the method is based on the Molodenskii coefficient  $Q_n$ , defined as:

$$(4.1) \quad Q_n = \int_{\psi_0}^{\pi} S(\cos\psi) P_n(\cos\psi) \sin\psi d\psi$$

where:

$$\begin{aligned} S(\cos\psi) &= \frac{1}{\sin\psi/2} - 3\cos\psi \ln\left(\sin\frac{\psi}{2} + \sin^2\frac{\psi}{2}\right) \\ &\quad - 6\sin\frac{\psi}{2} + 1 - 5\cos\psi \quad (\text{Stokes' coefficient}) \end{aligned}$$

$P_n(\cos\psi)$  = Legendre function

$\psi$  = central angle measured from computation point

$\psi_0$  = radial extent of integrated anomaly field

It can then be shown [Hirvonen and Moritz, 1963; deWitte, 1966a] that the error  $\Delta N_\psi$  in a computed undulation arising from truncation of the integration of Stokes' equation at  $\psi_0$  is equal to:

$$(4.2) \quad \Delta N_\psi = \frac{R}{2\gamma} \sum_{n=2}^{\infty} Q_n \Delta g_n$$

where  $\Delta g_n$  is the  $n^{\text{th}}$  order component in the development of anomalous gravity in spherical harmonics (ref: equation (3.31)):

$$(4.3) \quad \Delta g = \sum_{n=2}^{\infty} \Delta g_n$$

If expression (4.2) is squared and averaged over the earth, one obtains, after noting that the integral of two  $\Delta g_n$  of different order over the earth is zero:

$$(4.4) \quad \overline{\Delta N}_{\psi}^2 = \frac{R^2}{4\gamma^2} \sum_{n=2}^{\infty} Q_n^2 \overline{\Delta g}_n^2$$

In this expression,  $Q_n$  can be evaluated by direct integration [Molodenskii et al., 1962] or by numerical integration. Convenient formulae for the latter are given by Heiskanen and Moritz [1967, p. 262].

The  $\overline{\Delta g}_n^2$  appearing in expression (4.4) is the anomaly degree variance or the average square of the  $n^{\text{th}}$  degree term in expression (4.3). If an expression for  $\Delta g$  is given in the form of equation (3.31), then due to the orthogonality of spherical harmonic functions:

$$(4.5) \quad \overline{\Delta g}_n^2 = \gamma^2(n-1)^2 \sum_{m=0}^n (\overline{C_{nm}}^2 + \overline{S_{nm}}^2)$$

It should be noted that an exact evaluation of expressions such as (4.2) or (4.4) cannot be made since they require knowledge of  $\Delta g_n$  from  $n = 2$  to infinity. If such a knowledge existed, the problem of gravimetrically unknown areas would disappear. Our knowledge is deficient in that the high degree terms of  $\overline{\Delta g}_n^2$  are virtually unknown and the lower degree terms are known with an uncertainty that increases with the degree of the term. Expression (4.4) used with a reasonable set of  $\overline{\Delta g}_n^2$  can nevertheless give us a method of comparing the results of different integration cap radii and comparing the influence of dif-

ferent definitions of the reference surface based on a reasonable model of the earth's gravitational field.

#### 4.2 Comparison of Truncation Errors for Geoid Heights Computed with Respect to Ellipsoidal and Spherop Reference Surfaces

The anomaly degree variances used in this study are shown in Table 4 [Rapp, 1968b]. These degree variances were computed with reference to an ellipsoid with a reciprocal flattening of 298.25. They are derived from Rapp's (14,14) spherical harmonic coefficient set which is used in this study as a basis for Spherop 14. More specifically, a worldwide set of  $5^\circ \times 5^\circ$  mean free air anomalies, adjusted to be compatible with this coefficient set, were developed into a (30,30) spherical harmonic coefficient set by the summation formula [Rapp, 1968b]:

$$(4.6) \quad \left\{ \frac{\bar{C}_{nm}}{\bar{S}_{nm}} \right\} = \frac{1}{4\pi(n-1)\gamma} \iint \Delta g \bar{P}_{nm}(\sin\varphi') \begin{Bmatrix} \cos m\lambda \\ \sin m\lambda \end{Bmatrix} d\sigma$$

This coefficient set was used in equation (4.5) to obtain the degree variances. These degree variances are therefore completely compatible with the spherop reference surface described in Chapter 3 but theoretically contain more information on short wavelength anomalies than is given by Rapp's (14,14) coefficient set.

Anomaly degree variances with respect to the Spherop 14 reference surface can be computed in a similar fashion from equation (4.5). In this instance,  $\bar{C}_{nm}^*$  and  $\bar{S}_{nm}^*$  are formed by subtracting the coefficients defining the reference surface from the coefficients describing the anomaly field. Since these values are identical up through  $(n, m) = (14, 14)$ ,  $\bar{\Delta g}_n^2$  for  $n < 15$

Table 4

Anomaly Degree Variances According to Rapp  
(mgals<sup>2</sup>)

n	$\overline{\Delta g_n^2}$	n	$\overline{\Delta g_n^2}$	n	$\overline{\Delta g_n^2}$
2	7.1	11	3.3	21	2.5
3	30.4	12	4.5	22	4.2
4	16.2	13	4.4	23	4.0
5	12.3	14	5.6	24	3.4
6	14.5	15	3.8	25	3.7
7	9.4	16	4.1	26	3.0
8	6.7	17	3.3	27	2.5
9	5.3	18	3.7	28	3.3
10	6.7	19	4.2	29	3.4
		20	3.1	30	2.5

are zero. Since  $\overline{C_{nn}^*}$  and  $\overline{S_{nn}^*}$  for  $n \geq 15$  are assumed to be zero in the reference model, the values of  $\overline{\Delta g_n^2}$  for  $n \geq 15$  are identical to those given in Table 4.

These two sets of anomaly degree variances were then used in equation (4.4) to determine  $\overline{\Delta N_\psi}$ , the root mean square error in the undulation resulting from truncating the use of local gravity data at  $\psi_0$  instead of utilizing worldwide data. The results of these computations are shown in Table 5 and Figures 4 and 5. (Note the difference in vertical scale in these figures.)

It is immediately evident from Table 4 or Figures 4 and 5 that the use of the Spherop 14 reference surface in preference to an ellipsoid results in a dramatic reduction in  $\overline{\Delta N_\psi}$  for a specified truncation angle. It is furthermore evident that the reduction in  $\overline{\Delta N_\psi}$  is more rapid with increasing  $\psi_0$  for the Spherop 14 surface. For the ellipsoidal surface,  $\overline{\Delta N_\psi}$  decreases very slowly at larger  $\psi_0$ . In the next  $50^\circ$  past the region shown in Figure 4,  $\overline{\Delta N_\psi}$  decreases only by 1.3 meters to 8 meters at  $\psi_0 = 90^\circ$ .

Table 5

Root Mean Square Truncation Error  $\overline{\Delta N}_\psi$  (Meters)

Truncation Radius $\psi_0$ °	For Ellipsoidal Reference Surface	For Spherop 14 Reference Surface
0	28.11	2.45
1	26.98	1.61
2	25.84	.84
3	24.72	.43
4	23.64	.70
5	22.59	1.00
6	21.58	1.16
7	20.62	1.18
8	19.69	1.10
9	18.82	.98
10	18.00	.86
13	15.82	.58
16	14.06	.55
19	12.67	.55
22	11.58	.42
25	10.74	.28
28	10.12	.24
31	9.70	.19
34	9.45	.12
37	9.33	.07
40	9.32	.06

#### 4.3 The Effect of Neglected High Order Anomaly Degree Variances

The shape of the curve in Figure 5 raises some question as to the validity of the computation. It would appear from this curve that truncating the integration at  $3^\circ$  would be more accurate than any extension to less than  $\psi_0 = 22^\circ$ . It implies that the use of valid gravimetric data will increase the

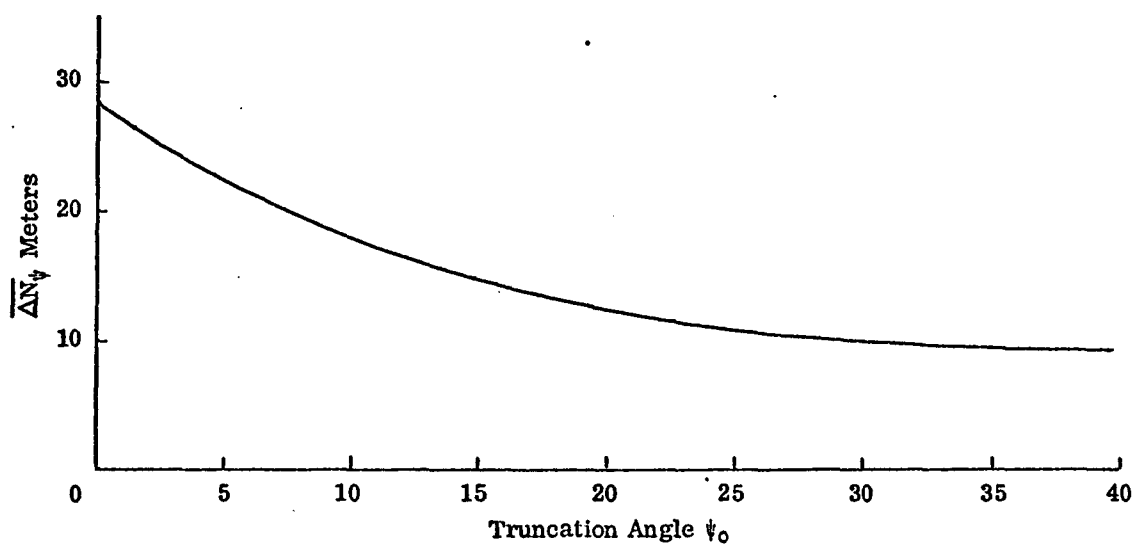


Figure 4

Undulation Error Due to Truncation of Anomaly Field  
Ellipsoidal Reference Surface  
(Degree variances used through  $n = 30$ )

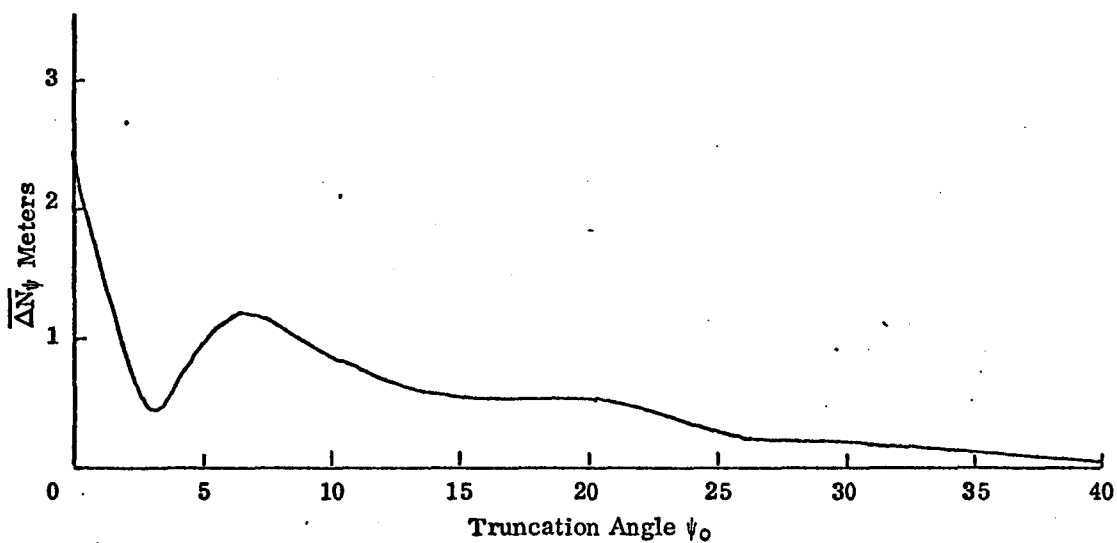


Figure 5

Undulation Error Due to Truncation of Anomaly Field  
Spherop 14 Reference Surface  
(Degree variances used through  $n = 30$ )

probability of error in the computation of an undulation.\* Intuitively this seems unreasonable. Several authors have published curves showing this characteristic [deWitte, 1966a; Wong and Gore, 1969; Hirvonen and Moritz, 1963]. Only Hirvonen and Moritz have commented on the phenomenon. They essentially reject the possibility of  $\overline{\Delta N}_\psi$  increasing with  $\psi_0$  and recommend "bridging" the dips empirically to obtain a continuously decreasing function. They tentatively suggested that the neglect of high order terms in equation (4.4) might be the cause of the dips. (The more limited data available at the time of their investigation restricted their summation to  $n = 8$ .) The complexity of the  $Q_n$  factors in equation (4.4) defies a ready visualization of the interaction of the components of different degree. It seems entirely possible, however, that the neglect of high order terms coupled with the suppression of terms in the range of 2 through 14 might cause the anomalous dip in the function. Data now available on the nature of higher order degree variances allow some speculative investigation of the reasonableness of Hirvonen and Moritz's suggestion.

Kaula has published degree variances data through  $n = 15$  [Kaula, 1967]; Kivioja's  $5^\circ \times 5^\circ$  mean anomaly data [1963] has been developed into degree variances through  $n = 36$  [Rapp, 1967a]; and Rapp has developed the set, through  $n = 30$ , given in Table 1.

---

\* It should be noted that truncation of the integrated gravity field may improve the accuracy of the computation if unknown constant errors occur in the gravity data. This is an entirely different problem which has been investigated in depth by deWitte [1966a].

Based on extrapolation of this data, various investigators have attempted to estimate the effect of the high degree portion of the anomaly field on undulation computation. On the assumption that  $\overline{\Delta g_n^2}$  is constant at 2.5 mgal<sup>2</sup> for  $n > 36$  (based on the Kivioja data), Rapp concludes that the error  $\delta \overline{\Delta N}$ , resulting from the neglect of  $\overline{\Delta g_n^2}$  above  $n$ , is given by [1967a]:

$$(4.7) \quad \delta \overline{\Delta N} = \left( \frac{105.69}{n-1} \right)^{1/2}$$

Wong and Gore [1967a] base an analysis on Kaula's rule that the variance of a fully normalized geopotential coefficients of degree  $n$  can be estimated by  $10^{-10}/n^4$  and derive that:

$$(4.8) \quad \delta \overline{\Delta N} < \left( \frac{ae^2}{10^{10}} \sum_{n=1}^{\infty} \frac{(2n+1)}{n^4} \right)^{1/2}$$

Pellinen and Demyanov, using Kaula's data to  $n = 15$ , derive an approximation [1969]:

$$(4.9) \quad \delta \overline{\Delta N} < \frac{R}{\gamma} \frac{\sqrt{60}}{n}$$

where  $R$  is the mean earth radius and  $\gamma$  the mean normal gravity.

Although the assumptions entering the derivation of the three preceding approximations are quite different, the three, when evaluated, are in reasonable agreement yielding the following approximations for the error incurred by the neglect of  $\overline{\Delta g_n^2}$  above  $n = 30$ :

<u>Approximation:</u>	<u><math>\delta \overline{\Delta N}</math>:</u>
Rapp	1.9 meters
Wong and Gore	< 2.2 meters
Pellinen and Demyanov	< 1.7 meters

Rapp	1.9 meters
Wong and Gore	< 2.2 meters
Pellinen and Demyanov	< 1.7 meters

The computations illustrated in Table 4 and Figures 4 and 5 neglect this error source. The error would be fully effective at  $\psi_0 = 0$  and should be quadratically summed with the  $\overline{\Delta N}$  values obtained through equation (4.4) evaluated at  $\psi_0 = 0$ . As  $\psi_0$  increases, the effect of the short wavelength variations in gravity anomalies will be incorporated into the computation through the inclusion of terrestrial data and the error in undulation from this source will diminish. Wong and Gore [1969] have estimated that  $\delta\overline{\Delta N}_\psi$  is less than 0.5 meters for  $\psi^o > 10^o$ . The total  $\overline{\Delta N}_\psi$  including the neglected higher order terms would then be given by:

$$(4.10) \text{ Total } \overline{\Delta N}_\psi = (\overline{\Delta N}_\psi^2 + \delta\overline{\Delta N}_\psi^2)^{1/2}$$

where:  $\delta\overline{\Delta N}_\psi \approx 2 \text{ meters at } \psi_0 = 0^o$   
 $\leq 0.5 \text{ meters at } \psi_0 = 10^o$

Under these conditions, the curve in Figure 4 is a very close approximation to the "Total  $\overline{\Delta N}_\psi$ " with respect to an ellipsoid since the large values for  $\overline{\Delta N}_\psi$  found with reference to an ellipsoid for  $n \leq 30$  would dominate the quadratic sum given by equation (4.10). The curve in Figure 5 would, however, be altered drastically for low values of  $\psi_0$  since the error derived from high degree variances would be a significant part of the total. This is precisely the "dip" area of the curve that Moritz advocated "bridging" to obtain a monotonically decreasing function. Simply to illustrate the possibility, a set of monotonically decreasing values of  $\delta\overline{\Delta N}_\psi = \left( \sum_{n=31}^{\infty} \overline{\Delta N}_\psi^2 \right)^{1/2}$  were arbitrarily selected that satisfied the estimated  $\psi_0 = 0$  and  $\psi_0 = 10^o$  values at  $\psi_0 = 0$  and  $\psi_0 = 10^o$  and that made "Total  $\overline{\Delta N}_\psi$ " in equation (4.10) a mono-

tonically decreasing function of  $\psi_0$ . These values are shown in Table 6 and the resulting Total  $\overline{\Delta N}_\psi$  curve in Figure 6.

Table 6

Hypothesised Undulation Computation Errors  
Due to Neglected High Order Terms  
(meters)

Integration Truncation Angle $\psi_0$	Due to Degree Variances Above $n = 30$ $\delta \overline{\Delta N}_\psi$	Total $\Delta N_\psi$ (14, 14) Reference Surface
0	2.00	3.16
1	1.90	2.48
2	1.85	2.03
3	1.80	1.84
4	1.70	1.84
5	1.54	1.84
6	1.42	1.84
7	1.40	1.83
8	1.20	1.70
9	.90	1.31
10	.50	.99

It is to be emphasized that these figures are purely arbitrary and were selected simply to show that conceivable values could exist for the influence of the high order degree variances that would make the shape of the  $\overline{\Delta N}_\psi$  curve more plausible. The values with the exception of the limiting values specified at  $\psi_0 = 0^\circ$  and  $\psi_0 = 10^\circ$  are of no consequence to the conclusions to be drawn from these computations.

An examination of Figure 6 shows that the use of terrestrial gravity data in a region with radius  $\psi_0$  of about  $13^\circ$  will result in an 80% reduction in the error of determining the undulation with respect to a Spherop 14 reference

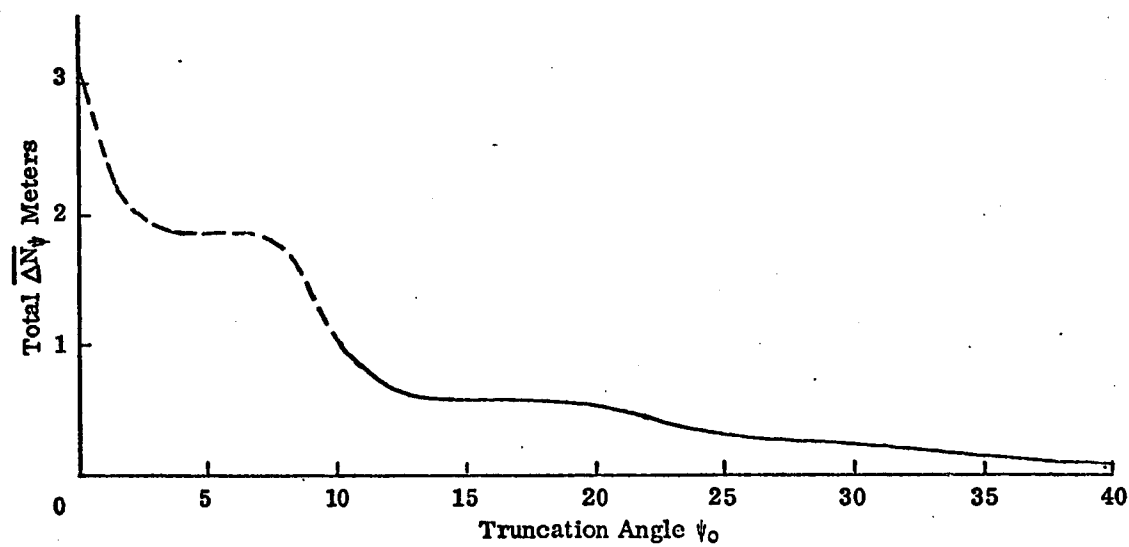


Figure 6

Total Undulation Error Due to Truncation of Anomaly Field  
Spherop 14 Reference Surface  
(Hypothetical Values in Region  $0 < \psi_0 < 10$ )

surface. The total error with respect to the reference surface is a relatively insignificant 0.6 meters which can be compared to a 15.8 meter error obtained if the computation is performed with respect to an ellipsoid ( $1/f = 298.25$ ) using the same  $\psi_0$ .

#### 4.4 The Effect of Discrepancies Between the Reference Model and the True Earth

The very favorable error elimination found in the preceding section occurs because we have assumed essentially that the reference figure is an exact representation of a comparably smoothed equipotential surface of the true geopotential. As a result, only the shorter wavelength components of the anomalous gravity (that is,  $\Delta g_n$ ,  $n > 14$ ) contribute to an undulation computation made with reference to this surface. It is unlikely, considering our present knowledge of the geopotential, that we will select a high order reference surface such that this situation prevails. It is therefore pertinent to consider how the preceding discussion is affected if the spherop reference surface is only a good approximation of a smoothed equipotential surface in the true geopotential field.

Let us retain our present definition of Spherop 14 based on Rapp's (14, 14) spherical harmonic coefficients. Let us assume, however, for purposes of defining a different gravity field, that each  $\bar{C}_{nn}$  and  $\bar{S}_{nn}$  for  $n < 15$  is changed by the standard deviation associated with that coefficient [see Appendix B]. Equation (4.5), after the reference figure coefficients were subtracted, would then become:

$$(4.11) \quad \overline{\Delta g_n^2} = \gamma^2(n-1)^2 \sum_{m=0}^n (\sigma_{C_{nm}}^2 + \sigma_{S_{nm}}^2)$$

for  $n = 2, 14$

These values are shown in Table 7.

Table 7

Anomaly Degree Variances for Altered Gravity Field  
Referred to Spherop 14

$n$	$\overline{\Delta g_n^2}$
2	.01
3	.08
4	.17
5	.35
6	.51
7	.97
8	1.27
9	1.72
10	1.99
11	2.05
12	2.26
13	1.99
14	1.91

The anomaly degree variances in Table 7 were combined with those for  $n > 15$  from Table 4 to provide a set of data representing a plausibly different gravity field. The computations for the Spherop 14 reference surface were then repeated using this data. The hypothesized contributions from  $\overline{\Delta g_n^2}$ ,  $n > 30$ , from Table 5 were added in accordance with equation (4.10). The results are shown in Figure 7.

The general conclusions from Figure 7 remain the same as from Figure 6. The error  $\overline{\Delta N_\psi}$  drops fairly rapidly at first as  $\psi_0$  is increased, but

the rate of improvement slows after  $\psi_0 = 10^\circ$ . For  $\psi_0 = 13^\circ$ , there is a 70% reduction in the root mean square error as compared to  $\psi_0 = 0$ . In this case, the influence of long wavelength anomalies emphasizes the importance of the more distant zones and the curve does not flatten as quickly. As was expected, the root mean square error is greater for all values of  $\psi_0$  when the reference figure is only an approximation of the true smoothed geoid. This example illustrates that the absolute error in geoidal undulation computation for a given integration radius is minimized by selecting a best fitting reference surface.

#### 4.5 Truncation Errors in the Computation of Gravitational Disturbance Components

Computations similar to those described in the preceding section can also be accomplished to analyze the effect of truncation on the determination of the components of gravitational disturbances.

The gravity disturbance at a point may be resolved into orthogonal components in the spherical coordinate system  $r$ ,  $\varphi'$ , and  $\lambda$  as [Heiskanen and Moritz, 1967, p. 233]:

$$(4.12) \quad \delta_r = \frac{\partial T}{\partial r}$$

$$(4.13) \quad \delta_{\varphi'} = \frac{\partial T}{\partial \varphi'}$$

$$(4.14) \quad \delta_\lambda = \frac{1}{r \cos \varphi'} \frac{\partial T}{\partial \lambda}$$

In a spherical approximation, these components can be related to gravity anomalies, deflections and undulations at a given point by the equations:

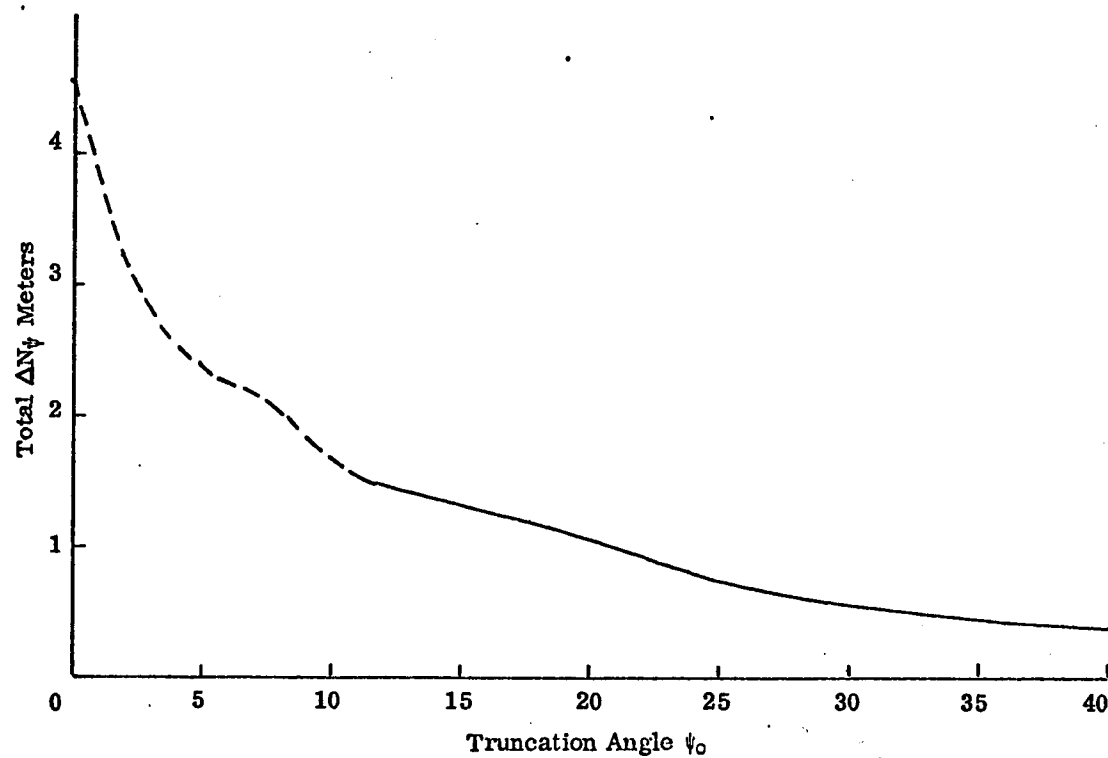


Figure 7

Total Undulation Error Due to Truncation of Anomaly Field  
Spherop 14 Reference Surface  
(Based on Altered Gravity Field)  
(Hypothetical Values in Region  $0 < \psi_0 < 10$ )

$$(4.15) \quad \delta_r = \Delta g + \frac{2\gamma}{R} N$$

$$(4.16) \quad \delta_\varphi' = -\gamma \xi$$

$$(4.17) \quad \delta_\lambda = -\gamma \eta$$

The anomaly  $\Delta g$  is a known quantity at the points of computation on the reference surface and  $n$ ,  $\xi$ , and  $\eta$  are subject to the errors  $\Delta N_\psi$ ,  $\Delta \xi_\psi$ , and  $\Delta \eta_\psi$  due to truncation of the area of integration at radius  $\psi_0$  so that the errors due to truncation may be expressed:

$$(4.18) \quad \Delta \delta_{r\psi} = \frac{2\gamma}{R} \Delta N_\psi$$

$$(4.19) \quad \Delta \delta_{\varphi'\psi} = -\gamma \Delta \xi_\psi$$

$$(4.20) \quad \Delta \delta_{\lambda\psi} = -\gamma \Delta \eta_\psi$$

Squaring and meaning over the earth, we obtain:

$$(4.21) \quad \overline{\Delta \delta_{r\psi}}^2 = \frac{4\gamma^2}{R^2} \overline{\Delta N_\psi}^2$$

$$(4.22) \quad \overline{\Delta \delta_{\varphi'\psi}}^2 = \gamma^2 \overline{\Delta \xi_\psi}^2$$

$$(4.23) \quad \overline{\Delta \delta_{\lambda\psi}}^2 = \gamma^2 \overline{\Delta \eta_\psi}^2$$

The expression for  $\overline{\Delta N_\psi}^2$  in terms of anomaly degree variances is given by equation (4.4). A similar expression for  $\overline{\Delta \xi_\psi}^2$  and  $\overline{\Delta \eta_\psi}^2$  is given by [Moritz and Hirvonen, 1963, p. 49]:

$$(4.24) \quad \overline{\Delta \xi_\psi}^2 = \overline{\Delta \eta}^2 = \frac{1}{8\gamma^2} \sum_{n=2}^{\alpha} n(n+1) Q_n^2 \overline{\Delta g_n}^2$$

The root mean square errors in gravity disturbance components are therefore given by:

$$(4.25) \quad \overline{\Delta \delta_{r\psi}} = \left( \sum_{n=2}^{\alpha} Q_n^2 \overline{\Delta g_n}^2 \right)^{1/2}$$

$$(4.26) \quad \overline{\Delta\delta}_{\varphi'} = \overline{\Delta\delta}_{\lambda\psi} = \left( \frac{1}{8} \sum_{n=2}^{\alpha} n(n+1) Q_n^2 \overline{\Delta g}_n^2 \right)^{1/2}$$

Equation (4.25) is the equivalent of:

$$(4.27) \quad \overline{\Delta\delta}_{r\psi} = .3086 \overline{\Delta N}_{\psi}$$

and can be evaluated under various assumptions from the tables and figures of the preceding sections.

Errors in the horizontal gravity components and deflections as functions of  $\psi_0$ , computed by equations (4.24) and (4.26) and truncated at  $n = 30$ , are shown in Figure 8. This composite figure shows the errors under the assumption of using a reference ellipsoid; a Spherop 14 reference surface that is an exact agreement with a completely smoothed geop and a reference surface, such as described in the preceding section, that is not an exact geopotential surface.

In these calculations, we must again assume that the neglect of high order anomaly degree variances has caused under-estimation of the errors associated with small truncation angles. Kaula has estimated the root mean square deflection of the vertical to be 6 seconds [1959]. This estimate was based on anomaly covariances and includes the effect of high order variations in the gravity field. For comparison to Figure 8, his estimate would correspond to a root mean square value of 4.2 seconds for a deflection component computed with respect to an ellipsoid at zero truncation angle. Kaula also did truncation error computations using his covariance data. The estimated errors shown on Figure 8 were consistently about 10 per cent higher

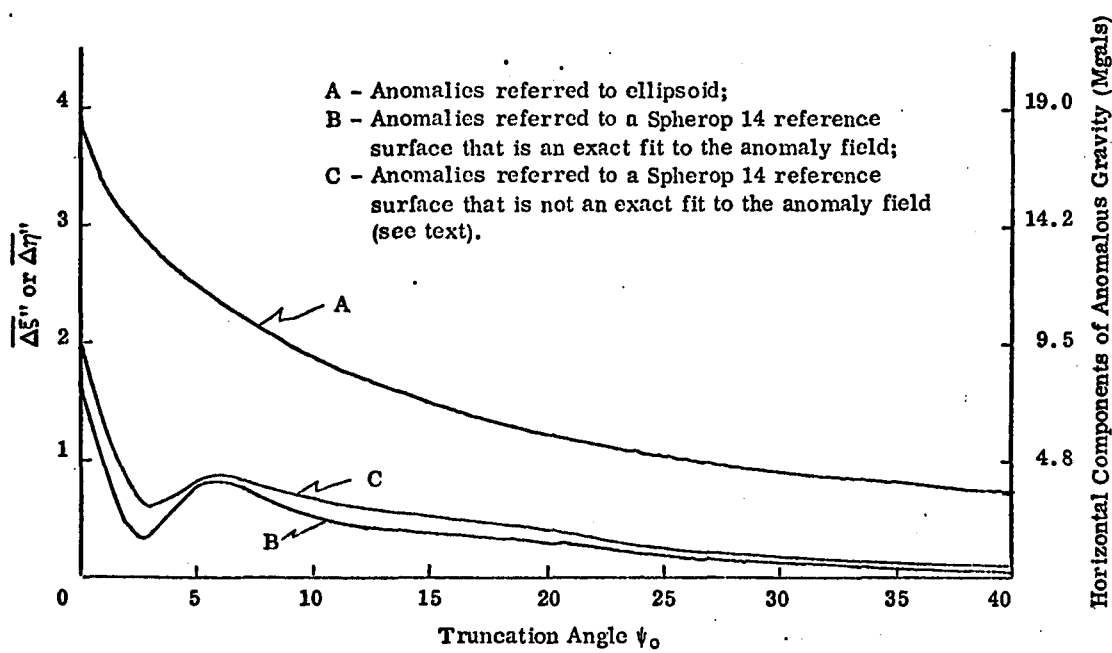


Figure 8

Errors in Deflections and Horizontal Components of Anomalous Gravity as a Function of the Truncation Angle  $\psi_0$

than Kaula's estimates except at truncation angles below about one degree. Kaula's computation shows the rapid increase in error that occurs when short wavelength variations in the anomaly field near the computation point are not considered. The effect of this neglect is suppressed in the truncated Moloden-skii type computation. If we assume the gravity data available for this current investigation is more reliable than the data available to Kaula in 1959, it would be appropriate to raise all of Kaula's error estimates by 10 per cent including the estimated error at zero truncation angle. The difference between the modified Kaula value and the value from equation (4.24), evaluated for the ellipsoid, provides the basis for a rough estimate based on decomposition of the total quadratic sum that the contribution of the neglected anomaly degree variances above  $n = 30$  is about 2 or 3 seconds for a zero truncation angle. This value could be summed quadratically with the  $\psi_0 = 0$  values on Figure 8 to obtain estimates of the total error under the different assumptions shown. Considering the relative rate of change of Stokes' function and Vening Meinesz's function [Heiskanen and Vening Meinesz, 1958, p. 81], one could expect the error due to high frequency anomaly variations to attenuate even more rapidly than the similar error discussed with relation to undulation computations. The errors for truncation angles greater than  $10^\circ$  are therefore probably realistic. For deflection computations, as in undulation computations, the use of a high order reference surface results in a very significant reduction in the errors arising from anomaly field truncation.

The fact that a high order reference surface permits the accurate

determination of a portion of the potential field from a localized field of gravity anomalies is one of the key factors making the concept of a point mass representation computationally feasible.

## CHAPTER 5

### THE COMPUTATION OF POINT MASS SETS

#### 5.1 General

This chapter will discuss the computer program and procedures used in determining point mass sets suitable for adding detail to spherical harmonic geopotential models. The procedures are based primarily on the discussions of Chapters 3 and 4, but also depend on certain collateral concepts and assumptions which will be developed in this chapter.

#### 5.2 Assumptions Regarding Data

In the following discussion we will assume that we have a set of spherical harmonic coefficients that are in agreement with our total knowledge of the gravity field of the earth. This assumption implies that this set of coefficients is the result of some method of adjustment that incorporates both satellite data and terrestrial gravity observations. Examples of such sets of coefficients are those of Kaula [1966], Rapp [1969b], and Gaposchkin and Lambeck [1970]. It is further assumed that the terrestrial gravity information used in the analysis, for example,  $5^\circ \times 5^\circ$  mean anomalies, can be traced backward to its origin, at least in general terms. This would imply that in areas of dense gravity coverage, it would be possible to specify a  $1^\circ \times 1^\circ$  mean anomaly field that could be combined to form the aforementioned  $5^\circ \times 5^\circ$  mean anomalies, a

$30^\circ \times 30^\circ$  field that is compatible with the  $1^\circ \times 1^\circ$  field and so forth down to the smallest mean element size justified by the observational density.

It is naturally assumed that the data entering into the adjustment has been properly weighted and that the mathematical model is correct so that an adjusted observation could be expected to be a closer estimate of the true value than was the original observation. This rather obvious remark is included for emphasis because it is a justification for certain modifications which will be made in the observed terrestrial gravity field.

### 5.3 Conditions Imposed on the Solution

The concept of adding localized detail to a model describing the geo-potential fields does not imply that we change the basic reference system that describes these fields. Rather we should impose conditions while developing this detail that will constrain the new model to be consistent with the parameters of the reference system.

Under the assumptions that we have properly weighted and utilized, all available observational data on the gravitational field to obtain a spherical harmonic coefficient set to a specified degree and order, we can assert that this set of coefficients is the best available set of descriptors of the geo-potential of that degree and order. If the degree and order are limited to (14, 14) for example, the described fields are heavily smoothed representations of the true fields. As such, one would expect the mean value of the true function and the mean value of the smoothed function over an area to approach a common value as the size of the area is increased. That is:

$$(5.1) \int_{\Delta S_1} F_{SH} ds \approx \int_{\Delta S_1} F_{TRUE} ds$$

where  $F_{SH}$  is an approximation expressed as a spherical harmonic series of the function  $F_{TRUE}$  evaluated on the spherical surface  $S$  and  $\Delta S_1$  is some portion of that surface. The expression  $F_{SH}$  is described by the  $(n+1)^2$  parameters making up the coefficients of the spherical harmonic series. The left side of equation (5.1) could therefore be approximated as a sum and rewritten as an expression in  $(n+1)^2$  unknowns. The right side is a single number for the integral of  $F_{TRUE}$  over  $\Delta S_1$ .

A solution for the  $(n+1)^2$  unknowns would therefore require a minimum of  $(n+1)^2$  discrete areas  $\Delta S_1$ . If the surface of the earth, taken as a unit sphere, is divided into this number of areas, then:

$$(5.2) \Delta S_1 = \frac{4\pi}{(n+1)^2}$$

If  $\Delta S_1$  is considered as a small tesseral element, then the sides subtend the central angle  $\Delta\theta$  where:

$$(5.3) \Delta\theta^\circ \approx \frac{203.1}{n+1}$$

By this argument a set of mean values defined as:

$$(5.4) \bar{F}_{TRUE} = \frac{1}{\Delta S_1} \int_{\Delta S_1} F_{TRUE} ds$$

where  $\Delta S_1$  has sides of  $\Delta\theta^\circ$  would suffice to determine the coefficients in the spherical harmonic expansion. Conversely one could expect that  $F_{SH}$  based on these coefficients would satisfy the relation:

$$(5.5) \quad \frac{1}{\Delta S_1} \int_{\Delta S_1} F_{SH} ds \approx \bar{F}_{TRUE}$$

Equation (5.2) therefore gives a minimum size to the area  $\Delta S_1$  where equation (5.1) could be expected to be valid. A conservative approach would be to apply the condition only to regions that were considerably greater than the area given by equation (5.2).

Rapp [1967a] uses a practically identical argument to propose that

$$(5.6) \quad F_{SH_1} \approx \frac{1}{\Delta S_1} \int_{\Delta S_1} F_{TRUE} ds$$

where  $F_{SH_1}$  is evaluated at the center of the block  $\Delta S_1$ . This would agree with my argument if:

$$(5.7) \quad F_{SH_1} \approx \frac{1}{\Delta S_1} \int_{\Delta S_1} F_{SH} ds$$

It is interesting to note that the validity of approximation (5.7) would increase as  $\Delta S_1$  decreased while the validity of approximations (5.1) and (5.5) would increase with the size of  $\Delta S_1$ .

Let us now return to equation (5.1) and specialize the preceding general discussion. Consider that  $F_{SH}$  in the left member is the expression for the anomalous potential of the form of equation (3.28) of degree and order 14 which forms the basis for our Spherop 14 system. The corresponding right member of equation (5.1) would be the mean anomalous potential with respect to an ellipsoid over the area  $\Delta S_1$ , or:

$$(5.8) \quad \frac{1}{\Delta S_1} \int_{\Delta S_1} T ds$$

Similar expressions could be defined for mean undulations, mean anomalies, etc., over the area  $\Delta S_1$ . If, however, we do not form the spherical harmonic expansion referred to an ellipsoid, but rather to the Spherop 14 surface, all coefficients in  $F_{SH}$  become zero and the left side of equation (5.1) disappears. Thus, if we have a set of spherical harmonic coefficients which we assert are a true smoothed representation of the actual potential field, then:

$$(5.9) \int_{\Delta S_1} T_{TRUE} ds \approx 0$$

under the conditions that the disturbances  $T_{TRUE}$  are measured with respect to the reference model previously described and that the dimensions of  $\Delta S_1$  satisfy equation (5.3). According to Bruns's equation (3.21), this is equivalent of asserting that the spherop encloses the same volume as the geoid within the volume region subtended by  $\Delta S_1$ .

If the point masses are determined from anomalies referred to the spherop system, the model anomalous potential  $T_{PM}$  arising from these masses can be taken as a detailed approximation of  $T_{TRUE}$  referred to the spherop system. It is appropriate therefore to impose the condition:

$$(5.10) \int_{\Delta S_1} T_{PM} ds = 0$$

This ~~can~~ <sup>can</sup> ~~not~~ <sup>not</sup> ~~be~~ <sup>be</sup> ~~in~~ <sup>in</sup> accordance with equation (2.6) as:

$$(5.11) \sum_j \sum_k \frac{k M_k}{l_{kj}} \cos_j d\phi d\lambda = 0$$

where  $\Delta S_1$  is divided into  $J$  area elements,  $ds = \cos_j d\phi d\lambda$ , for purposes of numerical integration.

If we couple this condition with the condition that the sum of the anomalous point masses under the region  $\Delta S_1$  is zero, then our point mass solution does not change the total mass or volume of our reference system in the volume region subtended by  $\Delta S_1$ . A compound model consisting of a number of localized point mass areas superimposed on a spherop reference system would retain the same mass and the same gross shape and volume as the original spherop reference system. These considerations seemed conceptually significant enough to justify the inclusion of the two conditions in the formation of a point mass model. In actual practice, it was found that the conditions were quite compatible with the observed data and had only a minor influence on the solutions. To illustrate, 180 point masses were fit to an area of  $285 1^\circ \times 1^\circ$  anomalies. This area is about 1.2 time the minimum  $\Delta S$  specified by equation (5.2). A solution was first found with no conditions, the integrated potential disturbance condition, equation (5.11), was then added, and finally the condition was added that the point masses must sum to zero. The slight strain imposed on the solution by the conditions can be illustrated by the very minor changes in the variance of unit weight or the root mean square residuals shown in Table 8.

The individual residuals exhibited the same general patterns in all solutions. In these and a number of other solutions that did not include the mass sum condition, it was observed that the sum of all of the positive and negative anomalous masses was only of the order of the absolute magnitude of an individual mass when masses were summed over an area satisfying equa-

tion (5.2). These results seem to verify the legitimacy of the imposed conditions when applied over adequately large regions.

Table 8

## Influence of Conditions on Point Mass Solutions

Conditions Imposed on Solution	Variance of Unit Weight (Normalized)	RMS Residual Anomaly (mgal)
NONE	1.00	7.19
$\int_{\Delta S_1} T_{PM} ds = 0$	1.01	7.26
$\int_{\Delta S_1} T_{PM} ds = 0; \sum_{kM} = 0$	1.03	7.32

## 5.4 Superposition of Mass Sets

The arguments presented thus far have implicitly imposed a number of requirements which must be considered in using point masses to determine a detailed local geopotential field. These requirements can be separated into those that must be met in order to determine a set of mass points and to those that must be met in order to determine potential related quantities at a given location from a set of mass points. Some confusion is possible with regard to the areal requirements. Chapter 2 pointed out that under the geometric restraints imposed on a point mass solution, a point mass was almost completely determined by the gravity anomalies within a radius of a few point mass

spacings. Chapter 4, however, indicated that geoidal undulations and therefore potential at a point were a function of gravity anomalies over a wider area. If the information on the potential field given by gravity anomalies is to be transformed into a representation by point masses underlying the anomaly field and these masses then used to generate potential fields, it is apparent that the area of anomalies and point masses must be of greater extent than the desired potential field. An estimate of the required radius of the area of anomalies and point masses can be obtained from Figures 6 and 8. These figures show that the most dramatic error reduction occurs in the case of a Spherop 14 reference surface if the integration cap extends to over  $10^{\circ}$ . Thus, if an accurate, detailed point mass densification of a spherical harmonic description of the geopotential is desired, even over a small area, several hundred square degrees of gravity anomalies must be considered in determining the point masses. The optimum number of point masses to be fit to an area is primarily a function of the size of the mean anomaly blocks used in the solution. As discussed in Chapter 2, the mass depth should theoretically be minimized. At the same time, the depth/side ratio should be maintained at a value that makes the observation equation coefficients consistent with equivalent layer theory. These guidelines argue for many shallow masses, but an upper limit is placed on the number of masses by the requirement that sufficient anomalies be available to over-determine the point mass set. To illustrate how these guidelines interact, some characteristics are shown in Table 9 for typical solutions that were accomplished in this study.

Out of the many experimental solutions that were computed, those that had the general characteristics shown in Table 9 appeared to provide satisfactory mass sets. Other solutions in this general range also were satisfactory. While no clear optimums could be identified, smaller depth/side ratios seemed undesirable and no advantage was noted for greater over-determination ratios. These figures are presented here primarily to indicate the number of masses involved in reasonable point mass configurations.

Table 9  
Point Mass Solution Characteristics

Anomaly Block Size	Depth to Point Mass Array (km)	Over-Determination Ratio Anomalies/Point Mass	Depth/Side Ratio
1° x 1°	100	1.6	.8
30' x 30'	50	1.1	1.0
5' x 5'	10	1.9	.9

Based on these configurations, it can be seen that the number of point masses--or unknowns--involved in an area of several hundred square degrees becomes formidable. Suppose, for example, we had a requirement for determining gravitational disturbance components along trajectories originating at a point. The usual procedure for such a computation is to use smaller anomaly blocks for nearby areas and progressively increase the size of the blocks as the distance from the computation point increases. Desirable anomaly block sizes for different distances from the computation point are discussed in general terms by many authors [Uotila, 1959; Hirvonen and Moritz, 1963; Rapp, 1966].

Some suggestions of Hirvonen and Moritz are shown in Table 10. These suggestions made for anomalies referred to an ellipsoid should be reasonable but conservative for computations using anomalies referred to a spherop reference surface. The spherop reference surface takes out the long wavelength features of the anomaly field, but has little influence on the relative variation of mean anomalies in the block sizes of one degree or less.

Table 10

Suggested Anomaly Block Sizes for Disturbance Computations  
[Hirvonen and Moritz, 1963]

Anomaly Block Size	Dimensions of Area Centered on Computation Point	
	Latitude	Longitude
5' x 5'	3°	4°
20' x 20'	7°	9°
1° x 1°	25°	30°
5° x 5°	Remainder of Earth	

Computations of Rapp [1966] suggest that the Hirvonen and Moritz estimate for area dimensions for 5' x 5' mean anomalies is conservatively large for disturbance computations at high elevations. His results showed no significant difference for disturbance components computed above 50 kilometers between computations using 30' x 30' anomalies and computations using 5' x 5' anomalies in a 5° x 5° area surrounding a computation point. Considering that a point mass solution is at best a smoothed solution that cannot show all the detail in the gravitational field at low elevations, it seems reasonable to reduce the area of 5' x 5' mean anomalies to a 2° x 2° rectangle sur-

rounding the computation point and specify that the computations cannot be carried successfully down to the surface. Even on the basis of conventional computations, Rapp [1966] has indicated that 15 to 20 kilometers in the lowest elevation at which the disturbance components can be accurately determined from  $5' \times 5'$  mean anomalies. If points are desired below that elevation, more detailed anomaly fields must be used.

If we assume we use an integration cap extended to the  $1^\circ \times 1^\circ$  mean anomaly block limits suggested above; use  $30' \times 30'$  anomalies in the area in which Hirvonen and Moritz use  $20' \times 20'$  anomalies; and use  $5' \times 5'$  anomalies in a central square  $2^\circ$  on a side; we can then compute the size of the point mass set that would be necessary to model this field. Using the over-determination ratios from Table 9, we could model the fields by the following sets of masses.

- a) 300 masses at 10 kilometers depth to represent the  $5' \times 5'$  field
- b) 210 masses at 50 kilometers depth in an annulus around the  $5' \times 5'$  field to represent the  $30' \times 30'$  field
- c) 430 masses at 100 kilometers depth outside the  $30' \times 30'$  field and extending to the limits of the  $1^\circ \times 1^\circ$  field

This total set of 940 masses could theoretically be determined by adjustment procedures using the 1499 anomalies in the described anomaly zones. This would be a formidable computational problem which would have to be repeated in its entirety for each area in which disturbance component computations were contemplated.

An alternate approach to the development of very detailed fields that is more compatible with the equivalent layer model is provided by point mass superpositioning. In the context of this study, superpositioning can be defined as the overlaying of an array of deep mass points by a more shallow array of more closely spaced mass points. The name arises from the principle of superposition of fields of force in potential theory [Ramsey, 1959, p. 22]. This principle states that the force exerted at a point by a system of particles is the vector sum of the forces exerted by each of the particles separately. It is a basic premise of the Newtonian theory of attraction. The principle can easily be seen to extend to the point wise vector addition of force fields and to the simple point wise addition of scalar potential fields. This concept has been used implicitly in earlier discussions when an anomalous field represented by a set of spherical harmonic coefficients was added to a normal field based on an ellipsoid of revolution to obtain the Spherop 14 field. It was also used when a point mass representation of an equivalent layer surface was added to the Spherop 14 field to obtain a more detailed field. In each of these instances anomalies referred to a model of a certain complexity were used to define a more detailed model. Point mass superposition simply continues this concept into reference models that incorporate point masses in their definition.

For example, suppose that point mass set  $M_j$  had been obtained by a solution using  $1^\circ \times 1^\circ$  anomalies referred to the Spherop 14 system. Suppose also that a set of  $30' \times 30'$  mean anomalies,  $\Delta g$ , referred to an ellipsoid were available over a central portion of the area of set  $M_j$ . Anomalies  $\Delta g_{PM}$

referred to the point mass model could be formed in accordance with equation (5.12).

$$(5.12) \quad \Delta g_{PM_1} = \Delta g_1 - \gamma \sum_{n=2}^{14} (n-1) \sum_{m=0}^n (C_{nm}^* \cos m\lambda_1 + S_{nm}^* \sin m\lambda_1) P_{nm} (\sin \varphi_1') \\ - \sum_j \left( \frac{R_1^2 - F_{1j}}{\ell_{1j}^2 R_1} - \frac{2}{\ell_{1j} R_1} \right) k M_j$$

These anomalies would be referred to the detailed model defined by a spherical harmonic coefficient set and point mass set  $M_j$ . They could be used as input to a solution that would yield additional detail in the form of local perturbations to that model. It would again be appropriate in this case to enforce the conditions that the sum of anomalous mass found in the new set should be zero and that the integral of the anomalous potential over the area of the solution be zero. It is assumed that any such solution would overlay an area that was several of the original mass set spacings on a side. This condition would be the equivalent of satisfying equation (5.2) to insure the validity of these conditions.

The procedure outlined above could be repeated to determine a mass set representing  $5' \times 5'$  mean anomalies. In this application, the mass set  $M_j$  in equation (5.12) would include the mass sets found from both the  $1^\circ \times 1^\circ$  mean anomalies and the  $30' \times 30'$  mean anomalies.

The superposition method would require more masses to represent the three sets of mean anomalies originally postulated than would a simultaneous solution. The mass sets required based on Table 9 characteristics would be:

$1^{\circ} \times 1^{\circ}$	-	470 masses
$30' \times 30'$	-	230 masses
$5' \times 5'$	-	300 masses
Total	-	1000 masses

While the total number of masses has increased slightly as compared to the simultaneous solution, the number of unknowns that must be determined simultaneously has, in this example, decreased by one-half. This greatly reduces the computational problems.

### 5.5 Generation of Contiguous Mass Sets

The program given in Appendix A and outlined in section 5.6 is capable of simultaneously determining up to 324 mass points underlying an area. This is very nearly the maximum number of unknowns that could be determined using direct matrix inversion processes with the available computer facilities. There are instances when it would be desirable to solve simultaneously for a greater number of unknown masses. It would be possible to solve for more unknowns in these instances using partitioning techniques but only at the expense of a very considerable increase in program complexity and computer usage time [Snowden, 1966]. While this approach would be theoretically correct, it did not seem justified in this exploratory investigation. The fact that point masses are determined almost entirely by gravity anomalies in a localized area, as pointed out in Chapter 2, makes it possible to use the basic point mass program outlined in section 5.6 to achieve a close simulation of a larger scale simultaneous solution.

The coefficients shown in Table 1 illustrate indirectly that a point mass

is determined primarily by the mean anomalies that are within three or four mass spacing intervals. Anomalies at a greater distance have essentially no relation to the point mass size since the coefficients relating the mass and the anomalies are near zero. One might expect therefore that adjacent point masses would be highly correlated because they are effectively determined by anomaly sets that have a large percentage of common members. Distant point masses would have little correlation. A typical set of correlation coefficients that was actually obtained in a point mass solution is shown in Figure 9. These coefficients apply to a mass point near the center of a  $16 \times 20$  array of mass points fit to a  $20^\circ \times 20^\circ$  field of  $1^\circ \times 1^\circ$  anomalies. Only those coefficients greater than .01 are shown.

**Figure 9**

## Correlation Coefficients for Members of a Point Mass Array

-.01  
 -.01 .96 -.02  
 -.03 .11 -.30 .12 -.04  
 -.02 .04 -.10 .25 -.58 1.00 -.60 .27 -.11 .04 -.02  
 .02 -.05 .15 -.35 .16 -.06 .02  
 -.02 .09 -.03  
 -.02

The asymmetry in this array of correlation coefficients is due to the fact that the gravity anomalies do not fall symmetrically about the center point mass

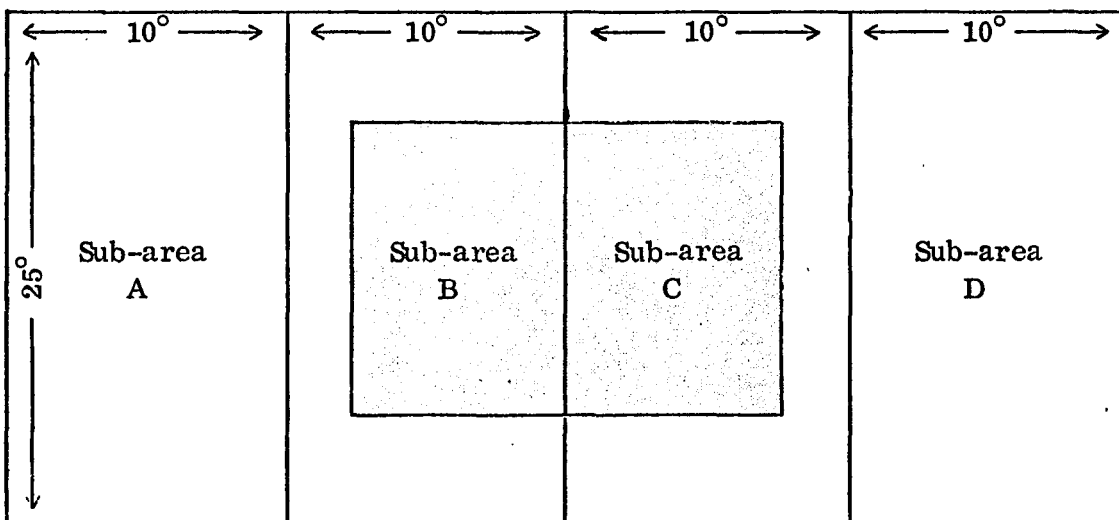
and because the north-south and east-west spacing of the point masses differ.

From Figure 9, it is apparent that the magnitudes of point masses separated by 5 or more intervals in an array are not closely related.

Consider a field of  $1000 \text{ } 1^\circ \times 1^\circ$  mean anomalies such as shown in Figure 10. Assume that this field comprises all of the  $1^\circ \times 1^\circ$  anomaly information available for determining the anomalous potential in the interior shaded over. Ideally a point mass set to be used in modelling this anomalous potential should be found by simultaneously fitting masses to the entire anomaly area.

Figure 10

Arrangement of Contiguous Anomaly Areas



If, however, masses are fit only to anomalies in sub-areas A and B, it could be assumed that the point masses found in A would be the equivalent to those that would be found in a solution based on all of the anomalies. The anomalies in sub-areas C and D are too far from sub-area A to have any significant influence on these point masses. The interdependence of point mass magnitudes

illustrated in Figure 9 attenuates too rapidly for point masses determined in sub-area A to be dependent on point mass values that might be found in sub-areas C and D. This argument cannot be used for point masses in sub-area B. The truncation of the anomaly field at the boundary between sub-areas B and C would eliminate observational data that is significant to the determination of point masses near that boundary. Point masses on both sides of the boundary would be correlated and would interact in a simultaneous solution.

Similarly, if a solution was accomplished for sub-areas C and D, the point masses found in sub-area D would be essentially the same as would be found from a solution covering the entire area while those in sub-area C would show the effects of the truncation of the available anomaly field.

By this reasoning, the two solutions described would define point mass sets in sub-areas A and D that are the equivalents of those that would have been found from simultaneous use of all of the available  $1^\circ \times 1^\circ$  mean anomaly information. It is therefore a reasonable approximation to hold these point mass sets fixed and accomplish a new solution for point masses, in the B and C areas, that will be compatible with the A and D mass sets. This can be accomplished by incorporating mass sets A and D in the definition of "normal" gravity used to form a new set of anomalies in sub-areas B and C. Point masses fit to this anomaly field will then smoothly bridge the area between the two previously defined point mass sets.

This type of solution is very similar to the superposition type of solution. The only differences are in the application of the conditions that are

imposed on the solution. The condition that the sum of the determined masses is zero is changed to a requirement that the sum of all of the mass sets (A, B, C and D) is zero. Similarly, the integral of the disturbing potential arising from all of the mass sets is constrained to zero over the area of the solution.

## 5.6 The Point Mass Solution Computer Program

### 5.6.1 General

The computer program used in this study to obtain point mass arrays is given in Appendix A. The program uses mean anomaly data in a specified rectangular area bounded by meridians and parallels to solve for a designated number of masses at a specified depth. As an option, the program will modify the input anomalies to refer them to a "normal" gravity field that includes pre-defined masses. (Reference equation (5.12).) After the mass set is defined, a geoid for the area, referred to an ellipsoid with the flattening of the GRS-67 ellipsoid may be computed as an option. (Reference equation (5.24).)

The program is written in Fortran IV, IBM 360 version [IBM, 1968a]. It requires a computer with core storage of 500,000 bytes and two peripheral storage devices. The program, as presented, is dimensioned to allow for the solution of 324 unknown mass points based on a maximum of 1000 mean anomaly observations. Provision is made for the inclusion of 2000 pre-determined masses.

The parameters of the Geodetic Reference System 1967 are built into the program. Use of another reference system would require minor internal modifications.

Unless specifically noted, the units used within the program and for input and output are meters, milligals, and degrees. The point "masses" are not actually given in mass units, but rather in kM units of centimeters cubed per second (where k is approximately  $6.673 \times 10^{-8} \text{ cm}^3 \text{g}^{-1} \text{sec}^{-2}$ ).

#### 5.6.2 Computation Control Parameters

The program is written to allow for considerable flexibility in the solutions without need for internal program changes. This is accomplished through input parameters that specify variable options. The options that must be specified are:

TOP	North latitude limit of anomaly field;
BOT	South latitude limit of anomaly field;
EAST	East longitude limit of anomaly field measured eastward from Greenwich;
WEST	West longitude limit of anomaly field;
NM1	Approximate number of masses to be determined (See section 6.54)
DEEP	Depth of masses below ellipsoid surface.
SIDE	The side length of a mean anomaly square in degrees; for example, for a $30' \times 30'$ mean anomaly, side = 0.5;
MIN	The spacing, in minutes of latitude and longitude, between grid points where the undulation is evaluated for geoid computations;
IGEOID	The value 1 indicates a geoid is to be computed; 0 indicates it is not to be computed;
ICOEF	The value 1 indicates that correlation coefficients between the masses are to be printed out; 0 that they are not;

## INITS

The value 1 indicates that the masses are to be fit under the condition that the integrated potential disturbance over the reference surface is zero when both the predetermined masses and the new masses are fit for the first time to an area, but other masses to be included in the model exist outside the area. (See section 5.5.)

The value 0 indicates that the masses are to be fit under the condition that the integrated potential disturbance contribution over the reference surface from the new masses will be zero. This option is used when mass sets are superimposed over an area in which deeper masses already exist. (See section 5.4.)

### 5.6.3 Input Data

The input data used consists of mean anomalies, predetermined masses and spherical harmonic coefficients. The latter two classes of data are required only for some options in the program.

The anomalies used are the Spherop 14 anomalies computed with reference to the normal gravity field defined by equations (3.17) or (3.32). An anomaly input card includes the anomaly value, the  $\varphi, \lambda$  coordinates of the anomaly block midpoint, the geocentric X, Y, Z coordinates of that point and the geocentric radius of the midpoint. These geocentric coordinates and radii were precomputed when the Spherop 14 anomalies were formed to avoid repetitious computations during the many solutions accomplished during these investigations.

The mass cards give the point mass magnitudes times the gravitational constant and Cartesian coordinates of predetermined masses. This data is required only when the superposition concept is used.

The spherical harmonic coefficients defining the Spherop 14 reference surface are required if the geoid computation option is exercised.

Formats and data sequences can be deduced from the program source-listing given in Appendix A.

#### 5.6.4 Mass Positioning

The subroutine NUMASL determines the geographic positions of a set of mass points arranged in a regular trapezoidal array under the area specified for the solution. The exterior points in this array are situated one half of an anomaly block dimension inward from the limits of the anomaly area. The interval between the points, in both latitude and longitude is selected so that the product of the number of rows times the number of columns in the array is approximately equal to the number of points specified by the parameter NM1 and so as to give approximately equal spacing in both directions. The subroutine MASL2 uses the output from NUMASL and the specified mass depth to compute the geocentric Cartesian coordinates of the mass points.

#### 5.6.5 Formation of Normal Equations

The system of equations in the point mass solution may be represented in partitioned matrix notation as [Uotila, 1967]:

$$(5.13) \quad \begin{bmatrix} A'PA & C1' & C2' \\ n \times n & n \times 1 & n \times 1 \\ \hline C1 & 0 & 0 \\ 1 \times n & & \\ \hline C2 & 0 & 0 \\ 1 \times n & & \end{bmatrix} \begin{bmatrix} M \\ n \times 1 \\ \hline K1 \\ 1 \times 1 \\ \hline K2 \\ 1 \times 1 \end{bmatrix} = \begin{bmatrix} A'PG \\ n \times 1 \\ \hline D \\ 1 \times 1 \\ \hline E \\ 1 \times 1 \end{bmatrix}$$

The A matrix is the matrix of observation equation coefficients. An individual element of this matrix for the  $i^{\text{th}}$  anomaly observation and the  $j^{\text{th}}$  mass is found by differentiating equation (2.19) with respect to the product of the mass and the gravitational constant to obtain:

$$(5.14) \quad a_{ij} = \frac{R_i^2 - F_{ij}}{l_{ij}^3 R_i} - \frac{2}{l_{ij} R_i}$$

The notation is that of Chapter 2. The coefficients are evaluated for the mid-point of the anomaly block. Note that the unknowns found by this procedure are masses multiplied by the gravitational constant.

Each observation is weighted according to the area represented by that mean anomaly. The P matrix is therefore a diagonal matrix with elements:

$$(5.15) \quad p_{ii} = \text{Area}_i \times \text{constant}$$

This may be approximated by:

$$(5.16) \quad p_{ii} = \cos\varphi_i' \Delta\varphi \Delta\lambda \times \text{constant}$$

$$(5.17) \quad p_{ii} = \frac{(X_i^2 + Y_i^2)^{1/2}}{R_i} \times \text{constant}$$

The G matrix is the vector of anomaly observations. If pre-defined masses are included in the solution, the input anomalies are altered to obtain anomalies such as those defined by equation (5.12).

The partitions C1 and C2 are the conditions discussed in section 5.3. The basic condition that the integral of the anomalous potential over the area of the point mass array is zero is given by equation (5.11). If, in addition, we accept the possibility of pre-defined masses outside this area, but wish to retain the condition that the total anomalous potential arising from the new

masses and the masses outside the area is zero, this equation must be expanded to:

$$(5.18) \sum_{j} \sum_i \frac{kM_j}{\ell_{ij}} \cos\varphi_i' \Delta\varphi \Delta\lambda + \sum_{k} \sum_i \frac{kM_k^*}{\ell_{ik}} \cos\varphi_i' \Delta\varphi \Delta\lambda = 0$$

where  $M_j$  is the set of unknown masses and  $M_k^*$  is the set of pre-defined masses.

The utility of this concept was discussed in section 5.5. With this condition, the elements of  $C1$  are:

$$(5.19) C1_j = \sum_i \frac{\cos\varphi_i' \Delta\varphi \Delta\lambda}{\ell_{ij}}$$

or if a normalizing constant is introduced:

$$(5.20) C1_j = \sum_i \frac{(x_i^2 + y_i^2)^{1/2}}{R_i \ell_{ij}} \times \text{constant}$$

If pre-defined exterior masses are used,  $D$  is given by:

$$(5.21) D = - \sum_k \sum_i kM_k^* \frac{(x_i^2 + y_i^2)^{1/2}}{R_i \ell_{ik}} \times \text{constant}$$

In the normal case, without masses external to the area,  $D$  would be zero.

The condition that the sum of masses fit to an area must equal zero can be extended in a similar fashion to allow for adjacent masses yielding the more general condition:

$$(5.22) \sum_j kM_j + \sum_k kM_k^* = 0$$

The coefficients  $C2_j$  are all ones or are normalized to a constant. If pre-defined external masses are used, the term  $E$  is given by:

$$(5.23) E = - \sum_k kM_k^* \times \text{constant}$$

In the usual case when there are no pre-defined masses external to the area,

E would be zero.

The partitions K1 and K2 are the usual Lagrange multipliers associated with this type of solution [Uotila, 1967].

Equation system (5.13) is built up simultaneously in computer core storage by sequentially adding the contributions of each observation, as the anomaly card is read, to the elements of the sub-matrices  $A'PA$ ,  $C1'$ ,  $C2'$ ,  $A'PG$ , D and E. This procedure is required because the A matrix alone, in the solution considered here, would greatly exceed the core storage capability of the IBM 360/75 computer. Actually, further space saving was accomplished by storing only the upper right triangular half of the symmetric left member of the normal equations as a "packed" matrix. "Packed" in this sense means that this upper triangular half-matrix is stored by column in a continuous single subscripted vector.

#### 5.6.6 Matrix Inversion

The matrix storage mode described in the preceding section is not compatible with the more familiar computer methods of matrix inversion based on Gaussian elimination and pivoting. An accurate and efficient method for inverting matrices in this storage mode is available, however, as the IBM subroutine DSINV which is based on the Cholesky or square root algorithm [IBM, 1968b; Faddeev and Faddeeva, 1963]. Unfortunately this algorithm is applicable only to positive definite matrices. Normal equations of the type shown in equation (5.13), that include zeros on the diagonal as a result of the condition equations, are not positive definite and cannot be inverted by this

method. The sub-matrix  $A'PA$  is, however, positive definite and can be inverted by the DSINV subroutine. This opens the possibility of using the efficient and accurate DSINV subroutine to invert almost all of system (5.13) and then to complete the inversion of the entire system by applying the method of bordering to the columns arising from condition equations. The method of bordering, described in Faddeev and Faddeeva [1963] and Snowden [1966] could theoretically be used for the entire inversion, but the accuracy of this technique deteriorates progressively as the computation continues through a large matrix. It is not as suitable for large systems as the Cholesky method. The dual inversion using the two different algorithms retains the advantages of the Cholesky method and essentially extends them to apply to the inversion of systems that incorporate a relatively small number of condition equations. The subroutine BINV in Appendix A is a modification of a bordering inversion for packed symmetric matrices that will accept a partially inverted matrix as a starting point. This dual inversion technique was a key element in determining large numbers of unknowns without having to resort to complicated matrix partitioning and the peripheral storage of sub-matrices.

#### 5.6.7 Results and Statistics Produced by Point Mass Solution Program

The basic output of the program is a set of mass points multiplied by the gravitational constant  $k$ , described by magnitudes ( $\text{cm}^3/\text{sec}^2$ ) and positions given in a geocentric X, Y, Z coordinate system. Other statistics and data useful in analyzing and interpreting the results are also given. This information includes:

- a) The mean and root mean square of the anomalies used to form the observation equations;
- b) The mean and root mean square difference between the observed gravity anomalies and model gravity anomalies derived from the point mass set;
- c) The correlation coefficients for the point masses and the diagonal elements of the covariance matrix. (This is an optional output. The complete covariance matrix can also be printed by removing one card from the program.);
- d) The variance of unit weight;
- e) Turing's N number which measures the conditioning of the normal matrix [Faddeev and Faddeeva, 1963];
- f) A listing of individual input mean anomalies, and the corresponding model anomalies derived from the point mass set.

#### 5.6.8 Geoid Computation

As a matter of convenience, subroutines were included with the basic point mass solution program to provide the option of computing a geoid in the area covered by the solution. The geoid computation follows the point mass solution and simply uses the results of that computation. It is not an integral part of the point mass solution.

The geoid is computed by the subroutine GEOH2. The geoid height above the reference ellipsoid is evaluated at the intersections of a grid of meridians and parallels. The mesh size of the grid is controlled by the control

parameter MIN as described in section 5.5.2. The following equation is used to determine the geoid height,  $N_{ij}$ , at latitude  $\varphi_i$  and longitude  $\lambda_j$ .

$$(5.24) \quad N_{ij} = R \sum_{n=2}^{14} \sum_{m=0}^n (\bar{C}_{nm}^* \cos m\lambda_j + \bar{S}_{nm} \sin m\lambda_j) \bar{P}_{nm}(\sin \varphi_i') \\ + \sum_k \frac{k M_k}{\ell_{(ij)k} \gamma} + \sum_k \frac{k M_k^*}{\ell_{(ij)k} \gamma}$$

In this equation,  $\ell_{(ij)k}$  refers to the distance between a computation point at  $\varphi_i$ ,  $\lambda_j$ , and mass  $k$ . The other symbols are as previously defined.  $M_k$  is again the mass set determined in the current solution and  $M_k^*$  is a pre-defined mass set. Note that  $P_{nm}(\sin \varphi_i')$  is evaluated at the geocentric latitude, rather than at the geodetic latitude. This subroutine prints  $N_{ij}$  at each grid point within and on the boundary of the mass solution area. Punched cards suitable for use in a contour program are also produced.

## CHAPTER 6

### DATA USED IN FORMING GEOPOTENTIAL MODELS

#### 6.1 Basic Data Used in Computations

The basic materials describing the geopotential that were used in this investigation were a set of spherical harmonic coefficients and four sets of mean anomaly data in various block sizes ranging from  $5^\circ \times 5^\circ$  means down to  $5' \times 5'$  means. These data sets are described in the following paragraphs.

##### 6.1.1 Spherical Harmonic Coefficients

The spherical harmonic coefficients used in this study are a set of the type described for equation (3.1) that were developed by Rapp [1969c, 1968b]. This set is complete to the 14th degree and order. The particular set used is one of a number of very similar sets developed by Rapp and is known as the "JGR 0<sup>th</sup> Iteration" coefficient set. The coefficients and their standard errors are given in Appendix B.

These coefficients are the result of a least squares adjustment that used both terrestrial gravity information and satellite derived spherical harmonic coefficients as input data. The terrestrial gravity information used was a worldwide set of  $5^\circ \times 5^\circ$  mean anomalies derived from gravity observations and anomaly estimates based on earth models. The sources of this material are described more fully in Rapp [1969b]. The satellite derived spherical

harmonic coefficients used as input data to the adjustment were taken from the SAO 66 Standard Earth Parameters [SAO, 1966]. The adjustment procedure is theoretically described in Rapp [1969b] and given in practical detail in Snowden and Rapp [1968].

#### 6.1.2 Five Degree by Five Degree Mean Anomaly Set

The  $5^\circ \times 5^\circ$  mean free air anomaly set used in this investigation is shown in Appendix C. This set of mean anomalies is an outgrowth of the combination solution adjustment which produced the spherical harmonic coefficient set described in the preceding section. It was formed from the terrestrial anomaly set used in the combination solution by imposing the condition that the adjusted anomaly field be compatible with the spherical harmonic coefficients found in the combined solution. This anomaly set was found through a separate adjustment based on condition equations of the form:

$$(6.1) \quad \left\{ \frac{\bar{C}_{nm}}{\bar{S}_{nm}} \right\} - \frac{1}{4\pi\gamma(n-1)} \int \int \Delta g \bar{P}_{nm} (\sin\varphi') \begin{Bmatrix} \cos m\lambda \\ \sin m\lambda \end{Bmatrix} d\sigma = 0$$

This equation is based on the summation method of determining spherical harmonic coefficients given a worldwide set of gravity anomaly data. A detailed description of the procedure is given by Snowden and Rapp [1968]. This method is not the equivalent of determining an anomaly field from spherical harmonic coefficients. The resulting field retains the detail of the original field but is made consistent with the spherical harmonic coefficients resulting from the combined solution.

These anomalies were based on the International Gravity Formula.

In the adjustment to determine this anomaly set, the condition was imposed that the mean value of terrestrial gravity anomalies over the earth, in this system, was  $\bar{\Delta}g_0 = 1.9$  milligals. The area weighted mean of this set of anomalies is therefore 1.9 milligals.

#### 6.1.3 One Degree by One Degree Mean Anomaly Set

A set of  $1^\circ \times 1^\circ$  mean free air anomalies covering most of the United States ( $25^\circ < \varphi^\circ < 50^\circ$ ,  $240^\circ E < \lambda < 280^\circ E$ ) was furnished for this investigation by Dr. Richard H. Rapp. This set has not been published but has been used for detailed geoid computations in the central United States [Rapp, 1969b, 1967b]. This data is closely related to the anomaly holdings of The Ohio State University Gravity Library and to the materials used to form the  $5^\circ \times 5^\circ$  mean anomalies used in the combination adjustment discussed in section 6.1.2. It is not, however, identical to the material used to establish the original estimates of the  $5^\circ \times 5^\circ$  means throughout this area. The  $1^\circ \times 1^\circ$  anomalies form a dynamic file that has been periodically improved and enlarged. The exact values used to form the  $5^\circ \times 5^\circ$  means are no longer identifiable.

These anomalies are referred to the International Gravity Formula. No formal accuracy data is available for the set.

#### 6.1.4 Thirty Minute by Thirty Minute and Five Minute by Five Minute Mean Anomalies

These sets of mean anomalies are described by Rapp [1965]. The  $5' \times 5'$  mean anomalies were formed by statistical prediction methods from point anomalies in The Ohio State University Gravity Library. The  $30' \times 30'$

mean anomalies were formed by meaning the included  $5' \times 5'$  means. These anomalies are referred to the International Gravity Formula. The  $30' \times 30'$  mean anomalies and their standard errors have been published by Rapp [1965].

### 6.2 The Relationship Between the Anomaly Sets

The  $5' \times 5'$ ,  $30' \times 30'$ , and  $1^\circ \times 1^\circ$  mean anomaly sets are basically consistent sets of data. The periodic changes in the  $1^\circ \times 1^\circ$  mean anomaly set, mentioned in section 6.1.3 have taken place primarily in the peripheral areas of the data set where the original values were uncertain and not in the areas of dense point coverage where the  $30' \times 30'$  and  $5' \times 5'$  anomaly sets were formed.

There is a basic difference between the  $5^\circ \times 5^\circ$  anomaly set and the other sets. This set is partially derived from the information included in the smaller block anomaly sets but also is influenced by satellite data. Assuming valid data and rational weighting, this set must be presumed more accurate than a set obtained solely from terrestrial observations.

It should also be noted that the  $5^\circ \times 5^\circ$  data has an enforced mean anomaly that is not present in the smaller block mean anomalies. This must be taken into account when the various data sets are used together.

### 6.3 Conversion of Mean Anomalies from The International Gravity Formula System to the GRS 67 and Spherop 14 Systems

All gravity anomalies used in this study were converted from the International Gravity Formula Reference System to anomalies based on the Geodetic Reference System of 1967 by means of the relation:

$$(6.2) \quad \Delta g = g - \gamma$$

Using the subscripts INT, GRS, and S14 to identify quantities referred to the

International, GRS 67, and Spherop 14 systems respectively,

$$(6.3) \quad g_{INT} = \Delta g_{INT} + \gamma_{INT}$$

$$(6.4) \quad \Delta g_{GRS} = g_{GRS} - \gamma_{GRS}$$

The absolute gravity value  $g_{INT}$  given by equation (6.3) derives ultimately from the assigned value of absolute gravity at Potsdam. Modern measurements of the absolute value of gravity indicate that this Potsdam value is in error. Some recent determinations are shown in Table 11 [Szabo, 1968].

Table 11

Recent Determinations of Absolute Gravity

Investigator	Year	Observed - Potsdam System (milligals)
Cook Teddington England	1967	-13.7
Sakuma Sevres France	1967	-13.8
Faller Gaithersburg Md.	1968	-13.6

We will assume a Potsdam correction of -13.7 milligals. The absolute value of  $g_{GRS}$  given in equation (6.4) is not referred to a Potsdam value but is rather derived from the parameters assumed to define a mean earth ellipsoid. Under this assumption:

$$(6.5) \quad g_{GRS} = g_{INT} - 13.7$$

Substituting equation (6.3) into (6.5) and (6.5) into (6.4):

$$(6.6) \quad \Delta g_{GRS} = (\Delta g_{INT} + \gamma_{INT}) - \gamma_{GRS} - 13.7$$

Normal gravity for the GRS 67 is given by equation (4.33). The International Gravity Formula is:

$$(6.7) \quad \gamma_{INT} = 978049 (1 + .005284 \sin^2 \varphi - .0000059 \sin^2 2\varphi)$$

To convert an International mean anomaly to a GRS 67 mean anomaly, equations (4.33) and (6.7) were evaluated at the mid-latitude of the anomaly block and  $\Delta g_{GRS}$  was then computed by equation (6.6).

Spherop 14 anomalies,  $\Delta g_{S14}$ , were computed in a similar fashion by:

$$(6.8) \quad \Delta g_{S14} = (\Delta g_{INT} + \gamma_{INT}) - \gamma_{S14} - 13.7$$

Normal Spherop 14 gravity,  $\gamma_{S14}$ , is given by equation (4.32) or (4.17). These equations were evaluated at the geocentric latitude of the midpoint of the anomaly block.

The mean anomaly sets described in Table 12 were formed by the above outlined methods.

Table 12

Mean Anomaly Sets Formed

Block Size	Type Anomaly	Latitude Limits	Latitude Limits
5° × 5°	GRS 67		World Wide
1° × 1°	GRS 67 Spherop 14	25°N - 50°N	240°E - 280°E
30' × 30'	GRS 67 Spherop 14	33°N - 41°N	256°E - 265°E
5' × 5'	GRS 67 Spherop 14	35°N - 39°N	258°E - 263°E

The relationships between the GRS 67 anomaly sets are basically the same as those described in section 6.2 for the anomalies based on the International Gravity Formula. The change of gravity formula does, however, change the magnitude of the zero order or worldwide mean anomaly imposed on the  $5^\circ \times 5^\circ$  anomaly set. Adapting an equation of Heiskanen and Moritz [1967, p. 111], this value may be calculated for the GRS 67 anomalies by:

$$(6.9) \quad \overline{\Delta g}_{\text{GRS}} = \overline{\Delta g}_{\text{INT}} - (\gamma_{\text{INT}} - 13.7) + \gamma_{\text{GRS}} + \frac{1}{3} \gamma_{\text{INT}} (f_{\text{INT}} - f_{\text{GRS}})$$

where  $\overline{\Delta g}_o$  refers to a mean anomaly over the earth and  $f$  is the ellipsoid flattening. This computation yields a mean anomaly of 0.8 milligals with reference to GRS 67. This value was confirmed by numerically integrating the  $5^\circ \times 5^\circ$  field over the earth. The existence of a mean anomaly indicates that there is some inconsistency between the  $5^\circ \times 5^\circ$  mean anomaly field and the GRS 67 model. This is not unexpected nor disturbing. Current estimates of the mean earth ellipsoid differ slightly from the GRS 67 [Moritz, 1968; Rapp, 1969b; Veis, 1968] and the anomaly field is certainly subject to error. In any event, in this investigation, the GRS 67 simply provides a basis for describing perturbations and need not have absolute accuracy.

The sets of 1000  $1^\circ \times 1^\circ$  mean anomalies are large enough in both number and area that some statistics concerning these sets are of interest to show the relation of the various types of anomalies used in this study.

The root mean square anomaly values are an indicator of the fit of the reference system to the observed terrestrial anomalies. As would be expected, the Spherop 14 system is the best fit.

Table 13

Statistics on  $1^\circ \times 1^\circ$  Mean Anomaly Sets

Reference System	Mean Anomaly (milligals)	RMS Anomaly (milligals)	Maximum Anomaly (milligals)
International	2.0	19.3	93.0
GRS 67	.4	18.8	89.6
Spherop 14	-1.2	16.7	73.4

In accordance with the logic of Chapter 4, the mean Spherop 14 anomaly over an area of  $25^\circ \times 40^\circ$  should be approximately zero. That is:

$$(6.10) \quad \frac{1}{\Delta s} \int_{\Delta s} \Delta g_{S14} ds \approx 0$$

According to Table 13, the GRS 67 anomalies more nearly satisfy equation (6.10) than do the Spherop 14 anomalies. A more critical examination of the data reveals that this is a coincidence for this particular integration block. If equation (6.10) is evaluated for smaller areas spaced across the  $25^\circ \times 40^\circ$  block, it is found that the Spherop 14 anomalies yield smaller and more nearly constant values for the mean anomalies of the areas than do the GRS 67 anomalies. This is illustrated in Table 14 which shows these values and the corresponding area weighted root mean square anomalies for areas extending  $19^\circ$  in latitude and longitude and centered along the central parallel of the  $25^\circ \times 40^\circ$  area. According to equation (5.2), a  $19^\circ \times 19^\circ$  area at this latitude is about 1.5 times the absolute minimum area over which equation (6.10) might be expected to have some validity for the Spherop 14 anomalies.

Table 14

Comparison of Spherop 14 and GRS 67  
 $1^\circ \times 1^\circ$  Mean Free Air Anomalies  
 Averaged Over  $19^\circ \times 19^\circ$  Blocks

Block Center		Spherop 14 Anomaly		GRS 67 Anomaly	
Lat	Long	Mean	RMS	Mean	RMS
37.50	249.50	-1.39	18.09	3.80	22.20
37.50	250.50	-1.49	17.95	4.11	21.79
37.50	251.50	-1.76	17.84	4.08	21.57
37.50	252.50	-1.58	17.97	4.37	21.44
37.50	253.50	-1.66	17.94	4.26	21.29
37.50	254.50	-1.22	17.80	4.56	21.00
37.50	255.50	-1.46	17.70	4.06	20.71
37.50	256.50	-0.96	17.37	4.21	20.23
37.50	257.50	-0.43	17.27	4.32	19.93
37.50	258.50	-0.14	17.29	4.13	19.62
37.50	259.50	-0.15	16.08	3.59	18.91
37.50	260.50	-0.16	16.76	3.02	18.27
37.50	261.50	-0.24	16.71	2.85	18.41
37.50	262.50	-0.08	16.49	1.96	17.78
37.50	263.50	-0.56	16.26	0.93	17.28
37.50	264.50	-1.57	15.15	-0.62	15.65
37.50	265.50	-1.61	15.00	-1.18	15.27
37.50	266.50	-1.65	14.73	-1.71	14.77
37.50	267.50	-1.55	14.83	-2.06	14.92
37.50	268.50	-1.11	14.61	-2.05	14.85
37.50	269.50	-0.66	14.31	-2.00	14.69
37.50	270.50	-0.09	14.04	-1.81	14.44

Other block sizes in the range from  $15^\circ \times 15^\circ$  to  $25^\circ \times 25^\circ$  yielded generally comparable results. The low mean GRS 67 anomaly for the entire  $25^\circ \times 25^\circ$  block is merely the result of a balance within the block of large regions with a positive mean anomaly against similar regions with a negative mean anomaly. The smaller negative mean anomaly for the Spherop 14 anomalies appears to be a consistent feature even on a limited area scale. On the basis of this set

of anomalies and equation (6.10), one might surmise that the equatorial gravity value used in defining normal gravity is too high. Unless the spherical harmonic model is exact and the mean anomaly values are very reliable, this would be a dangerous method of determining equatorial gravity. A few highly aberrant mean anomaly observations could seriously displace the mean in this small sample.

#### 6.4 Reconciliation of Anomalies

The sets of mean anomalies described above are derived directly and solely from terrestrial observations and are not consistent with the set of coefficients defining the Spherop 14 surface nor with the  $5^\circ \times 5^\circ$  mean anomalies adjusted to be consistent with those coefficients. The latter sets of data arose from a combination adjustment of satellite data and  $5^\circ \times 5^\circ$  mean anomalies. Some of the  $5^\circ \times 5^\circ$  mean anomalies that were used as input to the adjustment were derived from the smaller mean anomaly sets. In the context of a gravity field defined by a combination adjustment, these small block anomaly fields might be considered as unadjusted observations. If these anomalies are to be used to add detail to the basic gravitational field described by the Spherop 14 reference system, then some method must be used to make all of the anomaly sets consistent with the coefficients forming that system. In essence, we need to find "v's" or corrections to these smaller block anomalies just as corrections were found to the input  $5^\circ \times 5^\circ$  mean anomaly blocks. A rationale for finding these corrections can be given as follows.

The adjusted  $5^\circ \times 15^\circ$  mean anomaly set found through the application of

equation (6.1) is the best available estimate of the gravitational field in that degree of detail. In theory, at least, it is a resultant of all of our gravitational knowledge including all available  $1^\circ \times 1^\circ$  anomalies. Any detail that could be added in a specific area by use of these  $1^\circ \times 1^\circ$  anomalies could not logically change the value of the  $5^\circ \times 5^\circ$  mean anomalies. A consistent estimate of the  $1^\circ \times 1^\circ$  mean anomalies must therefore satisfy the condition:

$$(6.11) \quad \left( \overline{\Delta g}_5 - \frac{1}{A} \sum_{i=1}^{25} \overline{\Delta g}_{i1} dA_i \right) = 0$$

where:  $\overline{\Delta g}_5$  =  $5^\circ \times 5^\circ$  mean anomaly;

$A$  = area of  $5^\circ \times 5^\circ$  block;

$\overline{\Delta g}_{i1}$  =  $i^{\text{th}}$   $1^\circ \times 1^\circ$  mean anomaly; and

$dA_i$  = area of  $i^{\text{th}}$   $1^\circ \times 1^\circ$  anomaly.

Approximating  $dA_i$  by  $\cos\varphi_i (1^\circ/\rho)^2 R^2$ , this equation becomes:

$$(6.12) \quad \left( \Delta g_5 - \sum_{i=1}^{25} \frac{\cos\varphi_i}{\sum_{i=1}^{25} \cos\varphi_i} \overline{\Delta g}_{i1} \right) = 0$$

Following Uotila's nomenclature and notation [Uotila, 1967], equation (6.12) is the mathematical model for an adjustment by the method of condition equations. In matrix notation, the vector of corrections which must be added to the  $1^\circ \times 1^\circ$  mean anomalies to reconcile them to the adjusted  $5^\circ \times 5^\circ$  mean anomalies is given by:

$$(6.13) \quad V = -P^{-1}B'(BP^{-1}B')^{-1}W$$

where:  $B$  = partial differentials of equation (6.12) taken with respect to  $\overline{\Delta g}_i$ :

$$= \begin{bmatrix} \frac{\cos\varphi_1}{\sum_{i=1}^{25} \cos\varphi_i} & \frac{\cos\varphi_2}{\sum_{i=1}^{25} \cos\varphi_i} & \dots & \frac{\cos\varphi_{25}}{\sum_{i=1}^{25} \cos\varphi_i} \end{bmatrix}$$

$P$  = covariance matrix of the observed  $1^\circ \times 1^\circ$  mean gravity anomalies;

$W$  = misclosure obtained when evaluating equation (6.12) with the fixed  $\bar{\Delta g}_5$  value and the observed  $\bar{\Delta g}_1$  values.

Once the reconciled values of the  $1^\circ \times 1^\circ$  mean anomalies have been found through equation (6.13), they may be regarded as our best estimate of a  $1^\circ \times 1^\circ$  field consistent with the spherical harmonic coefficients. The same procedures can then be used to reconcile the  $30' \times 30'$  anomalies to the reconciled  $1^\circ \times 1^\circ$  anomalies and finally, the  $5' \times 5'$  to the reconciled  $30' \times 30'$  anomalies.

This process was accomplished for the anomaly fields listed in Table 12. In practice, covariance matrices were not available for the  $1^\circ \times 1^\circ$  and the  $5' \times 5'$  anomaly sets. Identity matrices were assumed. Variances obtained during the original estimation process were available for the  $30' \times 30'$  anomalies. A diagonal covariance matrix was therefore used in the  $30' \times 30'$  reconciliation adjustment. Except for the reconciliation of the  $1^\circ \times 1^\circ$  mean anomalies to the  $5^\circ \times 5^\circ$  means, the  $B$  matrix elements in equation (6.13) were essentially constant and equal to  $1/n$  where  $n$  is the number of mean anomalies. This simplification of the  $B$  matrix was used in the reconciliation of the  $30' \times 30'$  and  $5' \times 5'$  anomalies.

After the above outlined reconciliation process, the various anomaly

fields can be considered mutually consistent and compatible with the reference set of spherical harmonic coefficients.

Ideally the corrections to the smaller anomaly blocks could be attributed to the influence of the satellite data in the combination solution that produced the spherical harmonic coefficients, and to the fact that the worldwide field was constrained to have a mean anomaly. In the case of the data sets used in this investigation, this ideal was not met since the  $1^\circ \times 1^\circ$  anomalies are not identical to the sources of the gravity information used as input to the combination solution. Figure 11 shows the average correction to the  $1^\circ \times 1^\circ$  mean anomalies within each  $5^\circ \times 5^\circ$  block required to reconcile these  $1^\circ \times 1^\circ$  mean anomalies to the  $5^\circ \times 5^\circ$  mean. Figure 12 shows the average correction applied to the original  $5^\circ \times 5^\circ$  anomalies as a result of the condition equation adjustment following the combination solution [Rapp, 1968c]. The parenthetical numbers on this figure are the a priori standard errors associated with each  $5^\circ \times 5^\circ$  mean anomaly. With the exception of the peripheral blocks, the corrections to the  $1^\circ \times 1^\circ$  means were within a fraction of a milligal of the original correction applied to the corresponding  $5^\circ \times 5^\circ$  block means. These fractional differences are not significant since the original input  $5^\circ \times 5^\circ$  mean values were rounded to the nearest milligal. In some of the peripheral blocks the a priori standard errors assigned to the  $5^\circ \times 5^\circ$  means were significantly higher than in the central portion of the anomaly field. These are the areas where there are the greatest discrepancies between the corrections to the  $5^\circ \times 5^\circ$  and  $1^\circ \times 1^\circ$  anomaly sets. The Mexican area shows the largest deviation

tions. The deviations are not inconsistent with the assigned standard errors of these blocks in the combination solution adjustment.

The failure in complete agreement of the corrections to the  $5^\circ \times 5^\circ$  and  $1^\circ \times 1^\circ$  mean anomaly fields is unfortunate from a theoretical viewpoint and illustrates some definite areas of uncertainty in the actual gravity field. The reconciled anomaly sets are, however, completely consistent and are suitable for testing the point mass method even though the Spherop 14 reference system and the reconciled anomaly fields may not reflect the latest estimates of the terrestrial gravity field.

Average Reconciliation Correction to  $1^{\circ} \times 1^{\circ}$  Mean Anomalies (mgals)

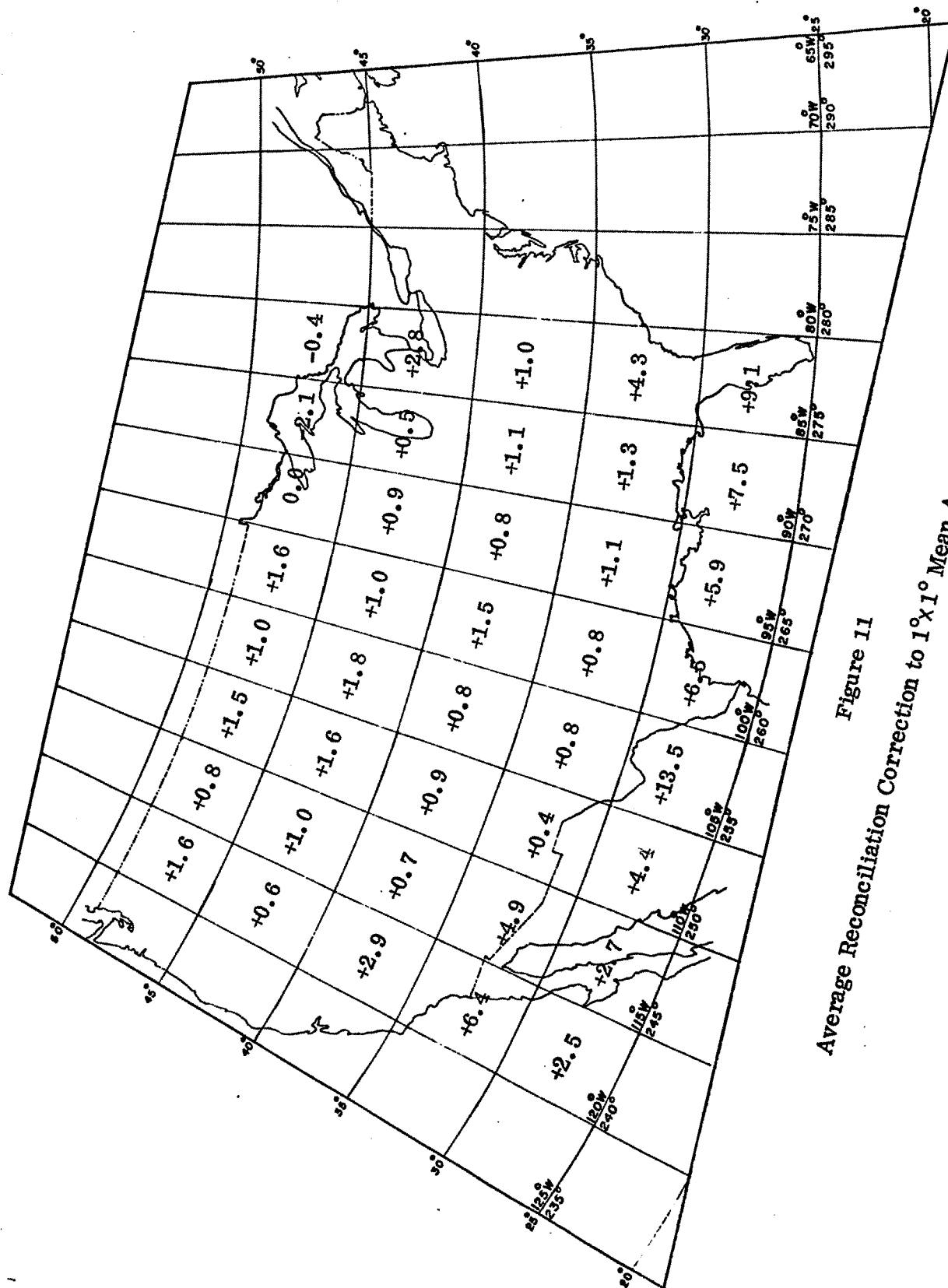


Figure 11

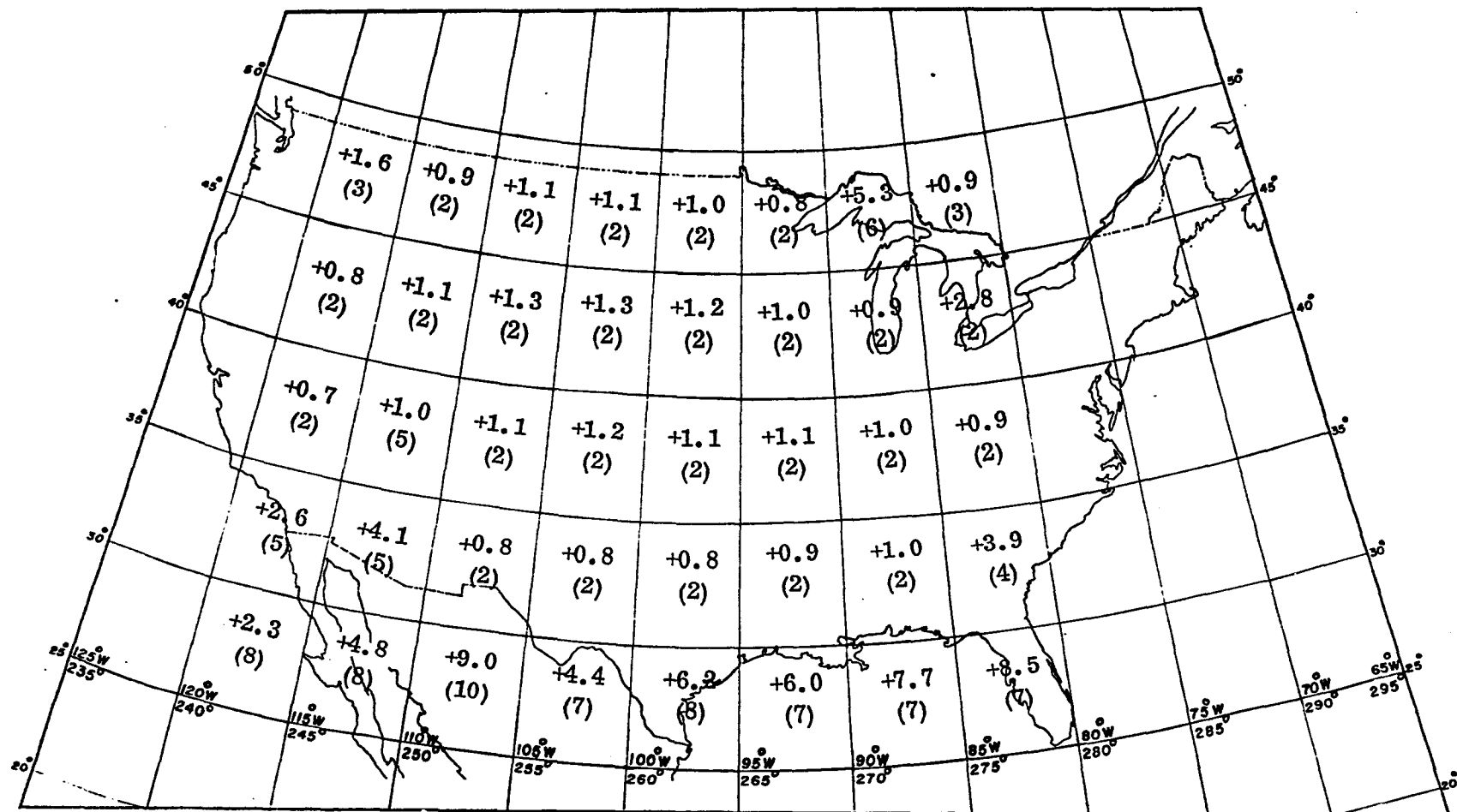


Figure 12

Corrections Applied to 5°x5° Mean Anomalies (milligals)  
(A Priori Standard Errors in Parentheses)

## CHAPTER 7

### COMPUTATION OF STANDARDS OF COMPAIRSON

#### 7.1 General

The preceding chapters have outlined a method of adding detail to a geopotential model through the use of point masses. The method by its nature is based on a series of approximations and assumptions. Attempts have been made throughout the preceding discussions to justify these assumptions and to evaluate the effects of the individual approximations. Convincing evidence of the validity of the overall process must come, however, from a comparison of point mass results and similar results obtained by more traditional and generally accepted methods. Before discussing point mass representations of the geopotential, it is therefore necessary to develop some standards against which these representations can be evaluated.

The geoid is a natural standard to use in comparing geopotential models. The geoid is directly related to the geopotential and can be regarded as a scaled expression of the anomalous potential measured with respect to a specified normal potential. By Stokes' Theorem, a proof that two models of the geopotential yield the same geoid is the equivalent of proving that the model geopotentials are equivalent throughout the empty space outside the

geoid. [Heiskanen and Moritz, 1967, p. 17]. The geoid also has the advantage of familiarity since most investigators illustrate their geopotential models by describing geoids. The significance of discrepancies between two models of the geopotential determined from similar data can therefore be evaluated with some realism when the discrepancies can be compared directly to the variations that appear between published models.

The currently proposed applications of point masses are primarily concerned with missile and space activities. The geopotential functions of most interest are the components of the anomalous gravity field. Complete worldwide agreement of geoids obtained from two different geopotential models would guarantee the agreement of the components of gravity as previously noted. The approximate agreement of such geoids over a limited area leaves the expected relationship between these components in theoretical doubt. An actual comparison between point mass derived anomalous components and those derived from more conventional formulations is therefore necessary to investigate the applicability of point masses to the determination of these geopotential functions.

Two types of comparison standards were therefore developed. The first consisted of a geoid of moderate detail developed over as large an area of the United States as could possibly be justified by the available observational material. This standard was designed to determine the adequacy of point mass models in describing larger scale features of the geopotential. The second standard consisted of a family of vertical trajectories, originating in a

$1^{\circ} \times 1^{\circ}$  square area, along which the anomalous components of gravity were computed at elevations ranging from 20 to 1500 kilometers. This standard was designed to obtain the maximum detail and accuracy that could be obtained from gravity anomalies given down to the detail of  $5' \times 5'$  means.

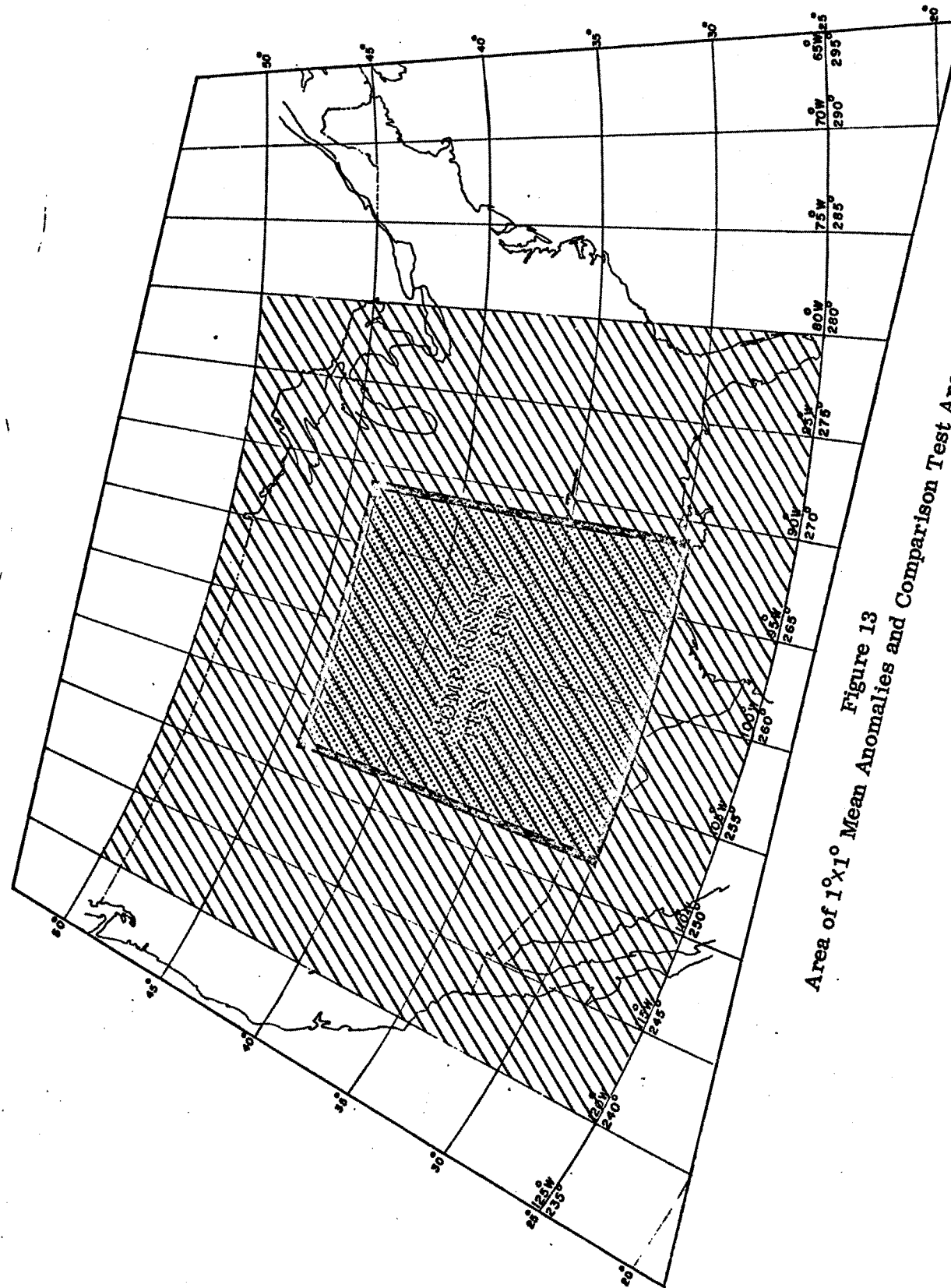
The two types of standards outlined permit an evaluation of the success of modelling both the disturbing potential and its first derivatives. In combination they provide a much more complete evaluation of the model than would either alone. It should especially be pointed out that the fact that a point mass model based on gravity anomalies permits the recovery of these anomalies tells little about the adequacy of the model. This agreement merely means that a linear combination of the model anomalous potential and its normal derivative agree with the starting gravity anomalies on one equipotential level. The agreement reveals nothing about the individual value of either function nor about their relationship to the true field at any other equipotential level.

## 7.2 The Comparison Gravimetric Geoid

### 7.2.1 General

An area in the south central United States has been used by Rapp for geoidal comparisons in a number of previous investigations [Rapp, 1967c, 1968d, 1968b, 1969b]. This area, shown in Figure 13, is centered in the block of  $1^{\circ} \times 1^{\circ}$  mean free air anomalies available for this study. To provide continuity with these previous studies, this area was selected as the comparison area for this study. The area is only slightly larger than the minimum

Figure 13  
Area of  $1^{\circ} \times 1^{\circ}$  Mean Anomalies and Comparison Test Area



area, determined in Chapter 5, over which the mean value of a function expressed as a (14, 14) spherical harmonic series might be expected to approximate the true value. It was therefore deemed to be a minimum area suited to representative investigations concerning surfaces associated with such a series.

The gravimetric comparison geoid was computed in this area using a conventional Stokes' formulation identical to that adopted by Rapp in the previously referenced studies. The geoid undulations were computed at the intersections of the grid formed by parallels and meridians spaced at one degree intervals. The undulations were given by:

$$(7.1) \quad N = \frac{R}{4\pi G} \iint_I \Delta g S(\psi) d\sigma + \frac{R}{4\pi G} \iint_{II} \Delta g S(\psi) d\sigma$$

In this expression,  $\Delta g$  is the mean free air GRS 67 anomaly over the area element  $d\sigma$ ,  $R$  and  $G$  are the mean radius and normal gravity over the reference ellipsoid,  $\psi$  is the angular distance from the computation point to the center of  $d\sigma$  and  $S(\psi)$  is the Stokes' coefficient defined for equation (4.1). The two integrals refer to area I, an inner zone of  $1^\circ \times 1^\circ$  anomalies surrounding the computation point and area II, a field of  $5^\circ \times 5^\circ$  anomalies covering the rest of the world.

Equation (7.1) does not actually yield geoid undulations with respect to the ellipsoidal reference surface used to define the anomalies. Rather, it gives undulations of the free air co-geoid with respect to a mean earth ellipsoid. The figure obtained is a co-geoid instead of a true geoid since no

consideration was given to the indirect effect of the theoretical mass transport implicit in the free air reduction of gravity to the geoid [Heiskanen and Moritz, 1967, p. 289]. This is not a direct matter of concern in this application since a point mass solution using the same anomalies will also result in a free air co-geoid. If the indirect effect is ignored in both computations, the two figures will err in the same manner and a comparison between the co-geoids will be the equivalent of a geoid comparison. In any event, the indirect effect introduced by the uncompensated use of free air anomalies is minor in relatively smooth areas such as the designated test area when compared to errors arising from uncertainties in the gravity field [Mather, 1970, p. 4]. In subsequent discussions, no distinction will be made between the free air co-geoid and the geoid except when such a distinction is relevant to that discussion.

The fact that equation (7.1) gives undulations with respect to a mean earth ellipsoid does not cause any difficulty in comparing gravimetric geoids and point mass geoids. The point mass geoid is developed as perturbations to a surface that is described by a set of spherical harmonic coefficients in accordance with equation (3.29). This latter surface is referred to a mean earth ellipsoid. The point mass geoid is therefore described as undulations above a mean earth ellipsoid and not above the adopted reference ellipsoid. The two geoid representations are directly comparable, but neither can be used to define the absolute undulation with respect to the reference ellipsoid. The difference between the reference ellipsoid and the mean earth ellipsoid must be found by other methods.

In equation (7.1), the worldwide anomaly field is split into two parts;

an inner field of one thousand  $1^\circ \times 1^\circ$  mean anomalies and an outer field of  $5^\circ \times 5^\circ$  mean anomalies. This data would not be adequate if the intent of this study was to produce a highly detailed geoid map throughout the comparison test area. Uotila [1959] and Mather [1968] have studied the influence of mean anomaly block size on the accuracy of the numerical integration required for undulation computation. Uotila concluded that detailed anomaly information should be used out to an angular radius of  $1^\circ.2$ . Mather suggested  $1^\circ.5$ . These recommendations were based on the assumption that a very accurate, very detailed geoid was desired. Mather, for example, was attempting to suppress integration errors to an order of magnitude less than the error of the order of the flattening that is inherent in the spherical approximation of Stokes' equation. If, as in the case of this study, a geoid is contemplated covering a large area with each computation point representing an area as large as one square degree, a requirement for this type of accuracy is not logically justifiable. Failure to use very detailed information around the computation point will merely smooth the resulting geoid to some extent. Both authors have modified their own suggestions when doing practical computations. Uotila actually used no area means smaller than  $1^\circ \times 1^\circ$  when doing large scale geoid computations [1959]. Mather, in one study where he wished to remove high frequency fluctuations in the geoid, intentionally omitted all anomaly information within  $1^\circ.5$  of the computation point [1970].

Uotila [1959] suggested that  $1^\circ \times 1^\circ$  anomalies be used out to a radius of  $13^\circ.3$  and Mather [1968] suggested  $20^\circ$ . Uotila reported numerical tests where this radius was varied. The results showed the resulting errors to be highly position dependent and significant when sub-meter accuracies are sought. Such absolute accuracies are unrealistic considering the available gravity data and little harm probably results in actual practice from using somewhat smaller  $1^\circ \times 1^\circ$  anomaly areas than these recommendations. Both Uotila and Mather appear to have little compunction about reporting geoids based on less material. In this current investigation, however, where geoids are to be determined from the same gravity material by two different computational methods, it would have been desirable to extend the  $1^\circ \times 1^\circ$  field to the theoretically recommended limit to remove this possible source of error. This was not possible considering the desired area of coverage and the available  $1^\circ \times 1^\circ$  set of anomalies. The outer edges of the gravimetric comparison geoid are therefore theoretically less reliable than the central portion. The actual effect should be minor unless there were pronounced regional trends in the unknown  $1^\circ \times 1^\circ$  mean gravity anomalies in the area immediately adjacent to the available  $1^\circ \times 1^\circ$  mean anomaly field. Such trends are not obvious in the border regions of the known anomaly field.

It is unlikely that the errors arising from the computational procedures used would exceed one meter in the geoidal comparison area.

#### 7.2.2 Compatibility of Anomaly Data

If a worldwide gravity field is integrated to solve Stokes' Formula for

geoid height at a point, a constant error applicable to all of the anomaly values is not significant. Integrating Stokes' Function over the entire earth:

$$(7.2) \quad \int_{\sigma} S(\psi) d\sigma = 0$$

If therefore an anomaly set,  $\Delta g$ , is defined that consists of true anomalies  $\Delta g_t$  plus a constant  $\Delta g_c$ , then:

$$(7.3) \quad \begin{aligned} \int_{\sigma} \Delta g S(\psi) d\sigma &= \int_{\sigma} (\Delta g_t + \Delta g_c) S(\psi) d\sigma \\ &= \int_{\sigma} \Delta g_t S(\psi) d\sigma + \Delta g_c \int_{\sigma} S(\psi) d\sigma \\ &= \int_{\sigma} \Delta g_t S(\psi) d\sigma \end{aligned}$$

The geoid obtained from the anomaly set that meant to  $\Delta g_c$  over the earth would thus be identical to a geoid computed from the true anomalies  $\Delta g_t$  that by definition have a zero mean value.

Rapp has pointed out a danger, related to the above discussion, that arises when equation (7.1) is applied [Rapp, 1967c]. If the anomaly sets used in integrals I and II are not part of a consistent set, i.e. with the same constant error,  $\Delta g_c$ , then the cancellation of the constant error term expressed by equation (7.3) does not occur. Great care must therefore be taken to insure that the anomalies used in evaluating the inner zone integral I are consistent with those used in evaluating the outer zone integral II. Inconsistencies between these anomaly sets can arise from several sources. If an outer field is computed directly from spherical harmonic coefficients,

$\Delta g_c$  is zero by definition since the 0<sup>th</sup> order harmonic is excluded. In this case the inner field must not contain a constant bias. Such a bias might arise from the gravity formula used in forming the anomalies or from the definition of the base station system used in obtaining the gravity measurements.

If an outer field of adjusted terrestrial anomalies is obtained from an adjustment based on equation (6.1), these anomalies have a specified worldwide mean value based on the zero order coefficient imposed. This technique in essence can be used to change the equatorial gravity value used in the normal gravity equation defining the anomalies. This zero order anomaly must be compatible with any constant bias that effects terrestrial anomalies used as an inner field. This condition will not normally be met by an arbitrary set of terrestrial anomalies specified for the inner area. The possible errors arising from differences in the anomaly definitions between the inner and outer zone are not trivial. If area I is defined as the 25°×40° area of 1°×1° mean anomalies shown in Figure 13, then:

$$(7.4) \quad \frac{R}{4\pi G} \int_I S(\psi) d\sigma \approx 2.0 \text{ meters/milligal}$$

for points in the center of the area. This means that a constant bias that increases only the inner zone anomalies by one milligal would increase the computed geoid height by two meters. A similar bias influencing only the outer zone would lower the height by the same amount.

The "reconciliation" adjustment described in section 6.4 insures compatibility of the inner field and outer field. In addition to introducing the effect of satellite observations on the terrestrial anomaly field, this adjustment removes differences between the inner and outer fields that might arise from minor inconsistencies in the definition of the anomalies. The significance of this reconciliation can be judged by reference to Figure 11. The reconciliation adjustment changed the area weighted mean anomaly over the inner zone by 2.6 milligals. This mean anomaly cannot be used directly with the result of equation (7.4) to determine an effect on geoid height since that relation assumes a constant change over the area. It does, however, indicate the general magnitude of the influence.

#### 7.2.3 Computation of The Comparison Gravimetric Geoid

The second integral in equation (7.1) was evaluated using the adjusted  $5^\circ \times 5^\circ$  mean anomaly set given in Appendix C converted to the GRS 67. The inner zone area shown in Figure 13 was excluded from this computation. The geoid heights were computed in the test area using the outer zone anomalies at a spacing of  $2^\circ$  in latitude and longitude. Linear interpolation was then used to obtain geoid heights at each degree intersection of latitude and longitude. This procedure was used to reduce the computer time required and is justified since the contribution of the outer zone is a slowly varying smooth function.

The first integral in equation (7.1) was evaluated at each degree intersection in the test area using the reconciled  $1^\circ \times 1^\circ$  GRS 67 mean anomaly set

for the inner zone shown in Figure 13. The contributions from the two zones were then added to obtain the geoid heights at the grid intersections. These geoid heights were used to draw a one meter contour interval map of the comparison area which is shown as Figure 14. This geoid is the comparison standard against which a point mass geoid will be evaluated. It is computed using conventional methods from gravity anomaly data that is consistent with Rapp's (14, 14) spherical harmonic set. It can logically be considered to be a more detailed representation of the same anomalous potential that gave rise to the (14, 14) set of spherical harmonic coefficients. Figure 15 shows a geoid computed by evaluating equation (3.29) with the (14, 14) set of coefficients at the same 270 grid intersections used to obtain the geoid shown in Figure 14. These common points were used for a numerical comparison of the two surfaces.

The mean geoid height at the 270 points from the Stokes' solution was 0.17 meters less than the mean height from the spherical harmonic solution. The root mean square difference between the two solutions, determined through the 270 grid points is  $\pm 1.77$  meters. The seventeen centimeter mean difference between the two surfaces is not considered significant. The close agreement of these mean differences, in fact, lends verification to the argument presented in section 5.3 regarding the equivalency of the means of spherical harmonic representation and true functions when taken over areas of appropriate size.

The  $\pm 1.77$  root mean square difference between the two surfaces is a

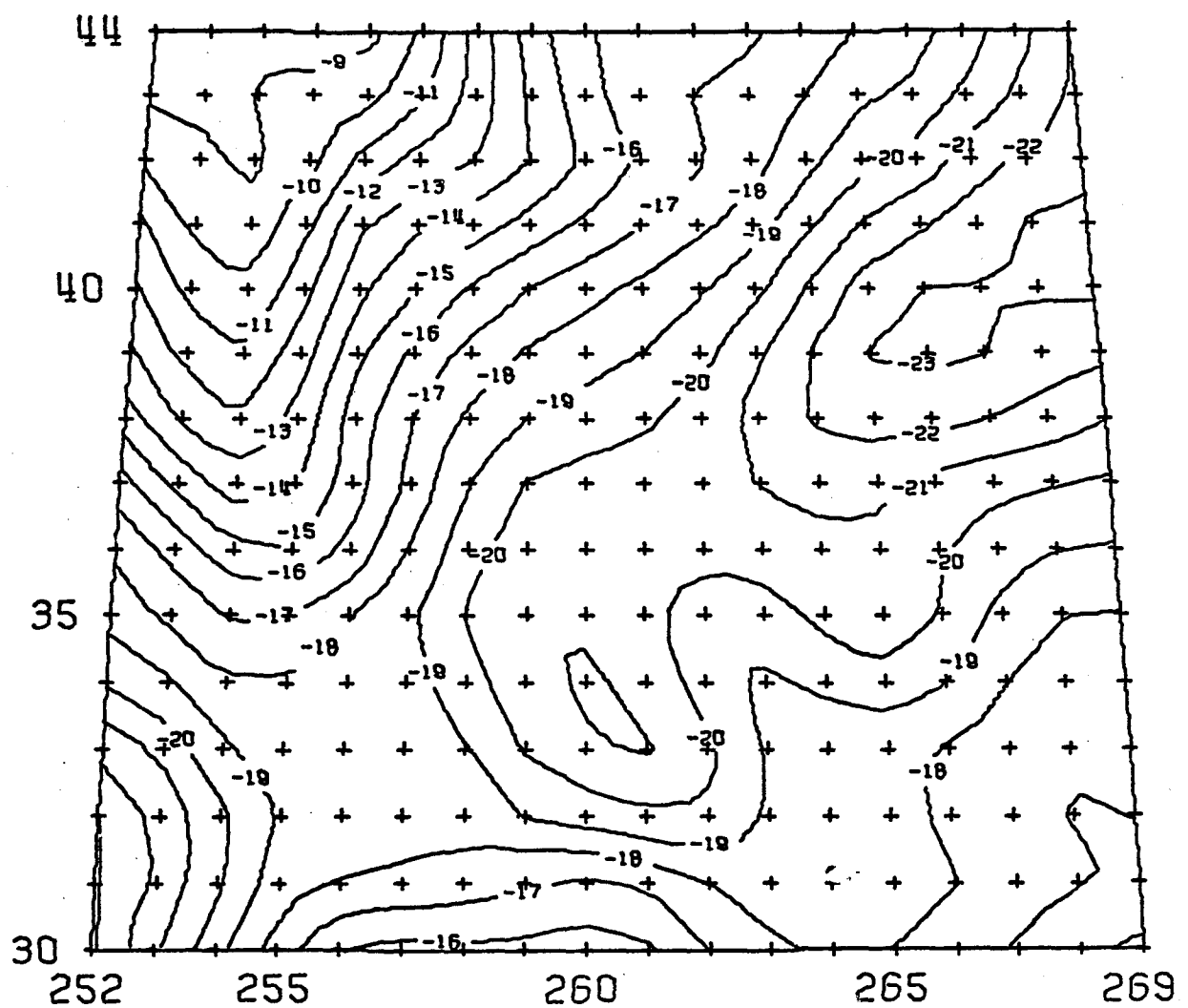


Figure 14  
Geoid from Stokes' Equation

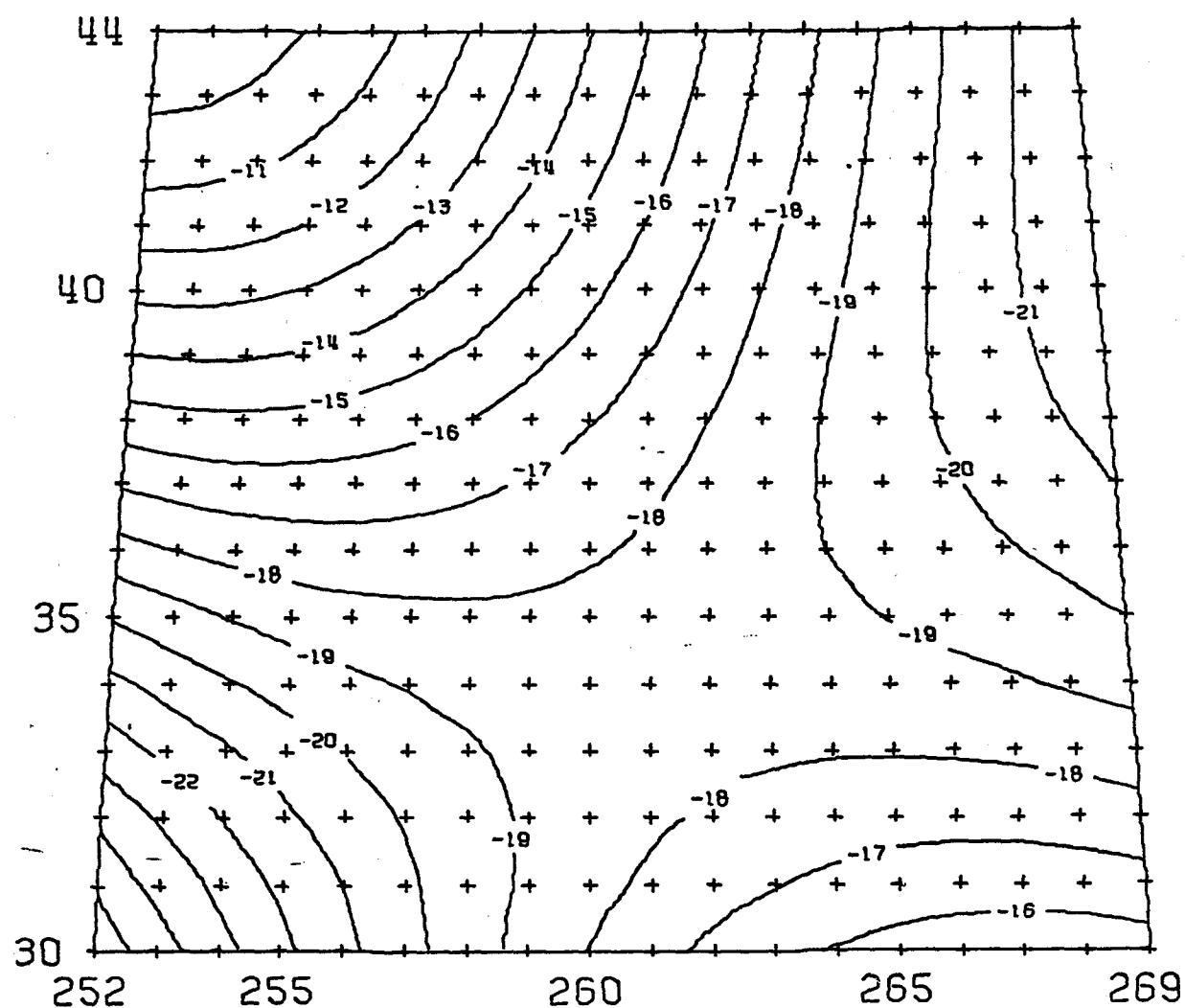


Figure 15  
Geoid from Spherical Harmonic Coefficients

measure of the additional detail in the Stokes' solution that is smoothed out in the spherical harmonic solution.

Rapp has reported the results of similar comparisons of geoids obtained through Stokes' equation and spherical harmonics [Rapp, 1967b, 1968b, 1969b]. All of his published comparisons exhibit much greater difference between the mean geoid heights obtained by the two methods than was found in this study. In a comparable computation covering the same area, using the same basic anomaly fields and the same spherical harmonic coefficients, he obtained [Rapp, 1968c]

Difference in Mean Geoid Height (Stokes - Spherical Harmonics)	-4.0 meters
RMS Difference	$\pm 4.5$ meters

This root mean square difference would be reduced to  $\pm 2.0$  meters if the constant mean difference were removed.

Rapp's procedures differed from those used in this investigation primarily in that he did not "reconcile" his inner and outer fields. He did insure that the gravity anomalies in the two fields were referred to the same normal gravity formula, but he accepted the unadjusted terrestrial  $1^\circ \times 1^\circ$  mean anomaly values as being compatible with the adjusted outer field. This has been the usual method of combining terrestrial and satellite data and has been used by Mather [1968] and Siebenhüner[1969].

The Mather data shows discrepancies similar to those quoted by Rapp [Rapp, 1968b]. It seems clear that these inconsistencies between the Stokes'

and spherical harmonic geoids can be traced directly to the use of inner zone mean anomalies that are not consistent with the spherical harmonic coefficients.

#### 7.2.4 Comparison with an Astrogeodetic Geoid

The gravimetric geoid described in the preceding section is the proper surface to use in evaluating the success of point mass computations as a method of describing the geopotential field. Both a point mass geoid and the conventional geoid obtained by Stokes' equation can be obtained from identically defined gravity fields so that discrepancies between the resulting geoids can be attributed solely to the computational method. Agreement of the two solutions reveals nothing, however, about the absolute accuracy of the geoids. It is not the intent of this study to argue that the gravimetric geoid developed as a comparison standard is the best geoid for central United States. It does seem appropriate, however, to attempt to demonstrate that this geoid is not inconsistent with other available information on the geoid in the test area.

An entirely independent check on the local features of the detailed gravimetric geoid can be obtained by comparing this surface with the U. S. Army Map Service Chart "Geoid Contours in North America" (AMS SN701593). This chart, which gives astrogeodetic contours referred to the 1927 North American Datum, is described by Fischer et al. [1967].

The gravimetric equipotential surface shown in Figure 14 is a free air co-geoid expressed as undulations with reference to a mass centered mean earth ellipsoid. An astrogeodetic surface in a true geoid expressed as undula-

tions measured with respect to a reference datum. In theory, even if the astrogeodetic geoid heights are precisely transformed to heights measured with respect to the mean earth ellipsoid, the gravimetric and astrogeodetic heights at common points will differ by the indirect effect that distinguishes the co-geoid from the geoid. In actuality, this effect, at least in areas of moderate topography is too small to significantly influence a comparison of astrogeodetic and free air gravimetric undulations [Mather, 1970; Heiskanen and Moritz, 1967, p. 146]. A comparison of a gravimetric and an astrogeodetic geoid can therefore be accomplished if transformation parameters can be found to relate the astrogeodetic and gravimetric reference ellipsoids.

Various sets of parameters can be used to accomplish this transformation. A discussion of some of these sets is given by Badekas [1969]. If we assume that the axes of the reference ellipsoid specified by the geodetic datum are parallel to the axes of the mean earth ellipsoid, a convenient set of transformation parameters is given by:

$$\Delta X = X_M - X_{AG}$$

$$\Delta Y = Y_M - Y_{AG}$$

$$\Delta Z = Z_M - Z_{AG}$$

$$\Delta f = f_M - f_{AG}$$

$$\Delta a = a_M - a_{AG}$$

In these definitions, the subscripts M and AG refer to the mean earth ellipsoid and astrogeodetic datum ellipsoid respectively, f is the ellipsoid flattening, and a, the equatorial radius. The subscripted Cartesian coordinates X, Y, Z

refer to identical points evaluated in the two coordinate systems.

Under the assumption of parallel axes, the differences  $\Delta X$ ,  $\Delta Y$ , and  $\Delta Z$  are constant throughout space and are identical to the vector separating the two ellipsoid centers. Using these parameters, the astrogeodetic undulations,  $N_{AG}$ , referred to a given datum, may be transformed to undulations,  $N_{TAG}$ , referred to the mean earth ellipsoid by the relation [Rapp, 1969d]:

$$(7.6) \quad N_{TAG} = N_{AG} + \cos\varphi \cos\lambda \Delta X + \cos\varphi \sin\lambda \Delta Y + \sin\varphi \Delta Z \\ - (1-e_{AG}^2 \sin^2\varphi)^{\frac{1}{2}} \Delta a + \frac{a_{AG}(1-f_{AG})}{(1-e_{AG}^2 \sin^2\varphi)^{\frac{1}{2}}} \sin^2\varphi \Delta f$$

The transformed undulations  $N_{TAG}$  are then comparable to the gravimetric undulations  $N_G$  so that an adjustment to determine the orientation parameters can be based on the mathematical structure:

$$(7.7) \quad N_G - N_{TAG} = 0$$

Ideally, both  $N_G$  and  $N_{AG}$  should be treated as stochastic quantities, and the adjustment accomplished accordingly. In this case, covariance matrices could not be obtained for either set of data so identity weight matrices were assumed for both and the quantities  $(N_G - N_{AG})$  were treated as simple observations.

The comparison test area was considered to be too small to permit a meaningful determination of  $\Delta a$  and  $\Delta f$ . Current estimates of these values were therefore held fixed in the adjustment. The  $\Delta f$  value was based on the assumption that the flattening of the mean earth ellipsoid was the same as that for the GRS 67. Current values for the best estimate of the equatorial radius of

a mean earth ellipsoid are, however, consistently smaller than that given for GRS 67. Several recent estimates have clustered near 6378140, so this figure was used in determining  $\Delta a$  [Veis, 1968; Moritz, 1968; Fischer, 1968; Rapp, 1969b]. It should be noted that  $\Delta a$  and the shifts  $\Delta X$ ,  $\Delta Y$ , and  $\Delta Z$  are highly correlated for small area solutions and the degree of fit of the surfaces is practically independent of the choice of  $\Delta a$ .

The values  $N_{AG}$  used in the adjustment were obtained by interpolating spot geoid heights from the Army Map Service Chart "Geoid Contours in North America" at each of the 270 points in the comparison test area where gravimetric geoid heights had been computed.

The results of the adjustment were as follows:

RMS Residual Difference ( $N_G - N_{TAG}$ )	1.25 meters
$\Delta X$	9.6 meters
$\Delta Y$	140.2 meters
$\Delta Z$	184.2 meters

The astrogeodetic geoid conforming to the AMS geoid chart but oriented in accordance with the above listed parameters is shown in Figure 16. The  $35^\circ$  parallel and  $95^\circ$  meridian astrogeodetic profiles that constitute the fixed framework of this geoid are indicated on the figure. This area around these primary strongly determined profiles should constitute a reliably determined portion of the North American astrogeodetic geoid.

The root mean square residual difference between the astrogeodetic and

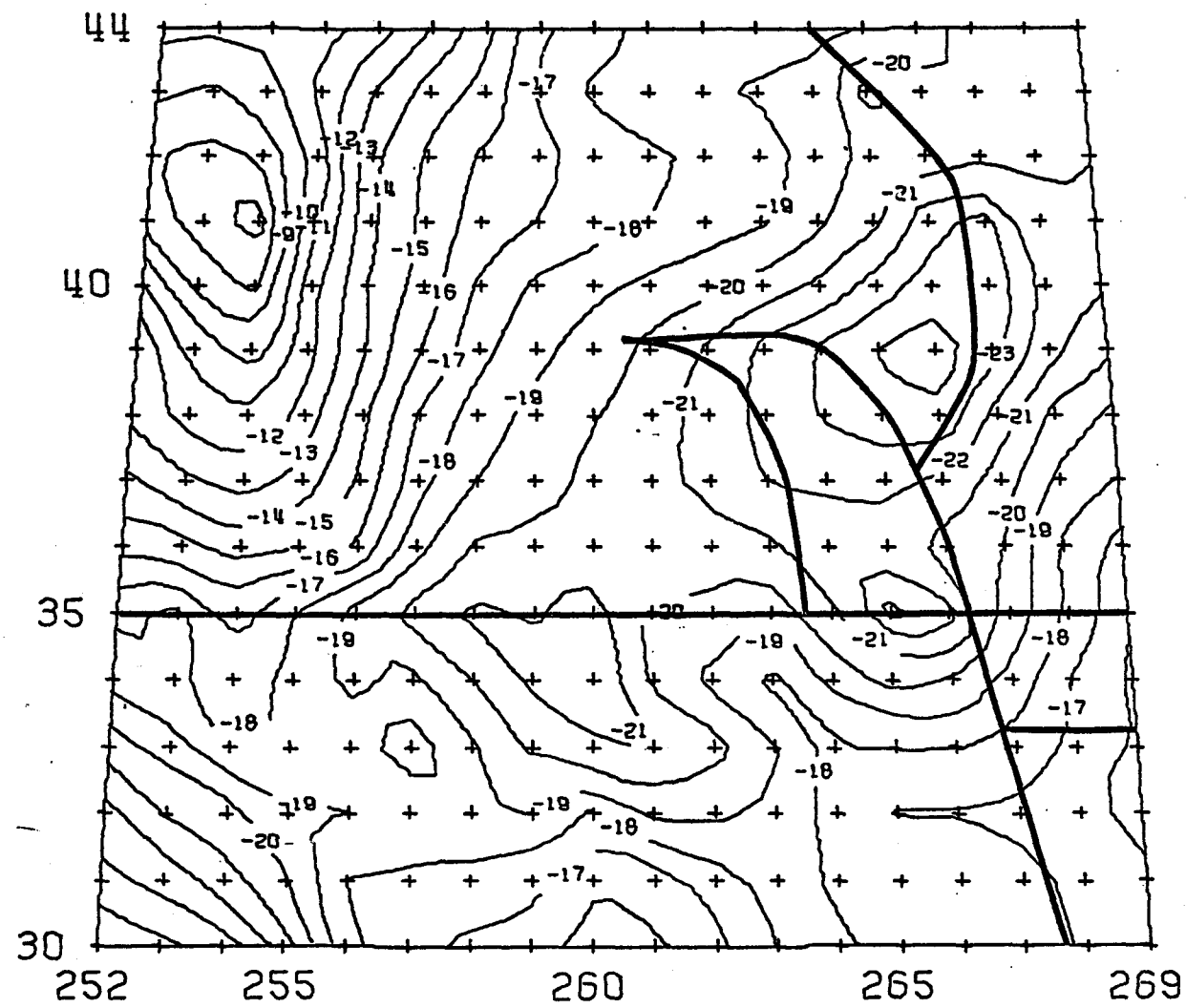


Figure 16  
Astrogeodetic Geoid;  $a = 6378140$ ,  $1/f = 298.247$

gravimetric surfaces is surprisingly small. This residual must absorb the local effects of errors in the mean gravity anomalies; approximations in the Stokes' integrations; errors in the 1927 NAD; errors in astronomic observations; the approximations of astrogeodetic computations; the indirect effect between the geoid and co-geoid and effects arising from different degrees of smoothing inherent in the two computational procedures. It must clearly be noted that these residual differences reflect only the local correlations of the two surfaces. The astrogeodetic geoid has been rotated and translated into a position that yields the best least squares fit to the gravimetric surface in the test area. For example, errors in the distant gravity field that change the slope or height of the entire gravimetric surface would simply result in changes in the orientation parameters  $\Delta X$ ,  $\Delta Y$ , and  $\Delta Z$  without increasing root mean square residual difference. For this reason, the standard errors of these parameters, based on the unsophisticated weighting system used would be meaningless. (The standard errors based solely on internal consistency were:  $\sigma_{\Delta X} = 0.9$  meters,  $\sigma_{\Delta Y} = 0.3$  meters,  $\sigma_{\Delta Z} = 0.5$  meters.)

It is difficult to compare the datum shifts obtained in this solution with other published datum shifts for the 1927 North American Datum. The shifts obtained in this study give a best fit for a portion of the datum in the central United States. Other solutions attempt to define mean shifts that apply to the entire datum. The internal discrepancies in the 1927 NAD are large enough that a best fit for a specific area could deviate very significantly from a mean

fit [Mueller, Reilly and Schwarz, 1969]. Typical examples of mean datum shifts as given by Veis [1968] and Fischer [1968] are shown in Table 14.

Table 15

## Mean 1927 NAD Datum Shifts

Investigator	$\Delta X$	$\Delta Y$	$\Delta Z$	Remarks
Fischer (1)	+ 8	+172	+183	Based on Doppler data. $a = 6378145$
Fischer (2)	-43	+106	+165	Based on Rapp's data. $a = 6378160.$
Veis	-26	+155	+185	Based on Baker Nunn positions. $a = 6378142$

The Fischer solutions are based on 303 data points spaced throughout the extent of the 1927 NAD. The Veis solution was based on comparison of the 1927 NAD and satellite positions of stations in New Mexico, Florida, and Alberta, Canada. Considering the spread of these mean datum shift solutions, the results of the solution presented here for the central U. S. are certainly reasonable possibilities.

By converting  $\Delta X$ ,  $\Delta Y$ , and  $\Delta Z$  datum shifts to deflections by means of Molodenskii's abridged equations [Lerch et al., 1969], the solutions previously discussed may be compared in terms of deflections at the origin.

Table 16

## Comparison of Deflections at 1927 NAD Origin

Investigator	$\xi$	$\eta$
Needham	.0"	+.4"
Veis	-.2	+1.6"
Fischer (1)	-.6	+ .6"
<u>Fischer (2)</u>	<u>+1.4</u>	<u>+1.9</u>

It is interesting to note that if a solution of the type designated as Fischer (2) (based on Rapp's (14, 14) geoid) is re-accomplished considering only data points in the test area, the deflections change to  $\xi = -0.1''$  and  $\eta = 0.0''$ . The deflection values seem to be as correlated with the portion of the datum considered as they are with the method of determination.

These results indicate that the gravimetric comparison geoid agrees remarkably well in detail with an astrogeodetic geoid. The low root mean square difference between the two surfaces is an indication of high correlation between the local features of the two surfaces. This is also evident from a comparison of Figures 14 and 16. The agreement between the gross features of the surfaces is more difficult to establish but the relationship found between the two surfaces does not seem to be controverted by external evidence from other solutions. A consideration of the various datum shift solutions does raise the possibility that mean datum shifts defined for all parts of large datums may be less useful than regional datum shifts.

### 7.3 The Gravity Disturbance Component Standard

#### 7.3.1 General

The computation of gravity disturbance components at high elevations is a relatively new facet of geodesy that has become important because of missile and space applications. Several methods for such computations are available. Reviews of these methods are given by Mueller [1966] and Heiskanen and Moritz [1967]. The three primary methods are:

- a) Direct integration method;
- b) Coating method;
- c) Upward continuation method.

The input data required for the three methods are different. The direct method requires free air anomalies; the coating method requires free air anomalies and free air co-geoid heights; and the upward continuation method requires anomalies and the deflections of the vertical on the reference surface. The direct method is computationally most complicated; the coating method less complicated and the upward continuation method, the least complicated. Analysis of truncation errors, carried out in the manner discussed in Chapter 4, show that the data fields must extend the furthest for the direct method, a lesser distance for the coating method, and the least distance for the upward continuation method to attain a specified root mean square accuracy. These latter observations on computation complexity and field truncation are somewhat illusory since they pre-suppose the existence of undulation and deflection values in the data area. In practice, these values would only be available as a result of additional computations using anomalies over a much wider area. In essence, the coating and upward continuation

methods are two step methods and the direct integration method is a one step method. All three methods ultimately depend on a worldwide knowledge of the free air gravity anomaly field. The direct integration approach seems to be the most straightforward method of using the available data to establish a comparison standard, and was therefore adopted for this computation.

### 7.3.2 The Direct Integration Method

The direct integration method of computing the disturbance components of gravity has been discussed thoroughly by Hirvonen and Moritz [1963]. The procedure followed in this investigation is based directly on their work. The details of the method will not be repeated here except to outline the derivation of the basic equations.

The anomalous potential  $T_p$  at a point P in the space external to the equipotential surface  $\sigma$  is given by the formula of Pizzetti.

$$(7.7) \quad T_p = \frac{R}{4\pi} \iint_{\sigma} \Delta g S(r_p, \psi) d\sigma$$

In this equation, R is the mean radius of the earth,  $r_p$  is the geocentric radius to the computation point P and the kernel is the extended Stokes' Function.

$$(7.8) \quad S(r_p, \psi) = \frac{2R}{\ell} + \frac{R}{r_p} - \frac{3R\ell}{r_p^2} - \frac{R^2}{r_p^2} \cos\psi \left( 5 + 3\ell n \frac{r_p - R\cos\psi + \ell}{2r_p} \right)$$

where:  $\ell = (r_p^2 + R^2 - 2Rr_p\cos\psi)$

$\psi$  = geocentric angle between P and  $d\sigma$

Expression (7.7) can be differentiated with respect to length units in orthogonal spherical coordinates at point P to obtain the gravity disturbance

components.

$$(7.9) \quad \delta r = \frac{R}{4\pi} \iint_{\sigma} \Delta g \frac{\partial S(r_p, \psi)}{\partial r} d\sigma$$

$$(7.10) \quad \delta \varphi = \frac{R}{4\pi} \iint_{\sigma} \Delta g \frac{\partial S(r_p, \psi)}{\partial r} d\sigma$$

$$(7.11) \quad \delta \lambda = \frac{R}{4\pi r_p \cos \varphi} \iint_{\sigma} \Delta g \frac{\partial S(r_p, \psi)}{\partial \lambda} d\sigma$$

Using the chain rule of differentiation and the identities [Heiskanen and Moritz, 1967, p. 113]:

$$(7.12) \quad \frac{\partial \psi}{\partial \varphi} = -\cos \alpha$$

$$(7.13) \quad \frac{\partial \psi}{\partial \lambda} = -\cos \varphi' \sin \alpha$$

where  $\alpha$  is the azimuth from  $p$  to  $d\sigma$ , these expressions can be transformed to:

$$(7.14) \quad \delta r = \frac{R}{4\pi} \iint_{\sigma} \Delta g \frac{\partial S(r_p, \psi)}{\partial r} d\sigma$$

$$(7.15) \quad \delta \varphi = \frac{-R}{4\pi r_p} \iint_{\sigma} \Delta g \frac{\partial S(r_p, \psi)}{\partial \psi} \cos \alpha d\sigma$$

$$(7.16) \quad \delta \lambda = \frac{-R}{4\pi r_p} \iint_{\sigma} \Delta g \frac{\partial S(r_p, \psi)}{\partial \psi} \sin \alpha d\sigma$$

Differentiating (7.8):

$$(7.17) \quad \frac{\partial S(r_p, \psi)}{\partial r} = \frac{-R(r_p^2 - R^2)}{r_p^3} - \frac{4R}{r_p^2} - \frac{R}{r_p^2} + \frac{6R\ell}{r_p^3}$$

$$\frac{+R^2}{r_p^3} \cos \psi \left( 13 + 6 \ln \frac{r_p - R \cos \psi + \ell}{2r_p} \right)$$

$$(7.19) \quad \frac{\partial S(r_P, \psi)}{\partial \psi} = \sin \psi \left[ -\frac{2R^2 r_P}{\ell^3} - \frac{6R^2}{r_P \ell} + \frac{8R^2}{r_P^2} \right. \\ \left. + \frac{3R^2}{r_P^2} \left( \frac{r_P - R \cos \psi - \ell}{\ell \sin^2 \psi} + \ln \frac{r_P - R \cos \psi + \ell}{2r_P} \right) \right]$$

Equations (7.14) through (7.18) form the basis for the computation of gravity disturbance components. A well-documented computer program exists for the practical evaluation of these equations. The quite intricate details of efficiently and economically accomplishing the required numerical integrations are fully described by Rapp [1966]. This program was used without modification to establish the comparison standard for the gravity disturbance computations.

### 7.3.3 Computation of the Gravity Disturbance Component Standard

Hirvonen and Moritz suggested regions surrounding the computation point in which mean anomaly blocks of various sizes should be used to insure that integration errors are minimized [1963]. These recommendations were discussed in Chapter 5 and shown in Table 10. The anomaly sets available for this investigation, which are shown in Table 12, satisfy these recommendations for computations carried out in a degree square centered on 37° N, 260° 5W. For the comparison standard, vertical trajectory origins were established at nine evenly spaced points within this area. The components of the gravity disturbance were computed at points along these trajectories using all of the GRS 67 mean anomaly data shown in Table 12. The elevations of the 65 points computed ranged from 20 to 1500 kilometers. With the exception of substituting 30 minute for 20 minute mean anomalies, these

computations met or exceeded the recommendations of Hirvonen and Moritz  
and should be acceptable for defining conventional comparison standards.

## CHAPTER 8

### POINT MASS COMPUTATIONS AND COMPARISONS

#### 8.1 Computation of a Point Mass Set to Describe the Potential Field in the Central United States

The 1000  $1^{\circ} \times 1^{\circ}$  mean free air Spherop 14 anomalies described in Chapter 6 were used to determine a point mass set modeling the anomalous potential field in the comparison test area. This computation was done in accordance with the general procedures outlined in Chapter 5. Details of the computation are given in the following paragraphs.

As was discussed in Chapter 4, the root mean square error in the determination of geoid height or anomalous potential is an asymptotically decreasing function of the size of the anomaly field considered in that determination. When the anomalies are based on a Spherop 14 system, this decrease is rapid until the angular radius of the anomaly field around the computation point reaches about  $13^{\circ}$ . The entire  $25^{\circ} \times 40^{\circ}$  block of mean anomalies should therefore be used to determine a point mass set suitable for representing the anomalous potential in the comparison test area. It would in fact be very desirable to have a larger area of anomalies so that a more extensive point mass set could be developed. Reference to Figures 13 and 6 will show that we can expect significantly larger errors caused by

truncation in the peripheral areas of the comparison test area than in the center of the area. This is unfortunate but unavoidable with the available data. It is a situation that could be expected in most practical applications.

An optimum sized set of point masses to represent  $1000\ 1^\circ \times 1^\circ$  anomalies cannot be determined simultaneously by the computer program written for this investigation. The  $25^\circ \times 40^\circ$  anomaly area was therefore broken up into segments and the point masses were determined as contiguous mass sets in accordance with the system outlined in section 5.5. Two independent solutions were first accomplished. One fit 320 masses at a depth of 100 kilometers in the western half of the anomaly area; the second fit a similar set of masses in the eastern half of the area. The western half of the first mass set and the eastern half of the second mass set were then used as predefined masses in a solution that determined 320 masses in the central half of the anomaly area. These solutions were identical to the hypothetical solutions outlined in section 5.5 and the arrangement of the areas was as shown in Figure 10. The comparison test area fell entirely within the third, centrally located, solution area.

Statistics and descriptive parameters concerning these solutions are shown in Table 17. The combined point mass set from these solutions is given in Appendix F. This set, taken in conjunction with Rapp's (14, 14) coefficients (Appendix B), defines a detailed potential field for the central United States. Using the approximations of section 5.3, which relate the number of defining parameters to mean surface integrals, this set of point masses can be com-

puted to be equivalent in detail to a set of spherical harmonic coefficients extending to about 180<sup>th</sup> degree and order.

Table 17

## Point Mass Solutions Using 1°×1° Mean Anomalies

	West Half of Area	East Half of Area	Central Area
Latitude limits	25°N - 50°N	25°N - 50°N	25°N - 50°N
Longitude limits	240°E - 260°E	260°E - 280°E	250°E - 270°E
No. anomalies used in solution	500	500	500
Mass depth (km)	100	100	100
No. of pre-defined masses	-	-	320
No. of unknown masses determined	320 <sup>b</sup>	320 <sup>b</sup>	320
Mean input anomaly (mgal)	1.20	1.50	1.78 <sup>a</sup>
RMS input anomaly (mgal)	17.89	15.99	17.62 <sup>a</sup>
Mean residual anomaly after fitting masses (mgal)	1.02	1.41	1.28 <sup>a</sup>
RMS residual anomaly after fitting masses (mgal)	7.57	6.23	7.06

<sup>a</sup> Input anomalies have been corrected for predefined masses.

<sup>b</sup> One half of these mass sets were included in the final composite set.

Some effects of the mathematical model used in the least square adjustment can be seen in the statistics of Table 16. It was not possible to define a set of point masses magnitudes in the specified mass locations that would completely satisfy the observed anomalies. The residual root mean square gravity anomalies after adjustment represent the portion of the gravity anomalies that arise from actual mass anomalies that were excluded by the mathematical model. The ratios of the magnitude of input anomalies to residual anomalies shown in Table 16 were characteristic of a number of solutions based on similar geometry that were accomplished during this investigation.

It was also characteristic of all of the solutions that the mean input anomaly and the mean residual anomaly agreed within a fraction of a milligal. This is a logical result of the conditions imposed on the point mass solution. A residual anomaly could be considered as an anomaly defined by subtracting a normal gravity field consisting of the Spherop 14 gravity field based on the GRS 67 supplemented by the field generated by the point masses. The conditions imposed on the solution have maintained a constant mass and nearly constant shape and volume for the earth during the addition of the point masses. The new "normal" field that includes the point mass contributions will therefore have nearly the same mean value over the area as did the original Spherop 14 normal field. A noteworthy consequence of these conditions is that even if the input anomalies have a non-zero mean anomaly over the solution area, the model anomalies or potentials generated from the point mass

set found from these anomalies will not contain zero order components.

The magnitude of the masses shown in Appendix F can be made more meaningful if we consider the influence of a single mass on the geopotential field. For a computation point on the earth's surface 100 kilometers directly above a mass  $M_k$ , the geoid undulation value will be affected by that mass by  $10^{-12} kM_k$  meters. The gravity disturbance at this point would be affected by  $10^{-11} kM_k$  milligals.

### 8.2 A Point Mass Geoid for the Comparison Test Area

The 640 point masses obtained as described in the preceding section were used to determine a geoid for the comparison test area. Geoid heights above the mean earth ellipsoid were computed at the same 270 points that were used to compute the comparison standard geoid. This computation was done as described in section 5.6.8 using equation (5.22). The resulting geoid heights were contoured to produce Figure 17.

The geoid shown in Figure 17 is referred to a mean earth ellipsoid with the flattening of the GRS 67. As can be seen from equation (5.22), the geoid is computed by adding the undulations resulting from point masses to the undulations defined by the (14, 14) spherical harmonic coefficients used as a basis for these computations. The point mass contribution is the detail that is added to the spherical harmonic field. This detail constitutes the difference between the geoid computed from the (14, 14) coefficient set, shown in Figure 15, and the point mass geoid shown in Figure 17. The difference between these two figures is so pronounced as to obscure the nature of this

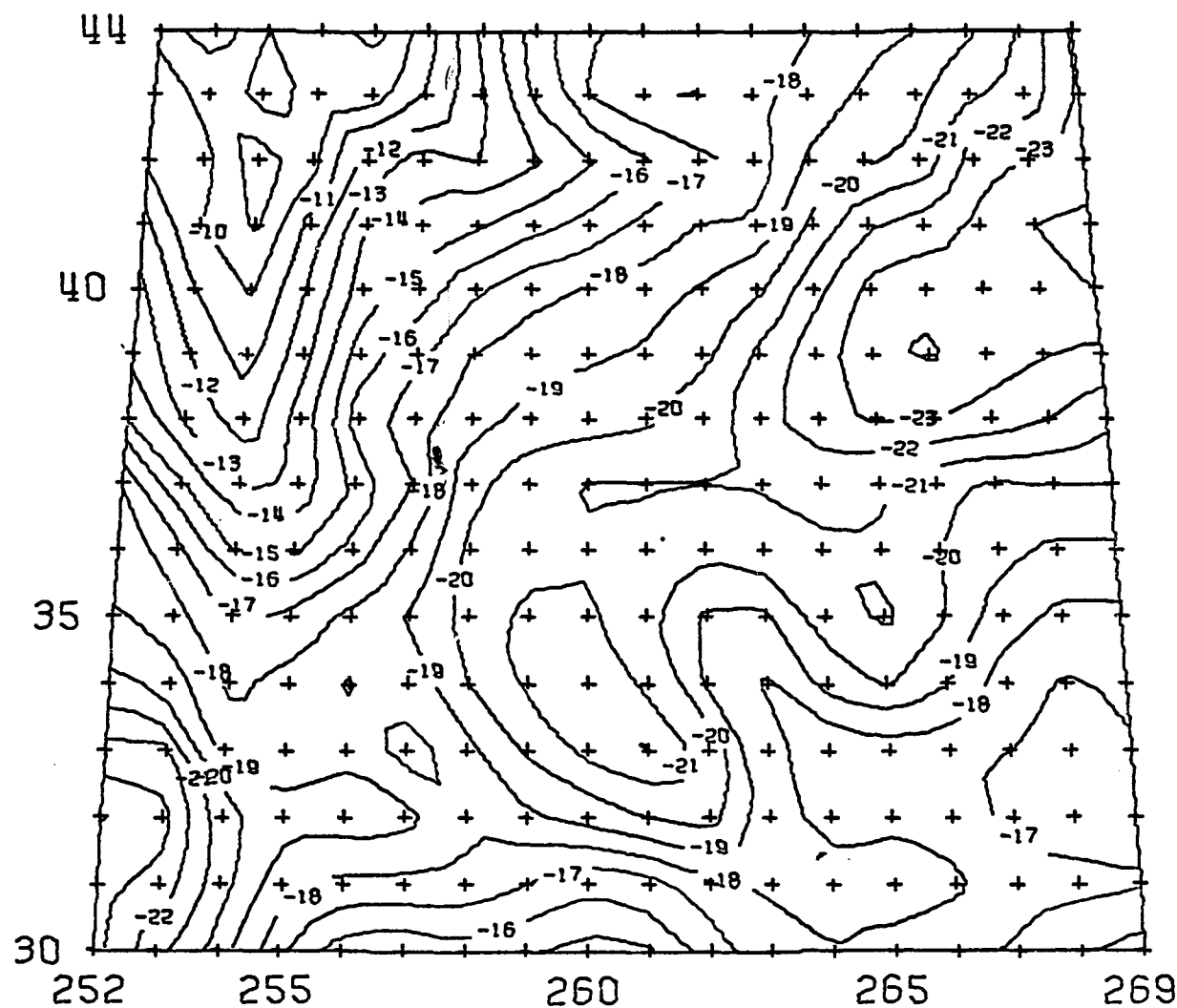


Figure 17  
Point Mass Geoid - 1 Meter Contour Interval

detail. It can be seen more clearly in Figure 18 which shows the contours of the differences between the spherical harmonic and point mass geoids. This figure demonstrates how much of the detail shown in Figure 17 is attributable to the inclusion of point masses in the geopotential model.

The point mass geoid was compared to the standard computed by Stokes' equation in several ways to estimate the success of the technique developed in this investigation.

The differences between the geoid heights computed by the Stokes' equation and point mass technique were formed at the 270 computation points in the comparison area. The mean value of these differences in the sense (Stokes' minus point mass) was 24 centimeters. The root mean square difference was 59 centimeters. This is a threefold improvement over the 1.77 meter root mean square difference between the (14, 14) geoid and the Stokes' comparison geoid, and proves the reality of the detail added by the point mass model.

The maximum difference between the two geoids at any of the points in the area was 2.04 meters. Less than 9 percent of the difference values exceeded 1 meter. The differences are shown graphically in Figure 19. It is apparent that the differences are systematic but the cause is not clear. There may be an imperfect relationship to the absolute geoid height or to the magnitude of the contribution of the point mass set to the anomalous potential. Either functional relationship could produce a pattern of the general type shown. It is entirely possible that no such relationship exists at all and the

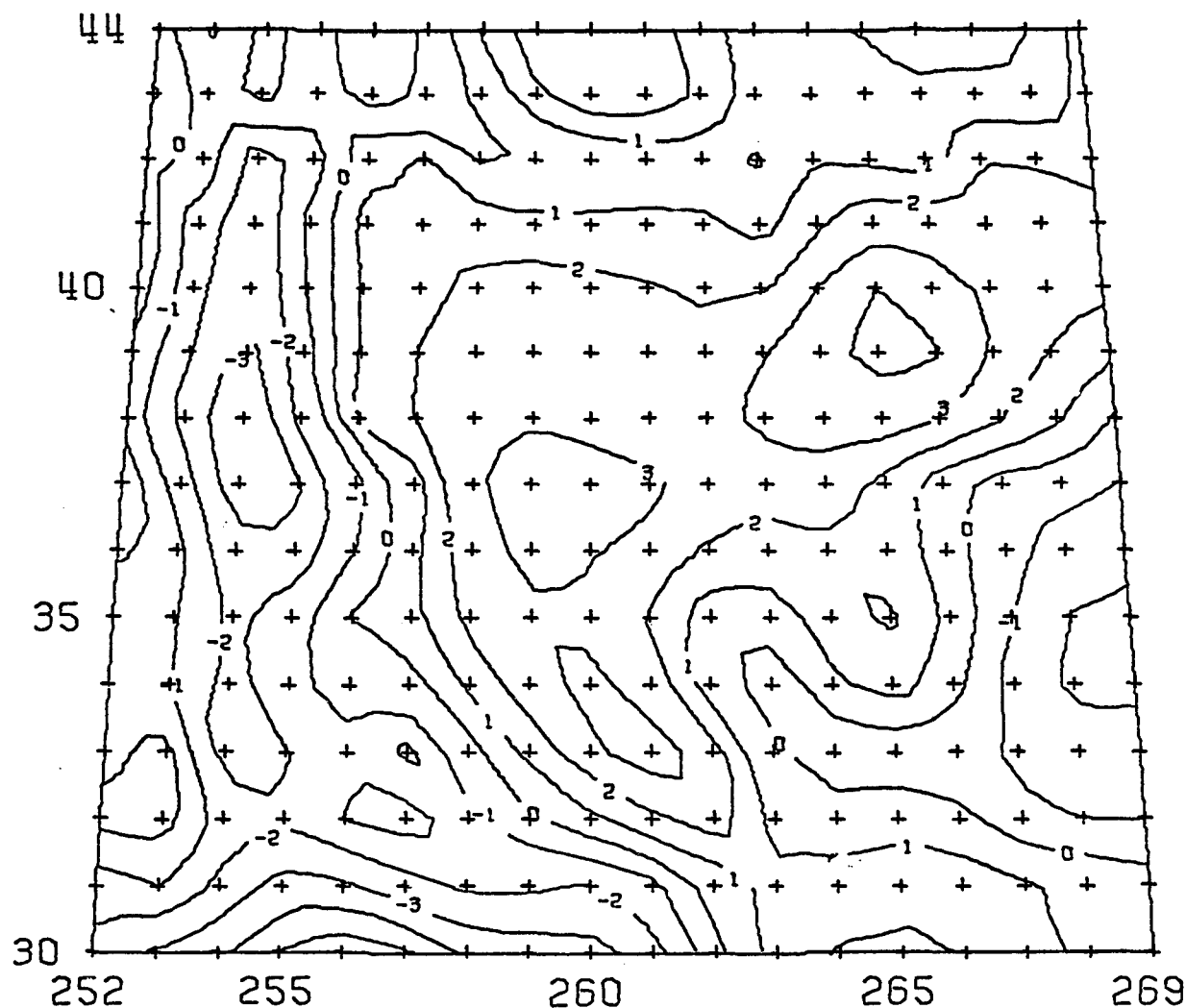


Figure 18  
Geoid Height Difference - (14,14) Spherical Harmonic Minus Point Mass

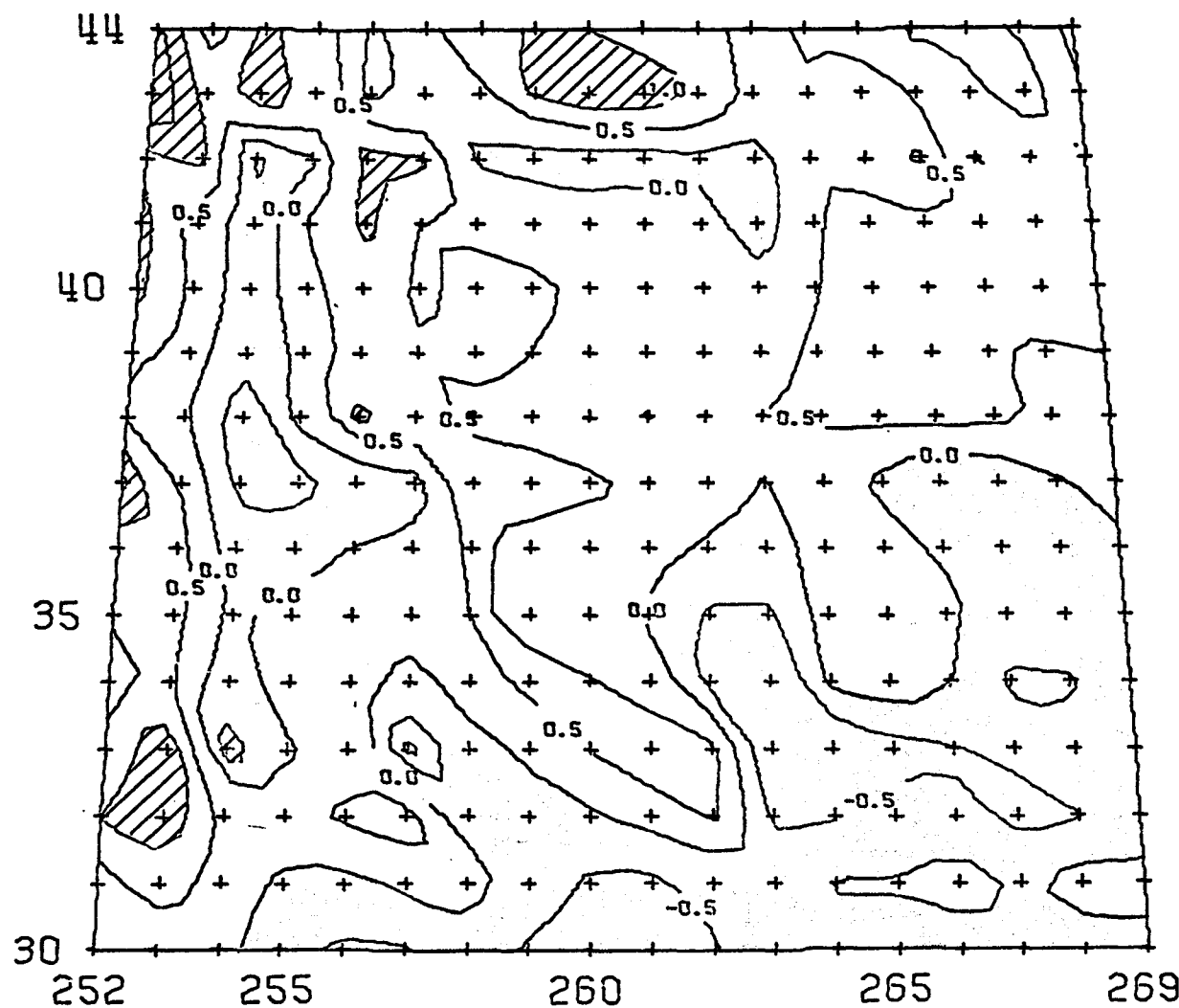


Figure 19  
Geoid Height Difference - Stokes Minus Point Mass

#### LEGEND

Point mass geoid  
above Stokes' geoid



Difference between  
geoids exceeds  
one meter



Contour Interval - 0.5 meters

differences between the two geoids are merely an expression of a position dependent truncation error in the point mass geoid. The differences are certainly compatible with the errors which might be expected from this source.

The distribution of the larger magnitude differences within the area is especially noteworthy. Practically without exception, the larger discrepancies occur on the very border of the comparison test area. In these areas, the average truncation angle to the edge of the anomaly field used to obtain the point masses is significantly less than the truncation angle for the center of the area. As shown in Figure 6, the errors in the point mass solution in these marginal regions should be expected to be larger than in the center of the area. The agreement between the theoretical statistical error estimates of Figure 6 and the actual discrepancies shown in Figure 19 is so good that it must be considered merely fortuitous. It is doubtful if the comparison standard can be considered accurate enough to show that these minor discrepancies have any significant interpretation. This is especially true in the border regions where the area of the available  $1^\circ \times 1^\circ$  mean anomalies was too restricted to allow use of the most desirable block sizes in the numerical integration of the Stokes' equation.

A different approach to the comparison of the point mass and Stokes' geoid was investigated by assuming that both methods estimated the true geoid but were subject to error. The statistical relationship between the two methods of computation was investigated by assuming a linear relationship between the point mass geoidal undulations  $N_{PM}$  and the undulations,  $N_{ST}$ , computed using

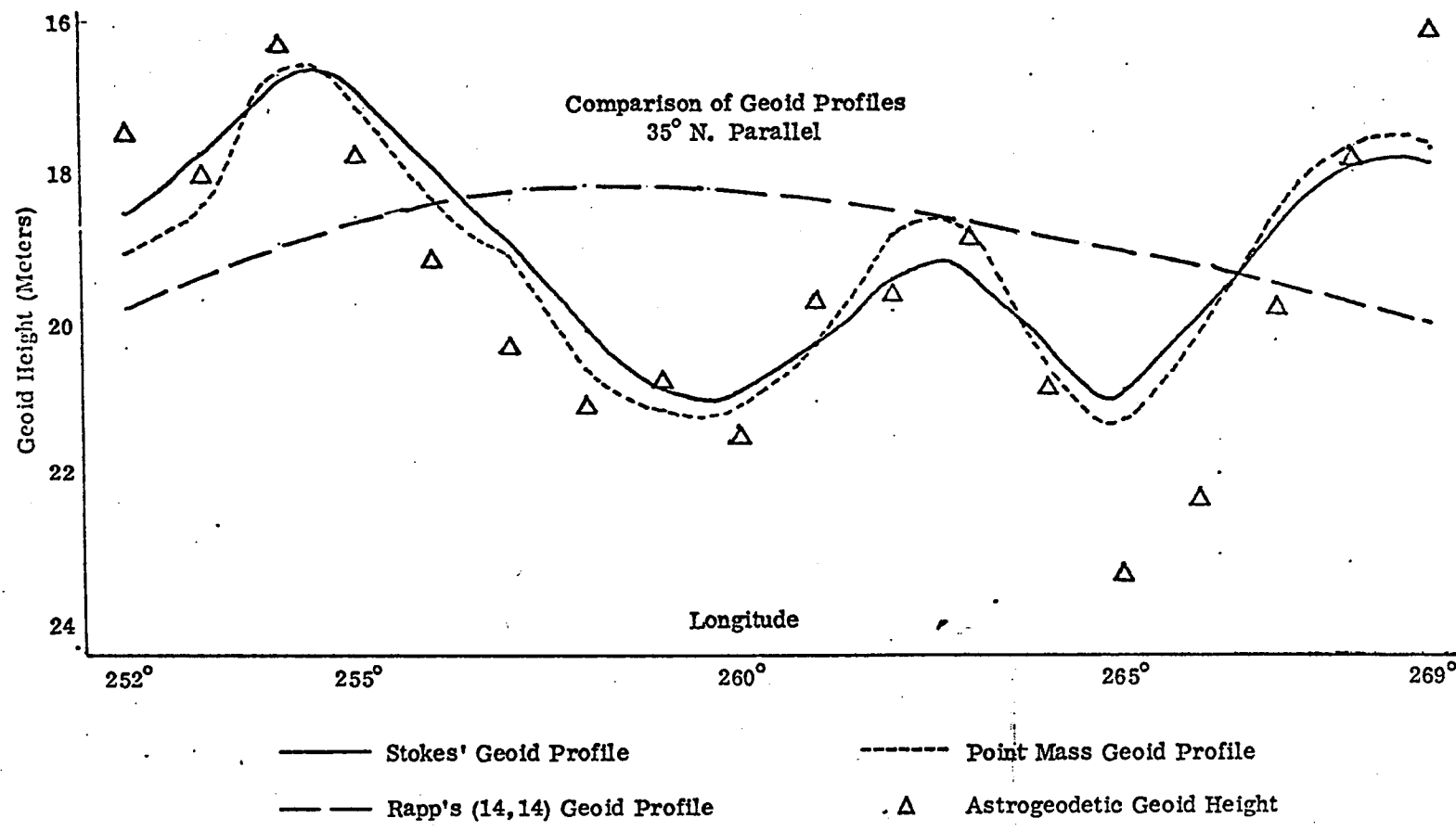


Figure 20

Stokes' equation. This relationship may be expressed as:

$$(8.1) \quad N_{PM} = \beta_0 + \beta_1 N_{ST}$$

Following procedures given by Natrella [1963], the computation points used in the comparison area were used to evaluate the coefficients of this equation with the results:

$$\beta_0 = - .240 \text{ meters}$$

$$\sigma_{\beta_0} = .165$$

$$\beta_1 = 1.000$$

$$\sigma_{\beta_1} = .009$$

The correlation coefficient between  $N_{PM}$  and  $N_{ST}$  was 0.989. On the basis of this data, it would not be possible to demonstrate any statistically significant differences related to geoid height between the two solutions even though one might suspect a systematic difference from an examination of Figure 19.

A last evaluation of these results was made by comparing geoid profiles along the 35<sup>th</sup> parallel of latitude. This parallel was selected to take advantage of the data provided by the 35<sup>th</sup> parallel geoid section [Rice, 1967], and because both the point mass and Stokes' solution should be reliable in this central area. The profiles from the Stokes' solution, the point mass solution, and Rapp's (14, 14) solution are shown in Figure 20. The astrogeodetic spot heights shown are compatible with Figure 16 and were obtained by rotating the astrogeodetic geoid to fit the Stokes' geoid as described in section 7.2.4.

The agreement between these profiles is considered to be entirely satisfactory. The point mass profile fits the astrogeodetic points slightly better than does the Stokes' profile. This may be an indication that the Stokes'

profile is more heavily smoothed than the point mass and astrogeodetic profiles but the data is not extensive enough to draw any firm conclusions. As might be expected, both gravimetric geoids have smoothed the detail in the vicinity of the very localized geoid low shown at 265°E on the astrogeodetic profile.

It is encouraging that all of the geoids agree so closely in an area where the predictable errors in each method may be expected to be small.

On the basis of all of the available evidence, I conclude that it is possible to form a geopotential model for an area like the central U. S., based on point masses, that is essentially equivalent to one based on  $1^\circ \times 1^\circ$  mean anomalies. The differences between the two models is insignificant when compared to absolute errors arising from deficiencies in the worldwide gravity data set.

### 8.3 Computation of Point Mass Sets for Gravity Disturbance Component Computation

Point mass sets providing the detail desired for the gravity disturbance component computation were developed by superimposing shallower point mass sets on the 640 point mass set obtained from the  $1^\circ \times 1^\circ$  mean anomalies. A set of point masses at 50 kilometer depth was first determined in the area of the  $30' \times 30'$  mean anomalies described in Table 12. A set of point masses at a depth of 10 kilometers was then determined using the  $5' \times 5'$  anomalies in an area  $2^\circ$  on a side that was centered on the point  $37^\circ\text{N}$ ,  $260^\circ.5\text{E}$ . The procedures used are described in section 5.4. Table 18 summarizes these solutions. The mass sets are listed in Appendix G.

The areas represented by these mass sets are shown in relation to the test trajectory foot points in Figure 21. The background contours in this figure represent a geoid computed from the 1201 mass points that make up the superposed mass sets. This geoid area has the same mean geoid height as the comparable area shown in Figure 17. The root mean square difference in the geoid height between the two surfaces, compared at 323 points, was 0.29 meters. This difference represents the additional detail added by the superposed mass sets.

#### 8.4 Computation of Gravity Disturbance Components from Point Masses

The anomalous potential of a spherical harmonic and point mass model such as has been developed is given by:

$$(8.2) \quad T_p = \frac{kM}{r} \left[ \sum_{n=2}^{14} \left( \frac{ae}{r} \right)^n \sum_{m=0}^n (C_{nm}^* \cos m\lambda + S_{nm} \sin m\lambda) P_{nm} (\sin \varphi') \right] \\ + \sum_j \frac{kM_j}{d_{pj}}$$

The gravity disturbance components equivalent to those determined for the comparison standard are found by differentiating this equation with respect to length units in orthogonal directions at the point p just as equation (7.7) was differentiated. The derivatives of the spherical harmonic term in equation (8.2) are:

$$(8.3) \quad \delta_{rSH} = \frac{kM}{r^2} \sum_{n=2}^{14} (n+1) \left( \frac{ae}{r} \right)^n \sum_{m=0}^n (\bar{C}_{nm}^* \cos m\lambda \\ + \bar{S}_{nm} \sin m\lambda) \bar{P}_{nm} (\sin \varphi')$$

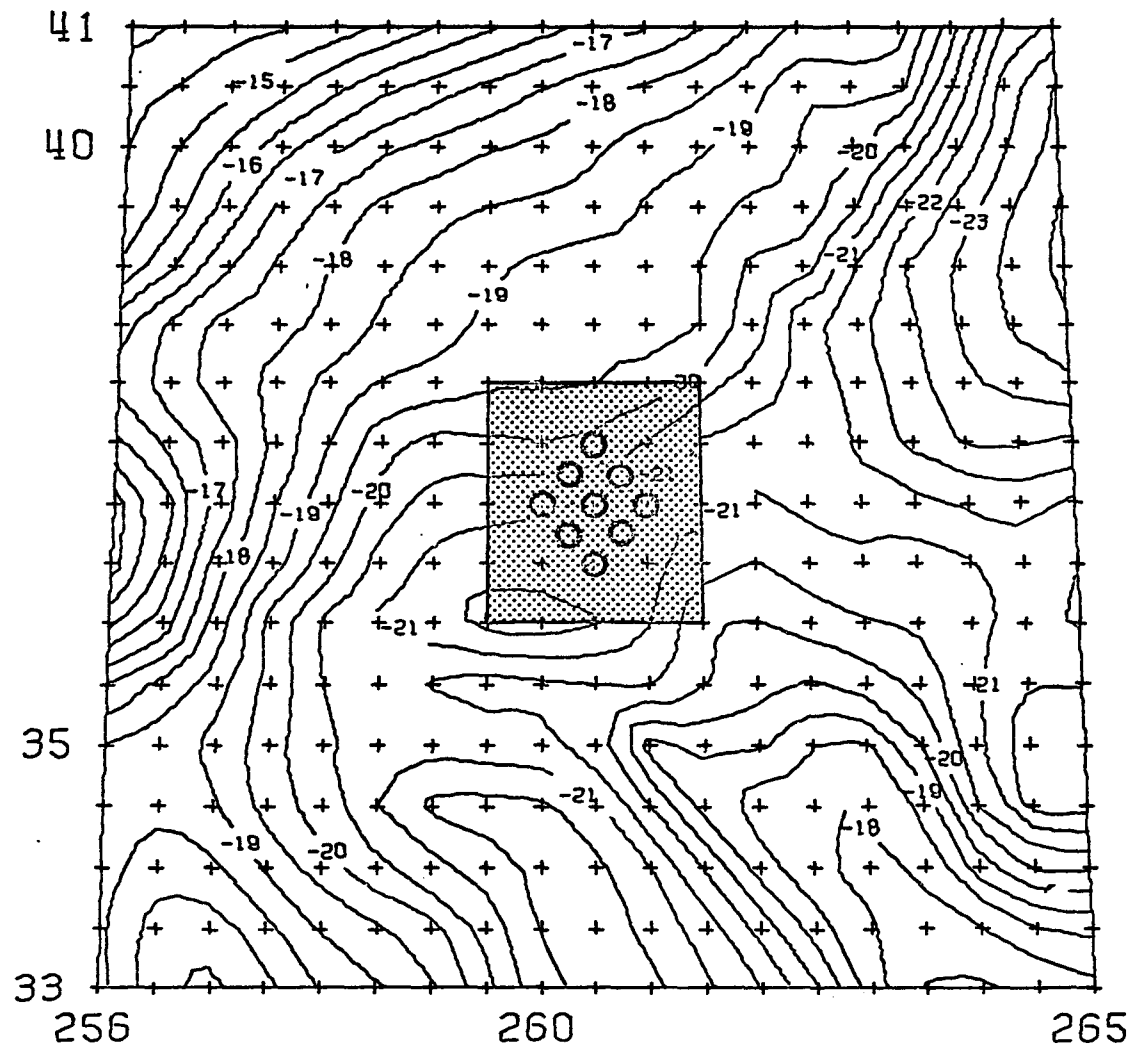


Figure 21  
Superposed Mass Set Area and Trajectory Foot Points

LEGEND

- Trajectory Foot Point
- Area of 10 Km Masses

$$(8.4) \quad \delta_{\varphi'} \text{SH} = \frac{kM}{r^2} \sum_{n=2}^{14} \left( \frac{a_e}{r} \right)^n \sum_{m=0}^n (\bar{C}_{nm}^* \cos m\lambda + \bar{S}_{nm} \sin m\lambda) \frac{d\bar{P}_{nm}(\sin\varphi')}{d\varphi}$$

$$(8.5) \quad \delta_{\lambda} \text{SH} = \frac{-kM}{r^2 \cos\varphi} \sum_{n=2}^{14} \left( \frac{a_e}{r} \right)^n \sum_{m=0}^n m(\bar{C}_{nm}^* \sin m\lambda - \bar{S}_{nm} \cos m\lambda) \bar{P}_{nm}(\sin\varphi')$$

The notation conforms to that of Chapter 3.

Table 18

Summary of Superimposed Point Mass Set Solutions

Depth of Masses (km)	50	10
Mean Anomaly Block Size	30'x30'	5'x5'
Latitude Limits	33°N - 41°N	36°N - 38°N
Longitude Limits	256°E - 265°E	259°.5E - 261°.5E
No. of Anomalies Used in Solution	288	576
No. of Predefined Masses	640	895
No. of Unknown Masses Determined	255	306
Mean Input Anomaly	0.56	-0.11
RMS Input Anomaly	9.40	7.10
Mean Residual Anomaly After Fitting Masses (mgal)	0.64	-0.21
RMS Residual Anomaly After Fitting Masses (mgal)	1.86	1.77

In the notation defined in section 2.2 and Figure 2, the derivatives of

the point mass term in equation (8.2) are:

$$(8.6) \quad \delta r_{PM} = \sum_j \frac{(R_i^2 - F_{ij})}{R_i \ell_{ij}^3} k M_j$$

$$(8.7) \quad \delta \varphi'_{PM} = - \sum_j \left[ \frac{(x_i x_{ij} + y_i y_{ij}) z_{ij} - z_i P_i^2}{R_i P_i \ell_{ij}^3} \right] k M_j$$

$$(8.8) \quad \delta \lambda_{PM} = - \sum_j \left( \frac{x_i y_{ij} - y_i x_{ij}}{P_i \ell_{ij}^3} \right) k M_j$$

The total disturbance components are formed by adding the components found from the spherical harmonic term and from the point mass term.

The computation point is defined as a point at a height  $H$ , measured along the normal to the ellipsoid that passes through a foot point specified in terms of geodetic latitude and longitude. These coordinates are used to determine the  $X, Y, Z$  coordinates and the geocentric latitude  $\varphi'$ , at the elevated point. These latter coordinates are then used to evaluate equations (8.3) through (8.8).

A computer program for the above outlined computation is given in Appendix D. It uses point mass sets in the card format produced by the point mass solution program and a set of spherical harmonic coefficients as input data. It computes and prints out the three disturbance components at points specified by geodetic latitude, longitude, and height. In addition, it prints the individual contributions to these components from the spherical harmonic model and from each distinct point mass set included.

### 8.5 Computation of Gravity Disturbances at the Test Points

The three mass sets described in Tables 17 and 18 were used to determine the anomalous gravity components of the same points used in the previously described comparison standard computations. Computation points were established at a total of 65 points on the ellipsoidal normals to the foot point positions shown on Figure 21. Results of these computations are shown in Appendix E. These computations are summarized together with the comparison standard computations in Table 19. This table is most explanatory when comparing variations between the solutions along a single vertical trajectory. Figure 22 presents the data more clearly when comparing the solutions on all trajectories at a given height.

Table 19 and Figure 22 show that the absolute difference between the two methods of solution is small. The maximum component difference is 1.7 milligals and occurs at the lowest elevation. The differences and the disturbances decrease in a regular manner with elevation. The magnitude of the discrepancies does not seem to be directly related to the magnitude of the disturbance, however, at a given elevation. This is evident from Figure 22. The  $\delta_r$  component varies over the area by over 250%, but the discrepancy between the two methods of computing the component varies only by about 20%. Evidently both solutions depict the local detail in the same manner, but regional bias exists between the solutions. A similar situation is found with the  $\delta_\varphi'$  component. At 20 kilometers, the differences between the solutions is position dependent, but this position dependence ceases with elevation and

Foot Point Location			Heights Above Ellipsoid									
$\sigma$	$\lambda$		20 km	30 km	50 km	100 km	200 km	300 km	500 km	1000 km	1500 km	
37.5	260.5	- 9.2 - 7.8 -1.4		-10.9 -10.0 -0.9		- 8.6 - 8.3 -0.3		- 4.9 - 5.0 0.1	- 3.7 - 3.9 0.2			
		13.8 12.1 1.7		9.4 8.0 1.4		3.3 2.5 0.8		1.7 1.1 0.6	1.0 0.6 0.4			
		- 4.5 - 4.6 0.1		- 3.8 - 3.9 0.1		- 3.1 - 3.1 0.0		- 1.1 - 1.0 -0.1	0.4 0.5 -0.1			
37.25	260.25	-15.5 -13.9 -1.6	-14.9 -13.5 -1.4	-13.9 -12.9 -1.0	-11.9 -11.3 -0.6	- 8.8 - 8.5 -0.3	- 6.8 - 6.7 -0.1	- 4.9 - 5.0 0.1	- 3.7 - 3.9 0.2	- 3.3 - 3.6 0.3		
		14.3 12.9 1.4	12.1 10.7 1.4	9.2 8.0 1.2	5.6 4.6 1.0	3.2 2.4 0.8	2.4 1.7 0.7	1.6 1.1 0.5	0.9 0.6 0.3	0.7 0.4 0.3		
		- 3.6 - 3.3 -0.3	- 3.4 - 3.2 -0.2	- 3.2 - 3.1 -0.1	- 3.1 - 3.1 0.0	- 2.9 - 2.9 0.0	- 2.3 - 2.2 -0.1	- 1.0 - 0.8 -0.2	0.5 0.6 -0.1	0.8 0.9 -0.1		
37.25	260.75	-16.0 -14.4 -1.6	-15.6 -14.3 -1.3	-14.4 -13.4 -1.0	-11.9 -11.3 -0.6	- 9.0 - 8.7 -0.3	- 7.1 - 7.0 -0.1	- 5.1 - 5.2 0.1	- 3.7 - 4.0 0.3	- 3.3 - 3.6 0.3		
		12.4 11.0 1.4	10.5 9.1 1.4	7.9 6.6 1.3	4.7 3.7 1.0	2.7 1.8 0.9	2.0 1.3 0.7	1.4 0.8 0.6	0.8 0.5 0.3	0.7 0.4 0.3		
		- 4.3 - 4.8 0.5	- 3.8 - 4.2 0.4	- 3.2 - 3.5 0.3	- 2.8 - 3.0 0.2	- 2.6 - 2.7 0.1	- 2.1 - 2.1 0.0	- 1.0 - 0.9 -0.1	0.4 0.6 -0.2	0.7 0.8 -0.1		
37.0	260.0	-19.3 -17.8 -1.5		-16.4 -15.3 -1.1		- 9.0 - 8.6 -0.4		- 4.8 - 4.9 0.1	- 3.6 - 3.9 0.3			
		10.1 9.0 1.1		7.9 6.8 1.1		3.0 2.3 0.7		1.6 1.0 0.6	0.9 0.6 0.3			
		- 3.8 - 3.2 -0.6		- 3.1 - 2.8 -0.3		- 2.8 - 2.7 -0.1		- 0.8 - 0.7 -0.1	0.6 0.8 -0.2			
37.0	260.5	-21.6 -19.9 -1.7	-19.5 -18.0 -1.5	-16.8 -15.6 -1.2	-13.0 -12.2 -0.8	- 9.2 - 8.8 -0.4	- 7.1 - 7.0 -0.1	- 5.1 - 5.1 0.0	- 3.7 - 4.0 0.3	- 3.3 - 3.6 0.3		
		9.9 8.8 1.1	8.7 7.6 1.1	6.8 5.7 1.1	4.2 3.3 0.9	2.5 1.7 0.8	1.9 1.2 0.7	4.1 0.8 0.6	0.8 0.4 0.4	0.6 0.4 0.2		
		- 2.4 - 2.5 0.1	- 2.4 - 2.4 0.0	- 2.2 - 2.3 0.1	- 2.3 - 2.4 0.1	- 2.4 - 2.4 0.0	- 1.9 - 1.9 0.0	- 0.8 - 0.7 -0.1	0.5 0.7 -0.2	0.8 0.9 -0.1		
37.0	261.0	-21.5 -20.0 -1.5		-16.7 -15.7 -1.0		- 9.2 - 8.9 -0.3		- 5.3 - 5.4 0.1	- 3.8 - 4.0 0.2			
		5.7 4.6 1.1		4.3 3.2 1.1		1.9 1.1 0.8		1.2 0.6 0.6	0.9 0.4 0.4			
		- 1.7 - 2.5 0.8		- 1.3 - 1.8 0.5		- 2.1 - 2.2 0.1		- 0.8 - 0.8 0.0	0.4 0.6 -0.2			
36.75	260.25	-21.9 -20.3 -1.6	-20.7 -19.2 -1.5	-18.3 -17.1 -1.2	-13.9 -13.1 -0.8	- 9.3 - 8.9 -0.4	- 7.1 - 6.9 -0.2	- 5.0 - 5.0 0.0	- 3.7 - 3.9 0.2	- 3.3 - 3.6 0.3		
		6.8 5.9 0.9	6.4 5.4 1.0	5.4 4.4 1.0	3.7 2.7 1.0	2.3 1.6 0.7	1.9 1.2 0.7	1.4 0.8 0.6	0.8 0.4 0.4	0.6 0.4 0.2		
		- 3.1 - 2.8 -0.3	- 2.4 - 2.2 -0.2	- 1.9 - 1.8 -0.1	- 2.0 - 2.0 0.0	- 2.2 - 2.2 0.0	- 1.8 - 1.7 -0.1	- 0.7 - 0.6 -0.1	0.6 0.8 -0.2	0.5 0.9 -0.1		
36.75	260.75	-23.3 -21.6 -1.7	-21.1 -19.6 -1.5	-18.0 -16.8 -1.2	-13.4 -12.7 -0.7	- 9.3 - 9.0 -0.3	- 7.3 - 7.1 -0.2	- 5.2 - 5.3 0.1	- 3.3 - 4.0 0.2	- 3.4 - 3.6 0.2		
		3.9 3.0 0.9	3.7 2.7 1.0	3.3 2.3 1.0	2.4 1.5 0.9	1.7 0.9 0.8	1.5 0.8 0.7	1.1 0.5 0.6	0.7 0.4 0.3	0.6 0.3 0.3		
		0.9 0.4 0.5	0.5 0.1 0.4	- 0.1 - 0.4 0.3	- 1.1 - 1.3 0.2	- 1.8 - 1.8 0.0	- 1.6 - 1.6 0.0	- 0.7 - 0.6 -0.1	0.5 0.7 -0.2	0.8 0.9 -0.1		
36.50	260.5	-23.5 -21.9 -1.6		-18.9 -17.7 -1.2		- 9.4 - 9.0 -0.4		- 5.2 - 5.2 0.0	- 3.7 - 4.0 0.3			
		2.5 1.7 0.8		2.4 1.5 0.9		1.6 0.8 0.8		1.1 0.5 0.6	0.7 0.3 0.4			
		1.1 1.0 0.1		0.4 0.3 0.1		- 1.6 - 1.6 0.0		- 0.5 - 0.4 -0.1	0.6 0.3 -0.2			

Key to Entries in Table for Each Computation Point

Computation Standard	Point Mass	Difference (Comparison Standard-Point Mass)
(1) $\delta r$	(4) $\delta r$	(7) $\Delta\delta r$
(2) $\delta\varphi'$	(5) $\delta\varphi'$	(8) $\Delta\delta\varphi'$
(3) $\delta\lambda$	(6) $\delta\lambda$	(9) $\Delta\delta\lambda$

Table 19

Comparison of Point Mass and Direct Integration  
Gravity Disturbance Component Computations

Figure 22

Gravity Disturbance Components at 20 km Elevation  
Arranged in Geographic Location

LATITUDE	- 9.2 - 7.8 - 1.4			13.8 12.1 1.7			- 4.5 - 4.6 0.1						
37.5 -													
37.25 -	-15.5 -13.9 - 1.4			16.0 -14.4 - 1.6			14.3 12.9 1.4						
37.0 -	-19.3 17.8 - 1.5	-21.6 -19.0 - 1.7		-21.5 -20.0 - 1.5	12.4 11.0 1.4		-3.6 - 3.3 - 0.3	- 4.3 - 4.8 .5					
36.75 -	10.1 9.0 1.1	9.9 8.8 1.1		5.7 4.6 1.1	- 2.4 - 2.5 0.1		- 3.8 - 3.2 - .6	- 1.7 - 2.5 0.8					
36.50 -	-21.9 -20.3 - 1.6			-23.3 -21.6 - 1.7			6.8 5.9 0.8						
	- 3.1 - 2.8 - 0.3			0.9 0.4 .5									
	-23.5 -21.9 - 1.6			2.5 1.7 0.8			1.1 1.0 0.1						
	260.0			260.25			260.5						
	260.75			261.0									
	LONGITUDE												

Entries in blocks conform to key for Table 18.

the difference becomes a constant bias. The  $\delta_\lambda$  component exhibits position dependent differences at low elevations. These differences are smaller than in the other components and little constant bias is apparent at higher elevations.

From Figure 8 we can estimate the possible effect of the areal truncation of the point mass solution on the horizontal components. At low elevations, the root mean square error for a  $\psi_0$  of  $13^\circ$  is somewhat less than 2 milligals. Such an error, since it is caused by the neglect of distant anomalies, would vary slowly with position. The apparent constant discrepancies between the horizontal components  $\delta_\phi'$  and  $\delta_\lambda$  computed by the two methods are smaller than the predicted worldwide root mean square truncation error. These discrepancies can therefore easily be explained as truncation error. The minor variations from a mean difference that are associated with position at low elevations reflect the differences between the point mass model and the direct integration procedure if truncation errors were removed.

The constant bias in the  $\delta_r$  component is not so easily explained. It does not appear reasonable to attribute this discrepancy to truncation errors. We have argued that gravity anomalies are determined almost entirely by the nearby mass distribution so that truncation effects would not be significant in the determination of  $\Delta g$  at the center of the point mass array. This argument also holds for  $\delta_r$  since:

$$(8.9) \quad \delta_r = \Delta g + .3086N$$

and the theoretical and actual errors found for N in the test area would result in a trivial contribution to the error in  $\delta_r$ .

Table 20 shows the mean difference between the two methods of computation for each component in the sense (Direct Integration-Point Mass). The bias in the  $\delta_r$  component falls off much more rapidly than does the bias in the  $\delta_\varphi'$  component. Assuming that the decay in the error follows an inverse square law with respect to the distance to an incorrectly modelled mass distribution, this would indicate that the sources of the  $\delta_r$  discrepancy were nearer than the sources of the  $\delta_\varphi'$  bias. This lends weight to the truncation error explanation for the  $\delta_\varphi'$  difference. Since the  $\delta_r$  difference would seem to be of more local origin, it was suspected that it might be related to the fact that a much smaller area of  $5' \times 5'$  mean anomalies was used for the point mass solution than was used for the direct integration solution.

To test this hypothesis, the direct integration method was repeated but the area of  $5' \times 5'$  mean anomalies was reduced to an area extending  $2^\circ$  in latitude and  $3^\circ$  in longitude. The results are shown in Table 21. The results differ only slightly from those shown in Table 18. The agreement between the two types of solutions is slightly improved but the systematic differences remain. This result verifies the legitimacy of reducing the size of the  $5' \times 5'$  anomaly field used in the point mass solution, as discussed in section 6.3, but does not resolve the difference in the  $\delta_r$  component determinations. This matter remains a subject of conjecture.

While considerable emphasis has been placed on the differences between the two solutions, it should be noted that these differences are primarily remarkable because the two solutions agree so well that small constant biases

Table 20

Mean Difference Between Comparison Standard  
and Point Mass Gravity Components

Elevation Kilometers	Component		
	$\delta_r$ mgal	$\delta_\varphi'$ mgal	$\delta_\lambda$ mgal
20	-1.6	1.2	.1
30	-1.4	1.2	.1
50	-1.1	1.1	.1
100	-0.7	1.0	.0
200	-0.3	.8	.0
300	-0.1	.7	.0
500	.1	.6	.1
1000	.2	.4	.2
1500	.3	.3	.1

can be clearly distinguished.

There is little in the literature that affords a basis of comparison to judge the success of the point mass solution relative to other methods. Comparisons have been made between accurately computed anomalous gravity components with those computed solely from spherical harmonics [deWitte, 1966b]. A review of Appendix E which gives the contribution of the spherical harmonic coefficients and the various mass sets shows that a pure spherical harmonic solution is a totally inadequate approach at lower elevations. The published comparison bears out this obvious conclusion.

Only one paper was found that compared gravity disturbance components computed by two methods designed to achieve high accuracy [Orlin, 1959]. Orlin computed components of the disturbance vector for points above two stations by the coating method and by a ring integration variant of the direct inte-

Table 21

Comparison of Point Mass and Direct Integration Gravity Disturbance Components  
(Reduced Field of 5'x5' Mean Anomalies)

$\varphi$	$\lambda$	20 km			50 km			200 km			500 km			1000 km		
37.5	260.5	- 9.2	- 7.8	-1.4	-11.0	-10.0	-1.0	- 8.6	- 8.3	-0.3	- 5.0	- 5.0	0	- 3.7	- 3.9	0.2
		13.6	12.1	1.5	9.2	8.0	1.2	3.3	2.5	0.8	1.7	1.1	0.6	0.9	0.6	0.3
		- 4.7	- 4.6	-0.1	- 3.9	- 3.9	0.0	- 3.2	- 3.1	-0.1	- 1.2	- 1.0	-0.2	0.4	0.5	-0.1
37.25	260.25	-15.5	-13.9	-1.6	-13.9	-12.9	-1.0	- 8.8	- 8.5	-0.3	- 4.9	- 5.0	0.1	- 3.7	- 3.9	0.2
		14.1	12.9	1.2	9.0	8.0	1.0	3.2	2.4	0.8	1.6	1.1	0.5	0.9	0.6	0.3
		- 3.7	- 3.3	-0.4	- 3.3	- 3.1	-0.2	- 3.0	- 2.9	-0.1	- 1.0	- 0.8	-0.2	0.5	0.6	-0.1
37.25	260.75	16.1	-14.4	-1.7	-14.5	-13.4	-1.1	- 9.0	- 8.7	-0.3	- 5.2	- 5.2	0	- 3.8	- 4.0	0.2
		12.2	11.0	1.2	7.7	6.6	1.1	2.6	1.8	0.8	1.4	0.8	0.6	0.8	0.5	0.3
		- 4.5	- 4.8	0.3	- 3.4	- 3.5	0.1	- 2.7	- 2.7	0.0	1.0	- 0.9	0.1	0.4	0.6	-0.2
37.0	260.0	-19.2	-17.8	-1.4	-16.3	-15.3	-1.0	- 9.0	- 8.6	-0.4	- 4.8	- 4.9	0.1	- 3.7	- 3.9	0.2
		9.9	9.0	0.9	7.7	6.8	0.9	3.0	2.3	0.7	1.6	1.0	0.6	0.9	0.6	0.3
		- 3.0	- 3.2	-0.7	- 3.2	- 2.8	-0.4	- 2.9	- 2.7	-0.2	- 0.9	- 0.7	-0.2	0.6	0.8	-0.2
37.0	260.5	-21.6	-19.9	-1.7	-16.8	-15.6	-1.2	- 9.2	- 8.8	-0.4	- 5.1	- 5.1	0	- 3.8	- 4.0	-0.2
		9.7	8.8	0.9	6.7	5.7	1.0	2.5	1.7	0.8	1.4	0.8	0.6	0.8	0.4	0.4
		- 2.6	- 2.5	-0.1	- 2.4	- 2.3	-0.1	- 2.4	- 2.4	0.0	- 0.9	- 0.7	-0.2	0.5	0.7	-0.2
37.0	261.0	-21.5	-20.0	-1.5	-16.7	-15.7	-1.0	- 9.2	- 8.9	-0.3	- 5.3	- 5.4	0.1	- 3.8	- 4.0	0.2
		5.6	4.6	1.0	4.2	3.2	1.0	1.9	1.1	0.8	1.1	0.6	0.5	0.7	0.4	0.3
		- 1.9	- 2.5	0.6	- 1.4	- 1.8	0.4	- 2.1	- 2.2	0.1	- 0.9	- 0.8	-0.1	0.4	0.6	-0.2
36.75	260.25	-21.9	-20.3	-1.6	-18.1	-17.1	-1.0	- 9.3	- 8.9	-0.4	- 5.0	- 5.0	0	- 3.7	- 3.9	0.2
		6.5	5.9	0.6	5.2	4.4	0.8	2.3	1.6	0.7	1.3	0.8	0.5	0.8	0.4	0.4
		- 3.3	- 2.8	-0.5	- 2.1	- 1.8	-0.3	- 2.3	- 2.2	-0.1	- 0.7	- 0.6	-0.1	0.6	0.8	-0.2
36.75	260.75	-23.3	-21.6	-1.7	-17.9	-16.8	-1.1	- 9.4	- 9.0	-0.4	- 5.2	- 5.3	0.1	- 3.8	- 4.0	0.2
		3.7	3.0	0.7	3.1	2.3	0.8	1.7	0.9	0.3	1.1	0.5	0.6	0.7	0.4	0.3
		0.7	0.4	0.3	- 0.3	- 0.4	0.1	- 1.9	- 1.8	-0.1	- 0.7	- 0.6	0.1	0.5	0.7	-0.2
36.50	260.5	-23.3	-21.9	-1.4	-18.7	-17.7	-1.0	9.4	- 9.0	-0.4	- 5.2	- 5.2	0	- 3.8	- 4.0	0.2
		2.1	1.7	0.4	2.2	1.5	0.7	1.6	0.8	0.8	1.1	0.5	0.6	0.7	0.3	0.4
		0.8	1.0	-0.2	0.2	0.3	-0.1	- 1.7	- 1.6	-0.1	- 0.6	- 0.4	-0.2	0.6	0.8	-0.2

Entries in blocks conform to key for Table 19.

gration method. His results are presented here in Table 22 for comparison purposes.

The deflection components may be roughly converted to milligal units by multiplying by five. The  $\delta_r$  results shown by Orlin are much less accurate than those obtained in this investigation. Orlin suggests that the discrepancies can be attributed to a difference in the size of the anomaly fields used in the two methods of integration. The coating method used anomaly fields truncated at a radius of  $5.5^\circ$  from station PAD and  $7.0^\circ$  from station EGG. The direct integration method used fields extending 516 kilometers from the computation points. Reference to Figure 4 and equation (8.9) shows that the difference found in the  $\delta_r$  component should not be unexpected under these circumstances. The field used for the direct integration method is inadequate for a high accuracy computation. The use of independent geoid heights in the coating method would diminish the importance of the distant fields so that quite different

Table 22

## Orlin's Computation of Gravity Disturbance Vector Components

Station	Elev. Kmg	$\delta_r$ (mg)		$\xi$ (sec)		$\eta$ (sec)	
		Coating	Direct Int.	Coating	Direct Int.	Coating	Direct Int.
Egg	0	+11.6	+17.0	-11.1	- 1.1	-0.6	-0.9
	32	+ 2.8	+ 8.2	- 0.3	+ 0.1	-1.8	-1.7
	64	- 1.1	+13.8	+ 0.1	+ 0.4	-1.5	-1.8
Pad	0	+21.7	+30.0	+16.6	+16.6	+0.2	-0.1
	32	-21.4	-13.2	+ 6.8	+ 6.8	-4.1	-4.2
	64	-20.8	-12.3	+ 3.5	+ 3.5	-4.6	-4.2

results could be obtained from the two methods under these conditions. Errors may exist in  $\xi$  and  $\eta$  in both of Orlin's methods that are caused by truncation, but these would compensate and not be fully reflected in the differences reported.

We are therefore left with no known published data that provides a meaningful standard of comparison. The point mass determination of the components of the gravity disturbance vector agree much better with a standard based on direct anomaly integration than any other method we have found in the literature.

#### 8.6 Comparison of Computer Time Requirements

Much of the interest in point masses has arisen because a point mass model is simple and should offer distinct computational advantages when compared to the use of gravity anomalies and complex surface integrals. This investigation was not concerned with measuring the extent of this advantage under a specific set of circumstances, but rather was concerned with the validity of the point mass model. The computer programs written in the course of the study were not "production type" programs. Features were included for flexibility and diagnostic purposes that would not be needed for routine applications and simplicity in programming was emphasized at the expense of efficiency during program execution. The programs used for establishing comparison standards were, conversely, adapted from production programs written by highly skilled programmers and were definitely designed for efficiency. A further difference was that the comparison standard programs

were written for the IBM 7094 computer system while those prepared for this study were written for the IBM 360. It is obvious that it is difficult to use these programs to compare the computational efficiency of the different methods. Some comparative figures on computation time will nevertheless be given simply to illustrate the general magnitudes of the required computational efforts using point masses and anomalies.

Table 23 shows the approximate IBM 360 computer time required to evaluate 1000 geoid heights using the two methods. The Stokes' method refers to the use of equation (7.1) with 1000  $1^\circ \times 1^\circ$  mean anomalies for an inner zone and worldwide  $5^\circ \times 5^\circ$  mean anomalies for an outer zone. The point mass method refers to the use of equation (5.22) with a (14, 14) spherical harmonic coefficient set and 640 point masses. In all cases, it was assumed that the processing included compilation of the program and loading of the data. The Stokes' program was actually accomplished on the IBM 7094. The time required on this computer was divided by five to give a time which would be roughly comparable to that required on an IBM 360. (The relationship between time requirements on the two machines is actually too complex to characterize accurately with a single number, but factors between three and five are commonly used as approximations.) Similar comparisons for the computation of the components of the gravity disturbance vector are shown in Table 24. In this case the times apply to computation of the 45 points shown in Table 21. The point mass method refers to equations (8.3) through (8.8), and was based on 1201 masses. The direct integration method refers to equations (7.14)

through (7.16). As expected, the point mass computations were significantly faster. This is offset, however, by the fact that extensive computations are required to form the point mass set. The time required to form the mass sets used in this study are shown in Table 25.

Table 23

**Comparison of Time Required  
To Compute 1000 Geoid Heights**

<u>Method</u>	<u>Equivalent IBM 360 Time (Seconds)</u>	<u>Ratio to Stokes' Method</u>
Stokes'	624	1:1
Point Mass	86	1:7.3

Table 24

**Comparison of Time Required  
To Compute Gravity Disturbance Components at 45 Points**

<u>Method</u>	<u>Equivalent IBM 360 Time (Seconds)</u>	<u>Ratio to direct Integration Method</u>
Direct Integration	72	1:1
Point Mass	20	1:3.6

Table 25

## Time Required to Form Point Mass Sets

Set	IBM 360 Time (Minutes)
640 Masses at 100 km Depth	49
255 Masses at 50 km Depth	9
306 Masses at 10 km Depth	20
Total - 1201 Masses	71

It is obvious that a purely economic justification for point mass computations using a given computer could be sustained only if the costs incurred in forming the mass sets could be amortized against a great many computations which subsequently used these masses.

## CHAPTER 9

### CONCLUSIONS AND RECOMMENDATIONS

#### 9.1 Summary and Conclusions

This investigation has shown that it is possible to form a complex and accurate model of the geopotential that is based on a spherop reference system and point masses. The point mass technique provides a simple method of using localized areas of detailed gravity information to add fine structure to a geopotential model that is based on spherical harmonic coefficients. The use of "reconciled" anomalies in this procedure results in a true densification of the detail in the model without distorting the long wavelength features of the original model.

Comparison of the anomalous geopotential computed from point masses with a standard based on Stokes' equation shows that the difference between the two methods is of the order of accuracy of the Stokes' comparison standard and is small when compared to the absolute error attributable to uncertainties in the knowledge of the gravity field. Similar conclusions are reached when components of the anomalous gravity vector computed from point masses are compared to those computed by more conventional means. In this case, however, there is evidence of small systematic differences between the two methods of computation.

The point mass technique can be used to model fine detail in localized areas that would be completely impractical to represent by an ordinary spherical harmonic model. Such fine detail could be represented by anomaly data but computations based on point mass sets are far more simple and efficient than comparable computations based directly on gravity anomalies.

The point mass techniques do, however, have disadvantages. A primary disadvantage is the large amount of computational effort entailed in forming the point mass set. More efficient methods for this purpose could be devised than those reported here, but it is inescapable that forming and solving the large systems of equations involved will require extensive computations.

A second disadvantage is that point mass "theory" is relatively ill-defined when compared to the bases of classical gravimetric geodesy. Both approaches require approximations and assumptions but the point mass method has the additional disadvantage that a given set of gravity observations could be used to develop a theoretically unlimited number of different point mass models of the geopotential. There seems to be no difficulty in establishing a model that is accurate enough for practical applications, but it would be difficult to defend a specific model as the optimum for use in theoretical studies. Point masses therefore seem more suited to solving practical problems than for theoretical scientific studies.

The usefulness of the techniques discussed in this study can only be evaluated in terms of specific proposed applications. In general, the decision

will not depend on the accuracy of the method since the differences found between the point mass methods and the conventional computations are small. The greatest advantage of point masses would be realized in a situation where huge numbers of computations were to be made on a routine basis. For example, a point mass set might be considered as a means of modelling the geopotential in a missile test area where gravitational acceleration components were desired along missile trajectories. The simplicity of a point mass model as compared to a model based on anomalies could speed computations, reduce the requirements for computer capability and perhaps permit in-flight computations that would not otherwise be feasible. In such a situation where prolonged use would be made of the model, the computations required to form the point mass set would not be an important consideration.

The apparent systematic errors in the point mass model noted in this study, although small, are a matter of some concern. For a limited area, it would be practical to compare the point mass model with a standard based on the direct integration approach, as was done in this study, to determine the nature and magnitude of any discrepancies. If significant systematic discrepancies were found, simple empirical corrections could be added to the model to achieve agreement with the comparison standard. This approach would retain the operational simplicity of the point mass model while yielding results that were practically equivalent to the direct integration method.

From the evidence obtained in this investigation, it appears that a point mass set would be a highly satisfactory means of forming geopotential

models needed to meet operational requirements generated by missile and space activities.

#### 9.2. Possibilities for Further Investigation

The variations possible in forming a point mass geopotential model offer an unlimited field for additional investigation. The general geometries of the solutions described in this study appear satisfactory, but it is possible that further experimentation could discover combinations of the various parameters such as the depth/side ratio and the over-determination ratio that would give even better results.

Improved models could undoubtedly be evolved if a capability were developed to obtain larger point mass sets. This would permit the use of smaller mean anomalies in forming the model, the description of finer structure in the field, and the elimination of more truncation error.

An allied problem that will become significant if more precise methods are to be developed is the definition of the comparison standards. It was assumed, for example, in this study that the direct integration method of determining the components of the anomalous gravity vector was without error at all altitudes. This assumption should be examined critically if all discrepancies between methods are to be regarded as errors in the point mass model.

Some experimentation, not reported here, was conducted in which point masses were used to predict gravity anomaly fields based on evenly distributed observation points. This subject was not pursued to the point

that firm recommendations can be made, but the results obtained did indicate that a more thorough study might be justified.

**APPENDIX A**  
**POINT MASS SOLUTION COMPUTER PROGRAM LISTING**

**PLEASE NOTE:**

**Some pages have indistinct  
print. Filmed as received.**

**UNIVERSITY MICROFILMS.**

```

C THE NORMAL UNITS USED IN THIS PROGRAM ARE METERS, DEGREES, MILLIGALS
C THE DIMENSIONING PERMITS THE FOLLOWING PROGRAM SIZE:
C           324 UNKNOWN POINT MASSES
C           2000 PREDETERMINED MASSES
C           1000 GRAVITY ANOMALY OBSERVATIONS
C           A (14,14) SET OF SPHERICAL HARMONIC COEFFICIENTS
C

C IMPLICIT REAL*8(A-H,O-Z)
REAL*8 MB(324),ML(324),XM(324),YM(324),ZM(324),A(324),C(326),
*MAS(326),N(533C1),U(326),B(1000),AL(1000),RES(1000),G(1000),
*UN(40,40),CNM(15,15),SNM(15,15),P(15,15),Q(15,15),
*L,L2,MIN,MD2,EEX(2000),EEY(2000),EEZ(2000),EEM(2000)
EQUIVALENCE (N(1),B(1)),(N(1001),AL(1)),(N(2001),RES(1)),
*(N(3001),G(1)),(N(4001),CNM(1)),(N(4501),SNM(1)),
*(N(5001),P(1)),(N(5501),Q(1)),(N(6001),UN(1)),
*(N(10001),EEN(1)),(N(15001),EEX(1)),(N(20001),EEY(1)),
*(N(25001),EEZ(1))

C BUILT IN GEOMETRIC PARAMETERS OF THE GRS-67
C
AE=6378160.00
E2=.00669460532856

C READ IN PROGRAM CONTROL PARAMETERS
C BOT, TOP, WEST, EAST ARE LATITUDE AND LONGITUDE LIMITS OF THE AREA
C TO WHICH MASSES ARE FITTED.
C NM1 IS THE APPROXIMATE NUMBER OF MASSES DESIRED
C SIDE IS THE SIDE LENGTH OF A MEAN ANOMALY BLOCK IN DEGREES
C MIN IS THE GRID SPACING IN MINUTES FOR COMPUTING GEOID HEIGHTS
C DEEP IS THE ASSIGNED MASS DEPTH
C ICOEF, IGEOD, AND INITIS ARE CONTROL PARAMETERS EQUAL TO 1 OR 0
C   IF ICOEF =1, CORRELATION COEFFICIENTS OF MASSES ARE PRINTED
C   IF IGEOD=1, A GEOID IS COMPUTED
C   IF INITIS=1, PREDETERMINED MASSES WILL BE USED IN FORMING CONDITIONS
C

      NAMELIST/INPUT/BOT,TOP,WEST,EAST,NM1,DEEP,MIN,SIDE
      READ(5,INPUT)
      NAMELIST/CCNTRL/ICCEF,IGEOD,INITIS
      READ(5,CCNTRL)

C COMPUTATION OF BEST FIT OF TRAPEZOIDAL ARRAY OF MASSES TO AREA
C
      CALL NUMASL(NM1,BOT,TOP,WEST,EAST,SIDE,NM,ML,MB)
      IF(NM.GT.324)STOP2
      CALL MASL2(MB,ML,NM,XM,YM,ZM,AE,E2,DEEP)
      N2=NM*(NM+1)/2

```

```

N4=NM+2
N3=N2+2*NM+3
NP1=15
K=0
TCTMAS=0.00
DO 2 I=1,N3
2 N(I)=0.00
DO 3 I=1,N4
3 U(I)=0.00
IC=0
C
C READ PREDETERMINED MASSES
C
713 READ(5,211,END=622)IZ,EM,EX,EY,EZ
IF(INITS.EQ.0)GOTO 9
U(N4)=U(N4)-EM*1.0-20
9 CONTINUE
IC=IC+1
WRITE (2) EM,EX,EY,EZ
GOTO713
622 REWIND 2
1 IF(SIDE.EQ.1.D0)GOTO1001
C
C READ GRAVITY ANOMALIES AND ASSOCIATED DATA. SELECT THOSE IN AREA
C
READ(5,117)PHI,ALAM,X,Y,Z,R,GG
GOTO 1002
1001 CONTINUE
READ(5,101)PHI,ALAM,X,Y,Z,R,GG
1002 CONTINUE
117 FORMAT(2F5.3,1X,3F10.2,F7.2,22X,F5.1)
101 FORMAT(2F3.1,5X,3F10.2,F7.2,22X,F5.1)
IF(PHI.GT.90.0C)GOTO13
IF(PHI.LT.BOT)GOTO1
IF(PHI.GT.TOP)GOTO1
IF(ALAM.LT.WEST-200.00)GOTO1
IF(ALAM.GT.EAST-200.00)GOTO1
K=K+1
C
C FORM OBSERVATION EQUATION COEFFICIENTS AND SIMULTANEOUSLY FORM AREA
C WEIGHTED NORMALS AND CONDITION EQUATIONS. STORE OBSERVATION EQUATION
C COEFFICIENTS AND ANOMALY DATA FOR LATER USE
C
R=R+63C0C00.00
R2=R*R
W=DSQRT(X*X+Y*Y)/R
C
C IF PREDETERMINED MASSES ARE USED, CONVERT ANOMALIES BY SUBTRACTING

```

```

C MASS EFFECT
C
IF(IC.EQ.0)GOTO 72
DO 714 J=1,IC
READ(2) EM,EX,EY,EZ
EF=X*EX+Y*EY+Z*EZ
EL2=(X-EX)*(X-EX)+(Y-EY)*(Y-EY)+(Z-EZ)*(Z-EZ)
EL=DSQRT(EL2)
GG=GG-((R2-EF)/(R*EL2*EL))-2.00/(EL*R))*1.00*EM
IF(INITS.EQ.0)GOTO 4
U(NM+1)=U(NM+1)-W*EM/(1.015*EL)
4 CONTINUE
714 CONTINUE .
REWIND 2
72 CONTINUE
M=0
DO 12 I=1,NM
F=X*XM(I)+Y*YM(I)+Z*ZM(I)
L2=(X-XM(I))*(X-XM(I))+(Y-YM(I))*(Y-YM(I))+(Z-ZM(I))*(Z-ZM(I))
L=DSQRT(L2)
A(I)=(R2-F)/(L2*L*R)-2.00/(L*R)
A(I)=A(I)*0.100
N(N2+I)=N(N2+I)+W/(L*1.015)
TEMP=A(I)*W
U(I)=U(I)+TEMP*GG
DO 12 J=1,I
M=M+1
12 N(M)=N(M)+TEMP*A(J)
WRITE(1) (A(I),I=1,NM),W,GG,PHI,ALAM
GOTO1
13 CONTINUE
DO 67 KL=1,NM
67 N(N2+NM+1+KL)=1.0-20
C TURING N NUMBER COMPUTATIONS
C
J=1
SSN=0.00
DO 5 I=1,N3
5 SSN=SSN+N(I)*N(I)*2.00
M=0
DO 6 I=1,N4
M=M+I
SSN=SSN-N(M)*N(M)
6 CONTINUE
IF(NM.GT.K)STOP3
C TWO STEP MATRIX INVERSION. FIRST INVERT OBSERVATION EQUATION

```

```

C PARTITION AND THEN ADD CONDITION EQUATION PARTITION SEQUENTIALLY.
C
C      CALL DSINV(N,NM,1.0-12,IER)
C      IF(IER.LT.0)STOP 1
C      IF(IER.NE.0)WRITE(6,202)IER
C      CALL BINV(N,NM,N4,C)
C
C TURING N NUMBER COMPUTATIONS
C
C      SSI=0.00
C      DO 7 I=1,N3
C      7 SSI=SSI+N(I)*N(I)*2.00
C      M=0
C      DO 8 I=1,N4
C      M=M+I
C      8 SSI=SSI-N(M)*N(M)
C      TUR=DSQRT(SSN*SSI)/DFLOAT(N4)
C
C COMPUTATION OF CORRELATION COEFFICIENTS
C
C      IF(ICOEF.EQ.1)CALL DSCORR(NM,1.00,N,C)
C
C PULL THE FOLLOWING CARD TO WRITE THE INVERSE MATRIX
C
C      GOTO513
C13  KK=0
C      DO 500 LL=1,N4
C      KK=KK+LL
C      J=J+LL-1
C      WRITE(6,220)(N(I),I=J,KK)
C500  CONTINUE
C513  CONTINUE
C220 FORMAT(/(1X,10E11.4))
C
C COMPUTATION OF MASS MAGNITUDES
C
C      DO 10 I=1,N4
C10  MAS(I)=0.00
C      M=0
C      DO 20 I=1,N4
C      DO 20 J=1,I
C      M=M+1
C20  MAS(J)=MAS(J)+N(M)*U(I)
C      M=0
C      DO 30 I=2,N4
C      M=M+1
C      DO 30 J=2,I
C      M=M+1

```

```

30 MAS(I)=MAS(I)+N(M)*U(J-1)
REWIND L
C COMPUTATION OF ANOMALY MISCLOSURES AND ADJUSTMENT STATISTICS
C
SGG2=0.00
VPV=0.00
VV=0.00
SGG=0.00
SV=0.00
DO 40 I=1,K
READ(1)(A(J),J=1,NM),W,GG,PHI,ALAM
GGG=0.00
DO 41 J=1,NM
41 GGG=GGG+A(J)*MAS(J)
RES(I)=GG-GGG
VV=RES(I)*RES(I)+VV
VPV=RES(I)*RES(I)*W+VPV
B(I)=PHI
AL(I)=ALAM+200.00
G(I)=GG
SGG=SGG+GG
SGG2=SGG2+GG*GG
SV=SV+RES(I)
40 CONTINUE
FK=K
FN=NM
RMSV=DSQRT(VV/FK)
RMSGG=DCRT(SGG2/FK)
M02=VPV/(FK-FN+1.00)
AVEV=SV/FK
AVEGG=SGG/FK
DO 571 J(K=1,NM
TOTMAS=TOTMAS+MAS(J,K)
571 CONTINUE
TOTMAS=TOTMAS-U(N4)
C OUTPUT OF INPUT PARAMETERS AND RESULTS OF COMPUTATIONS
C
WRITE(6,207)
WRITE(6,203)DOT,TCP,WEST,EAST
WRITE(6,214)IC
WRITE(6,204)K,NM
WRITE(6,205)DEEP
WRITE(6,212)AVEGG,RMSGG
WRITE(6,213)AVEV,RMSV
WRITE(6,206)TUR
WRITE(6,210)M02

```

```

      WRITE(6,210) TOTMAS
      WRITE(6,201)
      WRITE(6,202)(I,B(I),AL(I),G(I),RES(I),I=1,K)
      WRITE(6,207)
      WRITE(6,208)
      WRITE(6,209)(I,MAS(I),XM(I),YM(I),ZM(I),MB(I),ML(I), I=1,NM)
      WRITE(7,211)(I,MAS(I),XM(I),YM(I),ZM(I),I=1,NM)
      IF(IGECID.EQ.0)STOP5
      IF(IC.EQ.0)GOTO572
      DO 573 I=1,IC
      READ(2)EM,EX,EY,EZ
      EEM(I)=EM
      EEX(I)=EX
      ERY(I)=EY
      EEZ(I)=EZ
  573 CONTINUE
      REWIND 2
  572 CONTINUE
C
C   COMPUTATION OF GEOID BASED ON NEW AND PREDETERMINED MASSES
C
      CALL GECH2(BOT,WEST,TOP,EAST,MAS,XM,YM,ZM,UN,NM,E2,AE,MIN,IC,
     *EEM,EEX,ERY,EEZ,P,G,NP1,SNM,CNM)
  201 FORMAT('1',13X,'B',8X,'AL',8X,'DG',7X,'RES')
  202 FORMAT(15,4F10.1)
  203 FORMAT(1X,'LAT LIMITS',F5.1,' TO ',F5.1,' LONG',F6.1,'TO',F6.1)
  204 FORMAT(15,2X,'ANOMALIES USED TO FIT',14,' MASSES')
  205 FORMAT(1X,'DEPTH OF MASSES',F10.0)
  206 FORMAT(1X,'TURINGS N',E15.4)
  207 FORMAT('1')
  208 FORMAT(15X,'MASS',14X,'X',11X,'Y'11X,'Z',10X,'B',5X,'L')
  209 FORMAT(15,5X,D15.7,2X,F11.2,2X,F11.2,2X,F11.2,2X,F5.1,2X,F5.1)
  210 FORMAT(D15.6)
  211 FORMAT(13,D24.16,D17.10,D17.10,D17.10)
  212 FORMAT(1X,'MEAN INPUT ANOMALY',F6.2,' RMS INPUT ANOMALY',F6.2)
  213 FORMAT(1X,'MEAN RESID ANOMALY',F6.2,' RMS RESID ANOMALY',F6.2)
  214 FORMAT(14,' A PRICRI MASSES APPLIED TO ANOMALIES BEFORE ADJUST')
      STOP
      END

```

```

SUBROUTINE GECH2(B1,AL1,B2,AL2,TM,TX,TY,TZ,UN,NMTOT,E2,AE,MIN,IC,
*EEM,EEX,EY,EZ,P,Q,CN,SNM,CNM)
C
C B1 AND B2 ARE THE SOUTH AND NORTH LATITUDES OF AREA
C AL1 AND AL2 ARE THE WESTERN AND EASTERN LONGITUDES OF AREA
C TM IS THE NEW MASS MAGNITUDE ARRAY; TX, TY, TZ ARE THE NEW MASS
C COORDINATE ARRAYS, ALL OF LENGTH NMTOT. EEM, EEX, EY, EZ ARE THE
C SIMILAR ARRAYS OF LENGTH IC FOR THE PRE-DETERMINED MASSES.
C REFER TO THE MAIN PROGRAM AND TO SUBROUTINE NCNLY FOR OTHER
C VARIABLE DEFINITIONS AND THE MANNER OF STORAGE IN ARRAYS
C
IMPLICIT REAL*8(A-H,O-Z)
REAL*8 TM(1),TX(1),TY(1),TZ(1),MIN,UN(40,40),CNM(NP1,NP1),
*SNM(NP1,NP1),P(NP1,NP1),Q(NP1,NP1),EEM(1),EEX(1),EY(1),EZ(1)
RAD=57.2957795131
STEP=MIN/60.0DC
NB=(B2-B1)/STEP+1.001D0
NL=(AL2-AL1)/STEP+1.001D0
DO1 I=1,NB
B=B2-DFLOAT(I-1)*STEP
GB=DATAN((1.0-E2)*DTAN(B /RAD))*RAD
CALL PANC(GB,NP1,P,Q,CNM,SNM)
SB=DSIN(B/RAD)
CB=DCOS(B/RAD)
AN=AE/DSQRT(1.0-E2*SB*SB)
DO 1 J=1,NL
AL=AL1+DFLOAT(J-1)*STEP
CALL NCNLY(P,Q,CNM,SNM,AE,298.247167,978031.8456,NP1,AL,H)
SL=DSIN(AL/RAD)
CL=DCOS(AL/RAD)
X=(AN+H)*CB*CL
Y=(AN+H)*CB*SL
Z=(AN*(1.0-E2)+H)*SB
UN(I,J)=H
DO 2 K=1,NMTOT
UN(I,J)=UN(I,J)+TM(K)/(DSQRT((X-TX(K))*(X-TX(K))+(Y-TY(K))*
*(Y-TY(K))+(Z-TZ(K))*(Z-TZ(K)))*9798000.0D0)
2 CONTINUE
IF(IC.EQ.0)GOTO3
DO 4 KK=1,IC
4 UN(I,J)=UN(I,J)+EEM(KK)/(DSQRT((X-EEX(KK))*(X-EEX(KK))+(Y-EY(KK))*
*(Y-EY(KK))+(Z-EZ(KK))*(Z-EZ(KK)))*9798000.0D0)
3 CONTINUE
WRITE(7,600)I,J,B,AL,UN(I,J)
600 FORMAT(2I3,2F10.5,D24.8)
1 CONTINUE
WRITE(6,601)MIN
601 FORMAT('1 GEOID HEIGHT AT ',F5.2,' MINUTE INTERSECTIONS')

```

```
DO 5 I=1,NB
  WRITE(6,602)(UN(I,J),J=1,NL)
602 FORMAT(1H0,1GF10.2/(1X,1GF10.2))
5 CONTINUE
RETURN
END
```

```

C SUBROUTINE NONLY(P,Q,CNM,SNM,A,RF,GAME,NP1,AL,UND)
C P,Q,CNM,SNM, ARE STORED WITH INDICES RAISED BY ONE
C NP1 IS THE ORDER PLUS ONE. GAME IS EQUATORIAL GRAVITY
C IMPLICIT REAL*8 (A-H,O-Z)
C REAL*8 P(NP1,NP1),Q(NP1,NP1),CNM(NP1,NP1),SNM(NP1,NP1),
*CNL(37),SML(37)
C F=1.D0/RF
C FM=C.53174943312D-8*A/GAME*10.04
C C20=-DSQRT(.2DC)*(12.D0/3.D0)*F*(1.D0-.500*F)-(FM/3.00)
C *(1.D0-1.500*FM-(2.00/7.00)*F))
C C40=(4.00/105.D0)*F*(7.D0*F-5.00*FM)
C CNM(3,1)=CNM(3,1)-C20
C SNM(5,1)=SNM(5,1)-C40
C ALR=AL/57.2957795131
C CL=DCOS(ALR)
C SL=DSIN(ALR)
C CML(1)=1.D0
C CML(2)=CL
C SML(1)=0.D0
C SML(2)=SL
C DO 1 M=3,NP1
C CML(M)=2.D0*CL*CML(M-1)-CML(M-2)
C SML(M)=2.D0*CL*SML(M-1)-SML(M-2)
1 CONTINUE
UND=0.D0
DO 2 N=3,NP1
DO 2 M=1,N
HARM=(CNM(N,M)*CML(M)+SNM(N,M)*SML(M))*Q(N,M)*P(N,M)
UND=UND+6371.D3*HARM
2 CONTINUE
CNM(3,1)=CNM(3,1)+C20
SNM(5,1)=SNM(5,1)+C40
RETURN
END

```

```

SUBROUTINE PANG(PHI,NP1,P,Q,CNM,SNM)
IMPLICIT REAL*8 (A-H,O-Z)
REAL*8 P(NP1,NP1),Q(NP1,NP1),CNM(NP1,NP1),SNM(NP1,NP1)
INTEGER FST
DATA FST/0/
IF(NP1.LE.FST)GOTO 10
FST=NP1
113 READ(5,111)NN,MM,C,S
111 FORMAT(2I2,1X,2F10.5)
N=NN+1
M=MM+1
SNM(N,M)=S*1.0-6
CNM(N,M)=C*1.0-6
IF(N+M.LT.2*NP1)GOTO113
SNM(3,2)=0.00
CNM(3,2)=0.00
NMAX=NP1-1
DO 2 N=2,NMAX
CON=DSQRT(DFLOAT(2*N+1))
Q(N+1,1)=CCN*1.015
CON=CON*DSQRT(2.00)
DO 2 M=1,N
IA=N+M-1
IB=N-M+1
AC=DSQRT(DFLOAT((IA+1))*1.0-15
DO 1 I=IB,IA
1 AC=AC*DSQRT(DFLOAT(I))
2 Q(N+1,M+1)=CON/AC
DO 101 I=1,NP1
DO 101 J=1,NP1
P(I,J)=0.00
101 CONTINUE
P(1,1)=1.0-15
10 CONTINUE
PHR=PHI/57.2957795131
SB=DSIN(PHR)
CB=DCOS(PHR)
P(2,1)=SB*P(1,1)
P(2,2)=CB*P(1,1)
FN=1.00
FN2M1=1.00
DO 402 N=2,NMAX
FN=FN+1.00
FN2M1=FN2M1+2.00
P(N+1,1)=(FN2 M1*SB*P(N,1)-(FN-1.00)*P(N-1,1))/FN
DO 401 M=2,N
401 P(N+1,M)=P(N-1,M)+FN2M1*CB*P(N,M-1)
402 P(N+1,N+1)=FN2M1*CB*P(N,N)

```

RETURN  
END

```
SUBROUTINE DSCCRR (N,FMO,R,W)
REAL*8 R(1),W(1)
C COMPUTATION AND OUTPUT OF CORRELATION COEF FROM PACKED SYM MATRICES
C N SIZE OF MATRIX
C FMO MC TO BE USED IN COMPUTING STANDARD ERROR (REAL*8)
C R PACKED SYMMETRIC MATRIX (REAL*8)
C W WORK VECTOR OF LENGTH N (REAL*8)
C
I=0
J=0
DO 330 K=1,N
I=J+1
J=J+K
W(I)=R(J)*FMO
JJ=J-1
M=0
DO 320 L=I,JJ
M=M+1
NN=(M*(M+1))/2
320 W(M+1)=R(L)/DSQRT(R(NN)*R(J))
330 WRITE(6,900)K,(W(NN),NN=1,K)
900 FORMAT(1S,E12.4/(15F8.4))
RETURN
END
```

```
SUBROUTINE NUMASL(NM1,B1,B2,L1,L2,SIDE,NM,AL,B)
REAL*8 B1,B2,L1,L2,AL(1),B(1)
REAL*4 LINT
FM1=NML
NB=DSQRT(FM1*((B2-B1)/(L2-L1)*DCOS((B2+B1)/114.6D0)))+.5
NL=FM1/FLOAT(NB)+.5
LINT=(L2-L1-SIDE)/FLOAT(NL-1)
BINT=(B2-B1-SIDE)/FLOAT(NB-1)
DO 1 J=1,NB
DO 1 I=1,NL
K=(J-1)*NL+I
AL(K)=L1+SIDE/2.0+FLOAT(I-1)*LINT
B(K)=B1+SIDE/2.0+FLOAT(J-1)*BINT
1 CONTINUE
NM=K
RETURN
END
```

```
SUBROUTINE MASL2(MB,ML,NM,XM,YM,ZM,AE,E2,Q)
IMPLICIT REAL*8 (A-H,C-Z)
REAL*8 MB(1),ML(1),XM(1),YM(1),ZM(1),N,L
RAD=57.2957795131
DO1 I=1,NM
B=MB(I)/RAD
L=ML(I)/RAD
CB=DCOS(B)
SB=DSIN(B)
CL=DCOS(L)
SL=DSIN(L)
N=AE/DSQRT(1.000-E2*SB*SB)
XM(I)=(N-Q)*CB*CL
YM(I)=(N-Q)*CB*SL
ZM(I)=(N*(1.000-E2)-Q)*SB
1 CONTINUE
RETURN
END
```

```

SUBROUTINE BINV (A,N1,N2,B)
C   INVERSE OF A SYMMETRIC MATRIX BY BORDERING
C   A - FIRST WORD OF UPPER TRIANGULAR PART OF MATRIX PACKED BY COLUMN
C       WILL BE INVERSE ON RETURN
C   N1 - SIZE OF KNOWN INVERSE TO BE MODIFIED
C   N2 - SIZE OF DESIRED INVERSE
C   B - WORK VECTOR AT LEAST N2 LONG
C FOR EXAMPLE, THE PARTITIONED MATRIX
C   [ ] [ ] [ ] [ ] [ ] [ ] [ ] [ ] [ ] [ ] [ ] [ ] [ ] [ ] [ ] [ ]
C   |   |   |   |   |   |   |   |   |   |   |   |   |   |   |   |   |
C   |   N   |   C   |   |   |   |   |   |   |   |   |   |   |   |   |   |
C   |   |   |   |   |   |   |   |   |   |   |   |   |   |   |   |   |   |
C   |   |   |   |   |   |   |   |   |   |   |   |   |   |   |   |   |   |
C   [ ] [ ] [ ] [ ] [ ] [ ] [ ] [ ] [ ] [ ] [ ] [ ] [ ] [ ] [ ] [ ]
C   |   |   |   |   |   |   |   |   |   |   |   |   |   |   |   |   |   |
C   |   C'  |   0   |   |   |   |   |   |   |   |   |   |   |   |   |   |
C   [ ] [ ] [ ] [ ] [ ] [ ] [ ] [ ] [ ] [ ] [ ] [ ] [ ] [ ] [ ] [ ]
C   IF N IS A 5X5 MATRIX AND THE INVERSE IS
C   KNOWN AND C IS A 5X2 MATRIX, THEN THE
C   COMPLETE MATRIX CAN BE OBTAINED BY
C   CALL BINV (N,5,7,B)

C   [ ] [ ] [ ] [ ] [ ] [ ] [ ] [ ] [ ] [ ] [ ] [ ] [ ] [ ] [ ] [ ]
C   |   |   |   |   |   |   |   |   |   |   |   |   |   |   |   |   |   |
C   |   |   |   |   |   |   |   |   |   |   |   |   |   |   |   |   |   |
C   IF N1=0, THE COMPLETE INVERSE WILL BE
C   COMPUTED BY BORDERING. (NO PORTION OF
C   INVERSE IS KNOWN)    CALL BINV (A,0,7,B)

C FOR SINGLE PRECISION THE FOLLOWING STATEMENT SHOULD BE CHANGED
REAL*8 A(1),B(1),C,C0/0.000/,C1/1.000/
REAL*4 A(1),B(1),D,C0/0.0/,C1/1.0/
C
N=N1+1
10  IF(N-1) 99,10,20
N=2
20  A(1)=C1/A(1)
DO 90 N=N,N2
M1=(N*(N-1))/2
B(1)=A(1)*A(M1+1)
IF(N.EQ.2) GO TO 50
M2=1
DO 40 I=3,N
B(I-1)=C0
DO 30 J=3,I
M2=N2+1
B(J-2)=B(J-2)+A(M2)*A(M1+I-1)
30  B(I-1)=B(I-1)+A(M2)*A(M1+J-2)
M2=M2+1
40  B(I-1)=B(I-1)+A(M2)*A(M1+I-1)
50  D=A(M1+N)
DO 60 I=2,N
60  D=D-A(M1+I-1)*B(I-1)
DO 70 I=2,N
70  A(M1+I-1)=-B(I-1)/D
A(M1+N)=C1/D
M2=0
DO 80 I=2,N
D=A(M1+I-1)

```

```
DO 80 J=2,I  
M2=N2+1  
80 A(M2)=A(M2)-B(J-1)*D  
90 CONTINUE  
99 RETURN  
END
```

## APPENDIX B

RAPPS SPHERICAL HARMONIC  
POTENTIAL COEFFICIENTS AND THEIR ACCURACY TO (14,14)

N	M	C		S	
		ADJUSTED VALUE	STANDARD ERROR	ADJUSTED VALUE	STANDARD ERROR
2	0	-484.1750	0.0120		
2	2	2.3706	0.0551	-1.3422	0.0551
3	0	0.9365	0.0314		
3	1	1.8556	0.0497	0.2434	0.0531
3	2	0.7130	0.0491	-0.5486	0.0460
3	3	0.6331	0.0653	1.5234	0.0687
4	0	0.5522	0.0197		
4	1	-0.5513	0.0329	-0.4470	0.0272
4	2	0.2971	0.0437	0.5844	0.0441
4	3	0.8729	0.0305	-0.1975	0.0271
4	4	0.0936	0.0759	0.2741	0.0800
5	0	0.0495	0.0283		
5	1	-0.0816	0.0393	-0.0635	0.0390
5	2	0.5228	0.0419	-0.2134	0.0392
5	3	-0.3562	0.0456	0.0273	0.0461
5	4	-0.0492	0.0479	0.0744	0.0460
5	5	0.0859	0.0593	-0.5639	0.0600
6	0	-0.1366	0.0297		
6	1	-0.0647	0.0261	-0.0194	0.0226
6	2	0.0283	0.0396	-0.2635	0.0396
6	3	-0.0535	0.0411	0.0602	0.0373
6	4	-0.0250	0.0507	-0.4123	0.0518
6	5	-0.2906	0.0339	-0.4509	0.0316
6	6	-0.0087	0.0546	-0.1843	0.0540
7	0	0.0702	0.0327		
7	1	0.1289	0.0489	0.1060	0.0480
7	2	0.3065	0.0372	0.1372	0.0354
7	3	0.1796	0.0430	0.0092	0.0433
7	4	-0.1931	0.0430	-0.0906	0.0415
7	5	0.0704	0.0450	0.0355	0.0461
7	6	-0.1654	0.0441	0.0917	0.0426
7	7	0.0679	0.0464	-0.0298	0.0464
8	0	0.0460	0.0346		
8	1	-0.0433	0.0365	0.0250	0.0343
8	2	0.0401	0.0441	0.0981	0.0439
8	3	-0.0044	0.0388	0.0380	0.0379

EJECT

	C	ADJUSTED VALUE	STANDARD ERROR	ADJUSTED VALUE	STANDARD ERROR
M	4	-0.7922	0.0422	-0.0872	0.0386
5	5	-0.0632	0.0405	-0.0000	0.0327
6	6	-0.1073	0.0423	-0.0303	0.0412
7	7	0.0256	0.0348	-0.0258	0.0424
8	8	-0.1041	0.0412	-0.0432	0.0370
9	9	0.0243	0.0341	-0.0432	0.0422
0	0	0.1325	0.0405	-0.0154	0.0400
1	1	0.0125	0.0328	-0.0258	0.0400
2	2	-0.0752	0.0411	-0.0432	0.0400
3	3	0.0400	0.0406	-0.0432	0.0400
4	4	-0.0465	0.0399	-0.0432	0.0405
5	5	-0.0102	0.0391	-0.0432	0.0393
6	6	0.0421	0.0373	-0.0181	0.0380
7	7	0.2074	0.0377	-0.0032	0.0378
8	8	0.0129	0.0382	-0.0345	0.0384
9	9	-0.0127	0.0290	-0.0645	0.0311
0	0	10.0.0783	0.0326	-0.0706	0.0362
1	1	-0.0492	0.0359	-0.1314	0.0370
2	2	-0.0499	0.0371	-0.0866	0.0356
3	3	-0.0210	0.0353	-0.0037	0.0369
4	4	-0.0246	0.0364	-0.0202	0.0366
5	5	-0.0622	0.0363	-0.0160	0.0352
6	6	0.0745	0.0352	-0.0139	0.0343
7	7	0.0439	0.0337	-0.0026	0.0341
8	8	0.0934	0.0344	-0.0630	0.0349
9	9	0.0573	0.0347	-0.0167	0.0298
0	0	-0.0581	0.0218	-0.0120	0.0319
1	1	0.0244	0.0329	-0.0245	0.0315
2	2	0.0304	0.0313	-0.0049	0.0313
3	3	-0.0040	0.0317	-0.0597	0.0318
4	4	-0.0196	0.0320	-0.0615	0.0317
5	5	0.0087	0.0313	0.0098	0.0311
6	6	0.0339	0.0310	-0.0801	0.0309
7	7	0.0388	0.0308	-0.0106	0.0297
8	8	0.0409	0.0297	0.0060	0.0293
9	9	0.0334	0.0293	-0.0109	0.0295
0	0	-0.0140	0.0294	-0.0167	0.0298
1	1	0.0752	0.0297	-0.0596	0.0283
2	2	-0.0653	0.0236	-0.0865	0.0305
3	3	-0.0643	0.0302	-0.0655	0.0287
4	4	-0.0184	0.0293	-0.0169	0.0287
5	5	0.0681	0.0286	-0.0677	0.0290
6	6	-0.0175	0.0292	-0.0281	0.0283
7	7	0.0318	0.0286	-0.0281	0.0283
8	8	0.0033	0.0281	-0.0270	0.0279
9	9	-0.0423	0.0280	-0.0270	0.0279
0	0	12.0.0423	0.0280	-0.0270	0.0279

EJECT

## APPENDIX B CONTINUED

N	M	C		S	
		ADJUSTED VALUE	STANDARD ERROR	ADJUSTED VALUE	STANDARD ERROR
12	8	0.0121	0.0275	0.0507	0.0275
12	9	-0.0112	0.0263	0.0627	0.0267
12	10	-0.0033	0.0263	0.0027	0.0263
12	11	-0.0179	0.0267	0.0039	0.0269
12	12	0.0255	0.0272	-0.0313	0.0272
13	0	0.0462	0.0258		
13	1	-0.0198	0.0240	-0.0172	0.0228
13	2	-0.0028	0.0233	0.0061	0.0236
13	3	0.0196	0.0235	0.0535	0.0235
13	4	0.0092	0.0238	-0.0293	0.0236
13	5	0.0516	0.0236	-0.0476	0.0239
13	6	-0.0353	0.0233	0.0308	0.0235
13	7	0.0078	0.0230	0.0228	0.0231
13	8	-0.0460	0.0230	-0.0033	0.0229
13	9	0.0014	0.0224	0.0520	0.0227
13	10	0.0162	0.0219	-0.0576	0.0219
13	11	-0.0434	0.0218	-0.0011	0.0220
13	12	-0.0137	0.0222	0.0544	0.0225
13	13	-0.0203	0.0225	0.0465	0.0226
14	0	-0.0103	0.0222		
14	1	-0.0177	0.0243	0.0057	0.0232
14	2	-0.0533	0.0202	0.0006	0.0206
14	3	0.0179	0.0205	0.0149	0.0207
14	4	0.0216	0.0205	-0.0038	0.0203
14	5	0.0745	0.0204	-0.0631	0.0206
14	6	0.0144	0.0202	-0.0374	0.0203
14	7	0.0571	0.0199	0.0310	0.0198
14	8	-0.0159	0.0195	-0.0208	0.0195
14	9	0.0346	0.0193	0.0720	0.0193
14	10	0.0546	0.0191	-0.0461	0.0191
14	11	0.0120	0.0187	-0.0106	0.0187
14	12	0.0254	0.0190	-0.0073	0.0192
14	13	0.0145	0.0197	0.0171	0.0197
14	14	-0.0308	0.0197	-0.0075	0.0197

**APPENDIX C**  
**5° × 5° MEAN FREE AIR ANOMALIES,**  
**INTERNATIONAL REFERENCE SYSTEM**

	180°	210°	240°	270°	300°	330°	0°
90°	3 -0 -3 -3 6 0 14 14 6 7 10 7 16 -6 11 9 6 3 20 24 6 9 11 -3 22 19 3 -1 18 23 19 9 7 19 24 16	6 4 8 10 13 15 14 12 12 11 9 11 2 5 9 16 22 13 27 33 33 33 29 34 25 9 15 10 8 17 -9 2-10 3 2 1 42 59 17 5-10-13 -13-11 4 4 0 -3	14 12 10 9 8 13 34 35 18 21 24 26 27 33 33 33 29 34 34 32 29 13 10 39 3 12 -5 -2 0 -3 2 5 9 4 1 2 -7-10 -5 -7 -7 -2 -4-17-27 39 26 28	16 12 4 13 2 2 28 16 16 27 34 6 34 32 29 13 10 39 3 12 -5 -2 0 -3 1 4 22 20 24 27 2 5 9 4 1 2 -7-10 -5 -7 -7 -2 -4-17-27 39 26 28	2 3 2 2 2 1 37 38 39 38 37 34 33 15-14-11-15 22 1 4 22 20 24 27 23 22 24 23 24 8 4-17 11 46 23 36 -4-17-27 39 26 28 20 49 31 49 40 42	0 -1 1 1 0 1 30 24 16 12 16 13 19 48 40 17 31 15 23 22 24 23 24 8 34 31 37 47 28 19 20 49 31 49 40 42	
60°	7 14 18 42 29 29 -13-20 3-10 -3 16 8 6 13 15 9 12 -7-11 -8 -2 3 1 -6 -9-13-12 -6 -6 -6 -7-3-7-11 7 2	12 10 4 9 1 -0 9 6 -1 -7-36 3 0 -5 -9 -5 -8 15 3 22 18 22 11 11 14 24 27 13 4 -3 6 5 22 -1 -6 -3 0 -8 -5-12-15-20 -12-10 7 -0 -1 2	2 3 -9 0-11 -4 27 6 11 19 7 3 -8 -5-10-11 -6 3 11 17 33 18 39 13 -20 0 17 19 22 23 -3 7 -3 12 23 35 -9 7 -2 17 19 23	1 3-33-22 -5 11 -10-15 -9 -6 17 0 -8 -5-10-11 -6 3 11 17 33 18 39 13 -20 0 17 19 22 23 25 14 13 3 14 24 36 16 -2 11 30 19 16 -5 14 -4 +3 52	30 27 10 14 23 21 15 20 23 33 24 17 15 11 5 -5 -5 13 25 14 13 3 14 24 36 16 -2 11 30 19 16 -5 14 -4 +3 52		
30°	-13 -1 8 9 2 0 -5 2 11 36 26 3 -7 -8-12-16-18-19 -7 -4 -3 -3 2 -7 17-12 -4 1 9-16 -23 -8 -2 22 21-12 5 -7 -7 21 1 -9	10 10 -7-21-25-26 -21-11-12 17 -4 7 -15-10 -5 1 23 5 -22 2 -3 -4 0 4 -14 -1-12 -1 0 1 -7 -3 -6 -2 -3 6	-15-19 2 26 -4 2 -21-11-12 17 -4 7 -15-10 -5 1 23 5 -22 2 -3 -4 0 4 -14 -1-12 -1 0 1 -7 -3 -6 -2 -3 6	12 23-27-28-24-18 22 -2 -5-58-27-23 15 -7-20 4-49-16 18 22-11-26-36-18 12 17 34 12 18 -9 9 5 31 24 23 11	-28-19 11 24 -1-10 -28-13 3 -4-11-13 -27-26-15-17-20 -9 -50-29-34-13-14-17 -17-22-37-29 -8 4 -1 -4-11-19 -7 4	-10 -7 8 24 19 -2 -15 -8 -1 4 -7-11 -4 14 2 14 -3 11 -12-10 1 21 5 /6 1 3 5 16 29 18 6 2 -4 0 7 19	
0°	-1 -7 -3 -3 -6 -2 -2 -6 -7 7 12 10 11 -6 3 14 7 4 -1 5 9 13 -10-16 0 5 5 4 10 9 4 3 -3 -2	-6 -8 -6 -5 -1 -4 -1 -1 -7 -5 -7 -4 -2 -3-13 -3 -3 2 -4 2 1 0 2 -2 -3 2 -7 2 1 -3 -4 1 -5 4 -2 8 -1 5 1 8 -4 6	-6 -8 -5 2 -5 2 -5 -4 -3 -4 1 -5 -4 2 1 0 2 -2 -2 0 -8 26 18 15 -3 -6-20 -5 44 21 -12 21-12 -2 48 -8 -10 13 -4 21 27 15	9 3 11 24 19 4 -9 -6 13 3 -7 2 2 0 -8 26 18 15 -5-11 4 -9-11-10 7 -2 -5 10-11-13 -7-18 -7-11-16-11 10 8 -2-21-29 -9	-6 -6 -5-15 -7 -1 -7-10-36-34 1-19 -13-12 -5 -4 -4 -4 -9-12 -4 -9 4 -7 -10 -6 -4 5 0 -9 10 8 -2-21-29 -9	-6 -8 -4 5 10 1 -7-10 -4 2 0 -2 -13-12 -5 -4 -4 -4 -9-12 -4 -9 4 -7 -10 -6 -4 5 0 -9 -13 -5 -1 6 7 -2	
-30°	-20 4 6 11 4 -2 -2 4 9 9 7 7 9 9 7 8 10 8 3 -3 0 7 8 4 -7 -11 -6 -4 -6 -3 -3 2-10 -10 -7 -2	-3 -6 -3 -3 -1 -5 7 -1 -2 -2 -1 -2 0 3 4 0 -5 -1 3 3 5 8 9 12 6 8 8 6 5 9 8 8 5 5 10 15 11 9 6 5 9 11	-3 7 3 8 6 4 -1 7 5 5 8 10 3 3 5 8 9 12 14 0 7 11 7 3 12 3 0 28 5 14 7 1 29 6 2 0 8 5 6 7 9 2 0	-2 9 5 2 10 15 9 4 5 13 10 9 14 0 7 11 7 3 6 -4 -3 8 3 -1 -1 -5 -4 0 0 -2 -1 15 15 16 16 12 0 1 3 10 18 20	11 -0 16 -9 -4 11 16 3 1 4 -5 -3 -2 -3 4 8 8 5 -2 2 9 12 11 9 9 10 14 18 23 28 16 13 15 16 15 13		
-60°	-1 -2 -6 -7 -6 -4 -18-14-17-15-14-15 -13-14-24-28-31-32 -18-19-22-28-12-15 -14-15-19-14-12 -9 20 20 20 20 20	-6 -7 -6 -2 0 1 -16-16-13-10 -8 -7 -29-24-16 -8 -1 4 -8-22-16 -5 13 5 -10 -7 -5 -19 -2-22 21 20 20 20 20 -6	2 4 6 8 9 11 -6 -5 1 3 2 -1 7 8 10 11 -6 27 16 11 15 22 13-10 7 -9 -6 -4 18-10 -9 19 18 18 13 7	12 9 6 7 14 25 8 -2 5 17 31 21 20 12 15 40 40 32 16 11 15 22 13-10 7 -9 -6 -4 18-10 -9 19 18 18 13 7	30 25 16 12 15 18 30 17 4 -3 -1 1 21 9 -1 -6 -6 -4 8 3 0-14-13 2 -22 -9-14 7 7 7 6 -14-19 13-27 11	17 14 12 10 6 3 1 -3 -6 -8 -7 -6 -1 2 6 14 25 38 4 7 9 11 13 14 6 5 4 2 0 -2 10 9 8-22 7-26	
-90°							

## APPENDIX C

## 5°×5° MEAN FREE AIR ANOMALIES - WESTERN HEMISPHERE

	0°	30°	60°	90°	120°	150°	180°
90°	6 7 2 3 3 3 19 14 2 11 22 11 21 25 20 7 20 19 10 17 27 18 12 9 55 67 32 19 8 7 24 25 8 -2-15 0	3 3 2 3 3 3 13 15 8 16 16 15 39 36 32 28 11 21 20 20 17 17 4 7 12 22 19 7 3 6 9 4 10 14 5 21	-2 -3 2 2 3 3 14 13 5 4 2 8 18 16 15 15 16 16 12 8 4 2 -0 2 13 1 3 -4-10 -6 33 10 3 -5 -5-10	4 5 5 5 5 5 7 5 3 0 -2 -4 15 14 11 8 5 3 -12 -4-14 -4 0 -2 -2 -2 -2 -1 -5 5 -11 -9 -7 -6 -7 -9	5 5 5 5 5 5 -5 -6 -5 -4 -2 0 4 6 9 -8 18 22 6 1 7 8 9 10 8 11 12 14 15 13 -6 3 17 29 23 31	5 5 5 5 5 5 3 6 8 11 14 14 24 25 25 24 -2 6 10 10 9 10 12 16 10 8 11 18 23 24 25 21 22 25 20 22	
60°	5 18 10 -4 -6 3 -3 11 16 8 8 22 9 23 26 31 18 16 20 22 17 38 57 46 23 23 22 -5 -9 21 20-14 18 2 -1-35	1 12 11 18 17 20 8 14 13 8 11 3 16 5 10 -6 -6 -5 8 1 43-11 4 1 15 32 31 25 -5-14 -15 38 9 11 20 16	13 3 4 2 -1 -1 8 10 5-13-21 -2 -9 -9-15-22-18 -1 -8-28-24-11 -8 -0 -25-26-23-10 -8 -3 21 22-45 25 5 62	-30-35-21-20 -8 16 -3-27-19-15 -0 -0 0 9 10 1 -5 1 -25-26-23-10 -8 -3 -1 18-37-15 -6-11 39 39 16-17-26 -3	13 12 17 15 9 13 -3 4 16 22 6 13 8 7 5 8 6 16 4 3 7 1 30 -1 2 13 17 35 19 17 6 20 27 45-25 3	25 30 25 14 5 2 32 35 18 11 15 18 6 10 3 4 10 0 -5 2 9 11 6 -3 -3 5-16 -8 4 -6 -7 -9-19-13-16 0	
30°	-7-24-26 8 -7 -1 20 13 -2 -5-12 -3 12 10-15-10 -3 -4 1 4 31 -6 4 7 16 7 11 -6-14 3 20 1 4-14-20 3	2 4 7 -2-24 5 -3 13 19-19-24 17 4 5 29-11 -9 3 9 10 6 -5 -6-11 3 13 -0 3-51 -7 -3 -1-34-26-28-19	14 -3 1-31-49 -6 -18 -3 4 6 -4 -8 -12 -2-20-22 1-30 -15 -4 -5 -1 16 15 -14-28-45-20 -d-23 -21-34-42-47-50-36	-58 -6-14 -5 -7 1 -21-17-14-11 1 3 -11 -8-10-10 7 13 -16 -4 -5 -1 16 15 -30 3 3 7 -1 16 -16 9 14 18 19 27	1 10-15 19 11 15 13 5 7 1 3 -4 41 9 -2 -0 3 -0 32 2 4 -6 -2-22 31 2 15 48 8 12 28 19 52 3 15 19	-7 -5 -8-14-10 8 -3 1 -8-11-10-10 -8 -4 -5-11 -2 8 -4-11-11 -2-20 21 ? 2 -6 0 -5 8 3 9 -1 4 2 3	
0°	-11 -1-17-27-38 7 -10-28 -8-12 -6 -3 -14-25 -7 9-12-10 -1 3 -2 -6 -4 -0 7 8 8 17 -7 5 14 -1 3 23 8 26	-4 22-29-22-13-16 -2 0-31-22 1 -6 1-22-21 2-10-14 4 16-14 7 -8 12 -10 -5 4 13 -3 11 17 1 3 -4-16 1	-23-30-42-49-50-51 -16-10 -9-30-28-11 -15 -4 -8-25 -9 2 9 -4-13-12-34-25 25 35 19 -4 -6 -5 12 13 31 3 -1 -4	-14 -1 22 32 29 28 -13 2 -3 12 18 11 -11 5 8 2 -9-14 -25-34-10-14 -4 11 -3-34-28-17 2 12 -9-11-18-32 4 10	4 11 25 16 17 33 -2-18-12 15 26 2 -7 9 28 20 17 15 9 21 6 5 27 11 -6-16-14 0 12 24 44-12-24 -9 -0 2	+3 22 9 10 9 -7 -20 21 20-25 -1 7 11 23 37 9 12 10 53 8 4 21 17 19 10 5 36 23 22 21 20 6 11 21 19 11	
-30°	8 13 14 12 30 18 5 7 10 13 12 13 4 10 11 9 15 17 8 7 8 11 11 9 25 16 14 22 24-20 11 8 7 9 13 15	13 2 5 9 11 17 21 7 2 3 9 14 19 19 15 20 18 8 16 23 10 19 17 15 16 23 21 21 18 16 21 25 24 23 23 20	2 15 32 7 -2 -3 14 20 13 3 -7 5 16 23 10 19 17 15 29 26 35 30 21 18 19 28 32 30 20 11 18 24 33 33 23 13	-1-25-27-32-31 -3 -6-12-24-42-15-12 -11 0 -4 -6-10-12 -17 12 4 -4 -9-11 -11 3 4 -0 -1 6 12 13 11 7 6 5	-45-25-15 4 1 22 -22-25-14 1 8 22 -12 -9-10-14 9 27 -11 -3 4 -0 -1 6 -2 -1 5 9 9 7 4 4 4 5 4 1 1	16 9 25 14 17 22 21 0 2 9 27 14 8 -8 -5-11 -3 3 2 -8 -4 7 -2 10 -0 3 0 -2 13 2 4 1 -4-12-16-16	
-60°	3 5 6 8 12 16 -6 -8-10-12-12-10 50 58 62 60 54 45 15 14 11 7 3 -1 -4 -6 -6 -5 -3 0 -8 5 5 5 5 5	19 17 14 13 11 8 -5 36 15 29 38 37 37 33 32 34 34 32 -4 -5 -4 -2 2 6 5 10 16 22 28 32 6 6 6 6 6 6	2 -1 1 5 6 6 28 15 10 14 23 21 25 16 11 9 11 12 9 12 14 15 37 21 27 22 36 34 31 27 6 6 5 5 4 4	5 5 6 6 4 -1 13 28 26 25 21 23 23 14 11 10-37 7 17 17-45 1 11 7 23 18 14 11 8 7 -8 4 4-10 5 6	-4 -4 -1 -3 -6 -6 20 19 19 9 -2 8 6 5 4-52-11-17 4 0 -4-35-37-35 -25-27-19-16 8 8 7 9 10 -9-11 -8	0 6 4 -2 -5 -3 2 -3 -7-12-16-18 -23-24 3 3-16 -7 -29 21-30 -9-13-13 7 6 3 -0-21-16 6 -7 -4 0 11 20	
-90°							

APPENDIX C, CONT'D  
5° × 5° MEAN FREE AIR ANOMALIES - EASTERN HEMISPHERE

**APPENDIX D**  
**DISTURBANCE COMPONENT COMPUTER PROGRAM LISTING**

```

C THIS PROGRAM COMPUTES THE COMPONENTS OF THE GRAVITY DISTURBANCE
C VECTOR BASED ON A MODEL CONSISTING OF THE GRS-67 ELLIPSOID SUPPLEMENTED BY:
C
C   1) A (14,14) SET OF POTENTIAL COEFFICIENTS
C   2) UP TO 725 POINT MASSES BASED ON 1 DEGREE ANOMALIES
C   3) UP TO 325 POINT MASSES BASED ON 30 MINUTE ANOMALIES
C   4) UP TO 325 POINT MASSES BASED ON 5 MINUTE ANOMALIES
C UNITS ARE METERS, MILLIGALS, DEGREES AND CM3/SEC2
C
C IMPLICIT REAL*8(A-H,O-Z)
REAL*8 P(15,15),C(15,15),DP(15,15),CNM(15,15),SNM(15,15),N,
*M1(725),X1(725),Y1(725),Z1(725),M3(325),X3(325),Y3(325),Z3(325),
*M5(325),X5(325),Y5(325),Z5(325),H(15)
101 FORMAT(2I2,1X,2F10.5)
C
C C & S ARE SPHERICAL HARMONIC POTENTIAL COEFFICIENTS. THEY ARE STORED
C INTERNALLY AS THE ARRAYS CNM AND SNM IN WHICH THE INDICES ARE RAISED
C BY ONE
      READ(5,101)NN,MM,C,S
      N=MM+1
      N=NN+1
      SNM(N,M)=S*1.0-6
      CNM(N,M)=C*1.0-6
      IF(N+M.LT.30)GOT1
      NPI=15
      SNM(3,2)=0.00
      CNM(3,2)=0.00
C
C PARAMETERS OF THE GRS-67
C
      RF=298.247167
      F=1.00/RF
      E2=2.00*F-F**F
      GAME=978031.8456
      FK0=3.98603D20
      AE=6378160.00
      RAD=57.2957795131
      FM=.53174943312D-8*AE/GAME*10.D4
      C20=-DSQRT(.200)*((2.00/3.00)*F*(1.00-.500*F)-(FM/3.00)
      **(1.00-1.500*FM-(2.00/7.00)*F))
      C40=(4.00/105.00)*F*(7.00*F-5.00*FM)
      CNM(3,1)=CNM(3,1)-C20
      CNM(5,1)=CNM(5,1)-C40
      MAX1=C
      MAX3=C
      MAX5=0
C

```

```

C READ MASS SET DERIVED FROM 1 DEGREE ANOMALIES
C
 7 READ(5,104)I,M1(MAX1+1),X1(MAX1+1),Y1(MAX1+1),Z1(MAX1+1)
  IF(I.LT.0)GOTO59
  MAX1=MAX1+1
  GOT07
C
C READ MASS SET DERIVED FROM 30 MINUTE ANOMALIES
C
 59 READ(5,104)I,M3(I),X3(I),Y3(I),Z3(I)
  IF(MAX3.LT.I)MAX3=I
  IF(I.LT.0)GOTO60
  GOT059
C
C READ MASS SET DERIVED FROM 5 MINUTE ANOMALIES
C
 60 READ(5,104)I,M5(I),X5(I),Y5(I),Z5(I)
  IF(MAX5.LT.I)MAX5=I
  IF(I.LT.0)GOTO61
  GOT060
C
C READ NUMBER OF ELEVATIONS ON VERTICAL TRAJECTORY
C
 61 READ(5,102)NCEL
  IF(NCEL.EQ.0)STOP2
  WRITE(6,303)
  102 FCNMAT(I2)
C
C READ LATITUDE LONGITUDE OF TRAJECTORY FOT POINT AND ELEVATIONS OF
C COMPUTATION PCINTS CN TRAJECTORY
C
  READ(5,103)B,AL,(H(I),I=1,NOEL)
  BR=B/RAD
  103 FCNMAT(2F10.5,6F10.0/(8F10.0))
  104 FORMAT(I3,024.16,3D17.10)
  SR=DSIN(BR)
  CB=DCCS(BR)
  N=AE/DSQRT(1.00-E2*SB*SB)
  SL=DSIN(AL/RAD)
  CL=DCCS(AL/RAD)
  DO S1 I=1,NCEL
  X=(N+H(I))*CB*CL
  Y=(N+H(I))*CB*SL
  Z=(N*(1.00-E2)+H(I))*SB
  R2=X*X+Y*Y+Z*Z
  R=DSQRT(R2)
  GB=DATAN(Z/DSQRT(X*X+Y*Y))*RAD
  CALL LEG(GB,15,P,Q,DP)

```

```

C COMPUTE THE CONTRIBUTION TO THE DISTURBANCE COMPONENTS FROM THE
C SPHERICAL HARMONIC COEFFICIENT SET
C
C CALL SHDIS(P,Q,DP,NP1,CNM,SNM,R,FKM,AE,AL,GB,DBS,DLS,DRS)
C COMPUTE CONTRIBUTION FROM 1 DEGREE SET OF MASSES
C
C CALL PMDIS(X,Y,Z,R,R2,M1,X1,Y1,Z1,DB1,DL1,DR1,MAX1)
C COMPUTE CONTRIBUTION FROM 30 MINUTE SET OF MASSES
C
C CALL PMDIS(X,Y,Z,R,R2,M3,X3,Y3,Z3,DB3,DL3,DR3,MAX3)
C COMPUTE CONTRIBUTION FROM 5 MINUTE SET OF MASSES
C
C CALL PMDIS(X,Y,Z,R,R2,M5,X5,Y5,Z5,DB5,DL5,DR5,MAX5)
TDB=CLS+DB1+CB3+CB5
TCL=CLS+DL1+DL3+CL5
TDR=CRS+DR1+CR3+CR5
WRITE(6,201)B,AL,H(I),DRS,DR1,DR3,DR5,TDR
WRITE(6,202)B,AL,H(I),CLS,DB1,DB3,DB5,TDB
WRITE(6,203)B,AL,H(I),CLS,DL1,DL3,DL5,TDL
201 FORMAT(1X,'DN',2F9.2,F11.0,5F8.2)
202 FORMAT(1X,'DM',2F9.2,F11.0,5F8.2)
203 FORMAT(1X,'DL',2F9.2,F11.0,5F8.2)
303 FORMAT('IDIST',4X,'LAT',5X,'LONG',6X,'ELEV',5X,'HARM 100 KM 50
*KM 10 KM TOTAL'// 'CCMP',31X,51'DIST ')//)
      WRITE(6,204)
204 FORMAT(1HC)
51 CONTINUE
GOTO61
END

```

```

SUBROUTINE PMDIS(X,Y,Z,R,R2,M,XM,YM,ZM,DM,DL,DR,MAX)
C CALLING PARAMETER DEFINITIONS:
C   X,Y,Z ARE CARTESIAN COORDINATES OF COMPUTATION POINT
C   R AND R2 ARE GEOCENTRIC RADIALS AND RADIAL SQUARED TO
C   COMPUTATION POINT
C   M,XM,YM,ZM ARE VECTORS DEFINING THE MASS SET MAGNITUDES AND
C   POSITIONS IN CARTESIAN COORDINATES.  ALL ARE OF LENGTH MAX
C   DM,DL,DR ARE THE ORTHOGONAL DISTURBANCE COMPONENTS IN THE
C   MERIDIAN PRIME VERTICAL AND RADIAL DIRECTIONS
C
C IMPLICIT REAL*8(A-H,C-Z)
REAL*8 XM(1),YM(1),ZM(1),M(1),P,P2,L,L2,L3
P2=X*X+Y*Y
P=DSQRT(P2)
DM=0.00
DL=0.00
CR=0.00
DO 10 I=1,MAX
T=X*XM(I)+Y*YM(I)
F=T+Z*ZM(I)
L2=(X-XM(I))*(X-XM(I))+(Y-YM(I))*(Y-YM(I))+(Z-ZM(I))*(Z-ZM(I))
L=DSQRT(L2)
L3=L2*L
DM=DM-((T*Z -ZM(I)*P2)/(R*P*L3))*M(I)*.100
DL=DL-((XM(I)*Y-YM(I)*X)/(P*L3))*M(I)*.100
CR=CR+((R2-F)/(R*L3))*M(I)*.100
10 CONTINUE
RETURN
END

```

```

SUBROUTINE SHDIS(P,Q,DP,NP1,CNM,SNM,RM,FKM,AEM,AL,GB,GAMB,GAML,
*GAMR)

C CALLING PARAMETER DEFINITIONS:
C   P IS THE ARRAY OF LEGENDRE ASSOCIATED COEFFICIENTS
C   Q IS THE ARRAY OF NORMALIZING COEFFICIENTS
C   CNM & SNM ARE POTENTIAL COEFFICIENTS OF DEGREE AND ORDER
C   (NP1-1). ALL ARRAYS HAVE INDICES RAISED BY ONE FOR STORAGE
C   FKM IS KM OF REFERENCE SYSTEM (CM3/SEC2). AEM IS EQUATORIAL
C   RADIUS (METERS).
C   AL IS LONGITUDE, GB IS GEOCENTRIC LATITUDE, AND RM IS THE
C   GEOCENTRIC RADIUS OF THE COMPUTATION POINT
C   GAMR, GAMB, AND GAML ARE RADIAL, MERIDIAN AND PRIME VERTICAL
C   DISTURBANCE COMPONENTS.

C IMPLICIT REAL*8 (A-H,O-Z)
C P,Q,DP,CNM,SNM, ARE STORED WITH THE INDICES RAISED ONE
C NP1 IS ONE MORE THAN THE ORDER, FKM IS KM IN CM3/SEC2,
C PSI AND ETA ARE IN SECONDS, AL AND GB (LONG AND GEOCENTRIC LAT)
C ARE IN DEGREES. AEM IS EQUATORIAL RADIUS IN METERS.RM IS THE
C GEOCENTRIC RADIUS TO THE COMPUTATION POINT
REAL*8 P(NP1,NP1),Q(NP1,NP1),DP(NP1,NP1),CNM(NP1,NP1),
*SNM(NP1,NP1),CML(37),SML(37)
AE=AEM*100.00
R=100.00*RM
RAD=57.2957795131
ALR=AL/RAD
GBR=GB/RAD
CGB=DCOS(GBR)
CL=DCOS(ALR)
SL=DSIN(ALR)
CML(1)=1.00
CML(2)=CL
SML(1)=0.00
SML(2)=SL
DO 1 M=3,NP1
CML(M)=2.00*CL*CML(M-1)-CML(M-2)
1 SML(M)=2.00*CL*SML(M-1)-SML(M-2)
SUM1=0.00
SUM2=0.00
SUM3=0.00
DO 5 N=3,NP1
HARM3=0.00
HARM2=0.00
HARM1=0.00
DO 6 N=1,N
FM=DFLCAT(N-1)
HARM1=HARM1+(CNM(N,N)*CML(N)+SNM(N,N)*SML(N))*Q(N,M)*P(N,M)

```

```
HARM2=HARM2+(CNM(N,M)*CML(M)+SNM(N,M)*SML(M))*C(N,M)*DP(N,M)
6 PARM3=HARM3+FM*(CNM(N,M)*SML(M)-SNM(N,M)*CML(M))*Q(N,M)*P(N,M)
FNPI=DFLCAT(N)
ARNTH=(AE/R)**(N-1)
SUM1=SUM1+FNPI*ARNTH*HARM1
SUM2=SUM2+ARNTH*HARM2
5 SUM3=SUM3+ARNTH*HARM3
T1= FKM/(R*R)*SUM1
DUDB=(FKM/R)*SUM2
DUOL=-(FKM/R)*SUM3
T2=DUDB/R
GAML=DUOL/(R*CGB)
GAMB=T2*1CC0.D0
GAML=GAML*10C0.D0
GAMR=T1*1CC0.D0
RETURN
END
```

```

SUBROUTINE LEG(PHI,NP1,P,Q,DP)
IMPLICIT REAL*8 (A-H,O-Z)
REAL*8 P(NP1,NP1),C(NP1,NP1),DP(NP1,NP1)
INTEGER FST
CATA FST/0/
IF(NP1.LE.FST)GOTO 10
FST=NP1
NMAX=NP1-1
DO 2 N=2,NMAX
CCN=DSCRT(DFLCAT(2*N+1))
C(N+1,1)=CCN*1.D15
CCN=CCN*DSCRT(2.D0)
DO 2 M=1,N
IA=N+M-1
IB=N-M+1
AC=DSCRT(DFLCAT([IA+1])*1.D-15
DO 1 I=IB,IA
1 AC=AC*DSCRT(DFLOAT(I))
2 C(N+1,M+1)=CCN/AC
10 CONTINUE
DO 1C1 I=1,NP1
DO 1C1 J=1,NP1
P(I,J)=0.D0
CP(I,J)=0.D0
101 CONTINUE
P(1,1)=1.D-15
PHR=PHI/57.2957795131
SB=DSIN(PHR)
CB=DCCS(PHR)
P(2,1)=SB*P(1,1)
P(2,2)=CB*P(1,1)
FN=1.D0
FN2M1=1.D0
CO 4C2 N=2,NMAX
FN=FN+1.D0
FN2M1=FN2M1+2.D0
P(N+1,1)=(FN2 M1*SB*P(N,1)-(FN-1.D0)*P(N-1,1))/FN
DO 4C1 M=2,N
401 P(N+1,M)=P(N-1,M)+FN2M1*CB*P(N,M-1)
402 P(N+1,N+1)=FN2M1*CB*P(N,N)
FN=1.D0
FN2M1=1.D0
CP(1,1)=0.D0
CP(2,1)=P(2,2)
CP(2,2)=-P(2,1)
CO 5C2 N=2,NMAX
FN=FN+1.D0
FN2M1=FN2M1+2.D0

```

```
    CP(N+1,1)=(FN2M1/FN)*(SB*DP(N,1)+CB*P(N,1))-((FN-1.D0)/FN)*  
    *CP(N-1,1)  
    CC 501 M=2,N  
501 CP(N+1,M)=CP(N-1,M)+FN2M1*(CB*DP(N,M-1)-SB*P(N,M-1))  
502 CP(N+1,N+1)=FN2M1*(CB*CP(N,N)-SB*P(N,N))  
    RETURN  
    END
```

**APPENDIX E**

**RESULTS OF POINT MASS DISTURBANCE COMPONENT COMPUTATION**

DIST COMP	LAT	LONG	ELEV	HARM DIST	100 KM DIST	50 KM DIST	10 KM DIST	TOTAL DIST
DN	36.75	260.75	20000.	-4.41	-15.03	-0.74	-1.44	-21.62
DM	36.75	260.75	20000.	3.20	-1.30	-0.90	1.99	2.99
DL	36.75	260.75	20000.	-3.76	4.20	-0.91	0.93	0.45
DN	36.75	260.75	30000.	-4.37	-13.65	-0.74	-0.88	-19.64
DM	36.75	260.75	30000.	3.13	-1.26	-0.13	1.01	2.74
DL	36.75	260.75	30000.	-3.64	3.75	-0.38	0.34	0.08
DN	36.75	260.75	50000.	-4.29	-11.52	-0.64	-0.35	-16.79
DM	36.75	260.75	50000.	2.99	-1.23	0.37	0.17	2.30
DL	36.75	260.75	50000.	-3.41	2.99	0.03	-0.02	-0.41
DN	36.75	260.75	100000.	-4.11	-8.22	-0.30	-0.02	-12.66
DM	36.75	260.75	100000.	2.68	-1.22	0.17	-0.12	1.51
DL	36.75	260.75	100000.	-2.87	1.63	0.02	-0.06	-1.28
DN	36.75	260.75	200000.	-3.89	-5.05	-0.04	0.01	-8.97
DM	36.75	260.75	200000.	2.17	-1.07	-0.11	-0.05	0.94
DL	36.75	260.75	200000.	-1.99	0.28	-0.13	-0.01	-1.85
DN	36.75	260.75	300000.	-3.76	-3.37	-0.00	0.00	-7.13
DM	36.75	260.75	300000.	1.77	-0.90	-0.11	-0.02	0.75
DL	36.75	260.75	300000.	-1.32	-0.12	-0.13	-0.00	-1.57
DN	36.75	260.75	500000.	-3.68	-1.60	0.00	0.00	-5.27
DM	36.75	260.75	500000.	1.24	-0.64	-0.06	-0.00	0.54
DL	36.75	260.75	500000.	-0.41	-0.09	-0.08	-0.00	-0.58
DN	36.75	260.75	1000000.	-3.66	-0.33	0.00	0.00	-3.98
DM	36.75	260.75	1000000.	0.67	-0.31	-0.01	-0.00	0.35
DL	36.75	260.75	1000000.	0.51	0.19	-0.02	-0.00	0.67
DN	36.75	260.75	1500000.	-3.45	-0.10	0.00	0.00	-3.55
DM	36.75	260.75	1500000.	0.51	-0.17	-0.00	-0.00	0.33
DL	36.75	260.75	1500000.	0.68	0.20	-0.01	-0.00	0.87

DIST COMP	LAT	LONG	ELEV	HARM DIST	100 KM DIST	50 KM DIST	10 KM DIST	TOTAL DIST
DN	37.25	260.75	20000.	-4.02	-11.82	-1.34	2.76	-14.43
DM	37.25	260.75	20000.	3.56	4.82	3.08	-0.50	10.96
DL	37.25	260.75	20000.	-4.49	2.98	-3.35	0.11	-4.76
DN	37.25	260.75	30000.	-3.98	-11.05	-0.80	1.57	-14.26
DM	37.25	260.75	30000.	3.48	3.81	2.16	-0.32	9.13
DL	37.25	260.75	30000.	-4.36	2.64	-2.40	-0.10	-4.22
DN	37.25	260.75	50000.	-3.92	-9.78	-0.22	0.54	-13.39
DM	37.25	260.75	50000.	3.33	2.35	1.13	-0.16	6.65
DL	37.25	260.75	50000.	-4.09	2.05	-1.31	-0.17	-3.52
DN	37.25	260.75	100000.	-3.79	-7.60	0.67	0.01	-11.31
DM	37.25	260.75	100000.	2.98	0.50	0.26	-0.08	3.66
DL	37.25	260.75	100000.	-3.49	1.00	-0.41	-0.07	-2.96
DN	37.25	260.75	200000.	-3.63	-5.01	0.00	-0.02	-8.66
DM	37.25	260.75	200000.	2.42	-0.46	-0.07	-0.04	1.85
DL	37.25	260.75	200000.	-2.50	0.02	-0.17	-0.01	-2.66
DN	37.25	260.75	300000.	-3.57	-3.41	-0.01	-0.01	-6.99
DM	37.25	260.75	300000.	1.98	-0.58	-0.09	-0.02	1.30
DL	37.25	260.75	300000.	-1.74	-0.22	-0.13	-0.00	-2.10
DN	37.25	260.75	500000.	-3.56	-1.64	-0.01	-0.00	-5.21
DM	37.25	260.75	500000.	1.39	-0.50	-0.05	-0.00	0.83
DL	37.25	260.75	500000.	-0.70	-0.11	-0.08	-0.00	-0.89
DN	37.25	260.75	1000000.	-3.62	-0.35	-0.00	-0.00	-3.97
DM	37.25	260.75	1000000.	0.75	-0.28	-0.01	-0.00	0.46
DL	37.25	260.75	1000000.	0.39	0.19	-0.02	-0.00	0.55
DN	37.25	260.75	1500000.	-3.44	-0.11	-0.00	-0.00	-3.56
DM	37.25	260.75	1500000.	0.57	-0.16	-0.00	-0.00	0.41
DL	37.25	260.75	1500000.	0.63	0.20	-0.01	-0.00	0.82

DIST COMP	LAT	LONG	ELEV	HARM DIST	100 KM DIST	50 KM DIST	10 KM DIST	TOTAL DIST
DN	37.25	260.25	20000.	-3.42	-13.44	2.02	0.94	-13.90
DM	37.25	260.25	20000.	4.11	5.42	3.88	-0.53	12.83
DL	37.25	260.25	20000.	-4.33	2.75	-1.72	0.02	-3.28
DN	37.25	260.25	30000.	-3.40	-12.55	1.72	0.71	-13.52
DM	37.25	260.25	30000.	4.02	4.39	2.69	-0.38	10.72
DL	37.25	260.25	30000.	-4.19	2.36	-1.43	0.11	-3.15
DN	37.25	260.25	50000.	-3.37	-11.05	1.18	0.35	-12.88
DM	37.25	260.25	50000.	3.85	2.86	1.42	-0.18	7.95
DL	37.25	260.25	50000.	-3.92	1.69	-0.91	0.08	-3.07
DN	37.25	260.25	100000.	-3.30	-8.35	0.37	0.03	-11.26
DM	37.25	260.25	100000.	3.46	0.85	0.38	-0.08	4.61
DL	37.25	260.25	100000.	-3.31	0.52	-0.32	0.00	-3.11
DN	37.25	260.25	200000.	-3.25	-5.22	0.03	-0.01	-8.46
DM	37.25	260.25	200000.	2.80	-0.30	-0.04	-0.04	2.42
DL	37.25	260.25	200000.	-2.32	-0.41	-0.15	-0.00	-2.88
DN	37.25	260.25	300000.	-3.27	-3.42	0.00	-0.00	-6.69
DM	37.25	260.25	300000.	2.30	-0.51	-0.08	-0.02	1.69
DL	37.25	260.25	300000.	-1.56	-0.53	-0.12	-0.00	-2.21
DN	37.25	260.25	500000.	-3.38	-1.58	0.00	-0.00	-4.96
DM	37.25	260.25	500000.	1.61	-0.49	-0.05	-0.00	1.06
DL	37.25	260.25	500000.	-0.53	-0.24	-0.07	-0.00	-0.85
DN	37.25	260.25	1000000.	-3.57	-0.34	0.00	-0.00	-3.91
DM	37.25	260.25	1000000.	0.85	-0.28	-0.01	-0.00	0.56
DL	37.25	260.25	1000000.	0.50	0.17	-0.02	-0.00	0.65
DN	37.25	260.25	1500000.	-3.43	-0.12	0.00	-0.00	-3.55
DM	37.25	260.25	1500000.	0.62	-0.16	-0.00	-0.00	0.45
DL	37.25	260.25	1500000.	0.69	0.19	-0.01	-0.00	0.87

DIST COMP	LAT	LONG	ELEV	HARM DIST	100 KM DIST	50 KM DIST	10 KM DIST	TOTAL DIST
DN	36.75	260.25	20000.	-3.88	-16.55	1.06	-0.89	-20.26
DM	36.75	260.25	20000.	3.78	-1.03	1.08	2.07	5.89
DL	36.75	260.25	20000.	-3.60	2.76	-0.61	-1.40	-2.84
DN	36.75	260.25	30000.	-3.85	-15.13	0.47	-0.68	-19.19
DM	36.75	260.25	30000.	3.69	-0.93	1.59	1.07	5.42
DL	36.75	260.25	30000.	-3.47	2.47	-0.55	-0.64	-2.18
DN	36.75	260.25	50000.	-3.79	-12.84	-0.16	-0.28	-17.07
DM	36.75	260.25	50000.	3.54	-0.85	1.54	0.21	4.45
DL	36.75	260.25	50000.	-3.23	1.92	-0.34	-0.12	-1.77
DN	36.75	260.25	100000.	-3.68	-9.10	-0.32	-0.60	-13.11
DM	36.75	260.25	100000.	3.17	-0.85	0.52	-0.11	2.74
DL	36.75	260.25	100000.	-2.69	0.81	-0.12	0.01	-1.99
DN	36.75	260.25	200000.	-3.54	-5.34	-0.05	0.01	-8.93
DM	36.75	260.25	200000.	2.57	-0.89	-0.07	-0.05	1.56
DL	36.75	260.25	200000.	-1.81	-0.25	-0.12	-0.00	-2.17
DN	36.75	260.25	300000.	-3.50	-3.42	0.01	0.00	-6.90
DM	36.75	260.25	300000.	2.11	-0.83	-0.10	-0.02	1.16
DL	36.75	260.25	300000.	-1.13	-0.47	-0.11	-0.00	-1.71
DN	36.75	260.25	500000.	-3.52	-1.54	0.01	0.00	-5.05
DM	36.75	260.25	500000.	1.47	-0.63	-0.06	-0.00	0.78
DL	36.75	260.25	500000.	-0.24	-0.24	-0.07	-0.00	-0.55
DN	36.75	260.25	1000000.	-3.61	-0.32	0.00	0.00	-3.93
DM	36.75	260.25	1000000.	0.77	-0.31	-0.01	-0.00	0.45
DL	36.75	260.25	1000000.	0.62	0.17	-0.02	-0.00	0.77
DN	36.75	260.25	1500000.	-3.44	-0.11	0.00	0.00	-3.55
DM	36.75	260.25	1500000.	0.56	-0.17	-0.00	-0.00	0.38
DL	36.75	260.25	1500000.	0.75	0.19	-0.01	-0.00	0.93

DIST COMP	LAT	LONG	ELEV	HARM DIST	100 KM DIST	50 KM DIST	10 KM DIST	TOTAL DIST
DN	37.00	260.50	20000.	-3.94	-15.16	-1.06	0.30	-19.86
DM	37.00	260.50	20000.	3.67	2.38	1.30	1.42	8.77
DL	37.00	260.50	20000.	-4.05	3.22	-2.00	0.35	-2.48
DN	37.00	260.50	30000.	-3.91	-13.83	-0.62	0.36	-17.99
DM	37.00	260.50	30000.	3.59	1.82	1.27	0.89	7.57
DL	37.00	260.50	30000.	-3.92	2.87	-1.51	0.12	-2.45
DN	37.00	260.50	50000.	-3.85	-11.75	-0.20	0.21	-15.59
DM	37.00	260.50	50000.	3.43	0.98	1.04	0.28	5.74
DL	37.00	260.50	50000.	-3.67	2.23	-0.85	-0.03	-2.32
DN	37.00	260.50	100000.	-3.73	-8.49	-0.05	0.02	-12.25
DM	37.00	260.50	100000.	3.08	-0.11	0.38	-0.07	3.28
DL	37.00	260.50	100000.	-3.10	1.04	-0.26	-0.03	-2.35
DN	37.00	260.50	200000.	-3.58	-5.20	-0.02	-0.00	-8.80
DM	37.00	260.50	200000.	2.49	-0.67	-0.06	-0.04	1.72
DL	37.00	260.50	200000.	-2.16	-0.07	-0.14	-0.01	-2.38
DN	37.00	260.50	300000.	-3.52	-3.42	-0.00	-0.00	-6.95
DM	37.00	260.50	300000.	2.04	-0.70	-0.09	-0.02	1.23
DL	37.00	260.50	300000.	-1.44	-0.33	-0.12	-0.00	-1.89
DN	37.00	260.50	500000.	-3.53	-1.60	0.00	-0.00	-5.13
DM	37.00	260.50	500000.	1.43	-0.57	-0.05	-0.00	0.80
DL	37.00	260.50	500000.	-0.47	-0.17	-0.08	-0.00	-0.72
DN	37.00	260.50	1000000.	-3.62	-0.33	0.00	-0.00	-3.95
DM	37.00	260.50	1000000.	0.76	-0.29	-0.01	-0.00	0.45
DL	37.00	260.50	1000000.	0.50	0.18	-0.02	-0.00	0.66
DN	37.00	260.50	1500000.	-3.44	-0.11	0.00	-0.00	-3.55
DM	37.00	260.50	1500000.	0.56	-0.17	-0.00	-0.00	0.39
DL	37.00	260.50	1500000.	0.69	0.19	-0.01	-0.00	0.87

	DIST COMP	LAT	LONG	ELEV	HARM DIST	100 KM DIST	50 KM DIST	10 KM DIST	TOTAL DIST
DN	37.50	260.50	20000.	-3.50	-9.06	4.16	0.59	-7.80	
DM	37.50	260.50	20000.	3.59	6.74	2.43	-1.07	12.08	
DL	37.50	260.50	20000.	-4.78	2.57	-2.64	0.19	-4.65	
DN	37.50	260.50	50000.	-3.44	-8.47	1.64	0.21	-10.05	
DM	37.50	260.50	50000.	3.73	3.70	0.96	-0.37	8.03	
DL	37.50	260.50	50000.	-4.35	1.64	-1.15	-0.04	-3.91	
DN	37.50	260.50	200000.	-3.30	-4.98	0.04	-0.02	-8.26	
DM	37.50	260.50	200000.	2.71	-0.09	-0.06	-0.03	2.53	
DL	37.50	260.50	200000.	-2.66	-0.26	-0.17	-0.01	-3.10	
DN	37.50	260.50	500000.	-3.40	-1.62	-0.01	-0.00	-5.03	
DM	37.50	260.50	500000.	1.56	-0.42	-0.05	-0.00	1.09	
DL	37.50	260.50	500000.	-0.76	-0.18	-0.08	-0.00	-1.02	
DN	37.50	260.50	1000000.	-3.58	-0.35	-0.00	-0.00	-3.93	
DM	37.50	260.50	1000000.	0.84	-0.27	-0.01	-0.00	0.56	
DL	37.50	260.50	1000000.	0.38	0.18	-0.02	-0.00	0.54	

DIST COMP	LAT	LONG	ELEV	HARM DIST	100 KM DIST	50 KM DIST	10 KM DIST	TOTAL DIST
DN	37.00	261.00	20000.	-4.50	-13.23	-4.48	2.22	-19.99
DM	37.00	261.00	20000.	3.11	1.36	-0.60	0.74	4.61
DL	37.00	261.00	20000.	-4.20	3.97	-0.70	-1.56	-2.49
DN	37.00	261.00	50000.	-4.37	-10.36	-1.17	0.21	-15.69
DM	37.00	261.00	50000.	2.91	0.20	-0.02	0.16	3.24
DL	37.00	261.00	50000.	-3.83	2.76	-0.31	-0.39	-1.77
DN	37.00	261.00	200000.	-3.94	-4.92	-0.02	-0.01	-8.90
DM	37.00	261.00	200000.	2.10	-0.88	-0.10	-0.04	1.08
DL	37.00	261.00	200000.	-2.33	0.33	-0.16	-0.01	-2.18
DN	37.00	261.00	500000.	-3.71	-1.64	-0.01	-0.00	-5.36
DM	37.00	261.00	500000.	1.20	-0.58	-0.05	-0.00	0.56
DL	37.00	261.00	500000.	-0.64	-0.03	-0.08	-0.00	-0.75
DN	37.00	261.00	1000000.	-3.67	-0.34	-0.00	-0.00	-4.01
DM	37.00	261.00	1000000.	0.66	-0.29	-0.01	-0.00	0.36
DL	37.00	261.00	1000000.	0.39	0.20	-0.02	-0.00	0.57

DIST COMP	LAT	LONG	ELEV	HARM DIST	100 KM DIST	50 KM DIST	10 KM DIST	TOTAL DIST
DN	36.50	260.50	20000.	-4.34	-14.96	0.85	-3.48	-21.94
DM	36.50	260.50	20000.	3.29	-3.81	4.43	-2.23	1.68
DL	36.50	260.50	20000.	-3.31	3.52	0.69	0.14	1.04
DN	36.50	260.50	50000.	-4.22	-11.82	-1.21	-0.47	-17.72
DM	36.50	260.50	50000.	3.08	-2.66	1.78	-0.74	1.46
DL	36.50	260.50	50000.	-2.97	2.69	0.61	-0.03	0.30
DN	36.50	260.50	200000.	-3.84	-5.15	-0.07	0.02	-9.04
DM	36.50	260.50	200000.	2.24	-1.25	-0.14	-0.05	0.80
DL	36.50	260.50	200000.	-1.64	0.15	-0.10	-0.01	-1.60
DN	36.50	260.50	500000.	-3.66	-1.54	0.01	0.00	-5.19
DM	36.50	260.50	500000.	1.27	-0.70	-0.63	-0.00	0.51
DL	36.50	260.50	500000.	-0.18	-0.16	-0.07	-0.00	-0.42
DN	36.50	260.50	1000000.	-3.65	-0.31	0.00	0.00	-3.96
DM	36.50	260.50	1000000.	0.67	-0.32	-0.01	-0.00	0.34
DL	36.50	260.50	1000000.	0.62	0.18	-0.02	-0.00	0.78

	DIST COMP	LAT	LONG	ELEV	HARM DIST	100 KM DIST	50 KM DIST	10 KM DIST	TOT DIS
DN	37.00	260.00	20000.	-3.37	-16.77	-0.29	2.66	-17.78	
DM	37.00	260.00	20000.	4.24	2.47	2.17	0.10	8.97	
DL	37.00	260.00	20000.	-3.87	2.40	-1.49	-0.21	-3.11	
DN	37.00	260.00	50000.	-3.32	-13.06	0.63	0.41	-15.34	
DM	37.00	260.00	50000.	3.97	1.21	1.51	0.10	6.77	
DL	37.00	260.00	50000.	-3.48	1.30	-0.66	0.07	-2.71	
DN	37.00	260.00	200000.	-3.22	-5.40	-0.01	-0.00	-8.67	
DM	37.00	260.00	200000.	2.89	-0.55	-0.04	-0.04	2.27	
DL	37.00	260.00	200000.	-1.96	-0.64	-0.13	0.00	-2.71	
DN	37.00	260.00	500000.	-3.36	-1.52	0.01	-0.00	-4.83	
DM	37.00	260.00	500000.	1.66	-0.56	-0.05	-0.00	1.00	
DL	37.00	260.00	500000.	-0.30	-0.31	-0.07	-0.00	-0.40	
DN	37.00	260.00	1000000.	-3.57	-0.32	0.00	-0.00	-3.89	
DM	37.00	260.00	1000000.	0.86	-0.29	-0.01	-0.00	0.53	
DL	37.00	260.00	1000000.	0.61	0.16	-0.02	-0.00	0.76	

## APPENDIX F

POINT MASS SET DERIVED FROM ONE DEGREE ANOMALIES  
 (expressed as mass times the gravitation constant)

KM IN UNITS OF CM. CUBED PER SEC. SQRD.	GEOCENTRIC COORDINATES - METERS	X	Y	Z
-2.32594630 12	62673	-56662813	2686258	
-2.63655340 13	187995	-5667347	2686258	
2.16128570 13	313223	-5661506	2686258	
2.82427780 12	438298	-5653199	2686258	
-2.11503180 13	563159	-5642123	2686258	
2.36126840 13	697744	-5625301	2686258	
-2.62858490 12	811993	-5611722	2686258	
2.15582460 13	935845	-5592401	2686258	
2.40264460 12	62224	-5602156	2809715	
2.54382470 13	185993	-5606417	2809715	
2.41425240 13	309972	-5602935	2809715	
-2.65886010 13	423608	-5592717	2809715	
2.44736040 13	557133	-5591765	2809715	
2.24606750 12	580286	-5562095	2809715	
2.14021490 13	503226	-5571684	2809715	
2.29083370 13	925833	-5532572	2809715	
2.34783040 13	61222	-5545776	2932227	
-2.66942520 13	183882	-5542065	2932227	
-2.22963380 13	306371	-55527645	2932227	
2.29716820 13	428709	-5522520	2932227	
2.70265320 12	550838	-5512622	2932227	
-2.11335210 13	672698	-5525157	2932227	
2.53865010 12	724223	-5428251	2932227	
2.57621450 12	915371	-5472053	2932227	
2.29772170 13	60573	-5479700	3052934	
2.26501720 13	181621	-5477022	3052934	
2.60003440 12	302720	-5471657	3052934	
-2.24419260 12	423601	-5463673	3052934	
-2.10832270 13	544275	-5452932	3052934	
-2.96303280 11	664683	-5472575	3052934	
-2.13166190 12	734765	-5423552	3052934	
2.26812080 12	924465	-5424885	3052934	
-2.27127120 13	522813	-5410962	3172379	
-2.47557180 13	179412	-5405318	3172379	
2.13115310 12	298222	-5403070	3172379	
-2.28363490 12	416287	-53226122	3172379	
2.33172260 11	527448	-5334537	3172379	
-2.72276430 12	676245	-5371241	3172379	

EJECT

## APPENDIX F CONT.

KM IN UNITS OF CM. CUBED PER SEC. SQRD.	X	Y	Z
0.17559550 13	774921	-5355519	3172379
0.50347680 12	893119	-5337030	3172379
0.29304420 13	59024	-5339594	3290302
0.33193250 12	177045	-5326985	3290302
0.54667390 12	294000	-5321767	3290302
0.23210890 13	412770	-5323243	3290302
0.14902210 13	570359	-5313517	3290302
0.18994520 13	647638	-5300435	3290302
-0.12012500 13	764700	-5284852	3290302
0.68174770 12	891239	-5266697	3290302
-0.61192160 12	58207	-5265629	3406647
-0.28950450 13	174593	-5263055	3406647
-0.86177910 12	290824	-5257912	3406647
-0.16767180 13	427052	-5252194	3406647
-0.89637180 11	523012	-5239913	3406647
0.35213020 13	638716	-5227071	3406647
-0.17402190 13	754108	-5211675	3406647
0.28349970 12	869131	-5193731	3406647
0.17626220 12	57261	-5189101	3521357
0.29545390 13	172055	-5186565	3521357
0.49718840 11	285666	-5181494	3521357
-0.34621560 12	401137	-5173891	3521357
0.61146470 12	515411	-5162759	3521357
-0.19275520 13	629433	-5151104	3521357
0.15404410 12	743148	-5136931	3521357
0.14512560 12	856499	-5118249	3521357
0.28512260 12	56487	-5112047	3634375
-0.10910520 13	162434	-5107542	3634375
0.13972210 13	282299	-5102556	3634375
0.12005310 12	325025	-5095068	3634375
-0.31016470 13	507559	-5085091	3634375
0.58303440 13	619844	-5072629	3634375
-0.552292010 13	731826	-5057697	3634375
0.29658260 12	843451	-5040274	3634375
0.19943030 13	55585	-5028503	3745648
-0.32553540 12	166730	-5026045	3745648
0.14440230 12	277794	-5021131	3745648
-0.33121820 13	388722	-5012764	3745648
0.71723430 13	429479	-5003245	3745648
-0.55435200 12	509953	-4221582	3745648
0.67753120 13	720148	-4276272	3745648
-0.59012780 13	822291	-4252642	3745648
0.82875000 12	54657	-4244628	3855119
0.13740440 13	163945	-4242021	3855119
-0.16397170 13	273154	-4237250	3855119
-0.10395980 12	382229	-423215	3855119
-0.32589250 13	491117	-4222360	3855119

EJECT

## APPENDIX F CONT.

KV IN UNITS OF CM. CUBED PER SEC. SQRD.	X	Y	Z
0.2422601D 13	529764	-4208302	3855119
-0.3019799D 13	708119	-4893844	3855119
0.4629623D 13	816127	-4876995	3855119
0.3272215D 12	53722	-4858101	3962735
-0.1364739D 13	161080	-4855727	3962735
0.1719136D 13	268380	-4855979	3962735
-0.1874404D 13	375549	-4847361	3962735
0.5280606D 12	482534	-4834376	3962735
0.1613240D 13	532283	-4822528	3962735
-0.3652017D 13	695744	-4808323	3962735
0.1916648D 12	801865	-4791769	3962735
-0.1557177D 12	52720	-4769323	4068444
0.2770691D 13	158137	-4766992	4068444
-0.2575115D 13	263476	-4762332	4068444
-0.1171315D 13	368686	-4755344	4068444
0.2077131D 13	473716	-4746031	4068444
-0.2647336D 13	578514	-4734400	4068444
0.4629344D 13	693030	-4722455	4068444
-0.2305408D 13	787212	-4704202	4068444
-0.5970738D 11	51713	-4678216	4172193
-0.4341822D 10	155116	-4675930	4172193
-0.1271324D 12	258443	-4671352	4172193
0.1655181D 13	361643	-4664504	4172193
-0.5549531D 12	464667	-4655370	4172193
-0.2844058D 13	567463	-4643960	4172193
0.4401667D 12	659282	-4630281	4172193
-0.3079491D 12	772174	-4614340	4172193
-0.1473403D 13	50681	-4584824	4273932
0.1381469D 13	152019	-4582584	4273932
-0.2024410D 13	253283	-4578103	4273932
0.2740886D 13	354424	-4571385	4273932
0.6597006D 12	455321	-4562434	4273932
0.1000767D 13	556135	-4551252	4273932
0.1049222D 13	556607	-4527846	4273932
-0.1828243D 13	756769	-4522222	4273932
-0.4115722D 13	49624	-4489190	4273609
-0.9405696D 12	148848	-4496397	4273609
-0.5847225D 12	246000	-4482610	4273609
0.3187772D 13	347031	-4476072	4273609
-0.1348225D 13	445292	-4467267	4273609
0.1543565D 13	544537	-4456310	4273609
-0.1234697D 12	642011	-4443102	4273609
0.5219618D 12	740074	-4427895	4273609
0.2518502D 12	43540	-4321252	4471176
-0.2263447D 12	145605	-4389213	4471176
-0.1159731D 12	242526	-4384222	4471176
0.7823922D 12	339465	-4378483	4471176

EJECT

## APPENDIX F CONT.

KM IN UNITS OF CM. CUBED PER SEC. SORD.	X	Y	Z
0.73055700 12	426173	-4259914	4471176
-0.33493670 13	532668	-4259204	4471176
0.58595900 11	628201	-4246364	4471176
0.13700380 12	724826	-4231339	4471176
0.28608290 13	47437	-4221330	4566584
0.55105720 12	142220	-4229223	4566584
0.25170680 13	227072	-4285089	-4566584
-0.10161910 13	331739	-4278801	4566584
0.57280930 12	426244	-4277422	4566584
-0.10182200 12	520540	-4252257	4566584
0.35282720 13	614582	-4247409	4566584
-0.13661390 13	708224	-4232735	4566584
-0.51243030 13	463209	-4189293	4559785
-0.35662280 13	138905	-4187251	4559785
0.18552360 13	331433	-4183158	4559785
-0.26425210 13	222848	-4177019	4559785
0.49732270 12	416105	-4163640	4559785
0.50118140 12	508158	-4158623	4559785
-0.16946990 13	529263	-4146373	4559785
0.28684140 12	521474	-4132098	4559785
0.20302650 13	45158	-4055164	4750734
-0.18606210 12	135452	-4082158	4750734
0.76694490 12	225680	-4079176	4750734
-0.73327410 12	315798	-4073190	4750734
-0.52697940 12	425762	-4065214	4750734
0.10839240 13	425527	-4055251	4750734
0.17853490 12	535049	-4043306	4750734
-0.14084710 12	674286	-4022336	4750734
0.40861290 12	-2792122	-4935060	2686058
0.67628590 13	-2682247	-4925575	2686058
-0.46368480 12	-2571261	-5053650	2686058
0.56160720 12	-2458918	-5109255	2686058
-0.10669660 13	-2345273	-5152352	2686058
-0.53221860 13	-2230683	-5212247	2686058
0.56315250 13	-2114902	-5261984	2686058
-0.23535430 13	-1998087	-5306450	2686058
0.70492770 12	-2762250	-4982261	2809715
0.51944170 12	-2653649	-4942129	2809715
-0.12139750 13	-2543752	-4999582	2809715
0.30530560 13	-2432611	-5054592	2809715
0.16590790 12	-2220281	-5107131	2809715
0.14522530 13	-2206817	-5157173	2809715
-0.16791340 12	-2022275	-5204628	2809715
-0.31982200 13	-1976710	-5249677	2809715
0.30935000 12	-2771237	-4827222	2932127
0.10925240 13	-2623664	-4856264	2932127
0.70750330 12	-2616078	-4943098	2932127

EJECT

## APPENDIX F CONT.

KM IN UNITS OF CM. CUBED PER SEC.	SQRD.	GEOCENTRIC COORDINATES - METERS	X	Y	Z
-2.4920263D	13	-2425123	-42997476	2932027	
0.3147773D	13	-2294062	-5049422	2932027	
-2.2002028D	13	-2181881	-5098900	2932027	
-2.9611348D	11	-2068573	-5145886	2932027	
-2.1066957D	13	-1954374	-5190357	2932027	
0.5291268D	11	-2628498	-4769580	3052934	
0.4519024D	12	-2592404	-4828066	3052934	
-2.2135212D	13	-2485042	-4884173	3052934	
0.1902257D	13	-2376467	-4937933	3052934	
0.5206244D	13	-2266733	-4989260	3052934	
-2.7077889D	13	-2155385	-5033149	3052934	
0.2335472D	13	-2043936	-5084575	3052934	
-2.1297474D	13	-1931086	-5128516	3052934	
-2.1618267D	13	-2664648	-4729750	3172379	
0.7122837D	11	-2659984	-4767503	3172379	
-2.2089653D	12	-2453970	-4822926	3172379	
-2.2880998D	13	-2346656	-4875202	3172379	
-2.3908514D	13	-2278295	-4926557	3172379	
0.9197756D	12	-2128941	-4974250	3172379	
-2.2185175D	13	-2018746	-5022794	3172379	
0.1191484D	13	-1906855	-5064184	3172379	
-2.5727722D	11	-2629502	-4647500	3290302	
0.1143326D	13	-2526121	-4704621	3290302	
-2.1232316D	13	-2421504	-4752213	3290302	
0.3423287D	13	-2316726	-4811679	3290302	
-2.1035635D	12	-2228773	-4861604	3290302	
-2.2753884D	13	-2100762	-4800332	3290302	
-2.1832660D	12	-1991725	-4954572	3290302	
0.2777630D	13	-1881714	-4997762	3290302	
0.1137018D	13	-2593078	-4683250	3406647	
-2.4962526D	13	-2491128	-4622452	3406647	
0.6032044D	13	-2387261	-4693386	3406647	
-2.5344237D	13	-2236227	-4745027	3406647	
-2.6600719D	12	-2178177	-4794349	3406647	
0.1446667D	13	-2071662	-4841327	3406647	
-2.2920425D	13	-1964133	-4885240	3406647	
-2.5548211D	12	-1835648	-4728164	3406647	
0.2772153D	12	-2555721	-4515640	3521357	
-2.42299263D	13	-2454224	-4572025	3521357	
0.4020927D	13	-2353256	-4625175	3521357	
0.2269522D	12	-2250426	-4675065	3521357	
-2.2432529D	13	-2146520	-4724670	3521357	
0.1328449D	13	-2041554	-4770366	3521357	
0.3714197D	12	-1945589	-4814930	3521357	
0.1270343D	13	-1328679	-4855541	3521357	
-2.5480173D	12	-2516461	-4447830	3634375	
0.7015644D	13	-2417524	-4502371	3634375	

EJECT

## APPENDIX F CONT.

KM IN UNITS OF CV. CUBED PER SEC. SQRD.	GEOCENTRIC COORDINATES - METERS		
	X	Y	Z
-0.71038460 13	-2317405	-4654712	3634375
0.33793760 13	-2216153	-4604327	3634375
-0.22570130 13	-2113819	-4652621	3634375
0.37757830 12	-2010451	-4628252	3634375
0.20152290 12	-1926121	-4741576	3634375
-0.92236130 12	-1800820	-4782553	3634375
-0.68543560 13	-2476314	-4376853	3745648
0.10214160 14	-2378946	-4432524	3745648
-0.78693310 13	-2282423	-4482030	3745648
0.65962670 13	-2180789	-4531345	3745648
-0.73996760 13	-2080087	-4578446	3745648
0.34243480 13	-1978367	-4623309	3745648
-0.51585040 13	-1875685	-4665912	3745648
0.14201350 13	-1772083	-4706236	3745648
0.62238350 13	-2434941	-4303743	3855119
-0.41516220 13	-2379208	-4356518	3855119
0.45626740 13	-2242233	-4407163	3855119
-0.49117030 13	-2144761	-4455654	3855119
0.41575690 13	-2045342	-4501958	3855119
-0.26384860 13	-1945323	-4546082	3855119
0.55587170 13	-1844753	-4587974	3855119
-0.44492750 13	-1742482	-4627623	3855119
0.33665200 12	-2392259	-4228534	3962735
-0.22937130 13	-2298330	-4282386	3962735
0.17951160 13	-2203147	-4320146	3962735
0.33417800 12	-2106499	-4277730	3962735
0.95348300 12	-2029599	-4423295	3962735
-0.43860920 12	-1911328	-4466678	3962735
0.25617450 13	-1812123	-4507797	3962735
0.43475690 12	-1712032	-4546754	3962735
-0.24753790 12	-2348670	-4151261	4068444
-0.30735050 12	-2256330	-4202166	4068444
-0.16844070 13	-2162887	-4251017	4068444
0.47578080 12	-2058286	-4297770	4068444
0.31491510 12	-1972875	-4342463	4068444
-0.26413250 13	-1876400	-4285014	4068444
-0.32830630 13	-1779028	-4425421	4068444
0.35630280 13	-1680746	-4462666	4068444
0.10497100 13	-2303864	-4071361	4172193
-0.25029180 12	-2113228	-4121393	4172193
0.17563210 13	-2121570	-4162811	4172193
-0.21476430 12	-2028875	-4215691	4172193
0.76724240 12	-1935198	-4259510	4172193
-0.21267310 12	-1840556	-4301248	4172193
0.86395510 12	-1745024	-4345984	4172193
-0.12113610 13	-1648639	-4278398	4172193
0.33548160 12	-2257813	-3990672	4273932

EJECT

## APPENDIX F CONT.

KM IN UNITS OF CM. CUBED PER SEC. SQRD.	X	Y	Z
-2.14781670 12	-2162045	-4039607	4273932
-2.63816470 12	-2079216	-4086568	4273932
-2.17052310 13	-1985372	-4131532	4273932
2.20842250 13	-1805356	-4174477	4273932
-2.82477810 12	-1803812	-4215381	4273932
-2.87467100 12	-1710188	-4254226	4273932
2.37254210 12	-1615727	-4290921	4273932
2.58729760 12	-2213716	-3907431	4273629
2.14934550 13	-2123821	-3855346	4273629
-2.17614340 13	-2075847	-4001327	4373629
2.13402440 12	-1946897	-4045353	4373629
2.13399720 12	-1856026	-4087402	4373629
2.18281990 13	-1766187	-4127454	4373629
2.35297030 12	-1674515	-4165488	4373629
2.25932370 13	-1582025	-4201487	4373629
-2.37013520 13	-2162541	-3822273	4471176
2.12492520 13	-2077518	-3869142	4471176
2.32076340 12	-1991452	-3914123	4471176
-2.68463660 12	-1904460	-3957195	4471176
2.26261320 13	-1816727	-3998327	4471176
-2.30593680 13	-1727697	-4037506	4471176
2.54248300 12	-1673023	-4074711	4471176
2.16575420 13	-1547542	-4109925	4471176
-2.18638050 13	-2113305	-37755265	4566584
-2.26357410 13	-2030219	-3781288	4566584
-2.52062820 12	-1946141	-3825014	4566584
-2.66226810 12	-1861129	-3867100	4566584
-2.36021220 13	-1775170	-3907226	4566584
2.42822870 13	-1688262	-3945533	4566584
-2.53942590 13	-1600730	-3981241	4566584
2.41147120 13	-1512215	-4016333	4566584
-2.18461140 13	-2063035	-3646403	4659785
2.95990670 12	-1961226	-3621117	4659785
-2.20973280 13	-1800246	-3734026	4659785
2.23180180 13	-1816938	-3775111	4659785
-2.38383610 13	-1732942	-3914331	4659785
2.53157360 13	-1648292	-3851727	4659785
-2.25062020 12	-1562552	-3867221	4659785
-2.15073160 13	-1476341	-3920814	4659785
-2.17732770 13	-2011754	-3575763	4750734
2.24342790 13	-1972660	-3502236	4750734
2.12124520 13	-1852621	-3641229	4750734
-2.24113030 13	-1771677	-3631272	4750734
2.28040180 13	-1689267	-3712527	4750734
-2.31213560 13	-1607231	-3755234	4750734
-2.52792270 12	-1523202	-3720526	4750734
-2.24035720 13	-1472642	-3822254	4750734

EJECT

KM IN UNITS OF CM. METERS  
SOCONTACT COORDINATES - X Y Z

**APPENDIX E CONT.**

## APPENDIX F CONT.

KM IN UNITS OF CM.      GEOCENTRIC COORDINATES - METERS  
CUBED PER SEC.    SORD.    X            Y            Z

0.30962160	13	-48392	-5545933	2922727
0.13237510	13	-1829273	-5165708	3052934
-0.23635320	13	-1714624	-5204883	3052934
0.39432320	13	-1529158	-5241515	3052934
-0.10320590	13	-1482020	-5275584	3052934
0.18955190	13	-1365917	-5307076	3052934
0.18958220	13	-1248266	-5335973	3052934
0.13370670	13	-1120026	-5362267	3052934
0.53974220	12	-1011193	-5385933	3052934
0.15104370	12	-871286	-5406070	3052934
-0.99538010	12	-772147	-5425364	3052934
-0.88633670	12	-652023	-5441127	3052934
0.20322650	12	-521584	-5454191	3052934
-0.80480920	11	-410386	-5464609	3052934
-0.38592940	12	-289267	-5472357	3052934
0.19417250	12	-168246	-5477422	3052934
-0.34241570	12	-47823	-5479826	3052934
-0.13577210	12	-1926726	-5102929	3172372
0.45205930	12	-1623126	-5132523	3172372
-0.16675780	13	-1572028	-5175765	3172372
0.10225680	13	-1464228	-5222407	3172372
0.20576470	12	-1248723	-5242503	3172372
0.18221840	12	-1222622	-5262022	3172372
-0.26134810	12	-1115221	-5284722	3172372
0.14627710	12	-928522	-5318221	3172372
0.35225360	12	-880628	-5329144	3172372
0.19222210	12	-762453	-5357223	3172372
-0.11924260	12	-643844	-5372853	3172372
-0.10343470	12	-524916	-5385773	3172372
-0.13818090	12	-426732	-5392661	3172372
-0.16507320	12	-286749	-5403711	3172372
-0.27376850	12	-166827	-5408721	3172372
-0.11396670	12	-47223	-5411287	3172372
-0.24420680	12	-1732822	-5023630	3290302
0.26245170	12	-1670724	-5071924	3290302
-0.35225240	12	-1538272	-5107422	3290302
0.51147280	12	-1444987	-5140697	3290302
-0.77347320	12	-1230223	-5171383	3290302
-0.48523750	12	-1216252	-5172542	3290302
0.24575240	12	-1121114	-52227162	3290302
-0.18648260	12	-935232	-5248224	3290302
0.10722270	12	-969292	-5263723	3290302
-0.42382370	12	-752421	-5285547	3290302
0.20272830	12	-625222	-53201282	3290302
0.89284210	11	-517223	-53214727	3290302
-0.17732610	12	-422282	-5324552	3290302
0.25527470	12	-282572	-5332422	3290302

EJECT

APPENDIX E CONT.

GEOCENTRIC COORDINATES - METERS

## APPENDIX F. CONT.

KM IN UNITS OF CM. CUBED PER SEC. SEC'D.	X	Y	Z
-2.3822612D 13	-270425	-5123192	3634375
-2.3855710D 12	-157549	-5127232	3634375
-2.3863882D 12	-44527	-5111164	3634375
-2.3621532D 13	-1678651	-4742265	3745648
-2.4440224D 13	-1573452	-4775314	3745648
-2.1543227D 12	-1467432	-4802222	3745648
-2.3428272D 13	-1360728	-4841174	3745648
-2.1524512D 13	-1253447	-4872022	3745648
-2.3012724D 12	-1145484	-4826611	3745648
-2.2622473D 12	-1276251	-4920726	3745648
-2.1463222D 12	-927932	-4942456	3745648
-2.1181711D 13	-818448	-4961761	3745648
-2.7945278D 12	-728565	-4978641	3745648
-2.9383556D 12	-628736	-4993033	3745648
-2.8861248D 12	-487314	-5005034	3745648
-2.2231172D 12	-277254	-5014655	3745648
-2.2245245D 13	-266102	-5021754	3745648
-2.1257337D 12	-155023	-5026420	3745648
-2.5813821D 12	-43885	-5028619	3745648
-2.3536207D 12	-1650611	-4661183	3855119
-2.3138465D 13	-1547162	-4696532	3855119
-2.3002607D 12	-1442271	-4722535	3855119
-2.5223702D 12	-1332057	-4760227	3855119
-2.5372425D 12	-1232512	-4789743	3855119
-2.1420028D 12	-1126232	-4814813	3855119
-2.5765619D 12	-1012647	-4873541	3855119
-2.1863319D 11	-912422	-4859828	3855119
-2.1001428D 12	-824777	-4873381	3855119
-2.1609636D 12	-626730	-4895472	3855119
-2.1648206D 12	-588241	-4909684	3855119
-2.3960209D 12	-472656	-4921490	3855119
-2.1801282D 13	-370755	-4932891	3855119
-2.1369566D 12	-261654	-4937382	3855119
-2.3062335D 12	-152445	-4942472	3855119
-2.9265423D 12	-43152	-4944621	3855119
-2.1902101D 12	-1621756	-4972727	3962735
-2.1029321D 12	-1520132	-4614473	3962735
-2.1680428D 13	-1417754	-4646724	3962735
-2.4397462D 12	-1314684	-4677122	3962735
-2.1093253D 13	-1210272	-4705033	3962735
-2.1042226D 12	-1126557	-4722573	3962735
-2.2227542D 12	-1201322	-4752295	3962735
-2.1328222D 12	-826487	-4774272	3962735
-2.6257232D 12	-722714	-4792621	3962735
-2.1432732D 12	-634554	-4803222	3962735
-2.3555216D 12	-573060	-4822885	3962735
-2.3674226D 12	-471282	-4823485	3962735

EJECT

## APPENDIX F CONT.

KM IN UNITS OF CM. CUBED PER SEC. SQRD.	X	Y	Z
-0.18231920 13	-364276	-4844722	3962735
0.30274200 12	-267292	-4851521	3962735
0.28805250 12	-149761	-4865038	3962735
-0.10138550 13	-42322	-4858213	3962735
-0.15175240 13	-1522130	-4495036	4068444
-0.31567210 12	-1422353	-4522133	4068444
0.26124260 13	-1331846	-4562015	4068444
0.34557420 13	-1220652	-4591568	4068444
-0.57421260 13	-1188842	-4619077	4068444
0.24121420 12	-1086444	-4644222	4068444
-0.107339410 13	-983514	-4657111	4068444
-0.97288840 12	-880124	-4687711	4068444
-0.18608450 12	-776264	-4706021	4068444
-0.26994950 13	-672044	-4722031	4068444
0.33304990 13	-567496	-4735733	4068444
-0.23614450 13	-462671	-4747121	4068444
-0.11119710 13	-357619	-4756182	4068444
0.244795640 12	-252223	-4762932	4068444
-0.10826030 13	-147044	-4767347	4068444
-0.14345060 13	-41623	-4769433	4068444
-0.46505190 13	-1561716	-4412150	4172193
0.42127070 13	-1453845	-4443595	4172193
-0.49329240 13	-1365258	-4474869	4172193
0.56743860 13	-1266004	-4503955	4172193
-0.23172610 13	-1166132	-4530841	4172193
-0.39120860 13	-1055690	-4555512	4172193
0.33022410 13	-964726	-4577256	4172193
0.11585680 13	-863292	-4593164	4172193
0.31227720 13	-761435	-4616124	4172193
0.36282230 12	-659206	-4631828	4172193
0.32133140 13	-556656	-4645268	4172193
-0.33230790 13	-453833	-4656435	4172193
0.50267540 13	-350788	-4667333	4172193
-0.31772550 13	-247572	-4671247	4172193
-0.16360430 12	-144235	-4676273	4172193
0.90926720 12	-40826	-4678724	4172193
0.76172550 13	-1530532	-4322110	4273932
-0.76707390 13	-1434622	-4334687	4273932
0.49476610 13	-1338003	-4338535	4273932
-0.77291110 13	-1240731	-4414042	4273932
0.47714570 13	-1142652	-4442321	4273932
0.12106160 13	-1044415	-4454567	4273932
0.85825410 12	-945457	-4466536	4273932
-0.26742460 13	-846035	-4502570	4273932
-0.29373250 12	-746235	-4522371	4273932
-0.22500210 13	-646247	-4550362	4273932
0.10151460 13	-545342	-4552534	4273932

EJECT

## APPENDIX F CONT.

KM IN UNITS OF CM.      GEOCENTRIC COORDINATES - METERS  
 DIVIDED PER SEC. SQRD.      X      Y      Z

-0.7227957D 12	-444773	-4563481	4273932
0.6116253D 12	-243783	-4572198	4273932
-0.7222352D 12	-242630	-4578680	4273932
0.3336204D 13	-141376	-4582925	4273932
-0.1832769D 13	-40013	-4584930	4273932
0.3492429D 13	-1428514	-4231953	4373609
-0.5415297D 13	-1424627	-4264049	4373609
0.9526789D 13	-1210024	-4294059	4373609
-0.6552247D 13	-1214851	-4321371	4373609
0.5379107D 13	-1112014	-4347770	4373609
-0.6298122D 12	-1022631	-4371444	4373609
-0.1375661D 13	-925746	-4392982	4373609
-0.1693699D 13	-828410	-4412372	4373609
0.7036436D 12	-733669	-4429607	4373609
-0.4775285D 12	-632571	-4444676	4373609
0.2162444D 13	-534154	-4457574	4373609
-0.1622207D 13	-435495	-4463232	4373609
0.7977451D 12	-336614	-4476327	4373609
0.3981045D 12	-237569	-4483173	4373609
-0.3952551D 12	-138407	-4487331	4373609
-0.3387147D 12	-32175	-4492294	4373609
-0.7921371D 12	-1463255	-4133730	4471175
0.6462955D 12	-1374085	-4171125	4471175
-0.4335733D 13	-1231544	-4207481	4471175
0.1536762D 12	-1163276	-4227784	4471175
0.1133441D 12	-1094628	-4233021	4471175
0.1750247D 13	-1030344	-4276179	4471175
-0.1413277D 13	-726572	-4287247	4471175
0.5019217D 12	-810357	-4316215	4471175
0.7051728D 12	-714746	-4332074	4471175
-0.2231026D 12	-613785	-4347815	4471175
-0.1172264D 13	-522523	-4360432	4471175
0.3008821D 12	-426005	-4370017	4471175
-0.7869212D 12	-320278	-4379266	4471175
0.2454761D 13	-232392	-4383475	4471175
-0.1619428D 13	-135331	-4389540	4471175
0.1019583D 12	-78334	-4391460	4471175
-0.1251654D 12	-1432372	-4404540	4566584
0.2233139D 12	-1342811	-44076160	4566584
0.1392863D 12	-1232267	-44124847	4566584
-0.1712652D 12	-1161320	-44131520	4566584
0.7224882D 12	-1062706	-44156171	4566584
0.2122768D 13	-277569	-44175822	4566584
-0.8161718D 11	-384054	-44192410	4566584
-0.1836777D 12	-721327	-44217247	4566584
0.1067773D 12	-619473	-44244422	4566584
-0.7531716D 12	-604627	-44248627	4566584

EJECT

## APPENDIX F CONT.

KM IN UNITS OF CY. CURED PER SEC. SQRD.	X	Y	Z
-0.26207290 12	-310625	-4261156	4556584
0.15202740 12	-415306	-4271403	4556584
0.34484460 12	-321752	-4272562	4556584
-0.29205260 13	-227131	-4285629	4556584
0.74168420 13	-132329	-4289622	4556584
-0.22522320 13	-37472	-4291479	4556584
-0.30726240 12	-1328502	-3949248	4559785
-0.47607870 12	-1310850	-3972193	4559785
-0.11883130 13	-1222576	-4007223	4559785
0.21138070 12	-1133625	-4033250	4559785
-0.19073730 12	-1044261	-4057223	4559785
0.64127710 12	-254315	-4079418	4559785
0.17256260 13	-563203	-4099517	4559785
-0.87520740 12	-773070	-4117612	4559785
0.17721060 12	-681853	-4137625	4559785
-0.55545770 12	-520313	-4147753	4559785
-0.39639200 12	-436481	-4159734	4559785
0.12172560 12	-406423	-4162727	4559785
-0.61523320 11	-314127	-4177762	4559785
0.76262290 12	-221698	-4187635	4559785
-0.48579520 13	-122161	-4187562	4559785
0.71552780 13	-36561	-4189325	4559785
-0.34565280 12	-1363739	-3851031	4750734
0.43124210 12	-1278275	-3861236	4750734
0.58631200 12	-1132166	-3207595	4750734
-0.37872350 13	-1105515	-3222204	4750734
0.10356370 13	-1018303	-3956471	4750734
0.37672160 11	-930593	-3978215	4750734
0.44910860 12	-842429	-3997614	4750734
-0.12815280 13	-753363	-4015250	4750734
0.12563140 13	-564222	-4032943	4750734
0.79128470 12	-575640	-4044676	4750734
-0.23217230 13	-486092	-4056793	4750734
0.27582200 12	-336201	-4066147	4750734
-0.44705160 12	-326219	-4072214	4750734
-0.10526660 12	-216185	-4073690	4750734
0.24255320 13	-125251	-4093472	4750734
-0.35782630 13	-73672	-4095256	4750734
EJECT			

## APPENDIX G

POINT MASS SET DERIVED FROM THIRTY MINUTE ANOMALIES  
(expressed as mass times the gravitation constant)

KM IN UNITS OF CM.      GEOCENTRIC COORDINATES - METERS  
CUBED PER SEC. SQRD.    X            Y            Z

0.1604722D 12	-1259153	-5145733	3449692
-0.2972638D 12	-1211383	-5157167	3449692
-0.5419227D 11	-1163518	-5168127	3449692
-0.1512037D 12	-1115547	-5178763	3449692
0.5636895D 11	-1067484	-5188834	3449692
0.3703754D 12	-1019327	-5198538	3449692
0.2225361D 12	-971083	-5207766	3449692
-0.7091529D 12	-922755	-5216566	3449692
0.4024828D 12	-874348	-5224995	3449692
-0.1959341D 12	-825865	-5232730	3449692
0.6173026D 12	-777312	-5240212	3449692
0.1868077D 12	-728621	-5247194	3449692
-0.4881626D 12	-680008	-5255725	3449692
0.1781718D 12	-631257	-5259804	3449692
0.1842747D 12	-582471	-5265431	3449692
-0.7283134D 11	-533626	-5272635	3449692
-0.4893204D 12	-484734	-5275327	3449692
0.1564421D 11	-1251413	-5114114	3498839
0.3431539D 11	-1233944	-5125498	3498839
-0.7825553D 11	-1156369	-5135440	3498839
0.4499744D 12	-1108695	-5146841	3498839
-0.14119671D 11	-1060925	-5157000	3498839
0.3602255D 12	-1013064	-5166613	3498839
0.2845905D 12	-965116	-5175756	3498839
0.2429381D 12	-917085	-5184512	3498839
-0.9319149D 11	-866975	-5192792	3498839
0.5051491D 12	-820790	-5200623	3498839
-0.8425217D 12	-772533	-5208013	3498839
-0.1777171D 11	-724214	-5214752	3498839
0.7116122D 12	-675930	-5221443	3498839
-0.4668422D 12	-627356	-5227484	3498839
0.2878751D 11	-578932	-5233077	3498839
0.2058725D 12	-570547	-5238219	3498839
0.5546006D 12	-431755	-5242711	3498839
0.2749447D 12	-1243569	-5032048	3547684
0.1505261D 12	-1196725	-5033360	3547684
-0.2641708D 12	-1147113	-5104234	3547684
0.1425503D 12	-1101743	-5114563	3547684

EJECT

## APPENDIX G CONT.

KEY IN UNITS OF CM.  
CUTTED PER SEC. SEC'D. X Y Z  
GEORECTANGULAR COORDINATES - VECTORS

X	Y	Z	X	Y	Z
-0.1122803D 12	-1354273	-5124554	3547684	3547684	-5124213
-0.5711844D 12	-13542712	-5124554	3547684	3547684	-5124213
-0.1209719D 12	-359064	-514332	3547684	3547684	-514332
-0.1198165D 11	-311334	-5132004	3547684	3547684	-5132004
-0.3627422D 12	-863526	-5160232	3547684	3547684	-5160232
-0.1302352D 13	-215544	-5168017	3547684	3547684	-5168017
-0.6896244D 12	-757621	-5175357	3547684	3547684	-5175357
-0.2125872D 12	-719573	-5182253	3547684	3547684	-5182253
-0.8759650D 12	-671592	-5188793	3547684	3547684	-5188793
-0.8628639D 11	-623454	-5194767	3547684	3547684	-5194767
-0.5639738D 12	-575252	-5200264	3547684	3547684	-5200264
-0.6847437D 12	-527921	-5235374	3547684	3547684	-5235374
-0.5531328D 11	-478735	-5210034	3547684	3547684	-5210034
-0.1339231D 12	-1235613	-5349536	3547684	3547684	-5349536
-0.11956416D 12	-1195741	-5065775	3547684	3547684	-5065775
-0.2832174D 12	-1141747	-5071580	3547684	3547684	-5071580
-0.9581461D 11	-1024634	-5081748	3547684	3547684	-5081748
-0.2560825D 12	-1347595	-5091350	3547684	3547684	-5091350
-0.2654239D 12	-1332271	-5121373	3547684	3547684	-5121373
-0.7972662D 10	-9829269	-5110429	3547684	3547684	-5110429
-0.47399775D 12	-905504	-5110044	3547684	3547684	-5110044
-0.423201975D 12	-918802	-5127220	3547684	3547684	-5127220
-0.2617908D 13	-810426	-5134955	3547684	3547684	-5134955
-0.6214132D 12	-762732	-5142242	3547684	3547684	-5142242
-0.3713654D 12	-715~63	-5143130	3547684	3547684	-5143130
-0.3492652D 12	-667226	-5152553	3547684	3547684	-5152553
-0.5793919D 12	-613465	-5161474	3547684	3547684	-5161474
-0.4965526D 12	-571~32	-5166295	3547684	3547684	-5166295
-0.2350046D 12	-523650	-5172274	3547684	3547684	-5172274
-0.51593224D 12	-475672	-5176737	3547684	3547684	-5176737
-0.4312627D 12	-1227642	-5215582	3547684	3547684	-5215582
-0.2707460D 12	-1180383	-5227743	3547684	3547684	-5227743
-0.5460412D 12	-1134216	-5033462	3547684	3547684	-5033462
-0.1372176D 12	-1237550	-5048783	3547684	3547684	-5048783
-0.3636820D 11	-1040692	-5063649	3547684	3547684	-5063649
-0.2644264D 12	-723743	-5066669	3547684	3547684	-5066669
-0.9183816D 12	-945715	-5077077	3547684	3547684	-5077077
-0.5432744D 12	-329526	-5085637	3547684	3547684	-5085637
-0.5118667D 12	-562407	-5096759	3547684	3547684	-5096759
-0.8556826D 12	-365137	-5101443	3547684	3547684	-5101443
-0.32439717D 12	-7679202	-5106639	3547684	3547684	-5106639
-0.1442211D 12	-710402	-5115476	3547684	3547684	-5115476
-0.7411466D 11	-662041	-5121363	3547684	3547684	-5121363
-0.53739212D 11	-515461	-5127723	3547684	3547684	-5127723
-0.1403571D 12	-67952	-5133275	3547684	3547684	-5133275
-0.24992144D 11	-52322	-5138220	3547684	3547684	-5138220
-0.1936198D 12	-472568	-5142922	3547684	3547684	-5142922
			3547684	3547684	

EJECT

## APPENDIX G CONT.

K<sub>w</sub> IN UNITS OF CM.  
CUBED PER SEC. SEC'D. SCRD. X Y Z METERS  
GEOCENTRIC COORDINATES - METERS

0•3485910D	12	-1219378	-4293185	3692363
0•5230287D	12	-1173122	-4994280	3692363
-0•7192757D	12	-1125765	-5004942	3692363
-0•2930094D	12	-1080311	-5015174	3692363
-0•2992728D	12	-1033764	-5024675	3692363
0•2194458D	11	-987128.	-5034744	3692363
-0•1099998D	13	-940408	-5043281	3692363
-0•7138777D	12	-893627	-5051733	3692363
-0•9982538D	12	-846725	-506952	3692363
-0•1762469D	12	-739777	-5067485	3692363
0•9602017D	12	-752755	-5074682	3692363
-0•1377260D	12	-705677	-5081444	3692363
0•3638921D	14	-558828	-5087769	3692363
-0•3251752D	12	-611325	-509356	3692363
0•3078016D	13	-564272	-5099135	3692363
-0•2814417D	11	-516762	-5104115	3692363
0•3058209D	12	-469422	-5106633	3692363
0•6481986D	12	-1211135	-4942958	3739956
-0•1047722D	13	-1165153	-4562774	3739956
0•2612279D	12	-1119115	-4972954	3739956
0•5019227D	12	-1372977	-4881127	3739956
0•1027874D	11	-1026745	-4693031	3739956
-0•1118663D	12	-730427	-45030167	3739956
0•34601174D	12	-934024	-5039042	3739956
0•4171765D	12	-637541	-5017487	3739956
0•4337717D	12	-840981	-5042551	3739956
0•1275071D	12	-724348	-5034062	3739956
-0•1987206D	12	-747547	-5040231	3739956
0•424842D	12	-720982	-5046945	3739956
-0•637001D	12	-654057	-5034228	3739956
0•9739849D	11	-627176	-5059075	3739956
0•5840656D	12	-560243	-5064497	3739956
-0•29735654D	12	-513261	-5069464	3739956
-0•1267280D	12	-466235	-5074035	3739956
0•1432068D	12	-1202715	-4926034	3787226
0•1735034D	12	-115701	-4926551	3787226
-0•6356947D	12	-1111365	-4936560	3787226
0•3194144D	12	-1065542	-49465643	3787226
0•1712367D	12	-1019528	-49565716	3787226
-0•1534753D	11	-9735639	-4965551	3787226
0•2273297D	12	-727587	-4674765	3787226
-0•4770530D	12	-821705	-4932751	3787226
0•4776144D	11	-325153	-4991720	3787226
-0•4892986D	12	-758845	-4993233	3787226
0•1402755D	12	-742471	-5035637	3787226
0•2939030D	12	-635039	-5012035	3787226
0•1144571D	12	-6495229	-4918245	3787226
EJECT				

cm IN UNITS OF CM. SCRAP PEEF SCRAP METERS SCRAP

## APPENDIX G CONT.

## APPENDIX G CONT.

KM IN UNITS OF CV. CUBED PER SEC. SQRD.	GEOCENTRIC COORDINATES - METERS		
	X	Y	Z
0.2673004D 12	-771938	-4891089	3927055
0.3128251D 12	-726555	-4898036	3927055
0.3669885D 12	-681109	-4904562	3927055
-0.1190119D 13	-525625	-4910666	3927055
0.4425350D 12	-590046	-4916348	3927055
0.1851483D 12	-544437	-4921608	3927055
-0.1496631D 12	-428781	-4926444	3927055
0.1078247D 12	-453082	-4930857	3927055
0.3936732D 12	-1168132	-4773756	3972989
0.1149148D 12	-1123918	-4784381	3972989
-0.2782584D 12	-1079429	-4794596	3972989
0.1353745D 11	-1034928	-4804398	3972989
0.5734769D 11	-990317	-4813787	3972989
0.2965867D 11	-945642	-4822762	3972989
-0.7219301D 11	-900885	-4831323	3972989
-0.1069516D 12	-856050	-4839468	3972989
-0.1518379D 12	-811142	-4847197	3972989
0.1145287D 11	-766154	-4854510	3972989
-0.9961138D 11	-721121	-4861405	3972989
-0.1008245D 13	-676015	-4867832	3972989
0.1847671D 13	-630862	-4873941	3972989
-0.1310922D 13	-585624	-4879580	3972989
-0.1242353D 12	-540365	-4884831	3972989
0.1638777D 12	-495051	-4892601	3972989
-0.1933822D 12	-449623	-4893261	3972989
-0.2221409D 11	-1159226	-4737755	4018581
-0.4320673D 11	-1115251	-4747911	4018581
-0.1398044D 12	-1071181	-4758047	4018581
0.6592449D 11	-1027019	-4767775	4018581
-0.2067354D 12	-982768	-4777792	4018581
-0.5672026D 11	-938433	-4785999	4018581
0.1385216D 11	-894017	-4794494	4018581
0.3750761D 11	-849525	-4802578	4018581
0.5066545D 12	-804969	-4810248	4018581
-0.3262473D 12	-760324	-4817525	4018581
0.3676701D 12	-715624	-4824347	4018581
-0.3674418D 12	-670962	-4837775	4018581
0.1613617D 12	-626043	-4836786	4018581
0.5874014D 12	-581169	-4842334	4018581
-0.2605209D 12	-536246	-4847555	4018581
0.4315664D 12	-481277	-4852328	4018581
0.9184607D 11	-446267	-4856675	4018581
-0.1207511D 12	-1150227	-4700561	4063823
0.5848881D 11	-1106587	-4711024	4063823
-0.2203092D 12	-1062859	-4721081	4063823
0.1247500D 12	-1019243	-4730733	4063823
-0.1227116D 12	-975123	-4732278	4063823

EJECT

## APPENDIX G CONT.

KM IN UNITS OF CM. CUBED PER SEC. SQRD.	X	Y	Z
0.10120600 12	-231142	-4743816	4063823
-0.87832400 11	-887072	-4757245	4063823
-0.19767460 11	-842925	-4765265	4063823
-0.15657090 12	-728705	-4772376	4063823
-0.22751160 12	-754417	-4781077	4063823
-0.64403270 10	-710064	-4786866	4063823
0.20211020 12	-655650	-4733244	4063823
-0.32413340 12	-621179	-4792210	4063823
0.13722140 11	-576654	-4804763	4063823
0.16286000 12	-532280	-4809903	4063823
-0.18157530 12	-487460	-4814630	4063823
0.15690050 12	-442798	-4818943	4063823
0.33022440 12	-1141112	-4663343	4108714
-0.20251050 12	-1037825	-4673725	4108714
-0.25981130 11	-1054443	-4663701	4108714
0.18623640 12	-1010271	-4693275	4108714
-0.34341440 11	-767412	-4702448	4108714
0.85867620 11	-923770	-4711215	4108714
0.29805150 11	-880048	-4712578	4108714
0.77224840 11	-336250	-4727535	4108714
-0.21722770 12	-722331	-4733086	4108714
0.34612330 12	-748444	-4742229	4108714
0.13918940 12	-734442	-4748265	4108714
0.67360380 12	-660280	-4755292	4108714
-0.14607550 12	-616260	-4761211	4108714
0.32676190 12	-572088	-4766720	4108714
0.86621530 12	-527867	-4771819	4108714
-0.22478250 12	-483600	-4776509	4108714
-0.64647740 12	-439292	-4783737	4108714

EJECT

## APPENDIX G CONT.

POINT MASS SET DERIVED FROM FIVE MINUTE ANOMALIES  
(expressed as mass times the gravitation constant)

KV IN UNITS OF CM. CUBED PER SEC. SQRD.	GEOCENTRIC COORDINATES - METERS
--	---------------------------------

	X	Y	Z
-0.2419816D 10	-935781	-5069534	3725972
0.8573382D 10	-925803	-5071426	3725972
0.4134169D 10	-915822	-5073238	3725972
0.8469227D 10	-905837	-5075030	3725972
0.4824121D 10	-895849	-5076803	3725972
-0.2052348D 10	-885857	-5078636	3725972
0.5902118D 10	-875862	-5080239	3725972
0.5647234D 10	-865863	-5082003	3725972
0.2049514D 11	-855861	-5083697	3725972
0.1007815D 11	-845856	-5085371	3725972
-0.4394411D 10	-835848	-5087026	3725972
0.2808829D 10	-825836	-5088661	3725972
-0.4769367D 10	-815821	-5090276	3725972
-0.7289145D 10	-805803	-5091871	3725972
0.2911722D 10	-795782	-5093447	3725972
0.6497112D 10	-785758	-5095003	3725972
0.7594227D 10	-775733	-5096543	3725972
-0.1264832D 11	-765703	-5098056	3725972
0.1454009D 10	-934261	-5061905	3736695
0.6493522D 10	-924399	-5063734	3736695
0.5624136D 10	-914433	-5065543	3736695
0.1840185D 10	-904453	-5067332	3736695
0.8806744D 10	-894493	-5069102	3736695
0.3903147D 10	-884513	-5070853	3736695
0.6860998D 10	-874533	-5072583	3736695
0.5172258D 10	-864550	-5074234	3736695
0.1669502D 11	-854563	-5075935	3736695
0.5819560D 10	-844573	-5077638	3736695
0.1509504D 11	-834590	-5079310	3736695
0.5542528D 10	-824593	-5080942	3736695
0.3610675D 10	-814584	-5082635	3736695
0.4342331D 10	-804581	-5084148	3736695
-0.4563678D 10	-794575	-5085721	3736695
0.5481745D 10	-784566	-5087275	3736695
0.5505476D 10	-774554	-5088800	3736695
0.6571202D 10	-764539	-5090322	3736695
-0.1147309D 11	-932923	-5094193	3747402
-0.2422522D 10	-922920	-5096019	3747402

EJECT

KM IN UNITS OF CM. GEOCENTRIC COORDINATES - METERS KM IN UNITS OF CM. GEOCENTRIC COORDINATES - METERS

APPENDIX C CONT.

## APPENDIX G CONT.

KM IN UNITS OF CM. CUBED PER SEC. SQRD.	X	GEOCENTRIC COORDINATES - METERS Y	Z
-0.8912650D 10	-800893	-5062844	3768766
-0.6707543D 10	-790933	-5062410	3768766
0.2014116D 10	-780972	-5063957	3768766
0.2196193D 10	-771003	-5065484	3768766
0.8570847D 10	-761034	-5066991	3768766
-0.5358222D 10	-728643	-5031924	3779424
0.4067246D 10	-918741	-5032742	3779424
-0.3426027D 29	-908876	-5034540	3779424
-0.1394866D 10	-898927	-5036319	3779424
0.6566662D 29	-889015	-5038078	3779424
-0.3420425D 10	-879100	-5039818	3779424
-0.9033439D 29	-869131	-5041538	3779424
-0.2623839D 10	-859269	-5043238	3779424
-0.3995299D 10	-849333	-5044919	3779424
0.1243161D 10	-839404	-5046581	3779424
-0.2332353D 10	-829472	-5048223	3779424
-0.12389259D 10	-819537	-5049945	3779424
-0.4346533D 10	-809698	-5051446	3779424
-0.4631997D 10	-799657	-5053031	3779424
-0.2481403D 10	-789712	-5054595	3779424
0.9532896D 29	-779764	-5056139	3779424
-0.4527266D 10	-769813	-5057664	3779424
0.4396221D 10	-759853	-5059167	3779424
-0.8854459D 10	-727223	-5023124	3790065
-0.1723229D 29	-717317	-5024232	3790065
-0.2666821D 10	-907427	-5026734	3790065
0.5180119D 10	-897534	-5028510	3790065
-0.3804801D 29	-887637	-5030267	3790065
0.3415675D 10	-877737	-5032033	3790065
0.2844636D 10	-867823	-5033721	3790065
0.5858614D 29	-857926	-5035419	3790065
-0.7674021D 10	-848016	-5037097	3790065
-0.3581896D 10	-838103	-5038756	3790065
-0.1098956D 11	-828185	-5040395	3790065
0.2446732D 10	-818265	-5042216	3790065
-0.3672717D 10	-808343	-5043616	3790065
0.2832827D 10	-798417	-5045197	3790065
0.6514227D 10	-788487	-5046738	3790065
-0.4438227D 10	-778555	-5048200	3790065
-0.2654419D 10	-768512	-5049822	3790065
-0.5513322D 10	-758481	-5051325	3790065
-0.1408127D 10	-925750	-5015302	3800690
0.2313831D 10	-915685	-5017114	3800690
0.6733228D 10	-906014	-5018926	3800690
0.3988578D 10	-896126	-5020679	3800690
0.4422330D 10	-886255	-5022437	3800690
0.4007912D 10	-876272	-5024167	3800690

EJECT

APPENDIX G CONT.

GEOCENTRIC COORDINATES - METERS  
X Y Z

## APPENDIX G CONT.

KM IN UNITS OF CM. CUBED PER SEC. SQRD.	GEOCENTRIC COORDINATES - METERS		
	X	Y	Z
-0.5121775D 10	-755127	-5027660	3821891
0.2516373D 10	-921423	-4991703	3832467
0.1515902D 10	-911579	-4993507	3832467
0.3492885D 10	-901751	-4995291	3832467
-0.2497457D 09	-891919	-4997055	3832467
-0.2571270D 10	-882085	-4998801	3832467
0.3095385D 10	-872245	-5000527	3832467
-0.3913541D 09	-862405	-5002234	3832467
-0.8908740D 09	-852560	-5003921	3832467
0.9079432D 09	-842712	-5005589	3832467
-0.4419936D 10	-832860	-5007237	3832467
0.8556105D 10	-823025	-5008867	3832467
0.1370057D 10	-813149	-5010471	3832467
0.1044393D 11	-803286	-5012067	3832467
-0.2040506D 10	-793422	-5013638	3832467
0.7909017D 10	-783555	-5015189	3832467
-0.3913519D 10	-773685	-5016722	3832467
0.6374247D 10	-763812	-5018234	3832467
-0.7918413D 10	-753935	-5019728	3832467
0.1926368D 10	-744043	-4983793	3843026
0.1157813D 10	-7310134	-4985524	3843026
-0.5565366D 10	-7200322	-4987375	3843026
0.4155118D 10	-7000505	-4989137	3843026
-0.1976628D 10	-6900687	-4990280	3843026
0.7480428D 10	-6800864	-4992603	3843026
0.1015815D 10	-6700738	-4994307	3843026
-0.1233921D 10	-6510009	-4995992	3843026
0.2612223D 10	-6410376	-4997657	3843026
-0.1748557D 10	-6310540	-4999303	3843026
0.7415923D 10	-6210701	-50009929	3843026
-0.1187568D 10	-6110859	-5002537	3843026
0.5679539D 10	-6000104	-5004125	3843026
-0.8305091D 09	-592165	-5005623	3843026
-0.3127257D 10	-582213	-5007242	3843026
-0.9031562D 10	-5722459	-5008772	3843026
0.1210599D 10	-562501	-5010282	3843026
-0.2061548D 10	-552741	-5011773	3843026
-0.3140585D 10	-5418479	-4975861	3853568
-0.3706098D 09	-5318585	-4977659	3853568
-0.9154577D 10	-5200889	-4979437	3853568
-0.2178726D 10	-5100889	-4981196	3853568
-0.1981797D 10	-5072285	-4982036	3853568
-0.3440026D 08	-5060478	-4984657	3853568
-0.2242671D 10	-5000669	-4986338	3853568
-0.4576667D 09	-4949854	-4988040	3853568
-0.1502216D 09	-4840077	-4989703	3853568
-0.5260083D 10	-4830217	-4991346	3853568

EJECT

## APPENDIX G CONT.

KM IN UNITS OF CM. CURVED PER SEC. SQRD.	GEOCENTRIC COORDINATES - METERS
	X      Y      Z
-0.2574455D 10	-820394 -4992970 3853563
-0.1041333D 10	-810567 -4994575 3853563
-0.1581160D 09	-800737 -4996160 3853563
-0.2941332D 10	-790904 -4997726 3853563
0.6701138D 10	-781068 -4999273 3853563
0.1905490D 10	-771229 -5000800 3853563
-0.9273417D 09	-761387 -5002308 3853563
-0.1034653D 10	-751543 -5003797 3853563
-0.6677725D 10	-7417010 -4967937 3864094
-0.4891209D 09	-737233 -4969702 3864094
-0.4291500D 10	-7897452 -4971478 3864094
0.3203476D 09	-887567 -4973234 3864094
-0.3466248D 10	-877380 -4974971 3864094
0.3062350D 09	-868068 -4976669 3864094
-0.2928267D 10	-858294 -4978338 3864094
0.5552655D 10	-848426 -4980067 3864094
-0.2036458D 10	-838694 -4981727 3864094
-0.2442187D 10	-828890 -4982358 3864094
-0.1474285D 09	-819282 -4984282 3864094
0.1298617D 10	-809271 -4985691 3864094
0.3838155D 09	-799457 -4988174 3864094
0.1952061D 10	-789640 -4990737 3864094
-0.1612261D 10	-779820 -4991282 3864094
-0.2092687D 10	-769297 -4992807 3864094
0.7500583D 10	-760170 -4994212 3864094
-0.7643051D 10	-750341 -4995723 3864094
-0.3993173D 10	-915538 -4998032 3874603
-0.7039572D 10	-905776 -4961724 3874603
-0.2939261D 10	-896011 -4963497 3874603
0.8746267D 10	-886242 -4965250 3874603
-0.5917512D 10	-876470 -4966284 3874603
-0.50759224D 09	-866695 -4968700 3874603
-0.1813317D 10	-856916 -4970325 3874603
0.5263387D 09	-847133 -4972072 3874603
0.1725215D 09	-837346 -4973722 3874603
0.3122647D 10	-827559 -4975267 3874603
-0.4873101D 10	-817767 -4976936 3874603
-0.1626327D 10	-807972 -4978596 3874603
-0.1570026D 10	-798174 -4980156 3874603
-0.5813352D 09	-788272 -4981727 3874603
0.2376190D 10	-778568 -4983262 3874603
-0.2213228D 10	-768760 -4984731 3874603
-0.9694895D 09	-758950 -4986294 3874603
-0.2256842D 10	-749137 -4987773 3874603
0.2572255D 10	-7314062 -4981035 3886295
-0.6752047D 09	-704316 -4983724 3886295
0.6673191D 10	-834566 -4985424 3886295

EJECT

## APPENDIX G CONT.

KM IN UNITS OF CM. CUBED PER SEC. SQRD.	GEOCENTRIC COORDINATES - METERS		
	X	Y	Z
0.6264178D 10	-884813	-4957244	3885095
-0.1770211D 10	-875057	-4958276	3885095
-0.2827189D 10	-865297	-4960688	3885095
0.3776055D 10	-855534	-4962381	3885095
0.9442496D 09	-845768	-4964066	3885095
0.5878607D 10	-835993	-4965710	3885095
0.1764288D 10	-826225	-4967345	3885095
-0.1997592D 10	-816449	-4968961	3885095
-0.2159131D 10	-806669	-4970558	3885095
-0.3078825D 10	-796887	-4972136	3885095
-0.5231152D 10	-787101	-4973695	3885095
-0.4068046D 09	-777313	-4975234	3885095
0.1278416D 10	-767521	-4976754	3885095
0.6971315D 10	-757726	-4978234	3885095
0.4950144D 10	-747939	-4979736	3885095
-0.5277992D 10	-912582	-4980916	3895571
0.2070772D 10	-902652	-4945702	3895571
0.2543221D 09	-893118	-4947462	3895571
0.1122597D 11	-883381	-4949217	3895571
-0.2038622D 10	-873640	-4950946	3895571
-0.1154505D 10	-863896	-4952655	3895571
-0.3224226D 10	-854149	-4954245	3895571
0.3933114D 09	-844228	-4956016	3895571
0.3533211D 10	-834644	-4957658	3895571
0.6260768D 09	-824887	-4959201	3895571
0.3436518D 10	-815126	-4960715	3895571
-0.5512224D 10	-805363	-4962502	3895571
-0.7638971D 10	-795596	-4964254	3895571
-0.6280648D 10	-785827	-4965642	3895571
-0.5507430D 10	-776054	-4967177	3895571
-0.7010263D 10	-766278	-4968624	3895571
0.4454481D 10	-756492	-4970193	3895571
0.3255353D 09	-746713	-4971672	3895571

## BIBLIOGRAPHY

- Aldridge, L. R. and L. Hurwitz, (1964): "Radial Dipoles as the Sources of the Earth's Main Magnetic Field," *Journal of Geophysical Research*, Vol. 69, No. 12, (15 June 1964).
- Badekas, J., (1968): "Investigations Related to the Establishment of a World Geodetic System," *The Ohio State University, Reports of the Department of Geodetic Science, Rpt. No. 124.*
- Bomford, G., (1962): Geodesy, Oxford, Clarendon Press.
- Bullard, E. C. and R. I. B. Cooper, (1948): "The Determination of Masses Necessary to Produce a Given Gravitational Field," *Proceedings of the Royal Society, Series A*, 194.
- Cook, A. H., (1951): "A Note on the Errors Involved in the Calculation of Elevations of the Geoid," *Proceedings, Series A, Royal Society of London*, Vol. 308.
- Dampney, C. N. G., (1969): "The Equivalent Source Technique," *Geophysics*, Vol. 34, No. 1, (1 February 1969).
- DeWitte, L., (1966a): "Altitude Extension of the Three Anomalous Gravity Components," *Aerospace Corporation, Report No. APP-1001(S9990)-4, Revised 15 July 1967*, San Bernadino, California.
- DeWitte, L., (1966b): "Comparison of Altitude Extended Gravimetric Disturbances and Those Obtained from Spherical Harmonic Representations of the Gravity Field," *Aerospace Corporation Report No. TR-669 (S6230-37)-2.*
- Faddeev, D. K. and Faddeeva, V. N., (1963): Computational Methods of Linear Algebra, W. H. Freeman and Co., San Francisco.
- Fischer, I., (1968): "A Modification of the Mercury Datum," (A paper presented at the 49th Annual Meeting of the American Geophysical Union, Washington, D.C., April, 1968).
- Fischer, I., M. Slutsky, R. Shirley, and P. Wyatt, III, (1967): "Geoid Charts of North and Central America," *Army Map Science Technical Report No. 62.*

- Gaposchkin, E. M. and K. Lambeck, (1970): "1969 Smithsonian Standard Earth (II)," Smithsonian Astrophysical Observatory Special Report No. 315.
- Garland, G. D., (1965): The Earth's Shape and Gravity, Oxford, Pergamon Press, Ltd.
- Groten, E., (1968): "On the Spherical Harmonic Series of the Geopotential at the Earth's Surface," Bulletin Geodesique, No. 88, (June 1968).
- Heiskanen, W.A. and F.A. Vening Meinesz, (1958): The Earth and Its Gravity Field, New York, McGraw-Hill Book Company, Inc.
- Heiskanen, W.A. and H. Moritz, (1967): Physical Geodesy, San Francisco, W. H. Freeman and Company.
- Hirvonen, R. A. and H. Moritz, (1963): "Practical Computation of Gravity at High Altitudes," Reports of the Institute of Geodesy, Photogrammetry, and Cartography, Rpt. No. 27, Ohio State University, 1963.
- IAG, (1967): "Resolutions Adopted at the General Assembly," International Association of Geodesy, Lucerne, Bulletin Geodesique, No. 86.
- IAG, (1970): "Geodetic Reference System 1967," A special publication of the Bulletin Geodesique, Bureau Central de L'Association Internationale de Geodesie, Paris.
- IBM (1968a): "IBM System/360, FORTRAN IV Language," White Plains, New York, International Business Machines Corporation, Form C28-6515-7.
- IBM (1968b): "System/360 Scientific Sub-Routine Package (360A-CM-03x) Version III Programmer's Manual," White Plains, New York, International Business Machines Corporation, Form H20-0205-3.
- Kaula, W. M., (1957): "Accuracy of Gravimetrically Computed Deflections of the Vertical," Transactions, American Geophysical Union, Vol. 38, No. 3, (June 1957).
- Kaula, W. M., (1965): "The Use of Artificial Satellites for Geodesy," University of California, Institute of Geophysics and Planetary Physics, Publication No. 452.
- Kaula, W. M., (1966): "Tests and Computations of Satellite Determinations of the Gravity Fields with Gravimetry," Journal of Geophysical Research, Vol. 71, No. 22, (November 1966).

- Kaula, W. M., (1967): "Geophysical Implications of Satellite Determination of the Earth's Gravitational Field," Space Science Reviews, No. 7, Dordrecht, Holland, D. Reidel Publishing Company.
- Kaula, W. M., (1969): "The Appropriate Representation of the Gravity Field for Satellite Geodesy," University of California, Institute of Geophysics and Planetary Physics, Publication No. 760.
- Kivioja, L., (1963): "The Effect of Topography and Its Isostatic Compensation on Free Air Gravity Anomalies," The Ohio State University, Reports of the Department of Geodetic Science, Rpt. No. 28.
- Koch, K. and I. Morrison, (1969): "A Simple Layer Model of the Geopotential From a Combination of Satellite and Gravity Data," (Paper presented at the 50th Annual Meeting of the American Geophysical Union, Washington, D.C., April 1969).
- Lerch, F. J., J. G. Marsh, M. D. D'Aria and R. L. Brooks, (1969): "Geos I Tracking Station Positions on the SAO Standard Earth (C-5)," National Aeronautics and Space Administration, NASA TN D-5034.
- Levallois, J. J., (1969): "Note Sur La Convergence de Developpement du Potential en Harmonic Spheriques," (A paper presented at Symposium de Trieste 27-30 May 1969 with English Summary).
- Lundquist, C. A. and G. Veis, (1966): "Geodetic Parameters for a 1966 Smithsonian Institution Standard Earth," Smithsonian Astrophysical Observatory Special Report No. 200.
- Mather, R. S., (1968): "The Free Air Geoid in South Australia and Its Relation to the Equipotential Surfaces of the Earth's Gravitational Field," University of New South Wales, UNISURV Report No. 6.
- Mather, R. S., (1970): "The Australian Geodetic Datum in Earth Space," University of New South Wales, UNISURV Report No. 19.
- McGinnis, L. D., (1970): "Tectonics and the Gravity Field in the Continental Interior," Journal of Geophysical Research, Vol. 75, No. 2.
- Molodenskii, M. S, V. F. Eremeev, M. I. Yukina, (1960): Methods for the Study of the External Gravitational Field and Figure of the Earth, Trans by Israel Program for Scientific Translations, Jerusalem, (1962).

- Moritz, H., (1968): "The Geodetic Reference System 1968," Allgerneine Vermessungs Nachrichten 1/1968.
- Morrison, F., (1969): "Validity of the Expansion for the Potential Near the Surface of the Earth," (A paper presented to the Fourth Symposium on Mathematical Geodesy, Trieste 1969).
- Mueller, I. I., (1964): Introduction to Satellite Geodesy, New York, Fredrick Ungar Publishing Company.
- Mueller, I. I., (1966): "External Gravity Field of the Earth," Gravity Anomalies: Unsurveyed Areas, edited by H. Orlin, American Geophysical Union, Geophysical Monograph Series, No. 9.
- Mueller, I. I., (1969): Spherical and Practical Astronomy as Applied to Geodesy, New York, Fredrick Ungar Publishing Company.
- Mueller, I. I., J. P. Reilly and G. R. Schwarz, (1969): "The North American Datum in View of Geos I Observations," The Ohio State University, Reports of the Department of Geodetic Science, Rpt. No. 125.
- Mueller, I. I. and J. D. Rockie, (1966): Gravimetric and Celestial Geodesy, New York, Fredrick Ungar Publishing Company.
- Muller, P. and W. L. Sjogren, "Mascons: Lunar Mass Concentrations," Science, Vol. 161, No. 3842, (August 1968).
- Nagy, D., (1966): "The Gravitational Attraction of a Right Rectangular Prism," Geophysics, Vol. XXXI, No. 2.
- Natrella, M. G., (1963): Experimental Statistics, National Bureau of Standards Handbook 91, Washington, D.C., U.S. Government Printing Office.
- Obenson, G. F. T., (1970): "Direct Evaluation of the Earth's Gravity Anomaly Field from Orbital Analysis of Artificial Earth Satellites," Ohio State University, Reports of the Department of Geodetic Science, Rpt. No. 129.
- Orlin, H., (1959): The Three Components of the External Anomalous Gravity Field, J.G.R., Vol. 64, No. 12, December 1959.
- Pellinen, L. P. and G. V. Demyanov, (1969): "Quasigeoidal Heights Accuracy and Possibilities of Known Geocentric Distances Application in Geodetic Satellite Networks Processing," (A paper presented at the Joint Symposium of the Commission of the New Adjustment of European Triangulation and the Commission of the European Satellite Triangulation Net, Paris, February 1969).

- Pugh, E. M. and G. H. Winslow, (1966): The Analysis of Physical Measurements, Reading, Massachusetts, Addison-Wesley.
- Ramsey, A. S., (1959): An Introduction to the Theory of the Newtonian Attraction, Cambridge, University Press.
- Rapp, R. H., (1965): "Upward Continued Gravity in the Oklahoma Area," The Ohio State University, Reports of the Department of Geodetic Science, Rpt. No. 56.
- Rapp, R. H., (1966): "A FORTRAN Program for the Computation of the Disturbance Components of Gravity," Ohio State University, Reports of the Department of Geodetic Science, Rpt. No. 76.
- Rapp, R. H., (1967): "Comparison of Satellite Geoids and Anomaly Fields," Ohio State University, Reports of the Department of Geodetic Science, Rpt. No. 80.
- Rapp, R. H., (1967b): "Combination of Satellite and Terrestrial Data for a Detailed Geoid," (A paper presented at the 48th Annual Meeting of the American Geophysical Union, Washington, D.C., April 1967).
- Rapp, R. H., (1967c): "A Combination of Satellite and Gravimetric Data for a Detailed Geoid," (A paper presented to the 48th Annual Meeting of the American Geophysical Union, Washington, D.C., March 1967).
- Rapp, R. H., (1968a): "Further Studies in the Combination of Gravimetric and Satellite Data," Ohio State University, Reports of the Department of Geodetic Science, Rpt. No. 119.
- Rapp, R. H., (1968b): "Comparison of Two Methods for the Combination of Satellite and Gravimetric Data," The Ohio State University, Reports of the Department of Geodetic Science, Rpt. No. 113.
- Rapp, R. H., (1968c): Unpublished computations.
- Rapp, R. H., (1968d): "A Method for the Combination of Satellite and Gravimetric Data," The Ohio State University, Reports of the Department of Geodetic Science, Rpt. No. 101.
- Rapp, R. H., (1969a): "Gravitational Potential Coefficients from Gravity Data Alone (II)," (Paper presented at 50th Annual meeting of American Geophysical Union, Washington, D.C., April 1969).

- Rapp, R. H., (1969b): "The Geopotential to (14, 14) from a Combination of Satellite and Gravimetric Data," *Bulletin Geodesique*, No. 91, March 1969.
- Rapp, R. H., (1969c): "Analytical and Numerical Differences Between Two Methods for the Combination of Gravimetric and Satellite Data," *Bulletino di Geofisica Teorica Ed Applicata*, Vol. XI, No. 41-42.
- Rapp, R. H., (1970a): "The Direct Combination of Satellite and Gravimetric Data," (Paper presented at the 51st Annual Meeting of the American Geophysical Union, Washington, D.C., April 1970).
- Rapp, R. H., (1969d): "Geometric Geodesy Notes," The Ohio State University, Department of Geodetic Science, Processed lecture notes.
- Rice, D.A., (1967): "The Development of Geoidal Sections in the Central United States," (Paper presented at Festschrift Walter Grossman; "Aus der Geodatischen Lehre und Forchung," Konrad Wittwer, Stuttgart.
- Siebenhüner, Hajo, (1969): "A New Determination of the European Datum," *Studia Geoph. et. geod.* 13 (1969).
- Snowden, J. M., (1966): "An Investigation of Practical Solutions of Large Systems of Normal Equations," M.S. Thesis, The Ohio State University.
- Snowden, J. M., and R. H. Rapp, (1968): "Two FORTRAN IV Computer Programs for the Combination of Gravimetric and Satellite Data," Ohio State University, Reports of the Department of Geodetic Science, Rpt. No. 116.
- Szabo, Bela, (1968): Status of the First Order World Gravity Net and Absolute Gravity Experiment, (Paper presented at Defense Intelligence Agency Geodetic Objectives Symposium, Alexandria, Virginia, October 1968).
- Uotila, U.A.K., (1959): "Investigations on the Gravity Field and Shape of the Earth," Ohio State University, Reports of the Institute of Geodesy, Photogrammetry and Cartography, Rpt. No. 6.
- Uotila, U.A.K., (1967): "Introduction to Adjustment Computations with Matrices," Ohio State University, Department of Geodetic Science, Processed lecture notes.
- Veis, G., (1968): "The Determination of the Radius of the Earth and Other Geodetic Parameters as Derived from Optical Satellite Data," *Bulletin Geodesique*, No. 89, September 1968.

- Weightman, J.A., (1967): "Gravity, Geodesy, and Artificial Satellites. A Unified Analytical Approach," The Use of Artificial Satellites for Geodesy II, edited by George Veis. Athens: National Technical University of Athens.
- Wong, L., G. Buchler, W. Downs, R. Prislin, "Dynamical Determination of Mascons on the Moon," (Paper presented at the 50th Annual Meeting of American Geophysical Union, Washington, D.C., April 1969).
- Wong, L. and R. Gore, (1969): "Accuracy of Geoid Heights from Modified Stokes Kernels," Geophysical Journal of the Royal Astronomical Society, (1969)18.
- Young, R. G. E., (1970): "Combining Satellite Altimetry and Surface Gravimetry in Geodetic Determinations," Massachusetts Institute of Technology, Measurement Systems Laboratory Report TE-37, Cambridge, Massachusetts.
- Zidarov, D., (1965): "Solutions of Some Inverse Problems of Applied Geophysics," Geophysical Prospecting, Vol. 13.